Institut für Chemie
Arbeitskreis Angewandte Polymerchemie bei Prof. Dr. André Laschewsky

Twofold Switchable Block Copolymers Based on New Polyzwitterions

D I S S E R T A T I O N
zur Erlangung des akademischen Grades
„doctor rerum naturalium“ (Dr. rer. nat.)
in der Wissenschaftsdisziplin Kolloid- und Polymerchemie

eingereicht an der
Mathematisch-Naturwissenschaftlichen Fakultät
der Universität Potsdam

von

M.Sc. Viet Hildebrand

geb. Hoang

Potsdam. 18. April 2016

Published online at the
Institutional Repository of the University of Potsdam:
URN urn:nbn:de:kobv:517-opus4-101372
http://nbn-resolving.de/urn:nbn:de:kobv:517-opus4-101372

„*Gib jedem Tag die Chance, der schönste deines Lebens zu werden*“

- Mark Twain -

Für meine Liebsten Patricia, Jonah und Avi

Acknowledgements

Zu allererst danke ich Herrn Prof. Dr. André Laschewsky herzlichst für die Möglichkeit in seinem Arbeitskreis zu promovieren. Mit Ihrem Enthusiasmus, Inspiration und ständiger Bereitschaft führten Sie mich erfolgreich durch die Promotion, wobei Sie mir immer die Freiheit ließen meine eigenen Ideen in dieses spannende Forschungsthema einzubringen. Die zahlreichen Unterhaltungen über Chemie und allgemein-gesellschaftliche Themen waren immer lehrreich und ich möchte diese nicht missen. Ihre uneingeschränkte Unterstützung in Phasen der persönlichen Freuden, aber auch Krisen, werde ich nie vergessen, vielen Dank dafür! Und vielen Dank dafür, dass Sie mir das „Navigieren im Nebel“ beigebracht haben.

Ein großer Dank gilt Dr. Michael Päch (!) und Dr. Daniel Zehm für die Betreuung und das Korrekturlesen der Doktorarbeit. Eure Ratschläge, Geduld, Hingabe und grandiosen Ideen kombiniert mit eurem umfangreichen Fachwissen waren mehr als nur hilfreich.

Während meiner Promotion habe ich mit unterschiedlichen Kollegen zusammenarbeiten dürfen. Namentlich möchte ich mich hier bei Natalya Vishnevetskaya, Prof. Christine Papadakis und Prof. Peter Müller-Buschbaum (alle TUM) für die wunderschönen und fruchtbaren Diskussionen bedanken. Weiter möchte ich mich für die Messungen und für die hilfreichen Diskussionen der Ergebnisse bei Olaf Niemeyer (NMR, MPI) und Dr. Matthias Heydenreich (NMR, UP), apl. Prof. Michael Kumke und Sören Draffehn (Fluoreszenz, UP), und Prof. Joachim Koetz und Dr. Brigitte Tiersch (cryo-SEM, UP) bedanken.

ACKNOWLEDGEMENTS

Weiterer Dank gilt allen Weggefährten, Kollegen am IAP und UP für die produktive Zusammenarbeit, aber auch Freunden und Familie für eine angenehme und unterhaltsame Zeit neben der Promotion, insbesondere Clara Pobloth und Mats Knoop für das Korrekturlesen. Mein unendlicher Dank gilt meiner Frau Patricia, meinem Sohn Jonah und meinem Hund Avi (vollwertiges Familienmitglied) für die bedingungslose Unterstützung jeglicher Art.

Scientific publications

Parts of the results in this thesis were already published:

Scientific journals

- **Viet Hildebrand**, André Laschewsky, Eric Wischerhoff, "Modulating the Solubility of Zwitterionic Poly(3-methacrylamidopropyl)ammonioalkane sulfonate)s in Water and Aqueous Salt Solutions via the Spacer Group Separating the Cationic and the Anionic Moieties", *Polym. Chem.*, **2015**, 7, 731-740.
- **Viet Hildebrand**, André Laschewsky, Daniel Zehm, "On the hydrophilicity of polyzwitterion poly(N,N-dimethyl-N-(3-(methacrylamido)propyl) ammoniopropane sulfonate) in water, deuterated water and aqueous salt solutions", *J. Biomat. Sci., Polymer Ed.*, **2014**, 25, 1602-1618.

Poster presentations

- **V. Hildebrand**, A. Laschewsky, P. Müller-Buschbaum, C. M. Papadakis, N. Vishnevetskaya, "Twofold Switchable Zwitterionic Block Copolymers as a Promising Drug Delivery System", *Symposium: Transition Metal-Catalyzed Reactions with Organoboron Compounds – Potsdam*, **2016**.
- **V. Hildebrand**, A. Laschewsky, P. Müller-Buschbaum, C. M. Papadakis, N. Vishnevetskaya, "Twofold Switchable Zwitterionic Block Copolymers, and their "Schizophrenic" Micellar Self-organization Behavior", *62. SEPAWA Congress and EDC – Fulda*, **2015**.

- **V. Hildebrand**, A. Laschewsky, P. Müller-Buschbaum, C. M. Papadakis, N. Vishnevetskaya, "Twofold Switchable Zwitterionic Block Copolymers, and their "Schizophrenic" Micellar Self-organization Behavior", *European Polymer Congress EPF – Dresden*, **2015**.
- **V. Hildebrand**, A. Laschewsky, P. Müller-Buschbaum, C. M. Papadakis, D. Zehm, "UCST Phase Behavior of Poly(sulfobetaine)s in Water, Deuterated Water, and Aqueous Salt Solutions", *Polydays – Berlin*, **2014**
- Natalya Vishnevetskaya, **Viet Hoang**, André Laschewsky, Christine M. Papadakis, "Orthogonally switchable block copolymers", *DPG – Dresden*, **2014**.

Oral presentations

- **Viet Hildebrand**, "2-fold Switchable Zwitterionic Block Copolymers, and their "Schizophrenic" Micellar Self-organization", *62. SEPAWA Congress and EDC – Fulda*, **2015**.
- Natalya Vishnevetskaya, **Viet Hildebrand**, Martine Philipp, André Laschewsky, Peter Müller-Buschbaum, Christine M. Papadakis, "Aggregation behaviour of doubly thermo-responsive poly(sulfobetaine-b-*N*-isopropylmethacrylamide) diblock copolymers", *Field Controllable Functional Polymers DPG – Berlin*, **2015**.
- **Viet Hildebrand**, "Poly(sulfobetaine)s: Synthesis, Characterization, and Upper Critical Solution Behavior", *Colloquium "Switchable Polymers" – Potsdam*, **2014**.
- **Viet Hoang**, "Water-Soluble Block Copolymers showing Double Thermoresponsivity", *Annual Meeting of the DFG Priority Program "Hydrogels" – Aachen*, **2013**.

Abstract

Zusammenfassung

Diese Arbeit befasst sich mit der Synthese und Charakterisierung von doppelt thermisch-responsiven Blockcopolymeren mit einem polaren nicht-ionischen Block (der einen LCST-Übergang in wässriger Lösung induziert) und einem zwitterionischen Block (der einen UCST-Übergang aufweisen soll), der durch Salzzusatz über einen weiten Temperaturbereich modulierbar ist. Dafür wurden geeignete zwitterionische Polymerblöcke identifiziert und hergestellt, die ein derartiges Löslichkeitsprofil aufweisen. Da bislang nur relativ wenige Poly-sulfobetaine beschrieben sind und entsprechend das wässrige Phasenverhalten nur für einzelne ausgewählte Polymere bekannt ist, wurde ein Grundverständnis von chemischer Struktur und Phasenübergangsverhalten durch eine systematische Variation des Substitutionsmusters angestrebt. Die als geeignet erkannten Sulfobetain-Monomere wurden mit dem nicht-ionischen Monomer *N*-Isopropyl-methacrylamid („**NIPMAM**“) zu Blockcopolymeren von unterschiedlicher Größe und Blocklängen zusammengefügt. Die neuen Blockcopolymere wurden anschließend bezüglich der Lage der Phasenübergänge mit Trübheitsmessungen untersucht.

Es wurden 2 Serien neuer zwitterionischer Monomere synthetisiert, deren Struktur den sehr gut untersuchten 3-((2-(methacryloyloxy)ethyl)dimethylammonio)propane-1-sulfonate („**SPE**“) und 3-((3-methacrylamidopropyl)dimethylammonio)propane-1-

sulfonate („**SPP**“) ähnlich ist. Aus den Monomeren wurden fluoreszenz-markierte Homopolymere mit unterschiedlichen Molmassen mittels der Reversiblen Additions-Fragmentierungs Kettenübertragungs (RAFT) – Polymerisation unter Verwendung eines geeigneten RAFT Reagenzes synthetisiert. Die Polysulfobetaine wurden bezüglich ihrer Löslichkeit in Wasser, in deuteriertem Wasser und in Salzlösungen untersucht. Ihr wässriges Phasenverhalten mit einem UCST-Übergang ist stark abhängig von ihrer Molmasse und von der Polymerkonzentration der untersuchten Lösung. Auffällig ist, dass die Phasenübergangstemperatur in D_2O deutlich höher liegt als in H_2O. Des Weiteren konnten die Löslichkeit und Phasen-übergangstemperatur durch Salzzusatz effektiv moduliert werden. Prinzipiell stellte sich bei den untersuchten Anionen heraus, dass das Einsalzen bzw. das Aussalzen der empirischen Hofmeister Serie folgt. Dabei hängen die individuellen Effekte sehr stark von der Konzentration und von der Art des Salzes, aber auch in nicht-trivialer Weise von der detaillierten zwitterionischen Struktur stark ab. Durch die systematische Variation der Monomerstruktur wurden interessante Tendenzen offenbar. Die Methacrylamid-basierte Polysulfobetaine besitzen eine höhere Phasenübergangstemperatur als ihre Methacrylat-basierten Analoga. Die Vergrößerung der Distanz zwischen Polymerrückrat und der zwitterionischen Gruppe von 2 auf 3 Methylengruppen führt zu einer Erniedrigung der Phasenübergangstemperatur. Polysulfobetaine mit aliphatischen Resten (Methyl-gruppen) am Ammonium-Ion haben eine höhere Phasenübergangstemperatur als ihre Analoga, in denen der Ammonium-Stickstoff Teil eines Heterozyklus ist. Als letzte Strukturvariable wurde die Distanz zwischen Kation und Anion von 3 auf 4 Methylengruppen vergrößert; diese Änderung führt zu einer massiven Erhöhung der Phasenübergangstemperatur.

Die Polysulfobetaine wurden verwendet, um mit dem nicht-ionischen Monomer **NIPMAM** wasserlösliche Blockcopolymere mittels der RAFT Polymerisation herzustellen. Diese Blockcopolymere besitzen doppelt thermisch-responsives Verhalten (mit einem UCST- und einem LCST-Übergang). Die Besonderheit einer solchen Konstellation ist, dass eine Strukturinversion der solvophoben Aggregate induziert werden kann. Daher werden solche Blockcopolymer-Assoziate auch als

„schizophrene Mizellen“ bezeichnet. Je nach der relativen Lage der beiden Phasenübergänge, die sich durch Polymerkonzentration oder durch Salzzusatz einstellen lässt, läuft die Strukturinversion über ein molekular gelöstes oder über ein unlösliches Zwischenstadium ab. Der Polysulfobetain-Block bildet bei niedriger Temperatur Aggregate, die durch den gelösten **poly(NIPMAM)**-Block in Lösung gehalten werden. Dahingegen bildet der **poly(NIPMAM)**-Block bei hoher Temperatur Aggregate, welche ihrerseits durch den gelösten Polysulfobetain-Block in Lösung gehalten werden. Somit werden „schizophrene“ Aggregate in Wasser erzeugt, die fähig sind, reversibel ihr „Inneres“ nach „Außen“ und umgekehrt zu schalten durch Nutzen eines einfachen thermischen Impulses.

Abstract

In complement to the well-established zwitterionic monomers 3-((2-(methacryloyloxy)ethyl)dimethylammonio)propane-1-sulfonate (“**SPE**”) and 3-((3-methacrylamidopropyl)dimethylammonio)propane-1-sulfonate (“**SPP**”), the closely related sulfobetaine monomers were synthesized and polymerized by reversible addition-fragmentation chain transfer (RAFT) polymerization, using a fluorophore labeled RAFT agent. The polyzwitterions of systematically varied molar mass were characterized with respect to their solubility in water, deuterated water, and aqueous salt solutions. These poly(sulfobetaine)s show thermoresponsive behavior in water, exhibiting upper critical solution temperatures (UCST). Phase transition temperatures depend notably on the molar mass and polymer concentration, and are much higher in D_2O than in H_2O. Also, the phase transition temperatures are effectively modulated by the addition of salts. The individual effects can be in parts correlated to the Hofmeister series for the anions studied. Still, they depend in a complex way on the concentration and the nature of the added electrolytes, on the one hand, and on the detailed structure of the zwitterionic side chain, on the other hand. For the polymers with the same zwitterionic side chain, it is found that methacrylamide-

based poly(sulfobetaine)s exhibit higher UCST-type transition temperatures than their methacrylate analogs. The extension of the distance between polymerizable unit and zwitterionic groups from 2 to 3 methylene units decreases the UCST-type transition temperatures. Poly(sulfobetaine)s derived from aliphatic esters show higher UCST-type transition temperatures than their analogs featuring cyclic ammonium cations. The UCST-type transition temperatures increase markedly with spacer length separating the cationic and anionic moieties from 3 to 4 methylene units. Thus, apparently small variations of their chemical structure strongly affect the phase behavior of the polyzwitterions in specific aqueous environments.

Water-soluble block copolymers were prepared from the zwitterionic monomers and the non-ionic monomer *N*-isopropylmethacrylamide ("**NIPMAM**") by the RAFT polymerization. Such block copolymers with two hydrophilic blocks exhibit twofold thermoresponsive behavior in water. The poly(sulfobetaine) block shows an UCST, whereas the **poly(NIPMAM)** block exhibits a lower critical solution temperature (LCST). This constellation induces a structure inversion of the solvophobic aggregate, called "schizophrenic micelle". Depending on the relative positions of the two different phase transitions, the block copolymer passes through a molecularly dissolved or an insoluble intermediate regime, which can be modulated by the polymer concentration or by the addition of salt. Whereas, at low temperature, the poly(sulfobetaine) block forms polar aggregates that are kept in solution by the **poly(NIPMAM)** block, at high temperature, the **poly(NIPMAM)** block forms hydrophobic aggregates that are kept in solution by the poly(sulfobetaine) block. Thus, aggregates can be prepared in water, which switch reversibly their "inside" to the "outside", and vice versa.

Abbreviations and variables

A

A	absorbance
AIBN	azobisisobutyronitrile
APT	attached proton test
ATR	attenuated total reflection
ATRP	atom transfer radical polymerization

B

BHT	2,6-di-tert-butyl-4-methylphenol

C

c	concentration
$c_{CTA,0}$	initial molar concentration of the RAFT agent
CHPSNa	3-chloro-2-hydroxy-1-propane sulfonic acid sodium-salt
$c_{Mon,0}$	initial molar concentration of the monomer
COSY	correlation Spectra
CTA	chain transfer agent
CTA-#	chain transfer agent-#

D

DCC	N,N′-dicyclohexylcarbodiimide
DLS	dynamic light scattering
DMAP	4-(dimethylamino)pyridine
DMAPMA	N-(3-(dimethylamino)propyl) methacrylamide
DP_n	number average degree of polymerization
DSC	differential scanning calorimetry

E

ESI	electrospray ionization

F

FT-IR	Fourier transform-infrared

G

GPC	gel permeation chromatography

H

HMQC	heteronuclear multiple quantum coherence spectra
HR-MS	high resolution mass spectra

L

LCST	lower critical solution temperature

M

m	mass
M-#	monomer-#
M_{CRU}	molar mass of the constitutional repeat unit
m-CTA	macro-chain transfer agent
M_{CTA}	molar mass of the RAFT agent
MEHQ	4-methoxyphenol
MMA	methyl methacrylate
M_n^{theo}	theoretical number average molar mass
M_n^{UV}	number average molar mass calculated from UV-data
Mon	monomer

N

NMP	nitroxide-mediated polymerization
NMR	nuclear magnetic resonance

ABBREVIATIONS AND VARIABLES

P

PBS	phosphate buffered saline
pK_a	acid dissociation constant

R

RAFT	reversible addition-fragmentation chain transfer
RDRP	reversible deactivation radical polymerization

S

S_NAr	nucleophilic aromatic substitution
SPE	3-((2-(methacryloyloxy)ethyl)di-methylammonio)propane-1-sulfonate
SPP	3-((3-methacrylamidopropyl)di-methylammonio)propane-1-sulfonate

T

T	temperature
TFE	trifluoroethanol
TGA	thermogravimetric analysis
TLC	thin layer chromatography

U

UCST	upper critical solution temperature
UV-vis	ultraviolet-visible

V

V	volume
V-501	4,4´-azobis(4- cyanopentanoic acid)
ΔG_{mix}	change of Gibbs free energy of mixing
ΔH_{mix}	change in enthalpy
ΔS_{mix}	change in entropy
Đ	dispersity
ε	extinction coefficients
λ_{max}	maximum absorbance wavelength
λ_{PL}	maximum emission wavelength
θ	scattering angle
ν	wavenumber

Contents

CONTENTS

1 Introduction

In many cases, self-organization of stimuli-responsive polymers leads to manifold mesoscopic superstructures, especially in aqueous solutions. In this respect, water allows a complex and efficient cooperation of electrostatic, hydrophobic, and hydrogen bond interactions.[1] Particularly suitable for such responsive systems are block copolymers by virtue of their molecular structure which is able to outbalance miscellaneous interactions. By establishing the so-called controlled radical polymerization*, molecular designs and synthetic options have been tremendously improved. Thus, investigation and understanding of stimuli-responsive systems by novel model systems have been initiated. In the beginning, mainly thermoresponsive systems showing one phase transition in aqueous media were in the focus, typically exhibiting a lower critical solution temperature (LCST), but rarely showing an upper critical solution temperature (UCST).[2, 3] Many research groups have been interested in simple "on-off"-systems in which the polymers are dissolved before forming aggregates (**Figure 1.1a**). Alternatively, block copolymers of one permanently insoluble block have been investigated frequently as "on-off"-systems (**Figure 1.1b**). More complex systems passing through two[2] or three[4-6] thermal transitions have been much less explored. Besides, twofold switchable block copolymers exhibiting two different LCST-type transitions are known, in which the hydrophilic-hydrophobic balance decreases stepwise and leads to transitions from molecularly dispersed via superstructure 1 to superstructure 2 (**Figure 1.1c**). Also, block

* According to the International Union of Pure and Applied Chemistry (IUPAC): reversible deactivation radical polymerization (RDRP)

copolymers showing one LCST-type and one UCST-type transition have occasionally been reported (**Figure 1.1d-e**). This constellation induces a structure inversion of the solvophobic aggregate, called "schizophrenic micelles".[7] Depending on the relative positions of the two different phase transitions, the block copolymer passes through a molecularly dissolved or an insoluble intermediate regime.[7-23]

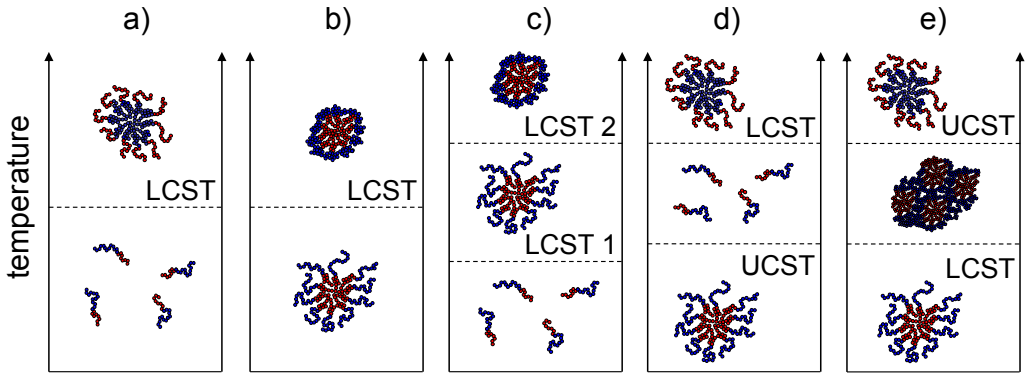

Figure 1.1. Schematic representation of possible thermoresponsive systems. Systems with 1 transition: a) molecular – collapse via LCST, b) superstructure 1 – superstructure 2 via LCST. Systems with 2 transitions: c) molecular – superstructure 1 – superstructure 2 via LCST, d) superstructure 1 – molecular – inverse superstructure 3 via consecutive UCST and LCST, e) superstructure 1 – superstructure 4 (precipitate) – inverse superstructure 3 via consecutive LCST and UCST.

Interestingly, an LCST-type transition is often found in water for non-ionic polymers. In contrast, the typical UCST-type transition for polymers in solution is rarely found in water.[24] The rare reports of polymers showing UCST-type transition in water are predominantly about poly(sulfobetaine)s, which display a permanently zwitterionic group.[25, 26] Poly(sulfobetaine)s are also known for their sensitivity to specific electrolytes[27-29], which improve the water-solubility with increasing electrolyte concentration.[30] The modulation of the transition temperatures of block copolymers possessing LCST- and UCST-type transition via a molecularly dissolved intermediate regime have been reported already, by utilizing the thermoresponsiveness and the electrolyte-sensitivity of poly(sulfobetaine)s.[31, 32] However, block copolymers showing twofold responsive behavior, where the relative position of LCST- and UCST-type transitions is inverted by the addition of electrolytes, have

not been developed yet (see **chapter 1.4**, **Figure 1.20b**). This kind of scenario will enable an orthogonal "switching" between all possible superstructures including their inversion.

1.1 Thermoresponsive polymers

The development of stimuli-responsive polymers is of great interest, e.g. as micellar carriers, switchable surfaces, or controlled release capsules.[1, 33-35] Such stimuli-responsive polymers undergo abrupt (nonlinear) physical changes in response to an external stimulus. Moreover, by suppressing the stimulus or applying a second 'reverse' stimulus, the induced property changes should be reversible.[1, 34, 36, 37] Responses of polymers on potential stimuli are illustrated in **Figure 1.2**.

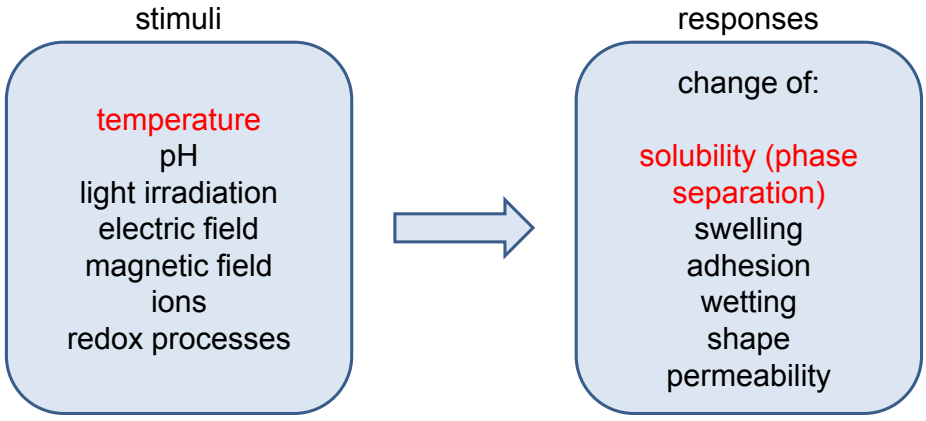

Figure 1.2. Selected responses of polymers on various potential stimuli.

Typical stimuli are temperature change, variation of pH, light, electric and magnetic fields, ions, or redox processes.[38-40] The change of physical property occurs, for instance, as phase separation, shape change, or swelling.[22, 38, 39, 41, 42] Soluble polymers that respond to temperature changes to generate property responses have attracted much interest in tissue engineering, bioseparations, and biosensors.[43]

Fundamental for this thesis is stimuli-response-behavior, due to temperature change induced phase separation in aqueous solution.

The thermodynamic criterion for spontaneous miscibility is the change of Gibbs free energy of mixing ΔG_{mix} (**equation 1.1**), which has to be negative ($\Delta G_{mix} < 0$).

$$\Delta G_{mix} = \Delta H_{mix} - T \cdot \Delta S_{mix} \qquad (\mathbf{1.1})$$

ΔH_{mix} = change in enthalpy
T = temperature
ΔS_{mix} = change in entropy

At a particular temperature, thermoresponsive polymers exhibit a transition from a single-phase regime into a two-phase regime. Depending on the direction of the phase transition, there are two types of thermoresponsive behavior[44]: polymers showing a lower critical solution temperature (LCST) (**Figure 1.3a**) precipitate upon heating, whereas polymers showing an upper critical solution temperature (UCST) (**Figure 1.3b**) dissolve upon heating.[45-47] Respectively, LCST and UCST are defined as the lowest or the highest temperature of the binodal curves. Both types of transitions are easily followed by turbidimetry. For instance, for polymer solution exhibiting an LCST, heating and cooling curves are recorded at a given concentration to provide the so-called cloud and clearing points, respectively (vice-versa for polymers showing an UCST). An inherent hysteresis between cloud and clearing points may occur due to the metastable regime, which is defined as the regime between the binodal and the spinodal curves of an isobaric phase diagram.

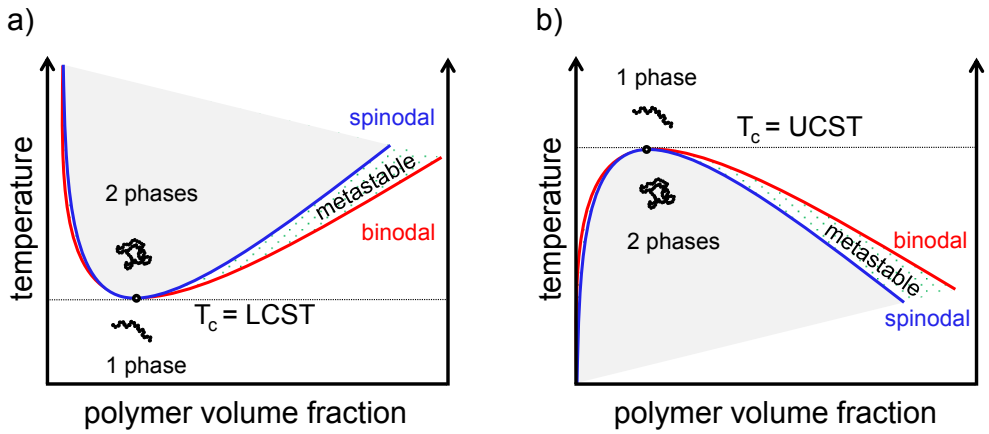

Figure 1.3. Schematic illustration of isobaric phase diagrams for polymer solutions showing a) lower critical solution temperature (LCST) and b) upper critical solution temperature (UCST). LCST and UCST are defined as the lowest or the highest temperature in the binodal curves, respectively.

In aqueous solution, polymers showing an LCST-type transition are by far the most studied ones compared to polymers exhibiting an UCST-type transition. Virtually, all uncharged water-soluble macromolecules investigated seem to show an LCST-type transition in water, although sometimes above 100 °C under high pressure.[1, 36, 48-50] In this case, the repeat units of such polymers include hydrophobic and hydrophilic segments. It is generally assumed that the delicate balance between hydrophilic segment-water interactions and hydrophobic segment-segment interactions is crucial for their transition temperature. At low temperature (T < LCST), the hydrophilic segments form hydrogen bonds with water whereas the hydrophobic segments are surrounded by a well-organized hydration shell (**Figure 1.4**). From the thermodynamic point of view, the hydrogen bond interactions lead to strong negative ΔH_{mix} resulting in negative ΔG_{mix}, although ΔS_{mix} (negative value) is unfavorable due to the high organization of water molecules. For the approximation that the enthalpy and the entropy are temperature independent constants[1], elevating the temperature, the $-T \cdot \Delta S_{mix}$ term (positive value) prevails after reaching the critical temperature: ΔG_{mix} becomes positive, polymer and water demix. Additional to this explanation, the temperature dependence of ΔH_{mix} is also to be considered.[51] At low temperatures, miscibility is driven by a strong negative enthalpy, originating from hydrogen bonds between water and hydrophilic segments. However, ΔS_{mix} is

unfavorable for miscibility due to the high organization of water molecules around the hydrophilic as well as hydrophobic segments. With increasing temperature, release of these highly ordered water molecules into the bulk phase is in general entropically favored over miscibility. Also, water molecules become more mobile, resulting in a weakening of the hydrogen bonds between water and the hydrophilic segments. Meanwhile polymer-polymer interactions become more favorable due to the increasing dehydration of the hydrophobic segments. These processes are closely related to the phenomenon known as 'hydrophobic effect'[52]. Thus, ΔH_{mix} becomes unfavorable for miscibility, resulting in positive ΔG_{mix} which forces the system to undergo phase separation.[1, 2, 36, 53]

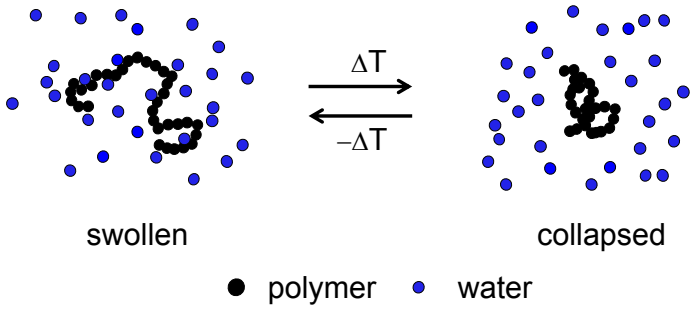

Figure 1.4. Schematic illustration for polymers showing LCST-type phase transition behavior. ● Polymer chain is dissolved in ● water, until above a certain temperature, the polymer chain collapses.

Examples of polymers showing an LCST-type transition are *N*-substituted poly(acrylamide)s and poly(methacrylamide)s, poly(vinylether), poly(oxazoline)s, poly(peptide)s, poly(glycine)s, poly(oligo ethylene glycol (meth)acrylate)s, poly(*N*-vinylamide)s, or poly(vinylphosphate)s.[1, 11, 13, 54-64] A selection of structures of well-investigated polymer exhibiting LCST-type transition is shown in **Figure 1.5**, of which poly(*N*-isopropylacrylamide) is by far the most studied one. Poly(*N*-isopropylacrylamide) displays a sharp phase transition, a very small hysteresis, and constant phase transition temperature (32 °C) over a broad polymer concentration range.[1, 48, 50] This benefits the wide use in different fields of application.[8, 65] Mostly, modifying polymers showing LCST-type transition with additional hydrophilic segments will increase polymer solubility and thus the LCST, whereas

modification with additional hydrophobic segments will decrease the LCST. However, the comparison of the LCST values of poly(*N*-isopropylacrylamide) (32 °C) and poly(*N*-isopropylmethacrylamide) (42 °C) and many analogous pairs exemplifies that the general prediction of phase transition temperatures via an increment system is impossible.[66, 67]

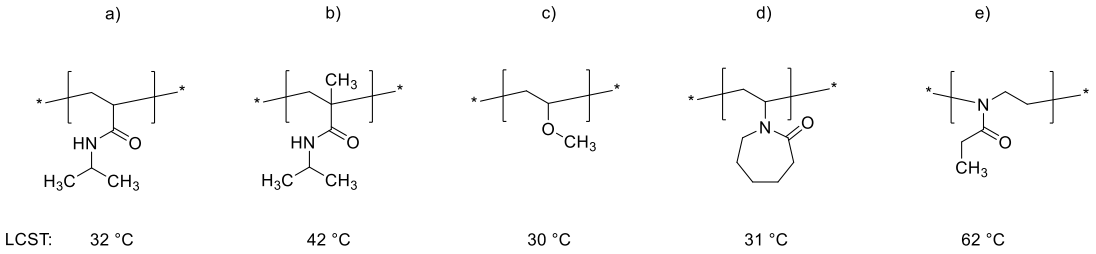

Figure 1.5. Chemical structures and LCST values of some well-investigated thermo-responsive polymers in aqueous solution. a) Poly(*N*-isopropylacrylamide), b) poly(*N*-isopropylmethacrylamide), c) poly(methylvinylether), d) poly(*N*-vinyl-ε-caprolactam), and e) poly(2-ethyl-2-oxazoline).[1, 41]

The phase behavior of polymers showing UCST-type transition implies that strong polymer-polymer interactions are formed at low temperatures, which are unfavorable for miscibility (positive ΔH_{mix}). Yet, these interactions are weak enough to be interrupted by increasing the temperature.[44, 48, 50] Thus, at high temperature, the resulting gain in entropy leads to an increasing by positive ΔS_{mix}, which results finally in a negative ΔG_{mix} value. In other words, the spontaneous miscibility is driven by the entropy.[44, 48, 50]

Generally, polymers exhibiting UCST-type transition in aqueous solution have been much less studied compared to polymers showing LCST-type transition.[24] The UCST behavior is more commonly observed in organic solvents or in organic/water mixtures.[44] Classical examples for organic polymer solutions displaying UCST are poly(styrene) in cyclohexane[68], poly(ethylene) in diphenylether[69], and poly(methyl methacrylate) in acetonitrile[70]. By now, current research focuses on water-based applications e.g. drug delivery systems, tissue engineering, bioseparation, etc. Although an UCST behavior is rather atypical in pure water[44], few biorelevant examples of applications have been published.[12, 71-75] The industrially relevant poly-(hydroxyethylmethacrylate) (**Figure 1.6a**) shows UCST behavior above 100 °C.[76-79] However, there are also polymers showing UCST-type transition between 0 °C and

100 °C. Exemplarily, non-ionic polymers exhibiting UCST behavior are poly(*N*-acryloyl glycinamide) with pronounced hysteresis[80], ureido-functionalized polymers[81], and also copolymers from acrylamide and acrylonitrile[82]. However, the phase separation of poly(*N*-acryloyl glycinamide) (**Figure 1.6b**) can be effectively suppressed by traces of ionic groups. Polymers relying on hydrogen bonds between polymer moieties and water are very sensitive to ionic contaminations.[80] Interestingly, poly(acrylic acid) (**Figure 1.6c**) exhibits an UCST-type transition only at high ionic strength.[83]

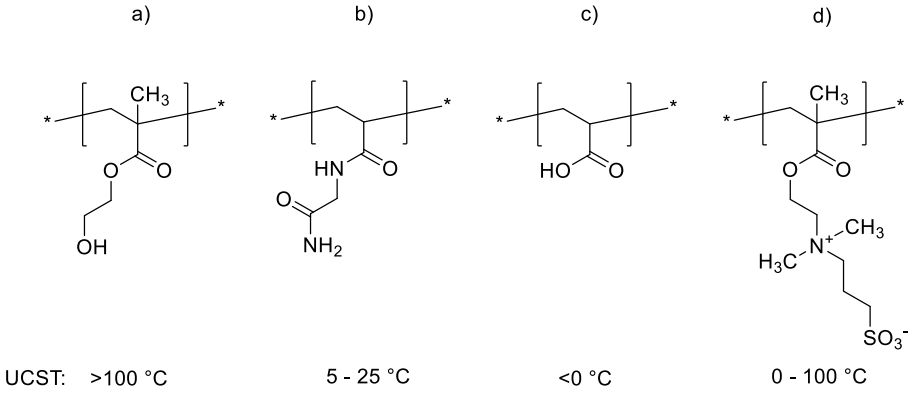

Figure 1.6. Chemical structures and UCST values of thermoresponsive polymers in aqueous solution. a) Poly(hydroxylethylmethacrylate), b) poly(*N*-acrylol glycinamide), c) poly(acrylic acid), and d) "**SPE**" 3-((2-(methacryloyloxy)ethyl)dimethylammonio) propane-1-sulfonate.

Another class of polymers showing UCST-type behavior in aqueous solution comprises ionic polymers, especially polyelectrolytes and zwitterionic polymers. In particular, the most studied polymers showing UCST-type transition are sulfobetaine-based (meth)acrylic polymers (**Figure 1.6d**).[26] These zwitterionic polymers can be also obtained in a controlled manner, e.g. via atom transfer radical polymerization (ATRP) or reversible addition-fragmentation chain transfer (RAFT) polymerization.[26, 40, 84-86] Thus, it is possible to obtain tailor-made polymers for model investigations.[8] The UCST-type behavior of such poly(sulfobetaine)s depends markedly on their molar mass.[8, 25, 87] Moreover, poly(sulfobetaine)s include ionic groups in their polymer side chains and are consequently sensitive to ion-ion interactions.[28, 30] Their phase transition temperature can decrease or increase

depending on the type and concentration of added ions.[88, 89] The challenge is to exploit such a behavior in responsive systems containing poly(sulfobetaine)s.

1.2 Polyzwitterions

1.2.1 Synthesis of sulfobetaines

Zwitterions are defined as electrically neutral molecules which carry an equal number of positively and negatively charged moieties. These charges are linked through covalent bonds, and are typically not electronically conjugated with each other. They are dipolar species with high dipole moments where cation and anion are separate units.[26, 90]

"Betaine" is originally the name for trimethylglycine (**Figure 1.7a**) because of its natural occurrence in the common turnip, beta vulgaris. Today, the IUPAC definition of "betaines" comprises all zwitterionic compounds with a positively charged functional group (e.g. quaternary ammonium or phosphonium cation) and with a negatively charged functional group (e.g. carboxylate, phosphate, or sulfonate anion, respectively (**Figure 1.7**)) thereby excluding ylides.[25, 86] Within a particular pH range, by means of reaching the isoelectric point, betaines are electrically neutral. Consequently, betaines do neither migrate in an electrical field nor bind to an ion exchanger.[90-92] Amidst the three main families of zwitterions (stable zwitterionic inner salts), namely carboxybetaines, phosphobetaines, and sulfobetaines, the latter are the chemically most inert.[26, 86]

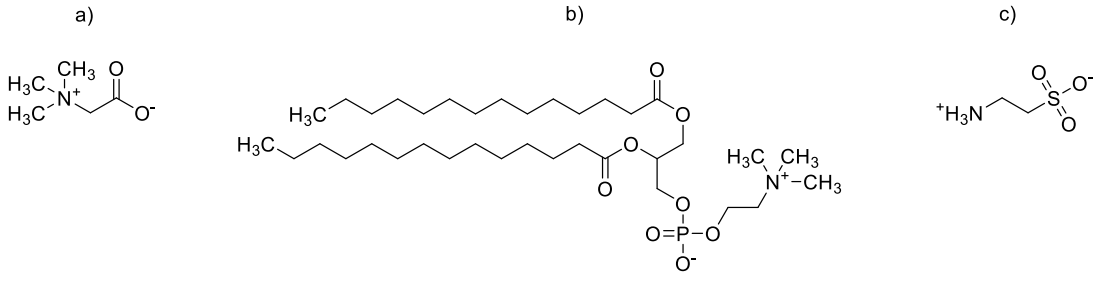

Figure 1.7. Examples for natural zwitterionic compounds. a) Trimethylglycine (carboxybetaine), b) phospholipid 1,2-dimyristoyl-*sn*-glycero-3-phosphatidylcholine (phosphobetaine), c) taurine (sulfobetaine) at pH ≤ 5.12.

The synthesis of sulfobetaines can be conducted in a single-step approach. This is performed by a ring opening alkylation of a tertiary amine with a sultone (e.g. 1,3-propanesultone or 1,4-butane sultone), resulting in quaternary amine and sulfonate moieties (**Figure 1.8a**).[93-96] This procedure ensures a salt-free synthesis of sulfobetaines.[28] Hence, the influence of salt admixtures on the UCST behavior of the poly(sulfobetaine)s produced is avoided. Another approach uses the heteroanalogous Michael addition of vinylsulfonylchloride, whereby hydrochloric acid is obtained as byproduct (**Figure 1.8b**).[97]

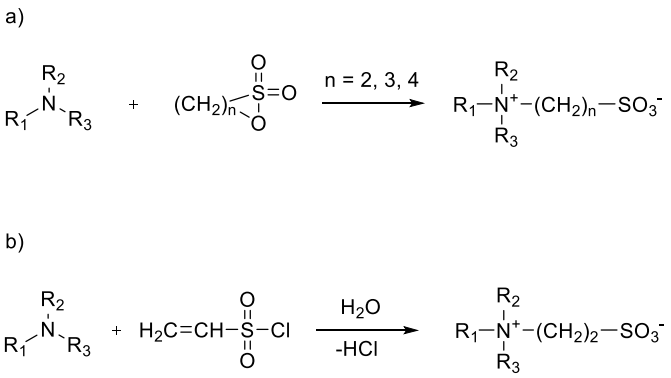

Figure 1.8. Synthetic routes to functional sulfobetaines utilizing tertiary amine and a) sultone, b) vinylsulfonylchloride.

Furthermore, two-step approaches are also known. Thereby, a tertiary amine is reacted with epichlorohydrin and sodium hydrogen sulfite. The formed 3-chloro-2-hydroxy-1-propane sulfonic acid sodium-salt reacts to a "hydroxypropane-sulfobetaine" via quaternization (**Figure 1.9**). A disadvantage of this reaction is that

sodium chloride has to be removed as phase transition temperature of produced polymers are strongly affected otherwise.[98]

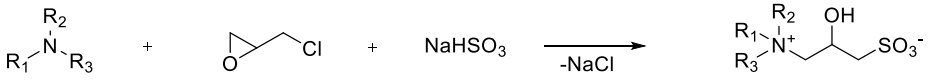

Figure 1.9. Two-step synthetic route to functional sulfobetaines with sodium chloride as byproduct.

Additionally, Ohme et al. described another synthetic approach at which a tertiary amine reacts with an allyl chloride leading to an intermediate quaternary allyl ammonium-salt, which reacts further to a sulfobetaine via sulfite addition by a radical mechanism.[91, 99, 100] Another possible synthetic route is to start with the sulfite addition and to continue with the quaternization subsequently.[99] Synthetic sulfobetaines show for instance good skin tolerance, compatibility with common surfactants, and low toxicity and are therefore attractive for the cosmetic industry, especially, as additive in perfumery and home care products.[101-105]

1.2.2 Poly(sulfobetaine)s

From the early 2000s on, poly(sulfobetaine)s have received increasing attention as materials to confer good biotolerance, extremely low friction or ultralow-fouling behavior to surfaces.[106-109] A tightly bound hydration layer around each zwitterionic group has been proposed to be the reason for effectively suppressing nonspecific protein adsorption and improving bio- and hemocompatibility (antibiofouling properties).[109, 110] Therefore, poly(sulfobetaine)s have been used for modification of ultrafiltration membranes[110], for blood-contacting devices[111], and in gene and drug delivery[109].

The name poly(sulfobetaine) refers to the zwitterionic polymers possessing quaternary ammonium and sulfonate groups on the same monomer unit.[26, 86] Copolymers of ammonium and sulfonate monomers are not called

poly(sulfobetaine)s although, when incorporated in stoichiometric amounts showing often similar properties.[112-115] The chemical structure of poly(sulfobetaine)s can be subsumed in several groups, where the different polymers bear an alkylsulfonate group. Most widespread are quaternary esters or amides of (meth)acrylic acid, poly(vinylimidazolium) or poly(vinylpyridinium) compounds, quaternary poly(pyrrolidinium) compounds, and zwitterionic ionenes (**Figure 1.10**).[25, 26, 92] Basically, poly(sulfobetaine)s are prepared via polymerization of respective monomers or via sulfite addition of polymeric tertiary amine polymer-analogously, applying synthetic the approaches described above.[25] Sulfobetaines of the polymers shown in **Figure 1.10a-e** were prepared by the usual sultone addition procedure.[92]

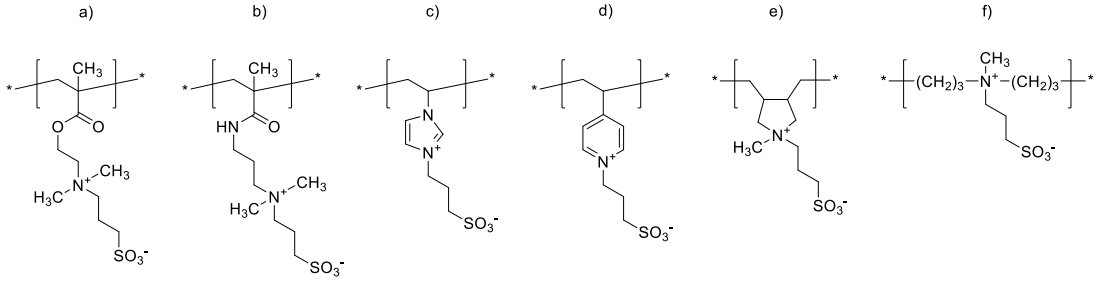

Figure 1.10. Examples of chemical structures of zwitterionic poly(sulfobetaine)s. a) Quaternary ammonium ester of methacrylic acid, b) quaternary ammonium amide of methacrylic acid, c) poly(vinylimidazolium), d) poly(vinylpyridinium), e) quaternary poly(pyrrolidinium), f) zwitterionic ionene.[25, 26, 92, 97, 116, 117]

Such poly(sulfobetaine)s (**Figure 1.10a-d**) are most conveniently prepared via free radical polymerization.[25, 29, 86, 90] However, only few sulfobetaine monomers suitable to free radical polymerization are commercially available at present. The most popular sulfobetaines are 3-((2-(methacryloyloxy)ethyl)dimethylammonio) propane-1-sulfonate ("**SPE**", **Figure 1.10a**) and 3-((3-methacrylamidopropyl) dimethylammonio)propane-1-sulfonate ("**SPP**", **Figure 1.10b**), which provides the best combination of polymerizability, hydrophilicity and resistance to hydrolysis.[29] The polymer featuring the pyrrolidinium ring was synthesized by cyclo-polymerization of the corresponding non-commercial diallylmethylammonium sulfobetaine (**Figure 1.10e**).[118] Different to other examples, the zwitterionic ionene (**Figure 1.10f**) was prepared via post-functionalization of a polymeric tertiary amine precursor using the classical sultone addition procedure.[116, 117]

The extraordinary behavior of poly(sulfobetaine)s in aqueous solution relies on the low acid dissociation constant (pK_a) value of sulfonic acid (pK_a ≈ -2).[119] Thus, poly(sulfobetaine)s exhibit a zwitterionic character over a broad pH window (pH ≈ 2 – 14) resulting in a broad window of electrically neutral behavior.[90, 101] In order to neutralize the charges, the ammonium cation and the sulfonate anion form an inner salt. By virtue of the balance of attractive or repulsive interactions between the numerous charged groups themselves and with water, many poly(sulfobetaine)s display UCST-type transition in aqueous media (**Figure 1.11**).[8, 15, 120] Moreover, poly(sulfobetaine)s are generally insoluble in aprotic solvents, such as chloroform, acetone, acetonitrile, dimethyl sulfoxide or dimethylformamide, and often also in many protic solvents, such as methanol and ethanol. They dissolve however mostly in solvents such as trifluoroethanol (TFE), hexafluoroisopropanol, or aqueous salt solutions.[15, 95, 121]

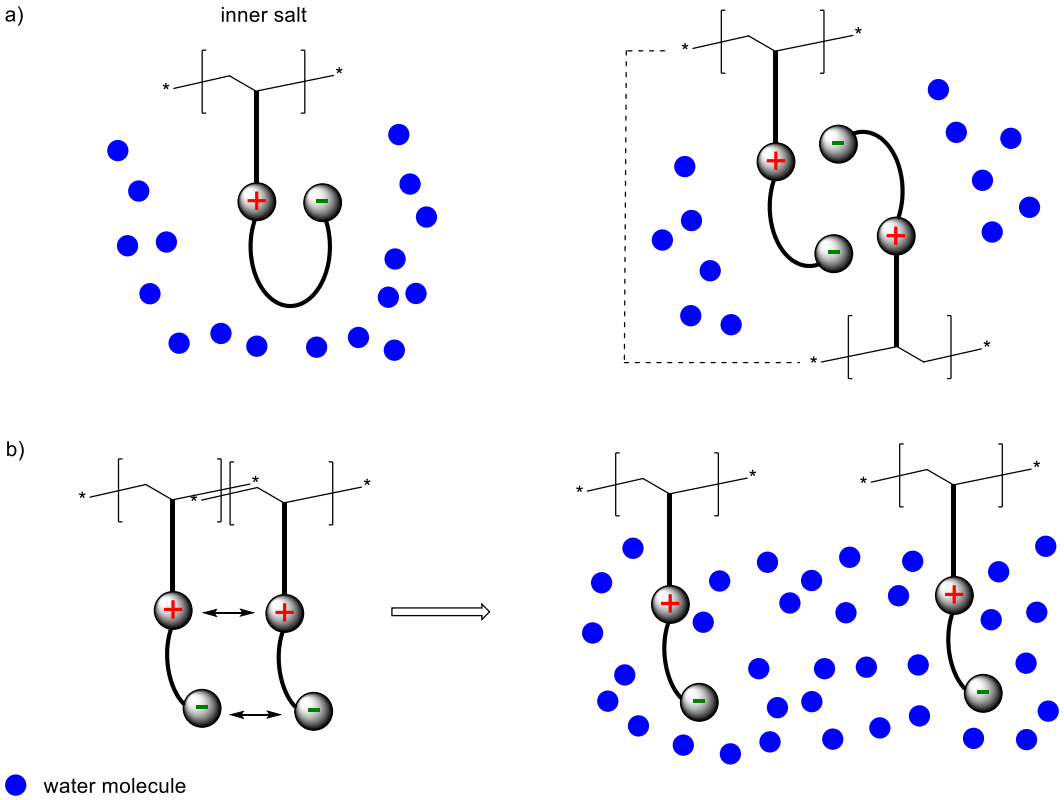

Figure 1.11. Attractive and repulsive interactions in zwitterionic polymers between charged groups themselves and with water. a) Attractive intra- and intermolecular polymer-polymer interactions and repulsive water-polymer interactions, b) repulsive intermolecular polymer-polymer interactions and attractive water-polymer interactions. ● Water molecules forms always attractive water-water interactions.

In aqueous salt solutions, the balance of all non-covalent attractive and repulsive interactions involving added ions, water molecules, and polymer segments controls the solubility behavior of poly(sulfobetaine)s, showing so-called "antipolyelectrolyte effect"[109]. The minimal salt concentration needed for dissolution of the poly(sulfobetaine) is called the critical salt concentration.[119, 122] In detail, the water-solubility of poly(sulfobetaine)s is strongly affected by the amount and the precise nature of added salt, in particular by the nature of the anion. In general effect of the cations on the critical salt concentration is rather small compared with the effect of the anions.[88, 89] Primarily, the effect of the anion on the critical salt concentration follows the empirical Hofmeister series (lyotropic series) (**Figure 1.12**).[89, 119, 121] Thereby, chaotropic anions lead to a "salting-in" effect (dissolution) whereas kosmotropic anions lead to a "salting-out" effect (precipitation).[88, 89, 119] With increasing chaotropic character, less amount of added salt is needed to obtain solubility (equal to decreasing the critical salt concentration). Among several theories, a very useful rule, the "law of matching water affinities" was formulated by Collins.[123, 124] In this concept, chaotropic ions are classified as large ions of low charge density (e.g. ClO_4^-, I^-, SCN^-, Br^-) which are considered to disorder the water structure (interfering with the water structure). While kosmotropic ions are characterized as small ions of high charge density (e.g. F^-) which are considered to support the order of water.[119, 123] Within this order, the large polymer random coil acts as a failure spot. In order to minimize the failure spots, the system pushes the coil to a small globule, which induces salting-out of the polymer. In contrast, chaotropic ions work oppositely and induce salting-in of the polymer due to disordering the water structure. The weakness of this concept is that ions are only considered as different sized point charges.[124] Still, it is unknown which interactions play the more dominant role, or whether it is a combination of all interactions.[123, 125] Therefore, the "surface charge layer" theory is rather focused on polymer-ion interactions. This concept claims that chaotropic ions enhance or generate a surface charge layer, and therefore improving the solubility and vice versa for kosmotropic ions.[88, 89, 119, 123-125]

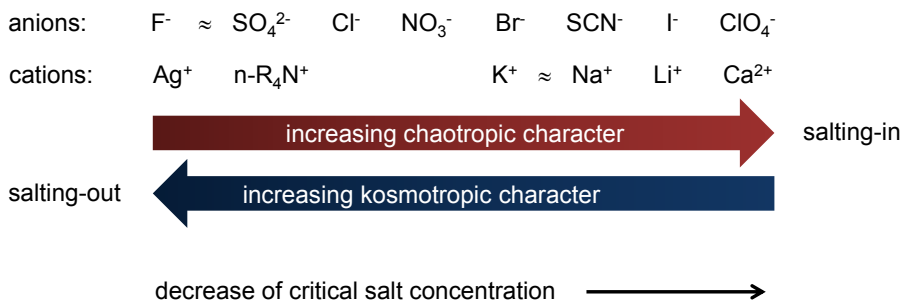

Figure 1.12. Hofmeister series of anions and cations for poly(vinyl sulfobetaine) explored by Salamone[122, 126] et al. From left to right: increasing chaotropic character (with anions: salting-in, increase of water-solubility). From right to left: increasing kosmotropic character (with anions: salting-out, decrease of water-solubility).[119] R = H, alkyl.

The improvement of water-solubility by addition of salts has been explored by Salamone et al., Monroy Soto et al., and Wielema et al. for different poly(sulfobetaine) series (**Figure 1.10a-d** and derivatives).[119, 121, 126] An increase in "side-binding" ability of the anion followed by "atmospheric-binding" at higher salt concentration has been proposed to be the reason for the improvement of the water-solubility (**Figure 1.13**).[119, 126] The binding process in "side-binding" is solely a consequence of coulombic interactions of the counterions with specific sites of the polyions. In this case, the profit of the coulombic interactions between charged side groups and counterions is higher than the energy expended in the dehydration of the counterions (**Figure 1.13a**). Whereas, "atmospheric-binding" describes the binding of (almost fully hydrated) counterions by the large electrostatic field which surrounds the polymer; binding of hydrated counterions is a long-range interaction and will occur if the charged site groups are large and the charges are delocalized. In this case, the profit of the coulombic interactions through decreasing the distance between ionic centers is smaller compared to the energy required to dehydrate the counterions (**Figure 1.13b**).[119] Furthermore, the addition of salts interferes with the intra- and intermolecular interactions of the poly(sulfobetaine)s with themselves and therefore, the critical salt concentration could reflect the strength of the interactions of poly(sulfobetaine)s with themselves.[122]

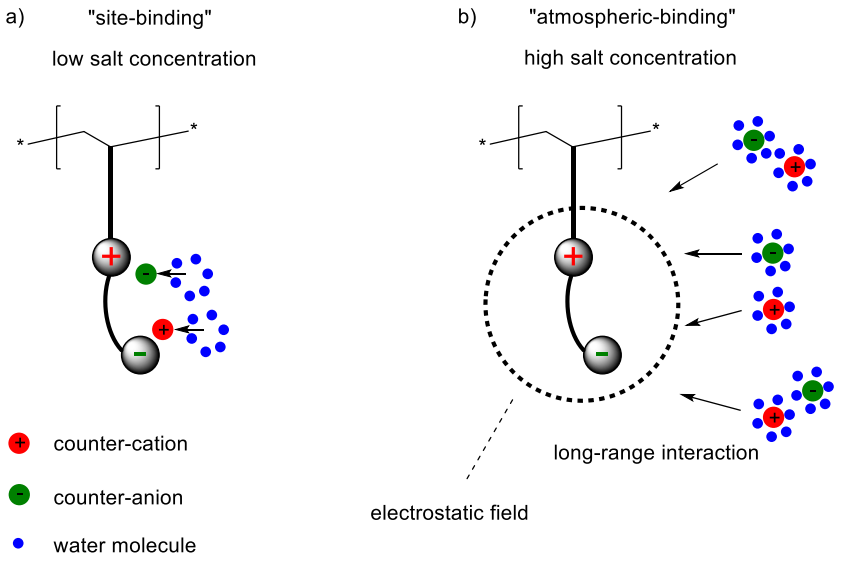

Figure 1.13. Schematic illustration of "side-binding" at low salt concentration and "atmospheric-binding" at high salt concentration proposed by Salamone et al.[126] Symbols represent ● counter-cation, ● counter-anion, and ● water molecule.

Interestingly, the attractive interactions of poly(sulfobetaine)s with themselves depend on their chemical structure. Hence, the critical salt concentration also depends on the chemical structure of poly(sulfobetaine)s. Thus, the critical salt concentration can be modulated by variation of the spacer group separating the cationic and anionic moieties, the distance between the polymer backbone and the zwitterionic group, the type of substituents on the ammonium moiety, and the incorporation of an aromatic ring into the ammonium moiety (**Figure 1.14**).[96, 97, 119]

The influence of the number of methylene units (n = 2, 3) between the opposite charges on the critical salt concentration was examined for poly(vinylimidazolium sulfobetaine)s and poly(vinylpyridinium sulfobetaine)s by Wielema et al.[119] They reported, that poly(sulfobetaine)s with n = 3 methylene units (**Figure 1.14a**) between the opposite charges show a higher critical salt concentration. In this case, the intramolecular interactions can be represented by a 6-membered ring interaction which leads to a very close proximity of the sulfonate to the quaternary nitrogen. Therefore strong attractive coulombic interactions are formed. Whereas, poly(sulfobetaine)s with n = 2 methylene units between the opposite charges exhibit a much smaller critical salt concentration. For n = 2, the intramolecular interactions

can be represented by a 5-membered ring interaction. Thus, the decrease in the distance between the sulfonate and the quaternary nitrogen and the increase in ring strain result in weaker coulombic interactions.[119] In contrast, increasing the distance between the polymer backbone and the zwitterionic group, e.g. from 2 to 11 methylene units (**Figure 1.14b**), leads to a decrease in critical salt concentration which has not been explained yet.[96] In the case of modification of the substituents on the ammonium moiety, Monroy Soto et al. reported that the critical salt concentration of polycation substituted by ethyl groups is lower than with methyl groups (**Figure 1.14c**).[94, 121] Additionally, aliphatic poly(sulfobetaine)s require a much smaller critical salt concentration than aromatic poly(sulfobetaine)s.[119, 122, 126, 127] These two observations have not been explained so far. However, Wielema et al. compared the influence to the integration of an aromatic ring to the ammonium moiety on the critical salt concentration for poly(vinylimidazolium sulfobetaine)s and poly(vinylpyridinium sulfobetaine)s (**Figure 1.14d**). They presumed that in the pyridinium ring, the positive charge is located on one nitrogen whereas in the imidazolium ring the positive charge is delocalized over both nitrogens, resulting in a weaker coulombic interaction. This difference in charge density was thought to lead to a lower critical salt concentration for poly(vinylimidazolium sulfobetaine)s.[119] However, the positive charge is not localized on the nitrogen, but rather delocalized over the neighboring carbons and hydrogens. This reveals the weakness of the explanation attempt. Thus, the dependence of the critical salt concentration on the chemical structure of the zwitterionic side chain seems to be more complex and cannot be easily predicted.

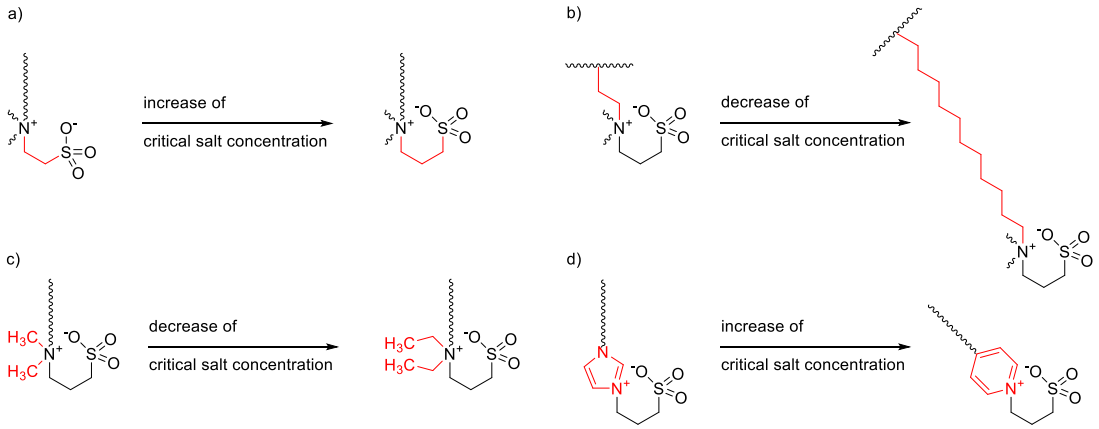

Figure 1.14. Dependence of critical salt concentration on chemical structure of the zwitterionic side chain. Variation of a) spacer group separating the cationic and anionic moieties, b) distance between the polymer backbone and the zwitterionic group, c) and d) type of substituents on the ammonium moiety.

1.3 Reversible addition-fragmentation chain transfer (RAFT) polymerization

The radical polymerization technique tolerates a high variety of nonpolar and polar monomers and shows a high tolerance against small amounts of impurities and water compared to living ionic polymerization. However, the conventional free radical polymerization technique is unsuitable to design complex polymer architectures like block copolymers, star, comb, and brush polymers. Moreover, control over molar mass and molar mass distribution is not feasible. Polymers of low and high molar masses are formed, which is indicated by a high dispersity (Đ). These features result from the polymerization mechanism, in which all polymer chains are not initiated simultaneously and inherent bimolecular chain termination leads to irreversible deactivation.[128] Therefore, in the past decades, much effort has been paid to adapt the advantageous characteristics of living ionic polymerization, known for low Đ and good accessibility of complex polymer architectures, to free radical polymerization. The developed and new established methods are described as reversible deactivation

radical polymerization (RDRP) (**Figure 1.15**), in which the active growing chain is reversibly deactivated by a specific agent.[129]

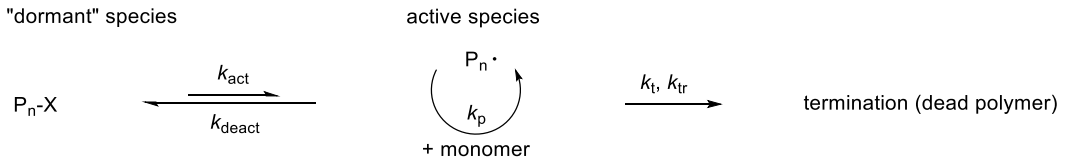

Figure 1.15. Schematic representation of the reversible deactivation radical polymerization methods. P_n-X is the deactivated chain by a specific agent, P_n· is the active growing chain, *k* is the reaction rate constant for activation (act), deactivation (deact), termination (t), and transfer (tr).

The most widespread RDRP methods are nitroxide-mediated polymerization (NMP), atom transfer radical polymerization (ATRP), and reversible addition-fragmentation chain transfer (RAFT) polymerization.[85, 130] General characteristics for those RDRP methods are:[131, 132]

- large excess of controlling agent over initiator
- fast exchange of "dormant" and active species
- fast and quantitative initiation
- linear correlation of molar mass and monomer conversion
- Đ decreases with increasing monomer conversion up to high conversion
- end group functionality is independent of slow initiation or low exchange reaction
- low percentage of irreversibly terminated polymer chains
- end group content in polymer only reduced by termination

In the late 1990s, Moad, Rizzardo, Thang et al. published the breakthrough of the RAFT polymerization concept. Polymers possessing high end group functionality could be synthesized with control over molar mass.[133, 134] Compared to the ionic polymerization, the RAFT polymerization method can be easily conducted and applied in a wide temperature range. Moreover, this method shows a high tolerance against water and the presence of functional groups. Furthermore, almost all vinyl monomer classes can be polymerized without loss of control. A schematic illustration of the RAFT polymerization method is shown in **Figure 1.16**. Most of the polymer chains carry "R" RAFT initiating ends as well as "Z" RAFT terminating

ends. Only a small percentage of the polymer chains bear initiator-derived ends, or lost the "Z" RAFT terminating ends.[135]

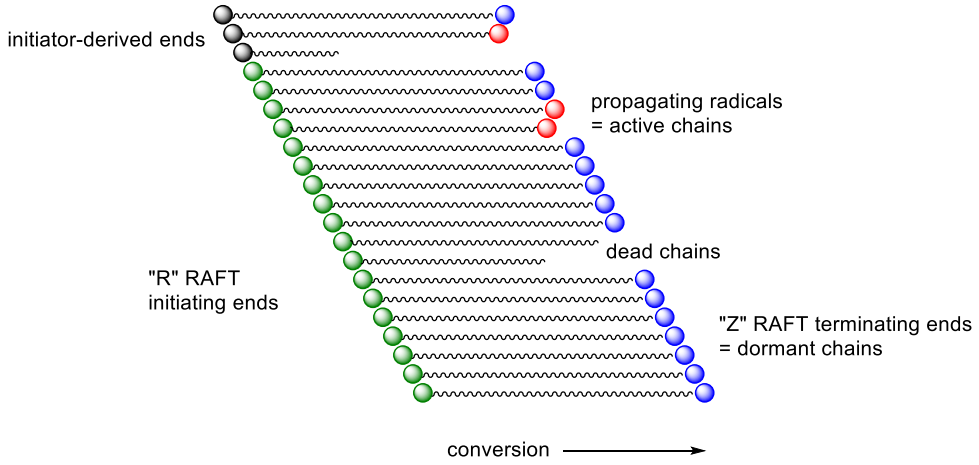

Figure 1.16. Schematic illustration of the RAFT polymerization.[129] "Z" and "R" are groups of the RAFT agent with precise functions.

Polymers of defined molar masses, narrow molar mass distributions, and noteworthy, defined end groups are accessible by the RAFT mechanism (**Figure 1.17**). Generally, a RAFT polymerization differs from a free radical polymerization only in the presence of a RAFT agent, acting as chain transfer agent (CTA). In this process, a series of reversible addition and fragmentation steps are involved, which overlap the steps of the free radical polymerization. In the early stages of the polymerization (initiation and RAFT pre-equilibrium, **Figure 1.17a-b**), addition of a propagating radical ($P_n\cdot$) to the C=S double bond of the CTA (**1**) gives the intermediate radical (**2**). Subsequently, fragmentation of **2** provides a polymeric CTA (**3**) and a new radical (R·). Hereby, the equilibrium between active and dormant species is defined by CTA to initiator ratio. Reaction of R· with monomers forms a new propagating radical ($P_m\cdot$) (re-initiation, **Figure 1.17c**). Importantly, when keeping the initiator concentration very low, $P_m\cdot$ takes part in the RAFT pre-equilibrium again to consume all remaining **1**.

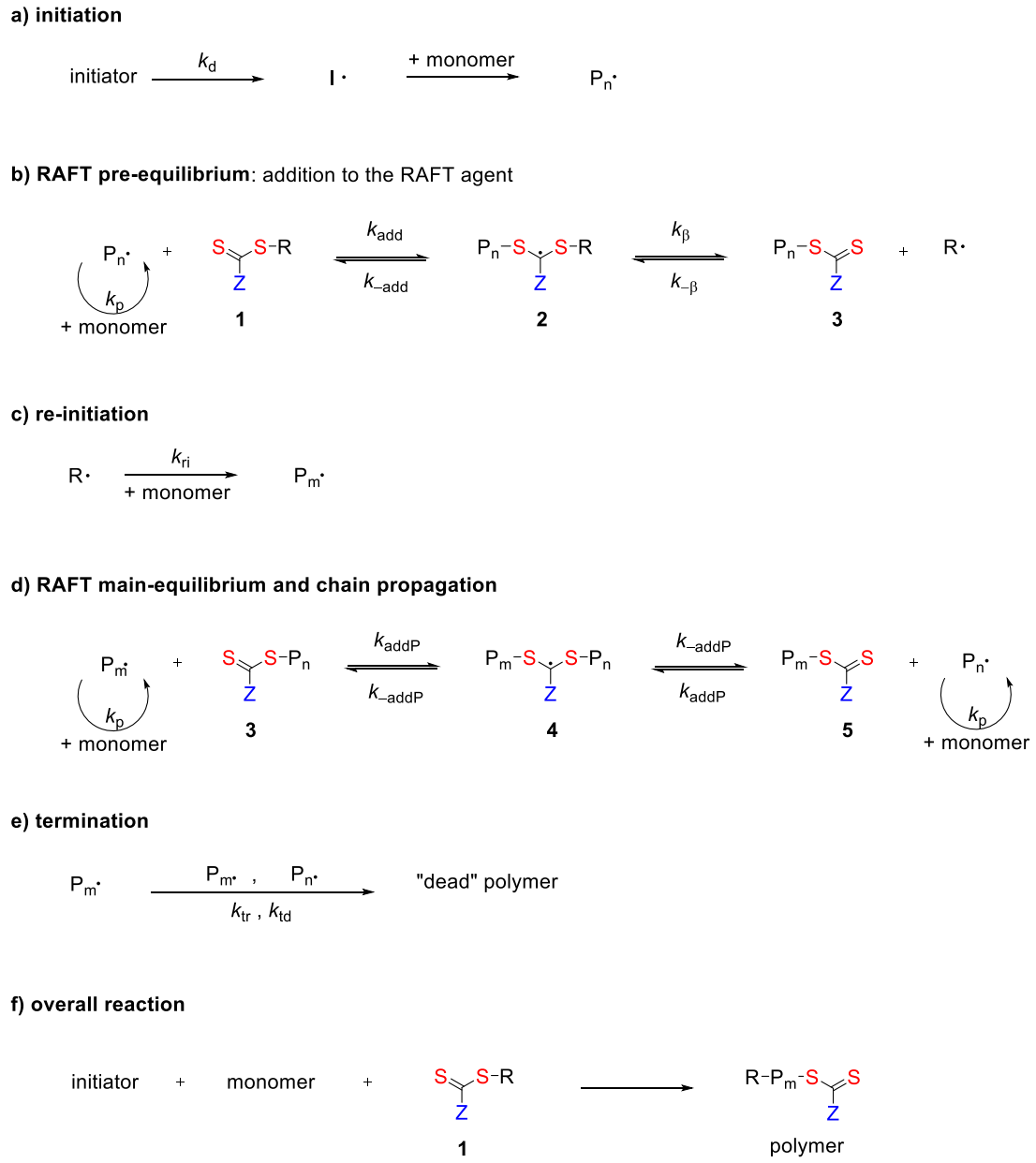

Figure 1.17. Simplified Mechanism of RAFT polymerization.[85, 129] a) Initiation, b) RAFT pre-equilibrium, c) re-initiation, d) RAFT main-equilibrium, and e) termination. I·: initiator radical, P_n·: propagating radical, R·: new radical, and P_m·: new propagating radical. *k* is the reaction rate constant for dissociation (d), re-initiation (ri), addition (add) with P for propagating, fragmentation (β), and termination through recombination (tr), and disproportionation (td).

Then rapid equilibrium between the active propagating radicals (P_n· and P_m·) and the dormant polymeric CTAs via the intermediate radical (**4**) provides equal probability for all chains to grow and thus the production of low dispersity polymers

(RAFT main-equilibrium and chain propagation, **Figure 1.17d**). A higher concentration of CTA than initiator with a typical ratio of 5 – 10[136] provides a low stationary radical concentration due to reversible deactivation of the active propagating species. Thus, despite the parallel growth of all polymer chains, chain terminations are kept as low as in conventional radical polymerization (**Figure 1.17e**). Therefore, the RAFT technique is only termed as "controlled" but not as "living". Moreover, in an ideal RAFT process, the CTA dominates the polymerization and remains as permanent end group as well as initiating reactive end group in the polymer (**Figure 1.17f**). These polymers are used afterwards as macro-RAFT agent for designing e.g. block copolymers.[85, 129, 133]

According to the mechanism, following criteria have to be fulfilled for an efficient RAFT polymerization:[85, 133, 134, 137]

- CTA **1**, **3**, and **5** exhibit a reactive C=S double bond (high k_{add})
- intermediate radicals **2** and **4** fragment rapidly (high k_{β}, weak S-R bond) without side reactions
- intermediate radicals **2** prefer to fragment to **3** and a new radical R· ($k_{\beta} \geq k_{-\beta}$)
- high re-initiation efficiency of new radicals R·
- large excess of CTA over initiator

Therefore, essential for the control of a RAFT polymerization is the design of the CTA. Typical CTAs exhibit a thiocarbonylthio unit and they differ in their stabilizing group (Z-group) and their leaving group (R-group) (**1** in **Figure 1.17b**). According to their Z-group, most chain transfer agents are classified as a) dithioester, b) trithiocarbonate, c) xanthate, and d) dithiocarbamate (**Figure 1.18**).[137]

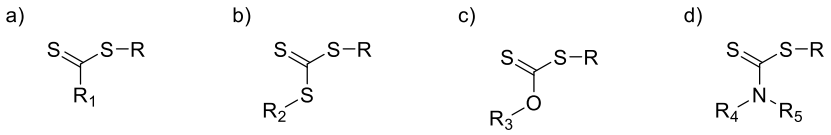

Figure 1.18. Class of CTAs. a) Dithioester, b) trithiocarbonate, c) xanthate, and d) dithiocarbamate. R indicates the R-group, $R_{\#}$ indicates any substituents.

The efficiency of a CTA is influenced by the reactivity and stability of the monomer derived radical as well as by the Z- and R-groups. The Z-group activates the C=S double bond and stabilizes the intermediate radicals, and therefore controls k_{add} and the lifetime of the intermediate radicals. An electron donating group such as a phenyl ring is an optimal Z-group which stabilizes the radical via resonance structures. However, a Z-group with an excessive stabilizing effect results in a stable intermediate radical, which leads to a rate-retarded RAFT polymerization. The R-group as a good leaving group is crucial for the direction of k_{β}. Optimal R-groups form stable radicals, are sterically demanding, and/ or exhibit electrophilic character. Furthermore, the resulting radical has to show sufficient reactivity for the re-initiation step. Otherwise a rate-retardation and an induction period will take place due to terminations. Retardation is described as the reduction of the rate of polymerization compared to the free radical polymerization. An induction period is known as the temporary inhibition in the beginning of the polymerization. With these considerations, appropriate combinations of Z- and R-groups for RAFT polymerizations are shown in **Figure 1.19**.[129, 135] Thereby, possible monomers are acrylates, methacrylates, acrylamides, styrene derivates, and vinyl acetate which include ionic and highly functionalized monomers.[85, 137]

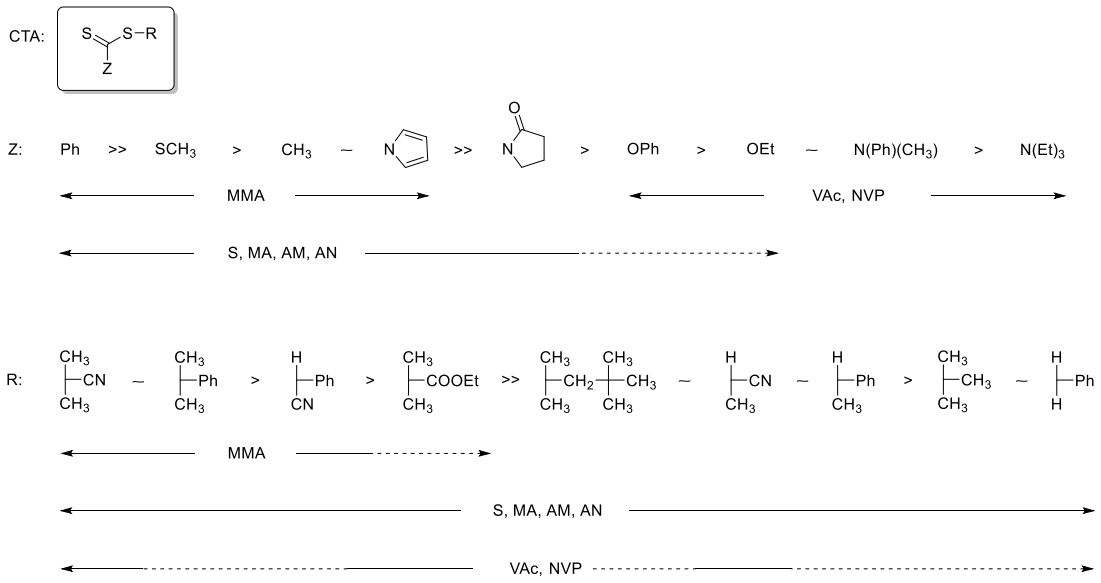

Figure 1.19. Appropriate combinations of monomers, Z-, and R-groups. From left to right: for Z-groups (Z:): decreasing k_{add} and increasing k_{β}, for R-groups (R:): decreasing k_{β}. Bold lines: controlled polymerization is possible, dashed lines: control over molar mass with broad molar mass distribution.[85, 129] CTA: chain transfer agent, MMA: methyl methacrylate, S: styrene, MA: methyl acrylate, AM: acrylamide, AN: acrylonitrile, VAc: vinyl acetate, and NVP: *N*-vinylpyrrolidone.

1.4 Objectives of the thesis

The following work describes the synthesis and characterization of new twofold thermoresponsive block copolymers. One of block is polar and non-ionic, exhibiting an LCST-type transition in aqueous media. In contrast, the other block consists of a polymeric sulfobetaine, displaying an UCST-type transition in aqueous media which can be modulated by addition of electrolytes over a broad temperature range (**Figure 1.20**). The modulation of phase transition temperatures of block copolymers with a molecularly dissolved intermediate regime (LCST > UCST, **Figure 1.1d**) has been already reported in literature (**Figure 1.20a**).[31, 32] In the case of block copolymers with an insoluble intermediate regime (LCST < UCST, **Figure 1.1e**), the

inversion of the relative position of LCST- and UCST-type transitions upon addition of electrolytes has been not mentioned yet (**Figure 1.20b**). Thereby, at low electrolyte concentration, the UCST-type transition is higher than the LCST-type transition, which turns vice versa with increasing electrolyte concentration. This kind of scenario enables an orthogonal switching depending on the combination of stimuli. Thus, a major objective is the identification and the synthesis of eligible zwitterionic poly(sulfobetaine)s displaying such aqueous solution behavior.

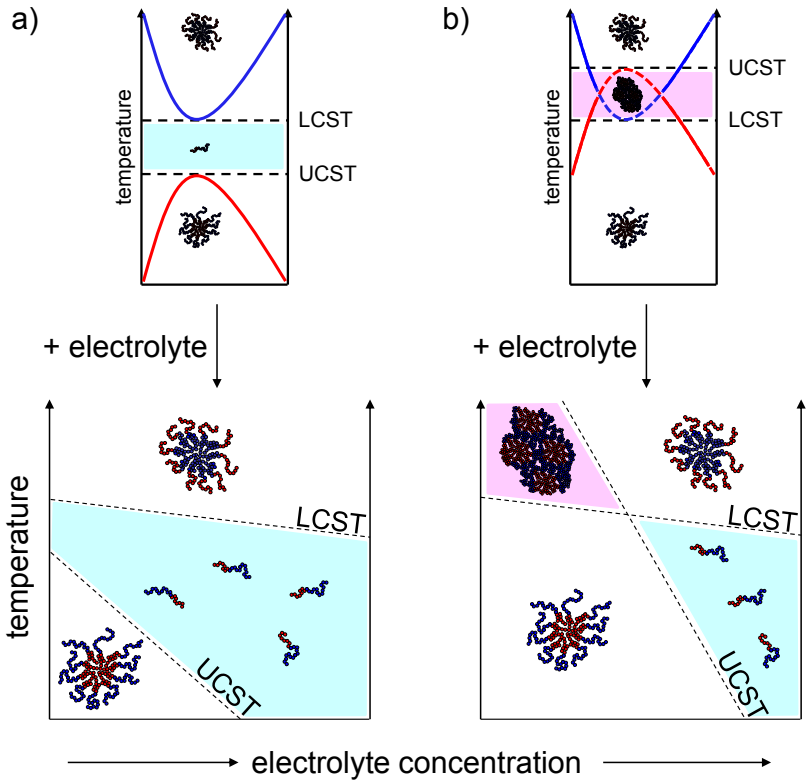

Figure 1.20. Induced self-organization of block copolymers by combined LCST- and UCST-type transitions via dual stimuli (temperature and electrolyte concentration). a) Modulation of UCST-type transition insufficient for orthogonal switching, b) orthogonal switchable (inversion of transitions) depending on combination of stimuli.

Relatively few poly(sulfobetaine)s are described so far and hence, the aqueous solution behavior has been only well-investigated for selected polymers. Therefore, better understanding of the influence of chemical structure on the phase transition

behavior was aspired by the systematic variation of the sulfobetaine structure. According to the literature, variations included:[96, 97, 119]

- the distance between the polymer backbone and the zwitterionic group
- the type of substituents on the ammonium moiety
- the spacer group separating the cationic and anionic moieties

Even with small structural variation, UCST-type transition temperature cannot easily be predict by applying the additive increment contribution due to the complex interactions and the salt-free monomer synthesis requirement.[28] Hence, suited, mostly new sulfobetaine monomers are to be synthesized, and to be copolymerized with the non-ionic monomer *N*-isopropylmethacrylamide "**NIPMAM**" (**M-12**) to block copolymers of different sizes and block lengths. Preliminary investigations of these block copolymers on their phase transition behavior and electrolyte dependence are conducted via turbidimetry.

By applying the RDRP technique, the usage of non-ionic **M-12** is matched to the reactivity of the zwitterionic methacrylamide sulfobetaines which enables a better chain extension compared to the well-used *N*-isopropylacrylamide (**M-13**). Besides, poly(methacrylamide)s are more resistant against hydrolysis than poly(acrylamide)s, and are therefore more eligible for long term measurements under harsh conditions, e. g. high temperature and salt addition. Furthermore, the RDRP technique enables the incorporation of defined functional end groups which will be useful for the complicated molecular characterization of poly(sulfobetaine)s. Therefore, polymers are synthesized by RAFT polymerization using a functional CTA, e.g. labeled with a fluorescent probe.

2 Synthesis and characterization of RAFT agent and new sulfobetaines

2.1 Design of labeled RAFT agent

Since the thermoresponsive behavior of poly(sulfobetaine)s depends sensitively on the molar mass, controlled polymerization methods were necessary to synthesize appropriate model polymers for the studies envisaged. The usage of the RAFT polymerization method seemed the most convenient technique among the RDRP methods, because through the RAFT polymerization method, well-defined end groups can be easily incorporated. These can facilitate the generally cumbersome molecular characterization of poly(sulfobetaine)s. In order to design a trithioester-type RAFT agent, which will polymerize methacrylamide and methacrylate monomers, a proper combination of Z- and R-group is crucial, including e.g. an alkyl and an isobutyronitrile group, respectively (see **Figure 1.19**). The functional **CTA-1** (**Figure 2.1**) with such groups has been successfully used to polymerize methacrylamide and methacrylate monomers.[138] The trithiocarbonate group of the RAFT agent can be used for molar mass determination by end group analysis via UV-vis spectroscopy.[139, 140] However, since the trithiocarbonate group is part of the Z-group, which can be lost during the polymerization process, an additional functional group linked to the R-group enhances its potential to facilitate the molecular characterization by end group analysis. Moreover, according to the

polymerization mechanism (see **Figure 1.15**), utilizing the R-group provides more reliable molar mass values than using the Z-group.[141] Thus, functionalization of the R-group especially with a strong fluorescent dye probe, which is permanently attached to the polymer, can facilitate the molecular characterization via nuclear magnetic resonance (NMR), fluorescence as well as ultraviolet-visible (UV-vis) spectroscopy. An attractive fluorescent dye probe is the 4-dimethylaminonaphthal-imide chromophore[142], which is a strong push-pull (amino group – imide ring) dye that is virtually inert against radical attack and therefore does not inhibit the polymerization process. Furthermore, 4-dimethylaminonaphthalimide is highly stable against photobleaching. Moreover, this chromophore is strongly fluorescent in many solvents, with the emission maximum close to the one of the widely used fluorophore rhodamine B.[142, 143] In contrast to the latter, however, the naphthalimide is non-ionic, considerably smaller, and is excited at lower wavelengths due to a pronounced Stoke shift.

In this context, the functional RAFT agents **CTA-1**, **CTA-2**, and **CTA-3** were synthesized (**Figure 2.1**). The basic structure of the R-group is similar to azobisisobutyronitrile (AIBN) which shows sufficient reactivity for the re-initiation step in a RAFT process.[144] 4-Cyano-4-(((phenethylthio)carbonothioyl)thio) pentanoic acid (**CTA-1**) was synthesized as described by Semsarilar et al.[145] 2-Phenylethyl bromide and thiourea reacted to 2-phenylethanethiol, which was subsequently deprotonated by NaH and reacted with carbon disulfide. The resulting trithiocarbonate anion was oxidatively dimerized to give the bis(trithiocarbonyl) disulfide. Then, the synthesis of **CTA-1** involved heating a solution of the bis(trithiocarbonyl) disulfide with 1.5 equivalents of 4,4'-azobis (4-cyanopentanoic acid) (V-501) under N_2 atmosphere to yield **CTA-1**. The esterification of **CTA-1** according to Steglich's procedure gives 4-methoxybenzyl 4-cyano-4-(((phenethylthio)carbonothioyl)thio)pentanoate (**CTA-2**) and 2-(6-(dimethylamino)-1,3-dioxo-1H-benzo[de]isoquinolin-2(3H)-yl)ethyl 4-cyano-4-(((phenethylthio) carbonthioyl)thio)pentanoate (**CTA-3**). The ^{1}H and ^{13}C NMR spectra of **CTA-2** and **CTA-3** are shown in the appendix (**Figure A.1** – **A.4**) as well as the IR spectra (**Figure A.24** – **A.25**).

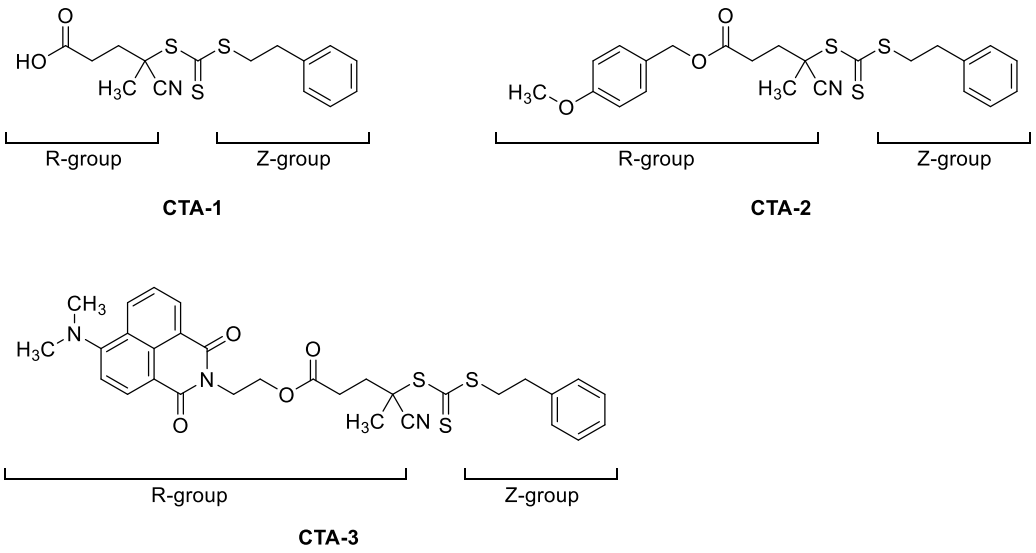

Figure 2.1. Structure of the RAFT agents **CTA-1**, **CTA-2**, and **CTA-3**.

CTA-3 bears the 4-dimethylaminonaphthalimide moiety as part of its R-group. The synthesis of this chromophore started with a nucleophilic aromatic substitution (S_NAr) of Cl or Br by dimethylamine. As the secondary amine could cause a competitive amidation of the anhydride ring, it was engaged in form of the protected tertiary amine 3-(dimethylamino)propionitrile for the substitution. For S_NAr reactions with the addition-elimination mechanism, Cl tends to be a better leaving group than Br. Interestingly, the reaction of 4-chloro-1,8-naphthalic anhydride in isoamyl alcohol by adapting the procedure reported by Zhang et al.[146] gave a yield of only 10 – 15 %, while the reaction of 4-bromo-1,8-naphthalic anhydride in isoamyl alcohol gave a yield of 75 – 80 %. Furthermore, the reaction of 4-bromo-1,8-naphthalic anhydride in 1-pentanol gave a yield of 75 – 80 %. However, 4-bromo-1,8-naphthalic anhydride as starting material is rather costly. Thus, the cheaper combination of 4-chloro-1,8-naphthalic anhydride and 1-pentanol was successfully tested and found to give a yield of 75 – 80 %. These results suggest that the quality of leaving group in a S_NAr mechanism can be influenced by the choice of the solvent. In the following step, 4-dimethylamino-1,8-naphthalic anhydride was reacted with ethanolamine to yield 4-dimethylaminonaphthalimide quantitatively.

The chromophore in **CTA-3** showed a broad and intensive characteristic maximum absorbance wavelength λ_{max} from 409 to 447 nm depending on the

solvent, while the maximum emission wavelength λ_{PL} varied from 502 to 546 nm (**Figure 2.2**).

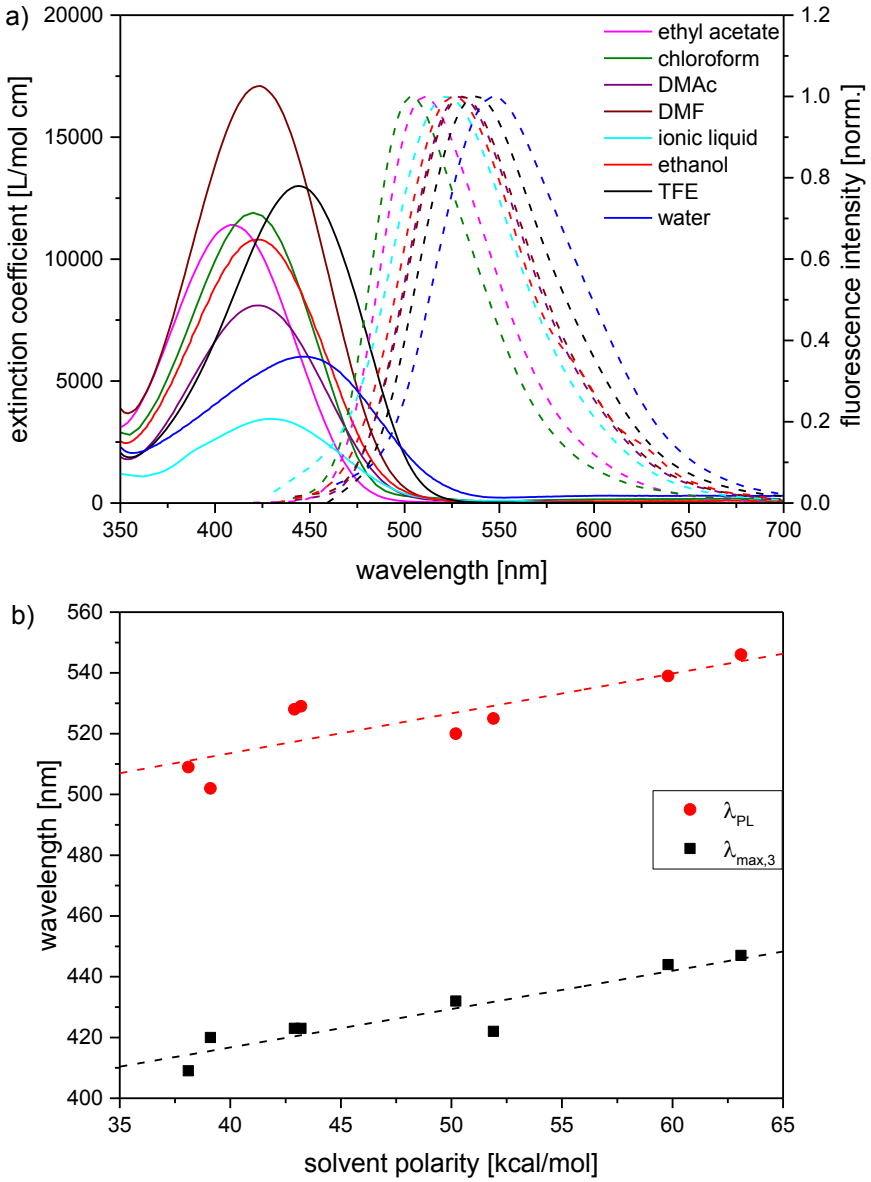

Figure 2.2. a) UV-vis absorbance spectra (solid lines) and normalized fluorescence emission spectra (dashed lines) of **CTA-3** in various solvents. Excitation at maximum absorbance wavelength. DMAc = dimethylacetamide, DMF = dimethylformamide, TFE = trifluoroethanol, and ionic liquid = 1-ethyl-3-methylimidazolium crotonate. The spectra of water and ionic liquid are only one point measurements. b) Evolution of λ_{PL} (●) and $\lambda_{max,3}$ (■) with empirical solvent polarity $E_T(30)$ parameter[147]. Increasing solvent polarity from left to right.

The extinction coefficients ε, the λ_{max}, the λ_{PL} of **CTA-1**, **CTA-2** (due to the trithiocarbonate moiety), and **CTA-3** in various solvents, and their empirical solvent polarity $E_T(30)$ parameters[147] are summarized in **Table 2.1**. Generally, λ_{max} and λ_{PL} of the chromophore in **CTA-3** increase with increasing solvent polarity. For example, changing the solvent from the polar trifluoroethanol to the less polar chloroform induces a hypsochromic shift ($\Delta\lambda_{max}$ = 24 nm, $\Delta\lambda_{PL}$ = 37 nm). As the chromophore shows a marked solvatochromism of the absorbance as well as of the emission bands, it may serve as a probe for the polarity of the molecular environment.[143, 148] In addition, spectroscopic characterization of the chromophore intermediate 4-dimethylamino-*N*-2-hydroxyethyl-1,8-naphthalimide **I-1** is shown in the appendix (**Figure A.36** and **Table A.1**). As a common feature, λ_{max} and λ_{PL} of **I-1** are not identical to the values of the chromophore incorporated in **CTA-3**. Also, the ε of **I-1** vary after incorporation in **CTA-3**. The spectroscopic parameters for **I-1** are higher than for **CTA-3** in TFE, but show the opposite trend in chloroform and in ethanol.

Table 2.1. Extinction coefficients ε, maximum absorbance wavelengths λ_{max}, maximum emission wavelengths λ_{PL} of **CTA-1**, **CTA-2**, and **CTA-3** in various solvents, and empirical solvent polarity $E_T(30)$ parameter[147]. Excitation and ε of **CTA-3** at λ_{max3}. Ionic liquid = 1-ethyl-3-methylimidazolium crotonic acid.

RAFT agent	solvent	ε_{max} [10^4 L·mol^{-1}·cm^{-1}]	$\lambda_{max1,2,3}$ [nm]	λ_{PL} [nm]	$E_T(30)$ [kcal·mol^{-1}]
CTA-1	chloroform	1.23	- , 295, -	-	39.1
CTA-1	ethanol	1.03	- , 301, -	-	51.9
CTA-1	trifluoroethanol	1.14	- , 306, -	-	59.8
CTA-2	chloroform	1.23	- , 296, -	-	39.1
CTA-2	ethanol	1.04	- , 302, -	-	51.9
CTA-2	trifluoroethanol	1.14	- , 307, -	-	59.8
CTA-3	ethyl acetate	1.14	259, 288, 409	509	38.1
CTA-3	chloroform	1.19	- , - , 420	502	39.1
CTA-3	dimethylacetamide	0.81	- , 292, 423	528	42.9
CTA-3	dimethylformamide	1.71	- , 290, 423	529	43.2
CTA-3	ionic liquid [a)]	-	- , - , 432	520	50.2
CTA-3	ethanol	1.08	259, 290, 422	525	51.9
CTA-3	trifluoroethanol	1.30	258, 290, 444	539	59.8
CTA-3	water [a)]	-	258, 297, 447	546	63.1

[a)] sparingly soluble.

Also, the trithiocarbonate moiety of the RAFT agents shows a strong absorbance band in the range from 295 to 306 nm (π-π*-transition of C=S bond) with extinction coefficients ε from $1.0 \cdot 10^4$ to $1.2 \cdot 10^4$ L·mol^{-1}·cm^{-1} (absorbance spectra of **CTA-1** and **CTA-2** in various solvents are shown in appendix **Figure A.35**). Absorbance bands of *n*-σ*- and *n*-π*-transitions are superposed by the solvent band, or are symmetry forbidden, respectively.[139] Likewise, ε of 4-dimethylaminonaphthalimide at λ_{max3} ranged from $0.8 \cdot 10^4$ to $1.7 \cdot 10^4$ L·mol^{-1}·cm^{-1}. Due to the partial overlapping of the absorbance bands of the trithiocarbonate and of the naphthalimide groups in **CTA-3**,

only the band of the naphthalimide at λ_{max3} in the range from 409 to 447 nm was useful for the molar mass determination via UV-vis spectroscopy.

As already mentioned, the trithiocarbonate functional RAFT agents were especially synthesized (**Figure 2.1**) to facilitate the molecular characterization of the poly(sulfobetaine)s via UV-vis spectroscopy. This sensitive spectroscopic technique is little time-consuming. Thereby, electromagnetic radiation of wavelength 190 nm ≤ λ ≤ 800 nm is used to stimulate transitions between electronic states. The wavelength of the absorbed light is proportional to the energy difference of the states. An UV-vis spectrometer measures the intensity of the transmitted light and the ratio of irradiated and transmitted light gives the absorbance *A*. According to the Lambert-Beer law (**equation 2.1**), *A* of a dilute solution depends on the extinction coefficient ε, the concentration *c* of the absorbing substance, and the path length *d* of the light in the solution.

$$A = \varepsilon \cdot c \cdot d \qquad (\mathbf{2.1})$$

In the case of a polymer, the molar concentration of the polymer can be described by **equation 2.2**, where *m* is the mass of the polymer, M_n is the number average molar mass, and *V* is the volume of the solvent.

$$c = \frac{m}{M_n \cdot V} \qquad (\mathbf{2.2})$$

Insertion of **equation 2.2** in **equation 2.1** followed by rearrangement results in **equation 2.3**:

$$M_n^{UV} = \frac{\varepsilon \cdot m \cdot d}{A \cdot V} \qquad (\mathbf{2.3})$$

Thus, the number average molar mass M_n^{UV} of polymers containing end groups, which absorb electromagnetic radiation of wavelength 190 nm ≤ λ ≤ 800 nm, can be determined via UV-vis spectroscopy. Such end groups were successfully incorporated through the Z- and/or R-group of the RAFT agent.

2.2 New sulfobetaines

In order to gain better understanding of the influence of chemical structure on the phase transition behavior of poly(sulfobetaine)s, the structure of sulfobetaine monomers was systematically varied. Variations included:

- the type of the polymerizable moiety
- the distance between the polymerizable moiety and the zwitterionic group
- the type of substituents on the ammonium moiety
- the spacer group separating the cationic and anionic moieties

New methacrylamide (**M-2** – **M-3**) and methacrylate (**M-5** – **M-11**) monomers (**Figure 2.3**) were successfully synthesized. An overview of all structures, e.g., monomers, RAFT agents, and initiator used in this study, is shown in the appendix (**Figure A.39**). The monomers 2-hydroxy-3-((3-methacrylamidopropyl)dimethyl-ammonio)propane-1-sulfonate (**M-2**), 4-((3-methacrylamidopropyl)dimethyl-ammonio)butane-1-sulfonate (**M-3**), and 4-((2-(methacryloyloxy)ethyl)dimethyl-ammonio)butane-1-sulfonate (**M-5**) were prepared by straightforward alkylation of the commercially available tertiary amine precursors. In the case of **M-2**, alkylation was performed with sodium 3-chloro-2-hydroxy-1-propane sulfonate. While avoiding the use of the rather potent sultone cancerogenes, the lower reactivity of the chloride required higher reaction temperatures to achieve satisfactory yields. Moreover, aqueous ethanol which may lead to side reactions, had to be employed as reaction medium due to the low solubility of the ionic alkylating agent in aprotic solvents, such as acetonitrile which are *a priori* more inert. Furthermore, the formation of sodium chloride as byproduct, which may tenaciously stick to the sulfobetaine moiety, required the purification of **M-2** with a mixed bed ion exchanger, to obtain the monomer free of inorganic salt contamination.[118, 149] Though reference data are missing, the ^{1}H NMR spectra of **M-2** (see in the appendix **Figure A.5** – **A.6**) fits well with the typical features of related sulfobetaine monomers.[150] In the case of **M-3** and **M-5**, alkylation was achieved by reaction with

butane sultone in acetonitrile.[93-96] Despite the lower reactivity of butane sultone[93] compared to propanesultone, the extended reaction times applied resulted in high yields. The ^{1}H NMR spectra of **M-3** (see in the appendix **Figure A.7** – **A.8**) and **M-5** (see in the appendix **Figure A.9** – **A.10**) agree precisely with published data.[93]

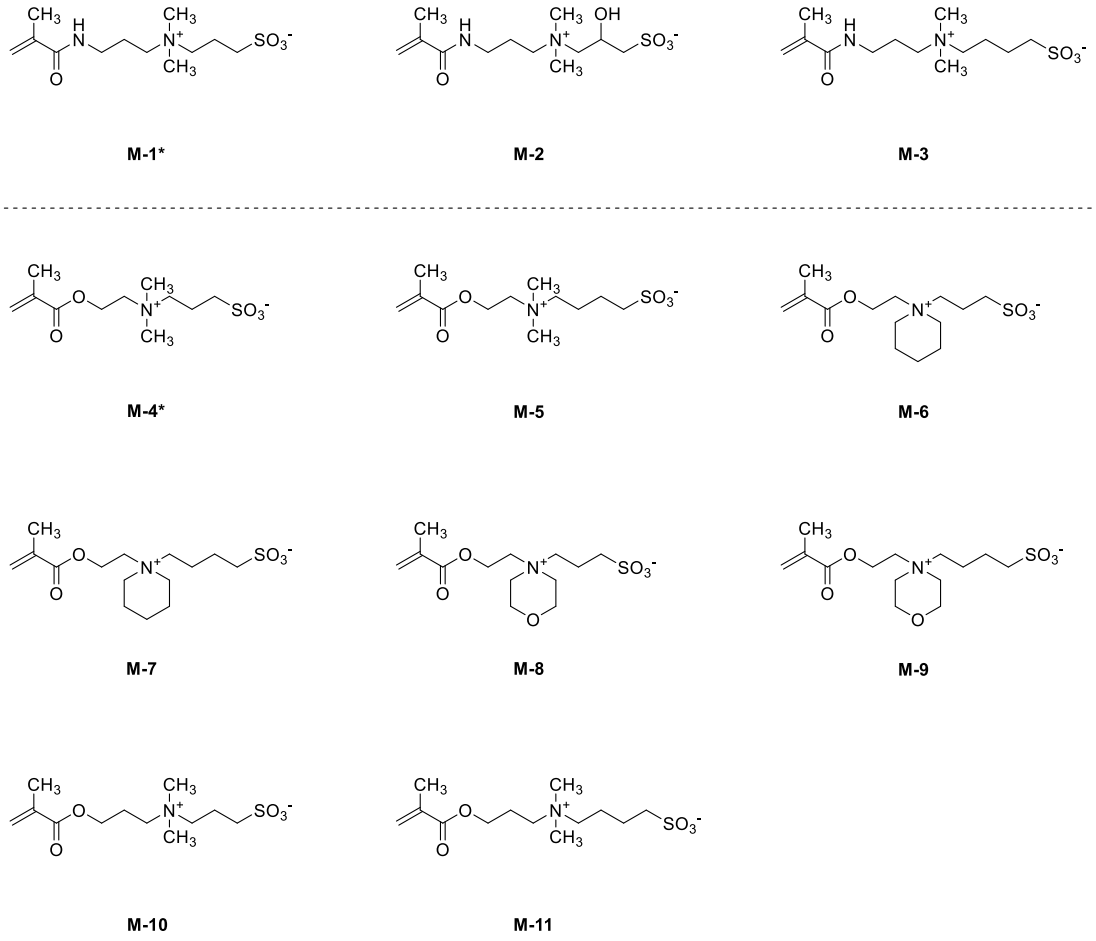

Figure 2.3. Structures of commercially available (*) and newly synthesized sulfobetaines employed. Monomers **M-1** – **M-3** are methacrylamide-based, whereas **M-4** – **M-11** are methacrylate-based.

The monomers 3-(1-(2-(methacryloyloxy)ethyl)piperidin-1-ium-1-yl)propane-1-sulfonate (**M-6**), 4-(1-(2-(methacryloyloxy)ethyl)piperidin-1-ium-1-yl)butane-1-sulfonate (**M-7**), 3-(4-(2-(methacryloyloxy)ethyl)morpholino-4-ium)propane-1-sulfonate (**M-8**), 4-(4-(2-(methacryloyloxy)ethyl)morpholino-4-ium)butane-1-sulfonate (**M-9**), 3-((3-(methacryloyloxy)propyl)dimethylammonio)propane-1-sulfonate (**M-10**), and 4-((3-(methacryloyloxy)propyl)dimethylammonio)butane-1-

sulfonate (**M-11**) were prepared by straightforward alkylation of synthesized tertiary amine precursors. The alkylation was achieved by reaction with propanesultone or butane sultone in acetonitrile. Pure monomers were obtained in high yields. The ^{1}H and ^{13}C NMR spectra are shown in the appendix (**Figure A.11** – **A.22**). The tertiary amine precursors were prepared by azeotropic transesterification of methyl methacrylate (**MMA**) with an amino alcohol at 300 mbar in the presence of potassium phosphate. The byproduct methanol and the unreacted excess of **MMA** were distilled off at 19 mbar. High yields of pure monomer precursors were obtained after ball tube distillation. Noteworthy, in a modified approach[†], the byproduct methanol in the synthesis of the precursor for **M-10** and **M-11** was successfully removed during the reaction with molecular sieve 4 Å.

The structures of the monomers **M-2**[151] and **M-10**[152-155] have already been reported. Yet, no synthetic information for **M-2** was provided by the authors. In the case of **M-10**, the authors did not provide satisfactory synthetic information, which in parts as even contradictory.

Fourier transform-infrared (FT-IR) spectra of the monomers (see in the appendix **Figure A.26** – **A.34**) reveal interesting information between monomer structure and phase transition behavior, especially comparing the wavenumber ν of the ammonium moieties (N^{+}-CH_3) (at about 3000 – 3040 cm^{-1}). Clearly, monomers which are alkylated with butane sultone have constantly lower values of ν(N^{+}-CH_3) (Δν(N^{+}-CH_3) ≈ -10 cm^{-1}) than monomers which are alkylated with propanesultone. Moreover, monomers bearing the piperidine or morpholine ring (**M-6**, **M-7**, **M-8**, and **M-9**) have lower values of ν(N^{+}-CH_2) (Δν(N^{+}-CH_2) ≈ -20 cm^{-1}) than monomers where the cation is substituted by methyl groups (**M-2**, **M-3**, **M-5**, **M-10**, and **M-11**). Still, ammonium moieties of monomers exhibiting C_2- or C_3-spacers between the polymerizable moiety and the zwitterionic group show similar wavenumbers. Also, the nature of the monomer (methacrylamide or methacrylate) did not influence the value of ν (N^{+}-CH_3). In general, the values of ν of the sulfonate anions (SO_3^{-}) follow the same trend (at about 1040 and 1200 cm^{-1}). In the series of M-1 – M-5 and

[†] personal communication, Dr. Michael Päch

M-10 – M-11, the monomers alkylated with butane sultone have lower values of $\nu(SO_3^-)$ ($\Delta\nu(SO_3^-) \approx -10 - 15$ cm^{-1}) than monomers which are alkylated with propanesultone, except for the monomers **M-6**, **M-7**, **M-8**, and **M-9**. In these cases, values of $\nu(SO_3^-)$ of monomers, which are alkylated with propanesultone, are slightly lower ($\Delta\nu(SO_3^-) \approx -5$ cm^{-1}) than values of $\nu(SO_3^-)$ of monomers which are alkylated with butane sultone. Anyhow, the monomers containing a piperidine or a morpholine ring have lower $\nu(SO_3^-)$ ($\Delta\nu(SO_3^-) \approx 0 - 50$ cm^{-1}) than monomers substituted by methyl groups. Furthermore, monomers exhibiting a C_2-spacer between the polymerizable moiety and the zwitterionic group show lower $\nu(SO_3^-)$ ($\Delta\nu(SO_3^-) \approx 0 - 50$ cm^{-1}) than monomers with a C_3-spacer. Lower $\nu(SO_3^-)$ ($\Delta\nu(SO_3^-) \approx 5 - 50$ cm^{-1}) are also recorded for methacrylates compared to methacrylamides. These differences point to different interactions between the cationic and anionic moieties of the zwitterionic groups within the different monomers. It was interesting to see if these results correlate somehow with their phase transition temperature (see **chapter 4.2**).

2 SYNTHESIS AND CHARACTERIZATION OF RAFT AGENT AND NEW SULFOBETAINES

3 Kinetic studies of RAFT polymerizations

In order to determine suitable reaction conditions for the synthesis of well-defined homo- and block copolymers, preliminary kinetic studies of RAFT polymerizations using **CTA-3** and azo initiator V-501 were performed. Poly(sulfobetaine)s typically require rather toxic, expensive, and exotic solvents such as trifluoroethanol (TFE), hexafluoroisopropanol, and formamide or aqueous salt solutions.[15, 95, 121] Also, RAFT polymerizations of sulfobetaine monomers in aqueous solutions have already been reported.[8, 27, 30, 151] However, as neither V-501 nor the fluorophore-labeled **CTA-3** dissolve in aqueous solutions, therefore to achieve a homogeneous reaction solution, TFE was the solvent of choice for the synthesis of the various poly(sulfobetaine)s. **CTA-3** was found to be stable under the chosen polymerization conditions (75 °C, 20 h, TFE) according to TLC and ^{1}H NMR.

3.1 Proof of principle with non-ionic monomers

To gain confidence in the functionality of **CTA-3**, a standard RAFT polymerization of **MMA** in benzene was carried out. RAFT polymerizations of **MMA** in benzene using a comparable RAFT agent (**CTA-1**) were established by Semsarilar et

al.[138, 145, 156] Therefore, it was expected that **CTA-3** enables a controlled polymerization process. Moreover, by polymerizing **MMA**, reliable molar masses and molar mass distributions can be determined via GPC by using PMMA calibration standards, which can prove the functionality of **CTA-3**. Afterwards, RAFT polymerizations of **MMA** and of *N*-isopropylmethacrylamide (**M-12**) (**Figure 3.1**) in the rather exotic TFE under comparable conditions were performed to check reactions more closely related to the RAFT polymerizations of the sulfobetaine monomers. The molar ratio monomer (Mon) : **CTA-3** : V-501 was 100 : 1 : 0.2, and the monomer concentration was 30 wt%. The reaction temperature was 75 °C.

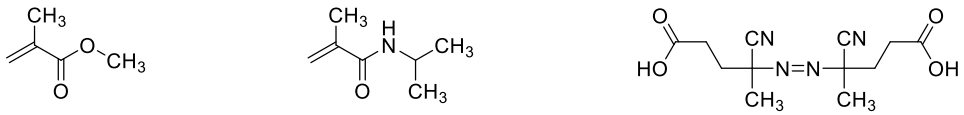

Figure 3.1. Structures of monomers **MMA**, *N*-isopropylmethacrylamide ("**NIPMAM**") **M-12**, and initiator V-501.

To follow the conversion of the monomer, samples were drawn after predefined reaction times. A small part of it was diluted by $CDCl_3$ and submitted to ^1H NMR. The majority of the sample was precipitated into diethyl ether. The isolated polymers were characterized by gel permeation chromatography (GPC) and by end group analysis via ^1H NMR and UV-vis. The approximate monomer conversion was calculated from the integral of the signals of the olefin C=C double bond, and the integral of the methyl group signal on the polymer backbone. A calculation example is shown in the appendix.

Conversions of **MMA** and **M-12** are almost equal up to 30 % after 1.5 h (**Figure 3.2a**). Then, only fast conversion of **MMA** is observed; thereby polymerization in TFE is faster than polymerization in benzene. After 3.5 h, conversion of 90 % is achieved for polymerization of **MMA** in TFE. For the polymerization in benzene, the same conversion is reached only after 9 h. In contrast, conversion of **M-12** slows down and achieves only 65 % after 19 h, this is presumably caused by the strong increase of viscosity.

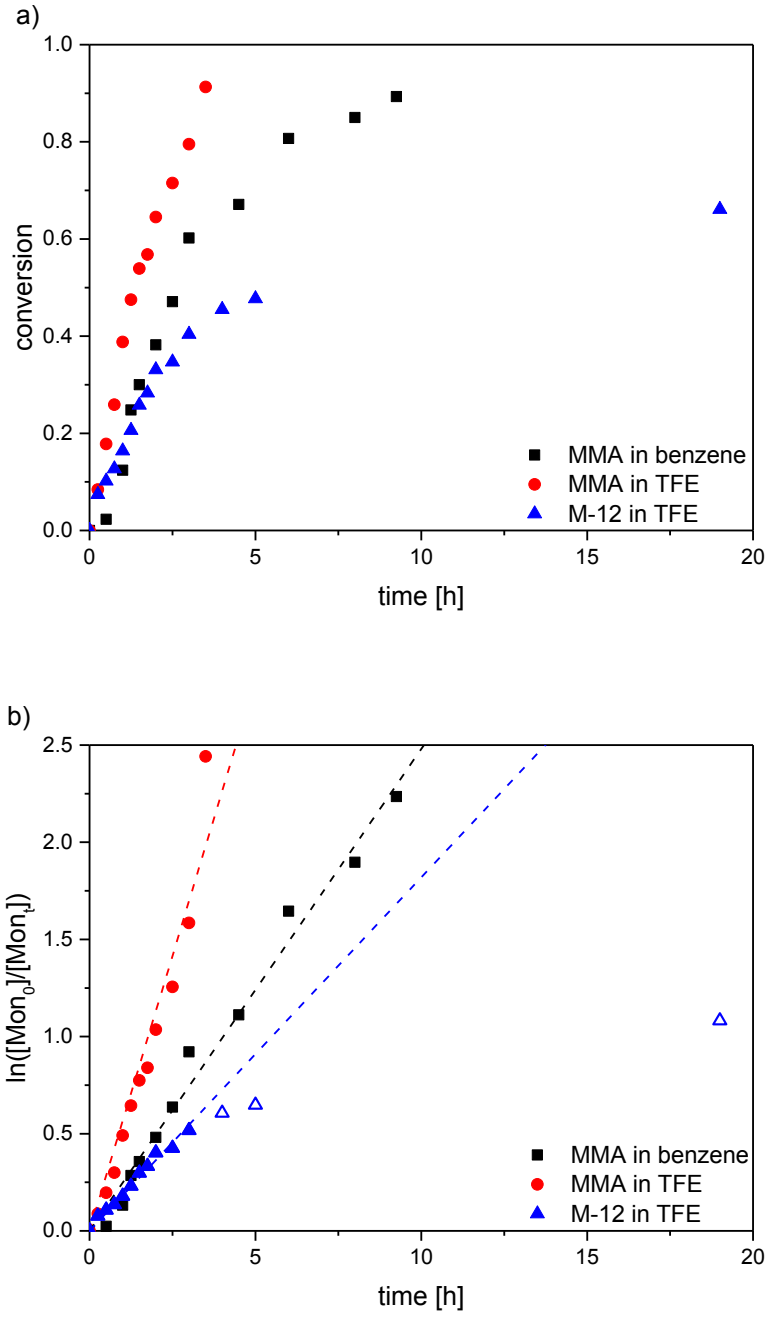

Figure 3.2. Evolution of polymerization of **MMA** in benzene (■) and TFE (●), and of **M-12** in TFE (▲/△). (△) data were not used for fitting. a) Conversion with time and b) verification of pseudo-first-order kinetic behavior. Polymerization at 75 °C, using **CTA-3** and V-501. The molar ratio Mon : **CTA-3** : V-501 was 100 : 1 : 0.2. Monomer concentration was 30 wt%.

The semi-logarithmic plot (**Figure 3.2b**) suggests that the polymerization follows a pseudo-first-order kinetic. Ideally, in the steady state, the number of formed radicals is equal to the number of terminated radicals and thus the concentration of the active propagating species is constant. Therefore, $\ln([Mon_0]/[Mon_t])$ is *a priori* expected to be a linear function of time. This behavior is found for the polymerization of **MMA** in benzene and TFE. For the polymerization of **M-12** in TFE, a downward curvature is observed after 4 h, suggesting a decrease in the concentration of the active propagating species, which may result from termination reactions.[84, 130] In contrast, an upward curvature in the kinetic plot indicates an increase in the concentration of the active propagating species which occurs in the case of slow initiation.[157] Note that the semi-logarithmic plot is not sensitive to chain transfer processes or slow exchange between different active species, since these processes do not affect the number of the active propagating species.[157] Though, GPC elugrams of the crude products after 2, 4, 5, and 19 h (see in the appendix **Figure A.37**) are monomodal with narrow molar mass distribution (Đ = 1.2). These findings do not suggest bimolecular termination reactions. However, for an efficient RAFT polymerization of **M-12** under the chosen reaction conditions, the conversion has to be lower than 40 %, which is achieved after 3 h, in order to avoid the downward curvature.

For RDRP, the number average molar mass is a linear function of the monomer conversion (**Figure 3.3a**) due to a constant number of active chains throughout the polymerization. Thus, the number average degree of polymerization DP_n can be pre-determined through monomer conversion, initial concentration of monomer $c_{Mon,0}$ and RAFT agent $c_{CTA,0}$ (**equation 3.1**)[158], neglecting the initiator concentration as well as side reactions. Theoretically expected number average molar masses M_n^{theo} were calculated according to **equation 3.2**.

$$DP_n = \frac{M_n}{M_{CRU}} = \frac{\Delta c_{Mon}}{c_{CTA,0}} = \frac{c_{Mon,0}}{c_{CTA,0}} \cdot conversion \qquad (\mathbf{3.1})$$

$$M_n^{theo} = DP_n \cdot M_{CRU} + M_{CTA} = \frac{c_{Mon,0} \cdot conversion \cdot M_{CRU}}{c_{CTA,0}} + M_{CTA} \qquad (\mathbf{3.2})$$

M_{CRU} = molar mass of the constitutional repeat unit
M_{CTA} = molar mass of the RAFT agent

The evolution of molar mass M_n with conversion is hardly affected by chain termination, as the number of polymer chains remains unaffected. The effect of termination is only observable on the plot when coupling reactions, resulting in higher molar mass polymers (upward curvature, **Figure 3.3a**), occur with a significant extent.[42, 84, 128, 130, 131, 157, 158] In contrast, a downward curvature from the ideal growth indicates additional formation reactions, such as, e.g. irreversible chain transfer, resulting in polymers of lower molar mass. Furthermore, inappropriately chosen RAFT agents result in a slow re-initiation entailing comparatively high molar mass in the beginning.[85, 144]

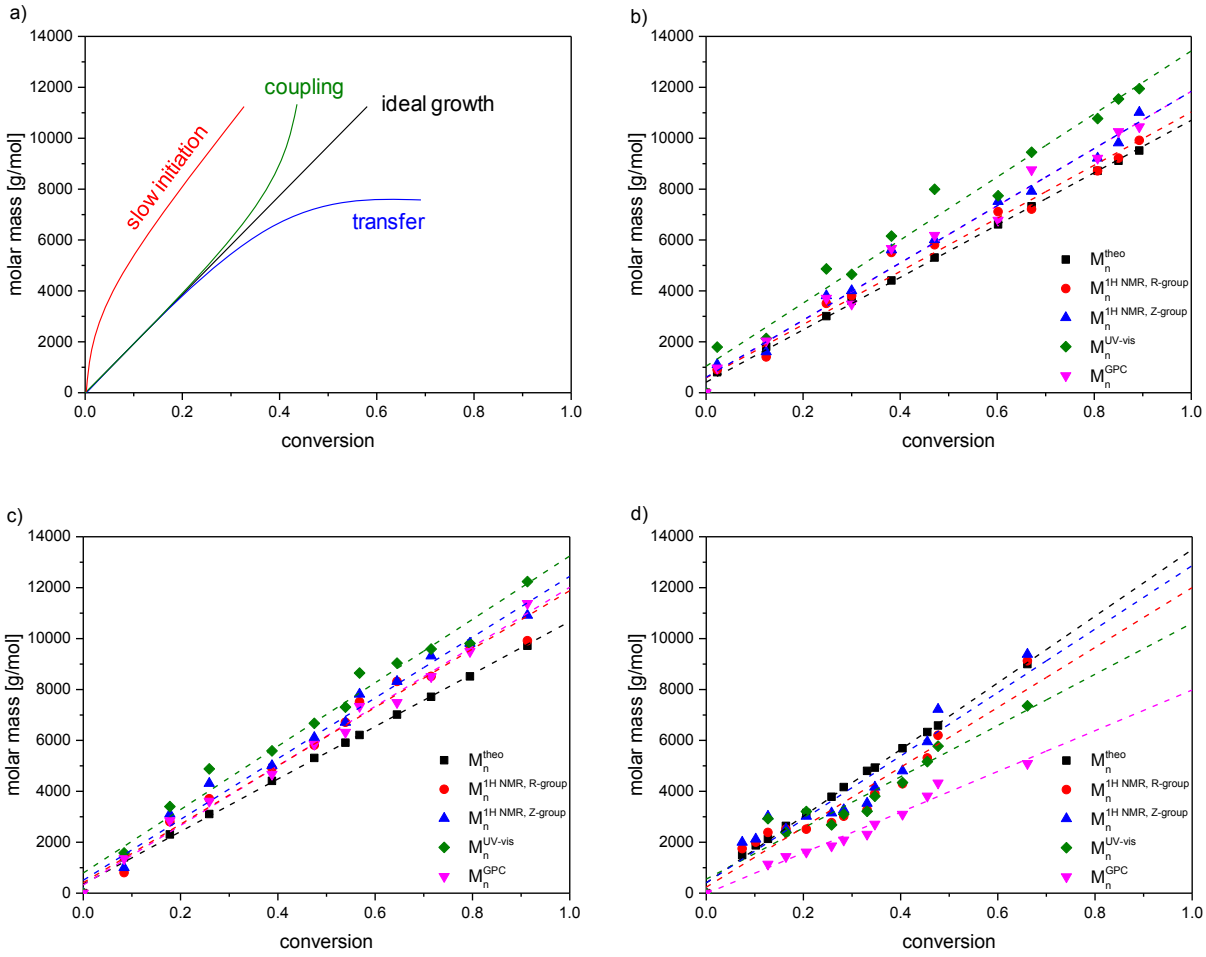

Figure 3.3. Dependence of molar mass on conversion a) theoretical for RDRP[130] and of the RAFT polymerization of b) **MMA** in benzene, c) **MMA** in TFE, and d) **M-12** in TFE. Molar masses: theoretical (■), via NMR (R-group) (●), via NMR (Z-group) (▲), via UV-vis (R-group) (◆), and via GPC (▼). GPC in THF using PMMA standards for analyzing the polymerizations of **MMA**, GPC in DMF + 0.1 % LiBr using PMMA standards for analyzing the polymerization of **M-12**. UV-vis in $CHCl_3$ (for **MMA**) and TFE (for **M-12**) using determined ε. Polymerizations at 75 °C, using **CTA-3** and V-501. The molar ratio Mon : **CTA-3** : V-501 was 100 : 1 : 0.2. Monomer concentration was 30 wt%.

Molar masses of the isolated polymers were determined by GPC and by end group analysis via ^{1}H NMR (M_n^{NMR}) (**equation 3.3**) and UV-vis. In the case of molar mass determination via UV-vis, the naphthalimide chromophore in the R-group of **CTA-3** with the $\varepsilon_{\lambda max}$ in $CHCl_3$ was utilized for analyzing polymers of **MMA**. R-group of the **CTA-3** with the $\varepsilon_{\lambda max3}$ in TFE was used for analyzing polymers of **M-12**.

$$M_n^{NMR} = \frac{\frac{N_{H(polymer)}}{N_{H(monomer)}}}{\frac{N_{H(end-group)}}{N_{H(end-group)}(theo.)}} \cdot M_{CRU} + M_{CTA} \qquad (3.3)$$

In the polymerization of **MMA** and **M-12**, the molar mass increases linearly with monomer conversions (**Figure 3.3b-d**). This strongly suggests that the majority of active propagating polymer chains are not prematurely deactivated irreversibly, they propagate during the whole polymerization. Clearly, a constant number of active chains throughout the polymerization is maintained which indicates an absence of chain transfer reactions that would increase the total number of chains and a sufficiently fast initiation, so that essentially all chains are propagating before the reaction stops.[85, 130, 159] Furthermore, in an ideal RAFT polymerization, molar mass distribution follows a Poisson distribution, which is very similar to what was obtained by GPC analysis of the polymers (see in the appendix **Figure A.38**). As described in previous publications[85, 135, 144, 160], the dispersity (Đ) generally decreases with monomer conversion, with Đ being the ratio between weight (M_w) and number average molar mass (M_n) (**equation 3.4**).[85, 158]

$$Đ = \frac{M_w}{M_n} \qquad (3.4)$$

For the RAFT polymerizations of **MMA** in benzene and in the exotic TFE, the values of M_n^{theo} are 10 % lower than the values of M_n^{GPC}, which may be caused by the loss of low molar mass polymers during the purification step. However, molar masses with low Đ (**Figure 3.4a**) determined via GPC by using PMMA calibration standards support the "controlled" character for the polymerization of **MMA** in the conventional solvent benzene as well as in the exotic solvent TFE by using the **CTA-3**.

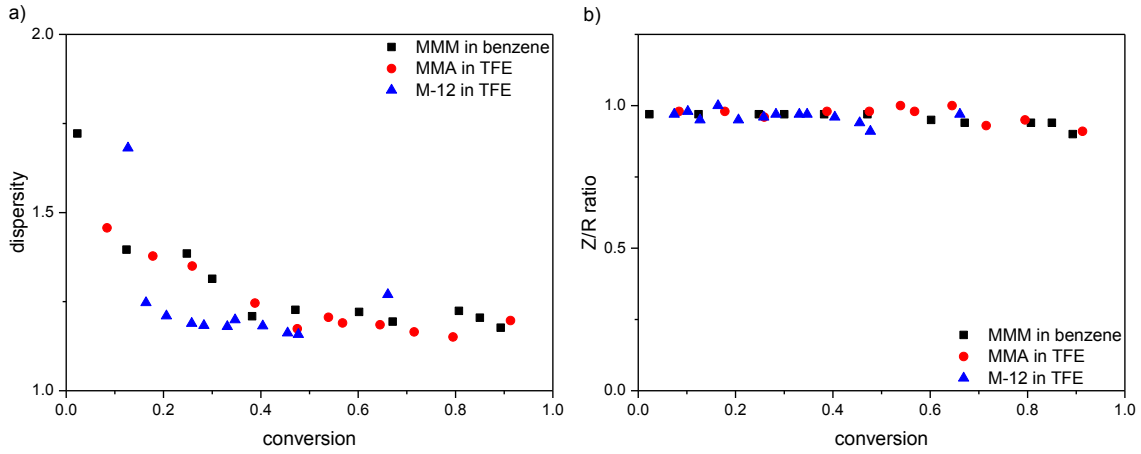

Figure 3.4. a) Evolution of dispersity Đ (determined by GPC) with monomer conversion and b) end group preservation (Z/R ratio) (determined via ^{1}H NMR). **MMA** in benzene (■), **MMA** in TFE (●), and **M-12** in TFE (▲).

Moreover, the values of M_n^{theo} are 5 – 12 % lower than the values of M_n^{NMR} determined via ^{1}H NMR end group analysis, which are also in good agreement with the M_n^{GPC} values. End group analysis by ^{1}H NMR (with Z- and R-group) provides values in excellent agreement to the theoretically expected ones which suggests that almost every polymer chain carries a Z- and an R-group (**Figure 3.4b**). Since the polymers contain high end group functionality, the difference of 20 % between M_n^{theo} and $M_n^{UV\text{-}vis}$ suggests that the determined $\varepsilon_{\lambda max}$ of the **CTA-3** and $\varepsilon_{polymer}$ of the polymer are not identical in a given solvent. The molar mass determination via UV-vis spectroscopy becomes more accurate by taking into account that ε of the chromophore changes with polymerization.[139, 161-163] Similar discrepancies were found for the RAFT polymerization of **M-12** in TFE. Clearly, the values of M_n^{theo} are 5 – 10 % higher than the values of M_n^{NMR} and 20 % higher than the $M_n^{UV\text{-}vis}$ values. These findings confirm the functionality of the **CTA-3**. Even though, the M_n^{theo} values are 50 % higher than the M_n^{GPC} values, because this discrepancy of 50 % can be explained by the different structure of **M-12** and the calibration standard PMMA.

The results of the kinetic experiments strongly support the “controlled” character of the polymerizations of **MMA** and of **M-12** in benzene and TFE in the presence of **CTA-3**. High **MMA** conversions were achieved rather fast (90 % conversion after 3.5 h) with linearly increasing molar masses, whereas conversions of **M-12** were

limited at 65 %. Moreover, different characterization methods prove the syntheses of polymers with high end group preservation, well-defined molar masses, and narrow molar mass distributions. For the latter, fast and quantitative initiation of active centers already occurs completely in the beginning of polymerization and further, the exchange between "dormant" and active species is sufficiently fast. Both criteria result in an equal propagation rate for all chains, which provides a narrow molar mass distribution. By successfully suppressing termination reactions, the RAFT agent **CTA-3** seems to be suitable for controlled polymerization of the sulfobetaine monomers under the chosen conditions. Additionally, end group analysis via UV-vis spectroscopy is a promising technique for molar mass determination.

3.2 Kinetic studies with sulfobetaines

Since the extinction coefficient ε depends on the chemical structure of the monomer, preliminary kinetic studies with sulfobetaines were performed under the same reaction conditions and procedures as described in **chapter 3.1**. To ensure homogenous polymerization solution of sulfobetaine in the presence of **CTA-3**, it was necessary to run the reaction in TFE. Exemplarily, results of the commercially available monomers 3-((3-methacrylamidopropyl)dimethylammonio)propane-1-sulfonate "**SPP**" (**M-1**) and 3-((2-(methacryloyloxy)ethyl)dimethylammonio) propane-1-sulfonate "**SPE**" (**M-4**) (**Figure 3.5**) and the synthesized monomers **M-6** and **M-11** are shown in this section. Additionally, the results of kinetic experiments of the other sulfobetaines are shown in the appendix (**Figure A.40** – **A.42**).

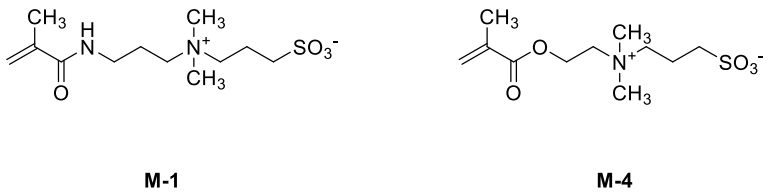

Figure 3.5. The chemical structures of sulfobetaine monomers **M-1** ("**SPP**") and **M-4** ("**SPE**").

The polymerization of all sulfobetaines (**M-1** to **M-11**) is fast (**Figure 3.6a** and **Figure A.40a**) compared to the polymerization of **MMA** and **M-12**. After 2 – 3 h the conversions of monomers significantly slow down to achieve their ultimate values after 4 h (**Table 3.1**).

Table 3.1. Maximum conversions after 4 h for sulfobetaines determined by the kinetic experiments.

sulfobetaines	maximum conversion	sulfobetaines	maximum conversion
M-1	0.91	**M-7**	0.52
M-2	0.76	**M-8**	0.61
M-3	0.86	**M-9**	0.62
M-4	0.98	**M-10**	0.99
M-5	0.98	**M-11**	0.99
M-6	0.84		

In comparison, fastest conversions are achieved by **M-4**, **M-5**, **M-10**, and **M-11**, whereas conversions were slowest for **M-7**, **M-8**, and **M-9**. In between, **M-1**, **M-2**, **M-3**, and **M-6** are found. Interestingly, conversions of the methacrylate sulfobetaines **M-10** and **M-11** are faster than of their analogous methacrylamides **M-1** and **M-3**. Another trend seen amidst the methacrylates is that the sulfobetaines derived from aliphatic esters react faster than sulfobetaines featuring cyclic ammonium cations.

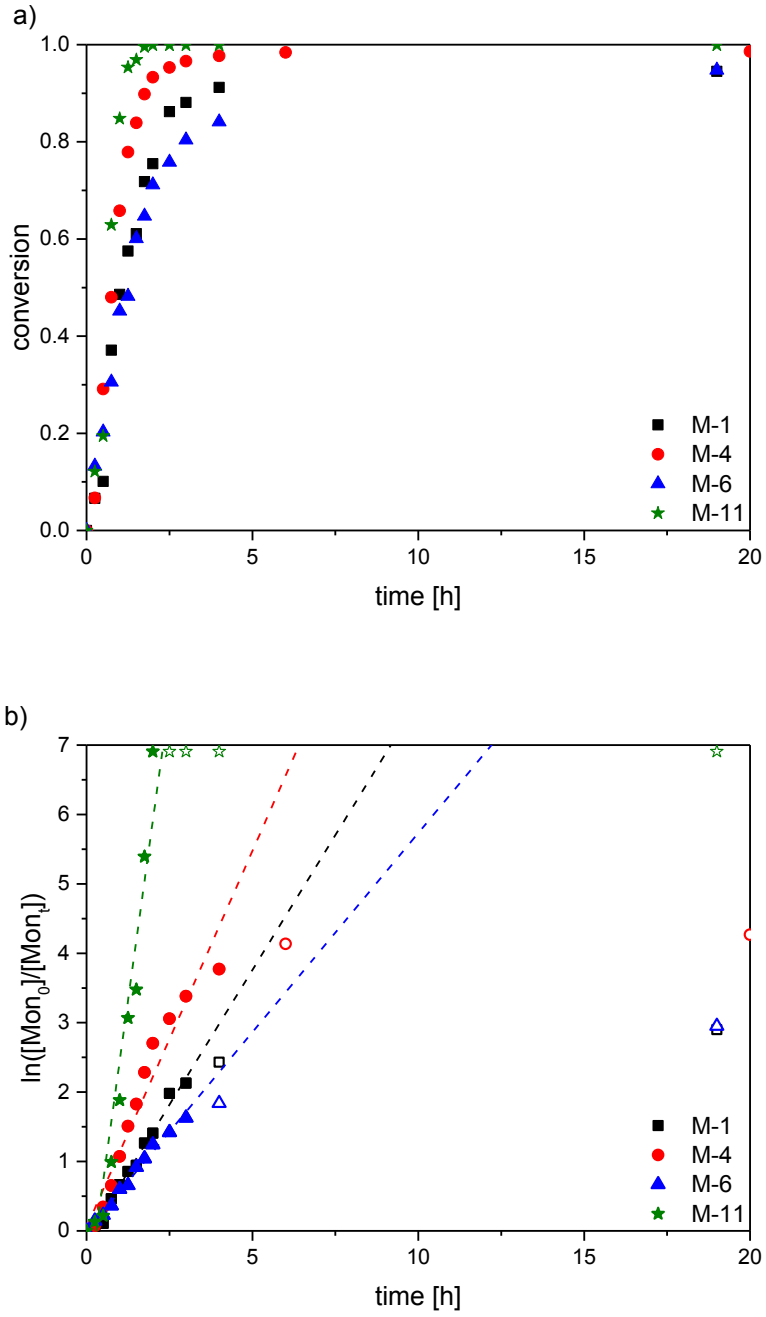

Figure 3.6. Kinetic experiments of sulfobetaine monomers in TFE. a) Conversion with time and b) verification of pseudo-first-order kinetic behavior of **M-1** (■), **M-4** (●), **M-6** (▲), and **M-11** (★). Data of **M-1** (□), **M-4** (○), **M-6** (△), and **M-11** (☆) were not used for linear regression. Polymerizations at 75 °C, using **CTA-3** and V-501. The molar ratio Mon : **CTA-3** : V-501 was 100 : 1 : 0.2. The monomer concentration was 30 wt%.

Up about 3 h, the polymerizations follow pseudo-first-order kinetics (**Figure 3.6b** and **Figure A.40b**). The subsequent apparent slowdown of the reaction is possibly caused by irreversible terminations through intrusion of O_2, or by an increase of viscosity. The downward curvature of the plot observed may indicate termination reactions and loss of control over the polymerization.[84, 130] Moreover, in some cases, the plot of the molar mass versus conversion shows a linear increase of molar masses only up to a certain monomer conversions (**Figure 3.7a-d** and **Figure A.41a-g**). A constant number of active chains are assumed in this section in which RAFT polymerizations of sulfobetaines using **CTA-3** is possible under controlled behavior.

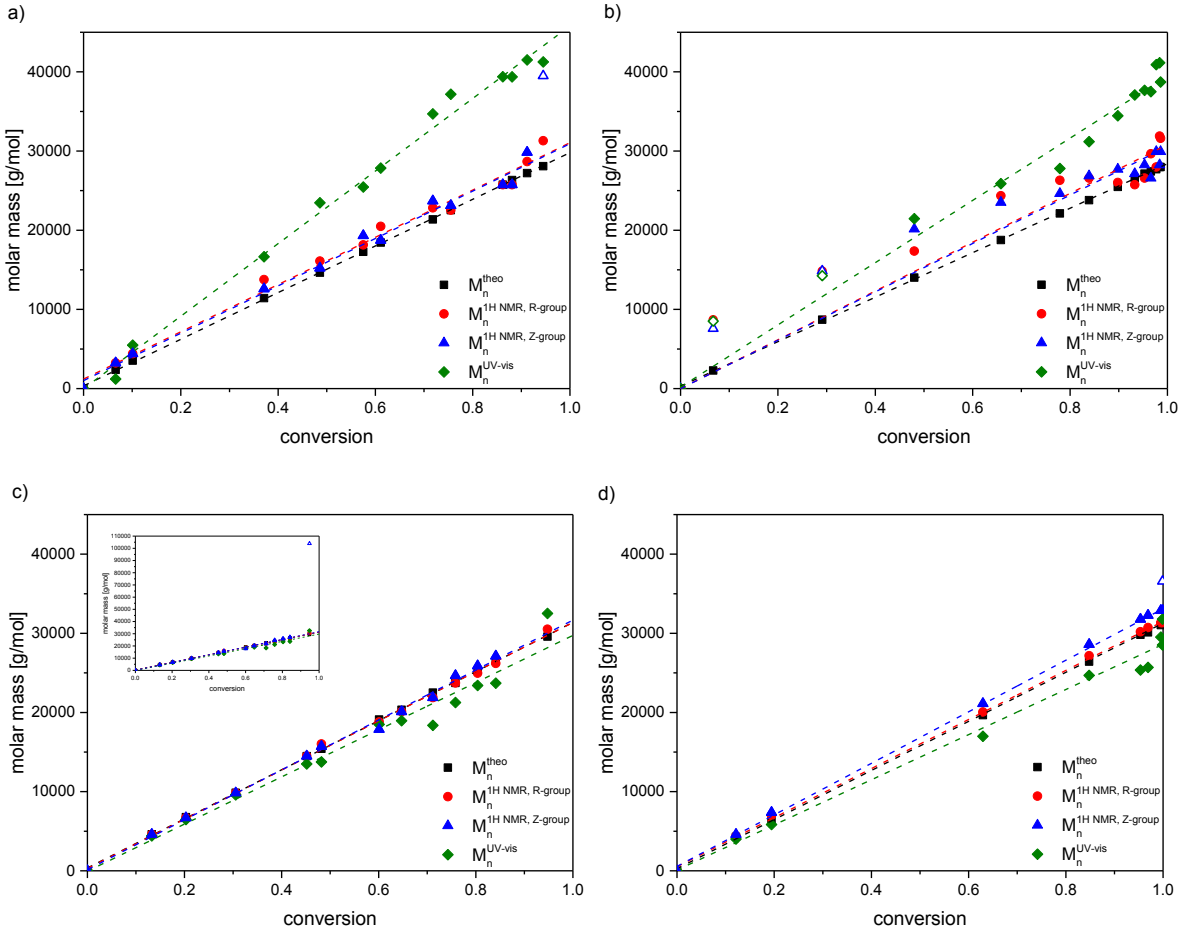

Figure 3.7. Dependence of molar mass on conversion of the RAFT polymerization of a) **M-1**, b) **M-4**, c) **M-6**, and d) **M-11** in TFE. Molar masses: theoretical (■), NMR (R-group) (●), NMR (Z-group) (▲), and UV-vis (R-group) (◆). (△, ○ ,◇) Data were not used for linear regression. UV-vis in TFE using ε at λ_{max3}. Polymerizations at 75 °C, using **CTA-3** and V-501. The molar ratio Mon : **CTA-3** : V-501 was 100 : 1 : 0.2. Monomer concentration was 30 wt%. Inset illustrates loss of Z-group functionality at high conversions. Inset illustrates the complete data set.

Loss of control of polymerization can be assumed for **M-1** – **M-11** when upward curvature of the plot (M_n^{NMR} by the Z-group) occurs, pretending overly high molar mass polymers. Such polymers lost partly their Z-group functionality and are "dead", i.e., they cannot serve as macro-RAFT agents for the synthesis of block copolymers anymore. Therefore, polymerizations of **M-1** – **M-6**, **M-10**, and **M-11** were stopped at ~75 % conversion, and polymerizations of **M-7**, **M-8** and **M-9** at ~50 % conversion (**Figure 3.8** and **Figure A.42**). At high conversion, it is possible that the rate of exchange between the polymeric CTA and the propagating polymer chain may decrease faster than the rate of addition of the monomer to the propagating chain ($k_p > k_{addP}$, see **Figure 1.16d**).[85, 158] In this case, loss of control and increase of Đ will be observed.[158] However, in the regime before the upward curvature of the plot (molar mass versus conversion), the discrepancy between M_n^{theo} and M_n^{NMR} (Z- and R-group) is smaller than 10 %, indicating high end group functionality. Accordingly, the reactions were stopped after approximately 2 – 3 h. Note that for the polymerization of **M-4**, a marked discrepancy between theoretical and experimental molar masses are observed, which may be caused by the loss of low molar mass polymers during the purification step. Therefore, these data were not used for linear regression.

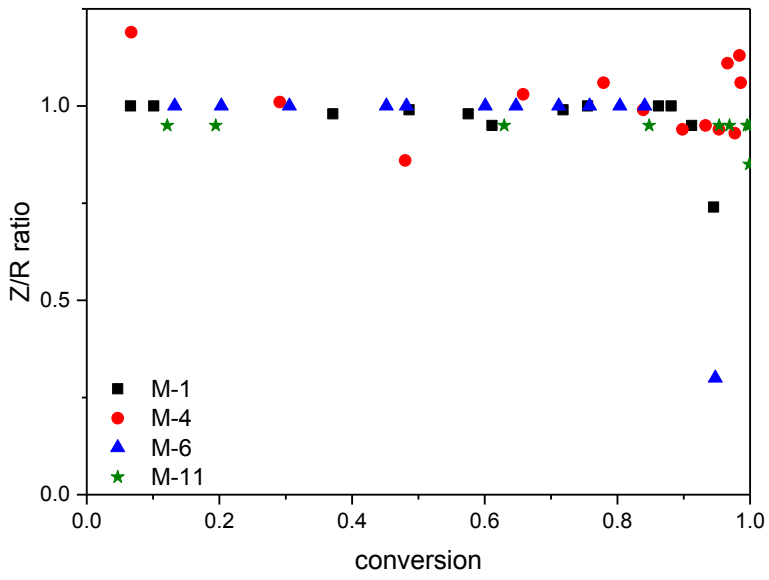

Figure 3.8. End group preservation in sulfobetaine polymerizations. **M-1** (■), **M-4** (●), **M-6** (▲), and **M-11** (★).

For molar mass determination via UV-vis spectroscopy, the R-group of **CTA-3** was used, with the $\varepsilon_{\lambda max3}$ in TFE, since high R-group preservation was confirmed. However, due to its marked sensitivity to its surroundings polarity, the ε value of the chromophore incorporated into the poly(sulfobetaine) cannot *a priori* be assumed to be equal (or at least close) to the value of ε determined for the isolated **CTA-3**, even if spectra are measured in the same solvent. In fact, a systematic difference in M_n^{NMR} (R-group) and $M_n^{UV\text{-}vis}$ is observed. Interestingly, small changes in chemical structure of the monomers have a very different impact on the extinction coefficient of the chromophore (see **Figure 3.7**), whereas, λ_{max3} remains generally unchanged. The discrepancy of M_n^{NMR} (R-group) and $M_n^{UV\text{-}vis}$ values is explained by the difference between local environments of the chromophore when either individually dissolved or bound to the polymer and thus being in the close neighborhood of the zwitterionic moieties. The corrected $\varepsilon_{\lambda max3}$ after incorporation into the polymer by a factor derived from ^{1}H NMR and UV-vis data of polymers with relatively low molar masses are shown in **Table 3.2**. The correction factors are in general higher for methacrylamide sulfobetaines (**M-1**, **M-2**, and **M-3**) than for methacrylate sulfobetaines. Polymers from **M-4** and **M-5** stronger affect ε than their analogs from **M-10** and **M-11**. Reproducible results of the kinetic experiments of sulfobetaines confirm the "controlled" character of the RAFT polymerizations by using **CTA-3**.

Table 3.2. Corrected extinction coefficient $\varepsilon_{\lambda max3}$ of **CTA-3** in TFE for molar mass determination via end group analysis by UV-vis spectroscopy.

monomers	ratio of $M_n^{UV\text{-}vis}$ and M_n^{NMR} (R-group) (correction factor)	corrected $\varepsilon_{\lambda max3}$ [10^4 L·mol^{-1}·cm^{-1}]	λ_{max3} [nm]
M-1	1.40	1.82	442
M-2	1.35	1.72	444
M-3	1.44	1.87	444
M-4	1.30	1.69	443
M-5	1.22	1.59	444
M-6	0.93	1.21	442
M-7	1.03	1.34	442
M-8	1.03	1.34	443
M-9	1.07	1.39	442
M-10	1.03	1.34	445
M-11	0.91	1.18	442
M-12	0.81	1.05	441

In conclusion, by restricting conversion to ~50 % or ~75 %, polymers with high end group preservation and well-defined molar masses can be obtained in TFE by the RAFT method. Note that reliable molar mass analysis of poly(sulfobetaine)s is generally cumbersome due to their tendency to aggregate. In particular, appropriate columns and eluents, let alone standards, for the characterization by GPC are generally not available. Therefore, molar masses of the end group labeled poly(sulfobetaine)s were determined via UV-vis spectroscopy by utilizing the appropriately corrected ε values.

3 KINETIC STUDIES OF RAFT POLYMERIZATIONS

4 Thermoresponsive poly(sulfobetaine)

4.1 Synthesis of the homopolymers

The homopolymers were synthesized by RAFT polymerization in TFE utilizing the azo initiator V-501 and the fluorophore functionalized trithiocarbonate **CTA-3** as RAFT agent.[85, 158] In order to modulate the molar masses, the ratio of monomer to **CTA-3** in the reaction mixtures was varied between 50 : 1 up to 600 : 1 (see **chapter 7.5**). According to the RAFT mechanism, the vast majority of the polymer chains starts with the R-residue of the **CTA-3** and is consequently labeled by the fluorophore.[139, 142] As signals due to the Z- and the R-groups can be resolved and quantified by both ^{1}H NMR (**Figure 4.1a**) and UV-vis (**Figure 4.1b**), they allow for the facile, rather precise and reliable determination of the number average molar mass of the homopolymers **poly(monomer)$_n$**. The results of the polymerizations are summarized in **Table 4.1** for the methacrylamide sulfobetaines, in **Table 4.2** for the methacrylate sulfobetaines, and in **Table 4.3** for the non-ionic monomers. The molar masses of the colored, fluorescent homopolymers increase linearly with decreasing amounts of **CTA** as expected for an efficient RAFT polymerization process.

Table 4.1. Analytical data for methacrylamide-based poly(sulfobetaine)s **poly(M-1)** – **poly(M-3)**. Conversions were determined by ^{1}H NMR analysis of the crude reaction mixtures.

sample		M_n [kg·mol^{-1}]				
	con-version	theo-retical	by ^{1}H NMR (via Z-group)	by ^{1}H NMR (via R-group)	by UV-vis (via R-group) [a]	ratio Z/R (NMR)
poly(M-1)$_{85}$ [c]	0.84	25	36	n.d. [b]	33 [e]	-
poly(M-1)$_{405}$ [c]	0.67	118	n.d. [b]	n.d. [b]	339 [e]	-
poly(M-1)$_{40}$ [d]	0.41	12	21	18	21 [e]	0.9
poly(M-1)$_{495}$ [d]	0.82	145	n.d. [b]	n.d. [b]	179 [e]	-
poly(M-1)$_{85}$	0.85	26	29	26	24	0.9
poly(M-1)$_{170}$	0.86	51	48	49	45	1.0
poly(M-1)$_{280}$	0.93	82	n.d. [b]	n.d. [b]	70	-
poly(M-1)$_{500}$	0.83	146	n.d. [b]	n.d. [b]	132	-
poly(M-2)$_{70}$	0.73	23	26	24	23	0.9
poly(M-2)$_{80}$	0.82	26	30	27	26	0.9
poly(M-2)$_{115}$	0.19	35	43	36	35	0.9
poly(M-2)$_{235}$	0.78	73	n.d. [b]	n.d. [b]	76	-
poly(M-2)$_{460}$	0.76	142	n.d. [b]	n.d. [b]	152	-
poly(M-2)$_{505}$	0.84	156	n.d. [b]	n.d. [b]	168	-
poly(M-3)$_{40}$	0.41	13	22	13	16	0.6
poly(M-3)$_{50}$	0.52	16	24	17	20	0.7
poly(M-3)$_{80}$	0.78	25	38	30	21	0.8
poly(M-3)$_{245}$	0.81	75	n.d. [b]	n.d. [b]	62	-
poly(M-3)$_{425}$	0.71	131	n.d. [b]	n.d. [b]	110	-

[a] calculated from sample weight, volume, absorbance at λ_{max3} in TFE, and the corrected extinction coefficients ε (**Table 3.2**). [b] signal intensity too weak to allow accurate integration. [c] using **CTA-1**. [d] using **CTA-2**. [e] using the uncorrected extinction coefficient of the Z-group derived in TFE (**Table 2.1**).

Table 4.2. Analytical data for methacrylate-based poly(sulfobetaine)s **poly(M-4)** – **poly(M-11)**. Conversions were determined by ^{1}H NMR analysis of the crude reaction mixtures.

sample		M_n [kg·mol^{-1}]				
	con-version	theo-retical	by ^{1}H NMR (via Z-group)	by ^{1}H NMR (via R-group)	by UV-vis (via R-group) [a]	ratio Z/R (NMR)
poly(M-4)$_{85}$	0.86	25	29	26	31	0.9
poly(M-4)$_{270}$	0.90	76	n.d. [b]	n.d. [b]	88	-
poly(M-4)$_{575}$	0.95	161	n.d. [b]	n.d. [b]	160	-
poly(M-4)$_{585}$	0.97	164	n.d. [b]	n.d. [b]	179	-
poly(M-5)$_{50}$	0.94	14	22	16	14	0.7
poly(M-5)$_{80}$	0.96	23	35	26	24	0.7
poly(M-5)$_{95}$	0.94	28	43	32	29	0.7
poly(M-5)$_{280}$	0.94	83	n.d. [b]	n.d. [b]	83	-
poly(M-6)$_{95}$	0.94	30	104	26	27	0.3
poly(M-6)$_{250}$	0.42	78	111	125	136	0.9
poly(M-6)$_{330}$	0.83	103	n.d. [b]	n.d. [b]	100	-
poly(M-6)$_{485}$	0.81	151	n.d. [b]	n.d. [b]	145	-
poly(M-7)$_{80}$	0.82	28	32	29	24	0.9
poly(M-7)$_{250}$	0.83	84	93	85	73	0.9
poly(M-7)$_{420}$	0.84	141	n.d. [b]	n.d. [b]	120	-
poly(M-7)$_{500}$	0.83	167	n.d. [b]	n.d. [b]	141	-
poly(M-8)$_{65}$	0.66	22	41	28	27	0.7
poly(M-8)$_{95}$	0.96	32	35	35	35	1.0
poly(M-8)$_{230}$	0.77	75	n.d. [b]	n.d. [b]	109	-
poly(M-8)$_{585}$	0.97	188	n.d. [b]	n.d. [b]	197	-
poly(M-9)$_{85}$	0.86	30	30	30	27	1.0
poly(M-9)$_{260}$	0.86	87	96	86	87	0.9
poly(M-9)$_{430}$	0.86	145	n.d. [b]	n.d. [b]	147	-
poly(M-9)$_{520}$	0.86	175	n.d. [b]	n.d. [b]	181	-

sample	M_n [kg·mol^{-1}]					
	con-version	theo-retical	by ^{1}H NMR (via Z-group)	by ^{1}H NMR (via R-group)	by UV-vis (via R-group) [a]	ratio Z/R (NMR)
poly(M-10)$_{75}$	0.75	23	24	24	23	1.0
poly(M-10)$_{295}$	0.98	87	n.d. [b]	n.d. [b]	74	-
poly(M-10)$_{480}$	0.96	141	n.d. [b]	n.d. [b]	145	-
poly(M-10)$_{585}$	0.97	172	n.d. [b]	n.d. [b]	185	-
poly(M-11)$_{100}$	0.99	31	37	31	33	0.9
poly(M-11)$_{290}$	0.97	90	n.d. [b]	n.d. [b]	88	-
poly(M-11)$_{480}$	0.96	148	n.d. [b]	n.d. [b]	155	-
poly(M-11)$_{540}$	0.89	166	n.d. [b]	n.d. [b]	160	-

[a] calculated from sample weight, volume, absorbance at λ_{max3} in TFE, and the corrected extinction coefficients ε (**Table 3.2**). [b] signal intensity too weak to allow accurate integration.

The ^{1}H NMR characterization of the homopolymers did not reveal anything unusual concerning the polymers' molecular structure, showing the typical signal broadening (see, e.g., **Figure 4.1a**). The spectrum indicates the presence of end groups derived from the RAFT agent, and the absence of residual monomer. The signals between 0.5 and 1.5 ppm, originating from the methyl groups attached to the polymer backbone, provide information on the polymer tacticity.[164] Their integration indicates identical tacticities for all samples, with about 60 – 65 % of syndiotactic, 30 – 35 % of atactic, and < 5 % of isotactic triades. This result is typical for the free radical polymerization of methacrylates at 75 °C, in spite of the use of a fluorinated alcohol as reaction medium.[165-167]

Table 4.3. Analytical data for polymers of **M-12** ("**NIPMAM**") and **M-13** ("**NIPAM**"). Conversions were determined by ^{1}H NMR analysis of the crude reaction mixtures.

sample		M_n [kg·mol^{-1}]						
	con-version	theo-retical	by ^{1}H NMR (via Z-group)	by ^{1}H NMR (via R-group)	by UV-vis (via R-group) [a]	by GPC	Đ	ratio Z/R (NMR)
poly(M-12)$_{180}$ [c]	0.46	23	26	n.d. [b]	21 [d]	18	1.3	-
poly(M-12)$_{40}$	0.40	6	5	4	5	3	1.2	1.0
poly(M-12)$_{45}$	0.45	6	6	6	6	4	1.2	1.0
poly(M-12)$_{65}$	0.60	9	10	9	9	5	1.3	0.8
poly(M-12)$_{195}$	0.48	25	28	25	29	20	1.3	0.9
poly(M-13)$_{195}$	0.96	24	n.d. [b]	n.d. [b]	36 [e]	24	1.5	-

[a] calculated from sample weight, volume, absorbance at λ_{max3} in TFE, and the corrected extinction coefficients ε (**Table 3.2**). [b] signal intensity too weak to allow reliable integration. [c] using **CTA-1**. [d] using the uncorrected extinction coefficient ε of the Z-group derived in TFE (**Table 2.1**). [e] using the uncorrected ε of the chromophore derived in TFE (**Table 2.1**). GPC in DMF + 0.1 % LiBr and PMMA standard.

The ^{1}H NMR data indicate also good agreement between the theoretically expected molar masses M_n^{theo} and the experimental M_n^{NMR} values determined by end group analysis up to 50,000 Da (corresponding to $n \leq 200$). Importantly, the ratio between the Z- and R-groups found is close to 1.0, corroborating that the polymerization process is well controlled and that the active end groups were mostly retained, albeit some losses may occur. Except for **poly(M-6)$_{95}$**, the ratio found is 0.3, indicating the loss of control over polymerization and the high loss of the Z-group functionality, which is possibly caused by irreversible terminations through intrusion of O_2. For higher molar masses, ^{1}H NMR end group analysis becomes increasingly imprecise due to the small number of end groups to be quantified and the increasingly poor signal-to-noise ratio (**Figure A.23**). Additionally, ^{1}H NMR measurements of exemplarily **poly(M-1)$_{85}$** and **poly(M-1)$_{500}$** in trifluoroethanol-d_3 instead of in D_2O provide the same results. Thus, the intense signal of the

naphthalimide chromophore in UV-vis spectra (exemplarily **Figure 4.1b**) was used with better sensitivity and precision.

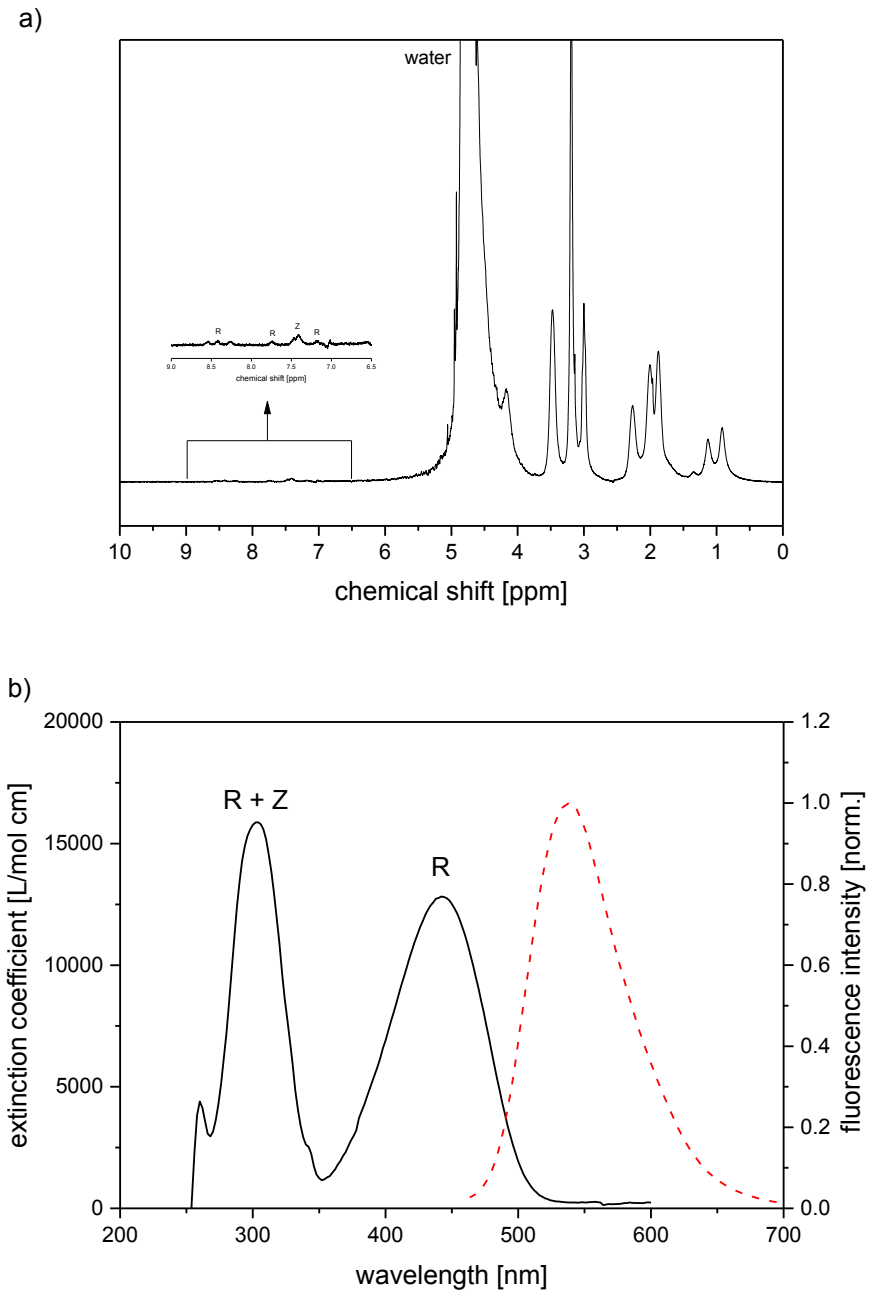

Figure 4.1. Resolved Z- and R-groups of **poly(M-11)$_{100}$**. a) ^{1}H NMR spectrum in dilute aqueous NaCl (0.9 g·L^{-1}) in D_2O, inset shows signals of the Z- and R-groups between 6.5 and 9.0 ppm. b) absorbance (——) and fluorescence emission spectra (------) in TFE, excitation at 442 nm. "R" indicates the absorbance bands of the naphthalimide chromophore; "Z" indicates the absorbance band of the trithiocarbonate moiety.

Introduced via the R-group of the RAFT agent, the fluorophore is stably attached to the polymers. By utilizing the corrected $\varepsilon_{\lambda max3}$ in TFE of **CTA-3**, theoretically expected and observed molar masses even for the high molar mass samples up to 180,000 Da are in good agreement (**Table 4.1** – **4.3**), as typical for a well-behaved RAFT polymerization. Note also that the polymers in spite the presence of the thiocarbonyl quencher group[168, 169] are all strongly fluorescent by virtue of the 4-dimethylaminonaphthalimide end group.

Concerning thermal properties, thermogravimetric analysis (TGA) of the poly(sulfobetaine)s and **poly(M-12)** shows the onset of decomposition accompanied by mass loss at ~300 °C, the onset is found at ~380 °C in the case of **poly(M-13)$_{195}$**. Differential scanning calorimetry (DSC) measurement shows no thermal transition for any of the poly(sulfobetaine)s before degradation starts, in agreement with reports on many poly(sulfobetaine)s.[29, 95] DSC of **poly(M-12)** shows a thermal transition at ~175 °C (glass-transition temperature: T_g) and DSC of **poly(M-13)$_{195}$** shows thermal transition at about 130 °C (T_g).

4.2 Aqueous solution behavior of poly(sulfobetaine)s

Solubility of poly(sulfobetaine)s in water as well as in deuterated water is complex, showing a miscibility gap, with an UCST-type phase transition (**Table 4.4**). In the turbidimetric studies of solutions of **poly(M-1)** to **poly(M-11)** in both H_2O and D_2O, the clouding transitions were all sharp and curves were highly reproducible (see in the appendix **Figure A.43**). The hysteresis between the UCST-type transitions for heating and cooling runs was marginal (≤ 1 °C). Accordingly, the binodal and spinodal lines of the poly(sulfobetaine)/water phase diagram coincide virtually. Turbidimetric curves of the methacrylamide-based (**poly(M-1)** – **poly(M-3)**) and methacrylate-based poly(sulfobetaine)s (**poly(M-4)** – **poly(M-11)**) in both H_2O and D_2O are shown in the appendix (**Figure A.44** – **A.45**). **Table 4.4** summarizes the derived UCST-type transition temperatures. Control experiment were performed with samples made with the unlabeled RAFT agent **CTA-1** and **CTA-2**, thus producing polymers bearing a carboxyl group or a 4-methoxybenzyl instead of the bulky aromatic (2-(naphthalimido)ethyl) end group. The UCST-type transition temperatures of these non-labeled polymers are a few degrees higher than the ones of their labeled analogs (**Table 4.4**). Accordingly, the transition temperatures are only moderately influenced by the nature of the end groups, though their influence is not negligible. These findings suggest that the chromophore somehow hinders the polymer chains from collapsing, and thus lowering the UCST-type transition temperature.

Table 4.4. UCST-type transition of 5 wt% aqueous solutions of the poly(sulfobetaine) series **poly(M-1)** to **poly(M-11)**.

sample	UCST-type transition [°C]		sample	UCST-type transition [°C]	
	in H_2O	in D_2O		in H_2O	in D_2O
poly(M-1)$_{85}$ [a]	11	18	**poly(M-6)$_{95}$**	<0	<0
poly(M-1)$_{405}$ [a]	30	37	**poly(M-6)$_{250}$**	<0	<0
poly(M-1)$_{40}$ [b]	<0	9	**poly(M-6)$_{330}$**	<0	<0
poly(M-1)$_{495}$ [b]	30	38	**poly(M-6)$_{485}$**	<0	<0
poly(M-1)$_{85}$	9	15	**poly(M-7)$_{80}$**	<0	17
poly(M-1)$_{170}$	11	19	**poly(M-7)$_{250}$**	4	28
poly(M-1)$_{280}$	14	21	**poly(M-7)$_{420}$**	11	36
poly(M-1)$_{500}$	26	32	**poly(M-7)$_{500}$**	15	40
poly(M-2)$_{70}$	<0	17	**poly(M-8)$_{65}$**	<0	17
poly(M-2)$_{80}$	6	18	**poly(M-8)$_{95}$**	24	34
poly(M-2)$_{115}$	10	25	**poly(M-8)$_{230}$**	38	48
poly(M-2)$_{235}$	13	30	**poly(M-8)$_{585}$**	47	56
poly(M-2)$_{460}$	22	38	**poly(M-9)$_{85}$**	70	75
poly(M-2)$_{505}$	34	51	**poly(M-9)$_{260}$**	88	94
poly(M-3)$_{40}$	60	66	**poly(M-9)$_{430}$**	>100	>100
poly(M-3)$_{50}$	67	76	**poly(M-9)$_{520}$**	>100	>100
poly(M-3)$_{80}$	74	78	**poly(M-10)$_{75}$**	<0	7
poly(M-3)$_{245}$	>100	>100	**poly(M-10)$_{295}$**	5	14
poly(M-3)$_{425}$	>100	>100	**poly(M-10)$_{480}$**	8	18
poly(M-4)$_{85}$	41	50	**poly(M-10)$_{585}$**	10	20
poly(M-4)$_{270}$	55	68	**poly(M-11)$_{100}$**	41	47
poly(M-4)$_{575}$	67	80	**poly(M-11)$_{290}$**	>100	>100
poly(M-4)$_{585}$	71	86	**poly(M-11)$_{480}$**	>100	>100
poly(M-5)$_{50}$	82	94	**poly(M-11)$_{540}$**	>100	>100
poly(M-5)$_{80}$	>100	>100			
poly(M-5)$_{95}$	>100	>100			
poly(M-5)$_{280}$	>100	>100			

[a] using **CTA-1**. [b] using **CTA-2**.

Furthermore, turbidity and DLS measurements are in good agreement indicating similar UCST-type transition temperatures, exemplarily, illustrated for **poly(M-3)$_{80}$** in **Figure 4.2** (more DLS measurements are shown in the appendix **Figure A.46** – **A.47**). Below the UCST-type transition, the poly(sulfobetaine) forms aggregates of > 1 µm and thus the transmittance is < 5 %. Whereas, above the UCST-type transition, the poly(sulfobetaine) is dissolved and therefore the transmittance strongly increases (≥ 90 %). However, the DLS result (~450 nm, which is markedly higher than the contour length) suggests that above the UCST-type transition, polymer chains are not individually dissolved possibly due to entanglement.

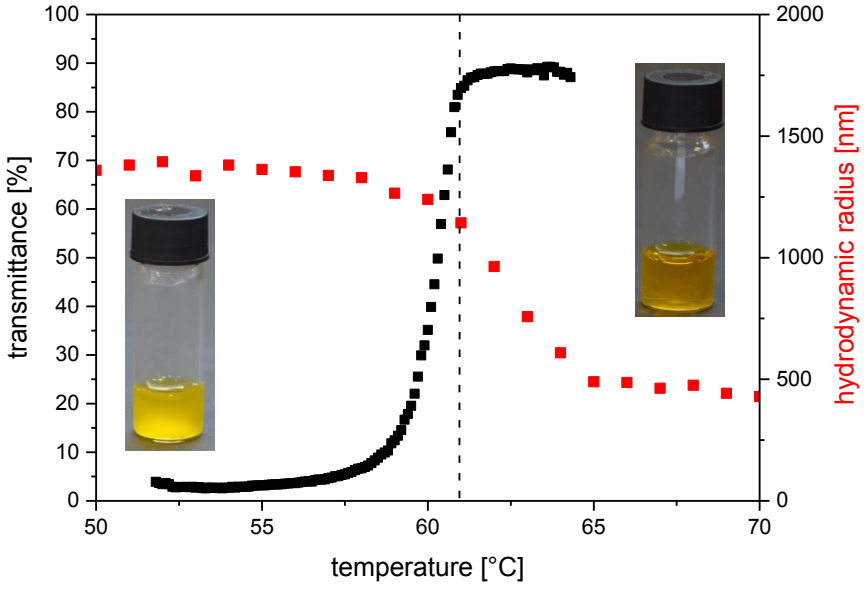

Figure 4.2. Turbidity and DLS measurements (cooling runs) of 1 wt% solutions in H_2O of **poly(M-3)$_{80}$**.

4.2.1 Methacrylamide-based poly(sulfobetaine)s

First of all, the UCST-type transition temperatures are much higher for **poly(M-3)** than for **poly(M-1)** and **poly(M-2)**, as anticipated. While the **poly(M-1)** and **poly(M-2)** samples with the lowest molar mass are fully soluble in H_2O, the **poly(M-3)** samples with the highest molar masses are no more soluble in H_2O at all. Still, as a common feature, the UCST-type transition temperatures increase monotonously with molar mass for the polymers in H_2O as well as in D_2O. Also, the UCST-type transition temperatures increase with concentration at least up to 50 $g \cdot L^{-1}$, apparently approaching asymptotically a maximum value. The concentration dependent evolution of UCST-type transition temperatures of selected polymers is shown in **Figure 4.3** (see in the appendix for more examples **Figure A.48**).

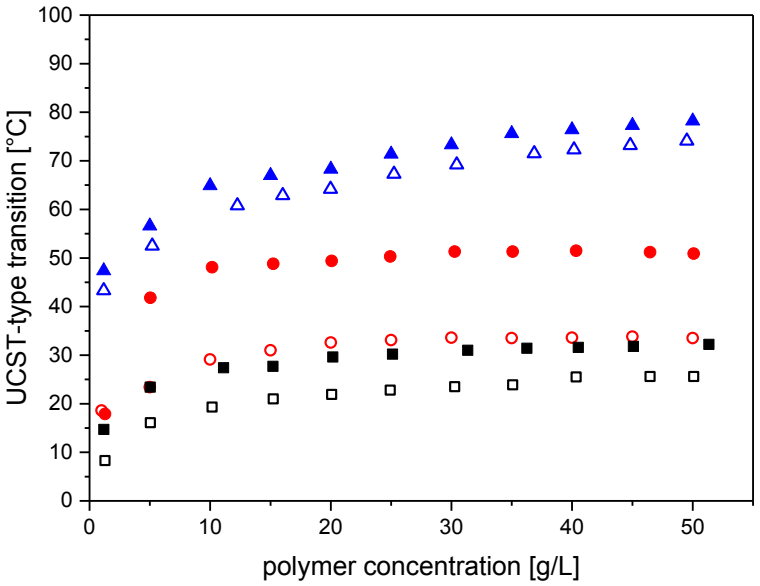

Figure 4.3. Concentration dependent evolution of UCST-type transition temperatures in aqueous solution of **poly(M-1)$_{500}$**: (▫) = in H_2O and (▪) = in D_2O, **poly(M-2)$_{505}$**: (○) = in H_2O and (●) = in D_2O, and **poly(M-3)$_{80}$**: (△) = in H_2O and (▲) = in D_2O.

The UCST-type transition temperature of a given sample is markedly higher in heavy water (D_2O) than in normal water (H_2O). The differences are in the range of

about 6 °C in the case of **poly(M-1)**, which corresponds closely to the behavior of **poly(M-3)**, and of about 15 °C in the case of **poly(M-2)**. This pronounced H-D-effect exceeds by far the analogous effect for the LCST-type coil-to-globule transition of, e.g., poly(N-isopropylacrylamide), that is in the range of 1 °C at most.[170, 171] The marked H-D-effect implies that the results of studies of these poly(sulfobetaine)s performed in D_2O, as e.g. characteristic for many ^1H NMR or neutron scattering studies, may not be directly transferable to their behavior in "normal" aqueous systems.

The reasons for the strong H-D-effect are not clear at present. Still, the strength of the observed effect as well as the finding, that effects are similarly strong for the sulfobetaine homologues **poly(M-1)** and **poly(M-3)**, while they are much stronger for the analogue **poly(M-2)** bearing an additional hydroxyl group (**Figure 4.4**), suggest a major role of hydrogen bonding for the effective hydration of the poly(sulfobetaine)s. Interestingly, similarly marked H-D-effects were reported for blends of poly(acrylamide) and poly(acrylic acid), or copolymers of acrylamide and acrylonitrile, both showing also UCST-type behavior in aqueous solution.[172, 173] Cooperative complementary hydrogen bonding between the different polymer segments has been evoked as explanation, which obviously cannot apply in our case. In any case, a major role of hydrogen bonding to provoke the strong H-D-effects is also consistent with the finding, that the UCST-type transition temperatures of the **poly(M-2)** series (**Table 4.4**) are the same (in H_2O) or even higher (in D_2O) than of the ones of the **poly(M-1)** series, albeit *a priori*, the additional hydrophilic hydroxyl group would have been expected to lower the UCST-type transition temperatures somewhat. In contrast, the UCST-type transition temperatures of the **poly(M-3)** series are much higher than for **poly(M-1)**, as may have been intuitively anticipated due to the longer, and thus more hydrophobic alkyl spacer group between the cationic and the anionic groups (**Figure 4.4**). The latter finding is in full agreement with a recent report on the behavior of poly(acrylamide) analogs of **poly(M-1)** and **poly(M-3)**.[93]

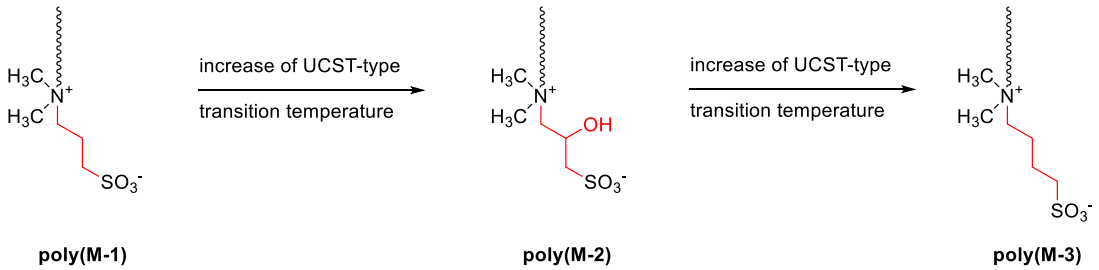

Figure 4.4. Variation of spacer group separating the cationic and anionic moiety. Schematic illustration of **poly(M-1)**, **poly(M-2)**, and **poly(M-3)**.

Control experiments were performed with samples made with **CTA-1** and **CTA-2**, thus producing polymers bearing a carboxyl or phenyl group instead of the bulky naphthalimide end group. The UCST-type transition temperatures of these polymers are higher than the ones of their fluorophore-labeled analogs (**Table 4.4**). Accordingly, the clouding transition temperatures are influenced by the nature of the end groups, though their influence is not negligible. Importantly, the UCST-type transition temperatures of the "non-fluorophore-labeled" polymers varied in the same range in H_2O and in D_2O as for the fluorophore-labeled polymers. Therefore, the H-D-effect cannot be caused by the incorporation of the fluorophore.

The UCST-type phase transition behavior of poly(sulfobetaine)s in aqueous media is known to be very sensitive to the presence of additives, in particular of inorganic salts. Not only the amount or the ionic strength of added salt is important, but also the precise nature of the ions added, in particular the nature of the anion.[28, 121, 174, 175] Therefore, the influence of selected salts on the UCST-type transition temperatures of **poly(M-1)** – **poly(M-3)** in aqueous solutions was also studied. The evolution of UCST-type transition temperatures in H_2O containing inorganic salts (NaCl, NaBr, Na_2SO_4, and $(NH_4)_2SO_4$) of selected polymers is shown in **Figure 4.5** (see in the appendix for more examples **Figure A.49** – **A.51**).

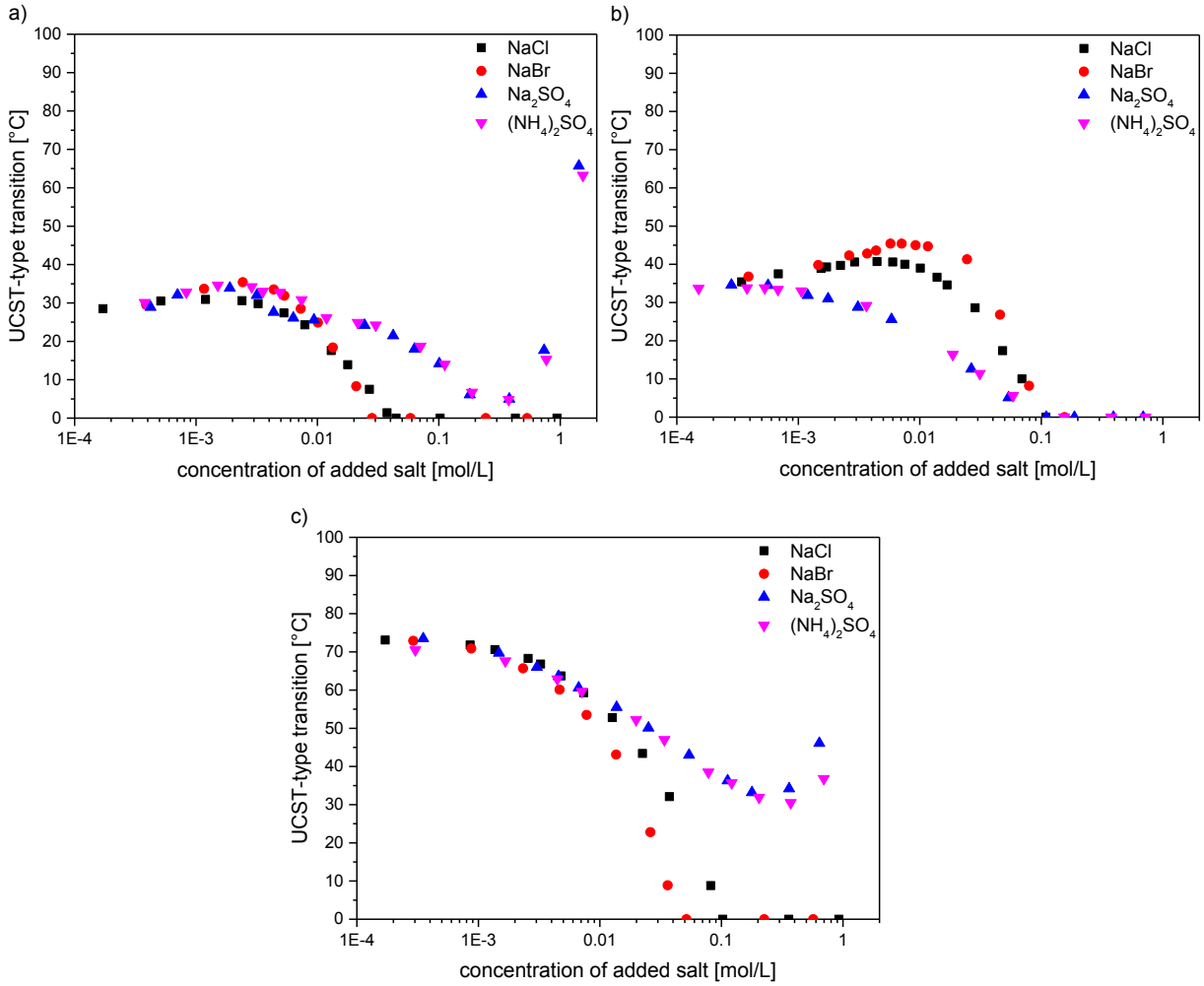

Figure 4.5. Evolution of UCST-type transition temperatures in 5 wt% H_2O containing inorganic salts of a) **poly(M-1)$_{500}$**, b) **poly(M-2)$_{505}$**, and c) **poly(M-3)$_{80}$**. (■) = NaCl, (●) = NaBr, (▲) = Na_2SO_4, and (▼) = $(NH_4)_2SO_4$.

When adding salt to aqueous solutions of **poly(M-1)** and **poly(M-2)** (**Figure 4.5a-b**), the UCST-type transition temperatures evolve in many respects with a similar pattern as observed for polyzwitterions bearing the ammoniopropanesulfonate moiety.[28, 174] Already small amounts of salt have a big impact, and their efficiencies vary markedly with the nature of the anion. While the difference between the cations Na^+ and NH_4^+ for a given anion is small. Still, the addition of salt does not lead automatically to a general "salting-in" effect as often assumed. Instead, the UCST-type transition temperatures increase first, when small amounts of salt are added, and pass through a maximum, before they decrease finally to below freezing point when salt concentrations reach the 100 mM range. This remarkable effect might have been missed in the past for other polymeric

ammoniopropanesulfonates, because these polymers tend to adsorb strongly inorganic salts up to stoichiometric amounts, once they have been exposed to them.[29, 176] However, the absence of contaminating inorganic salts, which possibly accumulate during synthesis and handling of such polymers, has been rarely verified before studying UCST-type transition temperatures. In fact, small contaminations by inorganic salt might be the reason for at least some of the apparently conflicting data on the phase transition temperatures of certain poly(sulfobetaine)s such as "**poly(SPE)**" in the literature.[28, 174, 177, 178]

A striking feature of the salt effects observed for the solutions of **poly(M-2)** is however, that the effectiveness of the anions correlates inversely with the empirical Hofmeister series,[88, 89, 124] namely, salting-in effectiveness increases in the order $Br^- < Cl^- < SO_4^{2-}$. This behavior is opposite to the order of **poly(M-1)** and to all previous findings for poly(sulfobetaine)s, such as "**poly(SPE)**" or analogues.[28, 30, 119, 121, 126, 174, 179] The reasons are not clear at present, but obviously, the hydroxyl group in the spacer separating the ammonium and the sulfonate moieties must affect the electrostatic interactions between the ionic groups. Possibly, an intramolecular hydrogen bond is formed between the hydroxyl and the sulfonate moieties, thus changing the ability of the latter to interact with the ammonium group.

Interestingly, the UCST-type transition temperatures evolve even differently for aqueous solutions of **poly(M-3)** (**Figure 4.5c**) in comparison to **poly(M-1)** when adding salt. Again small amounts of salt make a big impact, and their efficiencies increase in the Hofmeister anion series as $SO_4^{2-} < Cl^- < Br^-$. However, the UCST-type transition temperatures decrease continuously from the very first addition on, when NaCl or NaBr are added, and do not pass through a maximum. Increasing concentrations of Na_2SO_4 or $(NH_4)_2SO_4$ decrease the UCST-type transition temperature first, then make it pass through a minimum in the lower 100 mM range, before they make the UCST-type transition temperature slowly rise again above about 300 mM. Such a minimum of the UCST-type transition temperature at intermediate to high concentrations of sulfates is also observed for **poly(M-1)**. Additionally, salting-in and salting-out effects are independent from the molar mass as well as from the H-D-effect.

4.2.2 Methacrylate-based poly(sulfobetaine)s

Similar to the findings of **poly(M-1)** – **poly(M-3)**, UCST-type transition temperatures of methacrylate-based poly(sulfobetaine)s increase with molar mass and polymer concentration in H_2O as well as in D_2O (**Table 4.4**). The concentration dependent evolution of UCST-type transition temperatures of selected polymers is shown in **Figure 4.6** (see in the appendix for more examples **Figure A.52**). Moreover, the pronounced H-D-effect of UCST-type transition temperatures is also observed for the methacrylate-based poly(sulfobetaine)s. The differences are in the range of about 6 °C in the case of **poly(M-9)** and **poly(M-11)** and of about 10 °C in the case of **poly(M-4)**, **poly(M-5)**, **poly(M-8)**, and **poly(M-10)**, which correspond somehow to the behavior of **poly(M-1)** and **poly(M-3)**. The highest and remarkable differences of about 25 °C are obtained in the case of **poly(M-7)**, bearing a piperidine ring. This may indicate an influence of a sterically demanding substituent on the ammonium group on the H-D-effect. But in contrast, this H-D-effect is much stronger compared to **poly(M-8)** and **poly(M-9)**, which bear a similarly sterically demanding morpholine ring. These results show that reasons for the strength of the H-D-effect must be rather complex, though not clear at present.

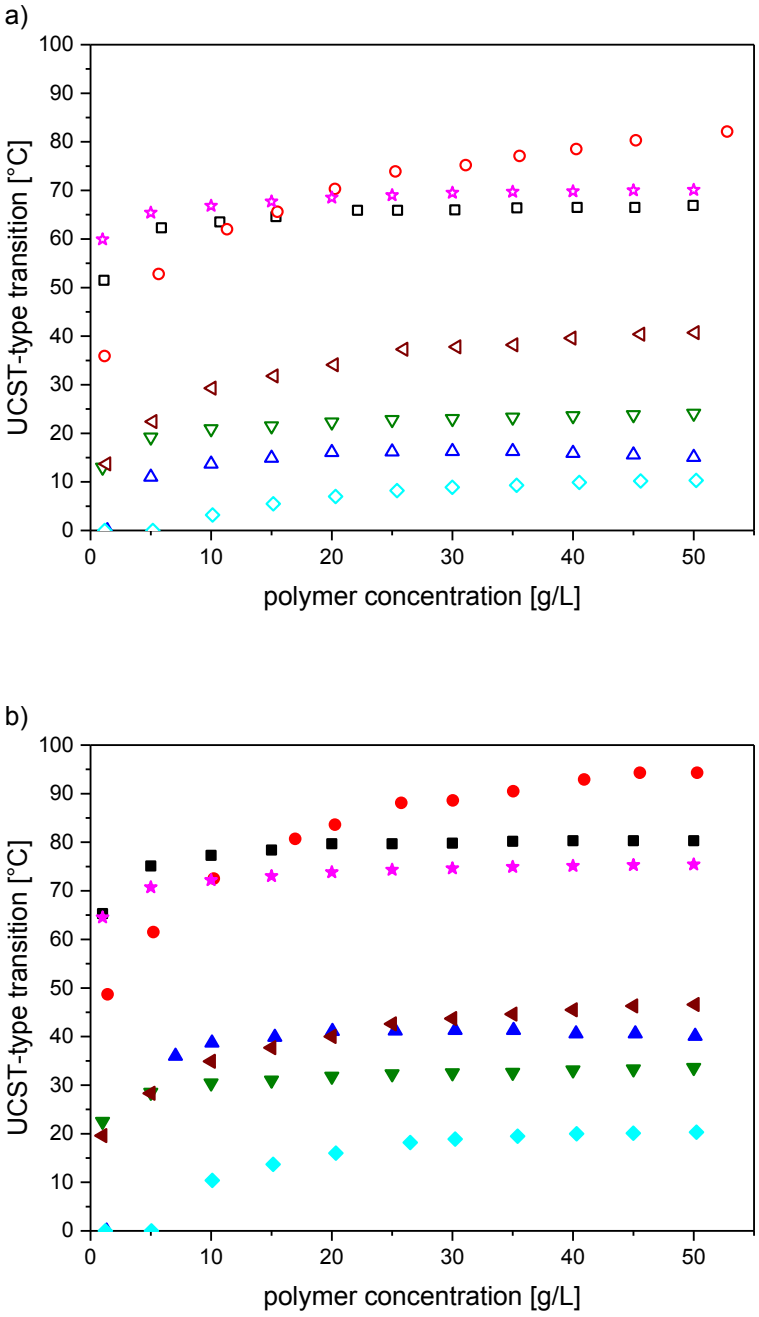

Figure 4.6. Concentration dependent evolution of UCST-type transition temperatures in a) H_2O (open symbols) and b) D_2O (close symbols) of **poly(M-4)$_{575}$** (▫, ▪), **poly(M-5)$_{50}$** (○, ●), **poly(M-7)$_{500}$** (△, ▲), **poly(M-8)$_{95}$** (▽, ▼), **poly(M-9)$_{85}$** (☆, ★), **poly(M-10)$_{585}$** (◇, ◆), and **poly(M-11)$_{100}$** (◁, ◀). The phase transition of **poly(M-6)** in H_2O and D_2O is below 0 °C.

The UCST-type transition temperatures are much higher for polymeric ammoniobutanesulfonates than for polymeric ammoniopropanesulfonates, as already found for the methacrylamide-based poly(sulfobetaine)s, clearly **poly(M-4)** < **poly(M-5)**, **poly(M-6)** < **poly(M-7)**, **poly(M-8)** < **poly(M-9)**, and **poly(M-10)** < **poly(M-11)**. Interestingly, **poly(M-6)** samples are fully soluble in H_2O as well as in D_2O, even for samples with the highest molar mass. Samples of **poly(M-7)**, **poly(M-8)**, and **poly(M-10)** with the lowest molar mass are also fully soluble in H_2O. In contrast, samples of **poly(M-5)**, **poly(M-9)**, and **poly(M-11)** with high molar masses are no more soluble in H_2O at all.

Interestingly, the type of substituent on the ammonium group shows a marked effect on the UCST-type transition temperatures. Comparing the **poly(M-4)** – **poly(M-9)** series, transition temperatures decrease in the order dimethyl > morpholine > piperidine (**Figure 4.7**). In other words, increasing the steric hindrance of the ammonium group decreases the UCST-type transition temperature, which is in agreement with the reports by Monroy Soto et al.[94, 121] However, the polymers with the morpholine ring were expected to show lower UCST-type transition temperatures than the polymers with the more hydrophobic piperidine ring, in contradiction to the results. This surprising finding correlates with the strength of the H-D-effect. Obviously, the oxygen of the morpholine ring must be responsible for the counterintuitive increase of the phase transition temperature. In the morpholine ring, it is assumed that the positive charge is more localized neighboring to the nitrogen, due to the stronger inductive effect (-I-effect) of the oxygen compared to the nitrogen. This possibly enables stronger interactions between the ammonium and the sulfonate moieties. Thus, the polymers bearing the morpholine ring show higher UCST-type transition temperatures than the polymers, in which the positive charge can be additionally delocalized in the whole piperidine ring.

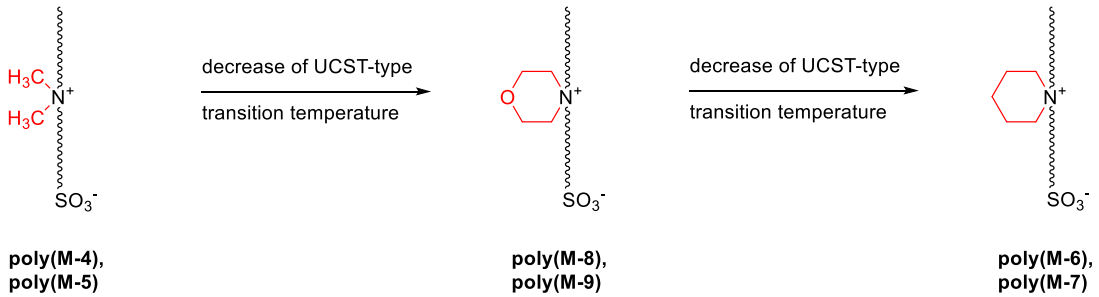

Figure 4.7. Variation of type of substituents on the ammonium group. Schematic illustration of **poly(M-4)** – **poly(M-9)**.

Furthermore, the distance between the polymer backbone and the ammonium group shows also a remarkable effect on the phase transition temperature. The UCST-type transition temperatures decrease by about 60 °C after extending the distance from 2 to 3 methylene units (**Figure 4.8**), by comparing the series of **poly(M-4)** and **poly(M-5)** with the series of **poly(M-10)** and **poly(M-11)**. This finding is consistent with the results discussed for the type of the substituent on the ammonium group and shows the same trend as reported for acrylate-based poly(sulfobetaine)s with 11 methylene units between the polymer backbone and ammonium group.[96] In any case, this effect may indicate that the mobility of the side chain affects the UCST-type transition temperatures. Possibly, the increase of the mobility and the steric hindrance of the zwitterionic side chain result in a weaker coulombic interaction between the ammonium and the sulfonate moieties, and therefore lead to lower UCST-type transition temperatures.

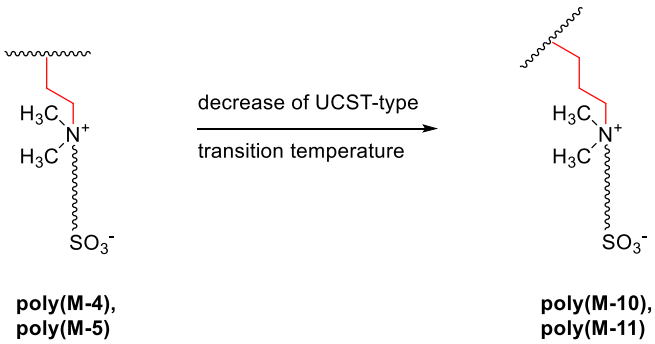

Figure 4.8. Variation of the distance between the polymer backbone and the ammonium group. Schematic illustration of **poly(M-4)**, **poly(M-5)**, **poly(M-10)**, and **poly(M-11)**.

The effect of inorganic salts was also investigated for the methacrylate-based poly(sulfobetaine)s. The evolution of UCST-type transition temperatures in H_2O containing NaCl, NaBr, Na_2SO_4, and $(NH_4)_2SO_4$ of selected polymers is shown in **Figure 4.9** (see in the appendix for more examples **Figure A.53** – **A.57**). The UCST-type transition temperatures of **poly(M-4)**, **poly(M-5)**, **poly(M-7)**, **poly(M-10)**, and **poly(M-11)** evolve with a similar pattern as observed for the methacrylamide-based **poly(M-3)**. UCST-type transition temperatures of **poly(M-8)** and **poly(M-9)** (bearing the morpholine ring) evolve similarly as found for **poly(M-1)**, when adding salts to the aqueous solutions. As a common feature, already small amounts of added salt make a big impact, and efficiencies depend notably on the nature of the anion as $SO_4^{2-} < Cl^- < Br^-$, following the empirical Hofmeister anion series. Again, the difference between the cations Na^+ and NH_4^+ for a given anion (SO_4^{2-}) is small. According to a "**poly(M-3)**-behavior", the UCST-type transition temperatures decrease continuously below freezing point after addition of NaCl or NaBr. In contrast, increasing concentrations of Na_2SO_4 or $(NH_4)_2SO_4$ decrease the UCST-type transition temperature first, then make it pass through a minimum at ~300 mM, before they make the UCST-type transition temperature rise again. Interestingly, the increase of UCST-type transition temperatures at high Na_2SO_4 or $(NH_4)_2SO_4$ concentration is not observed for **poly(M-10)**, but it is observed for **poly(M-11)** of high molar masses. In the case of **poly(M-8)** and **poly(M-9)**, the UCST-type transition temperatures increase first and pass through a maximum when salt concentration reach the 100 mM range. Afterwards, increasing the salt concentration above the 100 mM range, UCST-type transition temperatures of **poly(M-8)** and **poly(M-9)** decrease below freezing point (for NaCl and NaBr) or pass through a minimum at ~300 mM (for Na_2SO_4 and $(NH_4)_2SO_4$), as also observed for **poly(M-1)**.

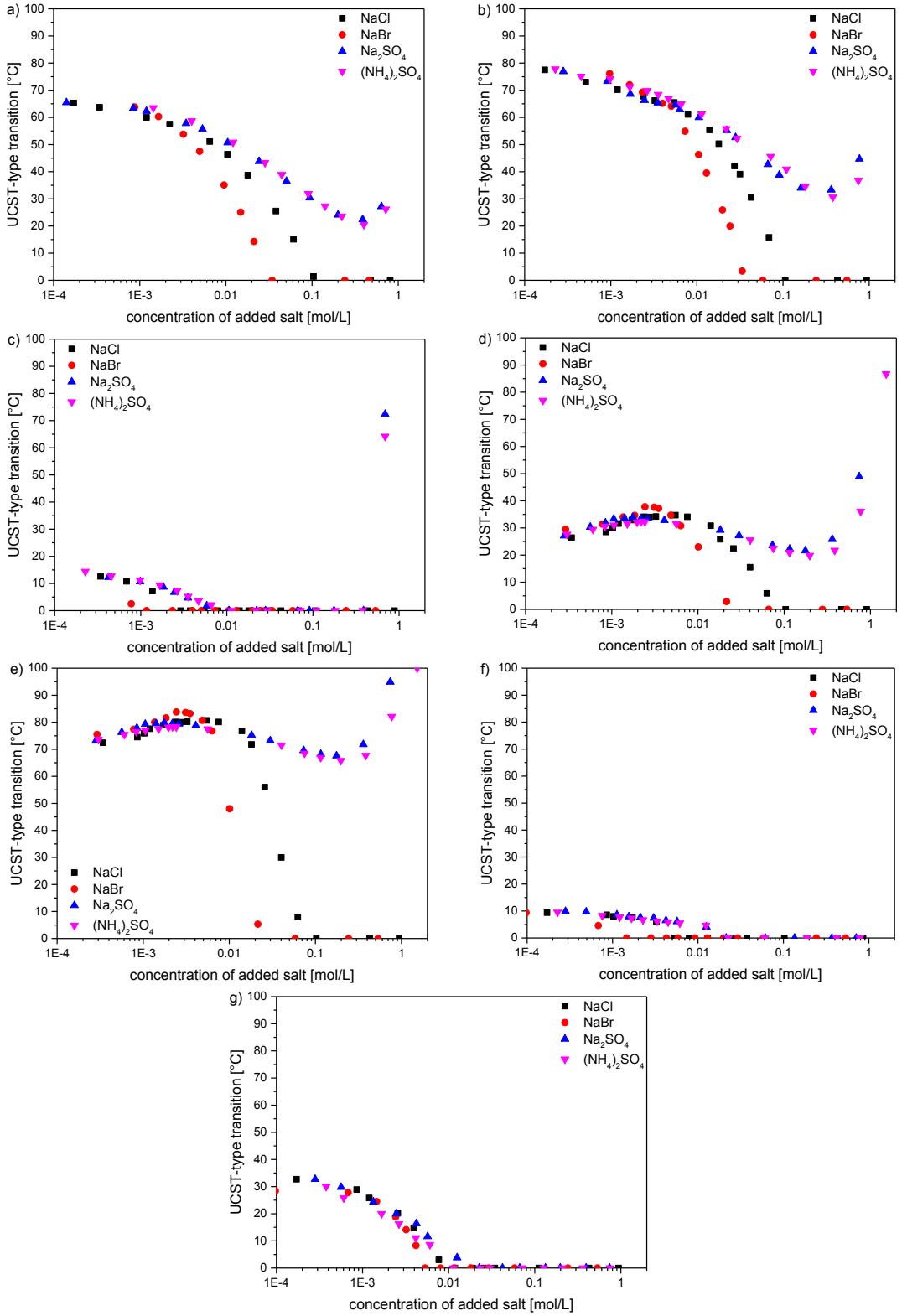

Figure 4.9. Evolution of UCST-type transition temperatures in 5 wt% H_2O containing inorganic salts of a) **poly(M-4)$_{575}$**, b) **poly(M-5)$_{50}$**, c) **poly(M-7)$_{500}$**, d) **poly(M-8)$_{95}$**, e) **poly(M-9)$_{85}$**, f) **poly(M-10)$_{585}$**, and g) **poly(M-11)$_{100}$**. The phase transition of **poly(M-6)** in H_2O and D_2O is below 0 °C. (■) = NaCl, (●) = NaBr, (▲) = Na_2SO_4, and (▼) = $(NH_4)_2SO_4$.

4.2.3 Relation between chemical structure and phase transition behavior

The UCST-type transition temperatures depend sensitively on the precise chemical structure of the poly(sulfobetaine)s. An order of poly(sulfobetaine)s according to their UCST-type transition temperature in H_2O is shown in **Figure 4.10**.

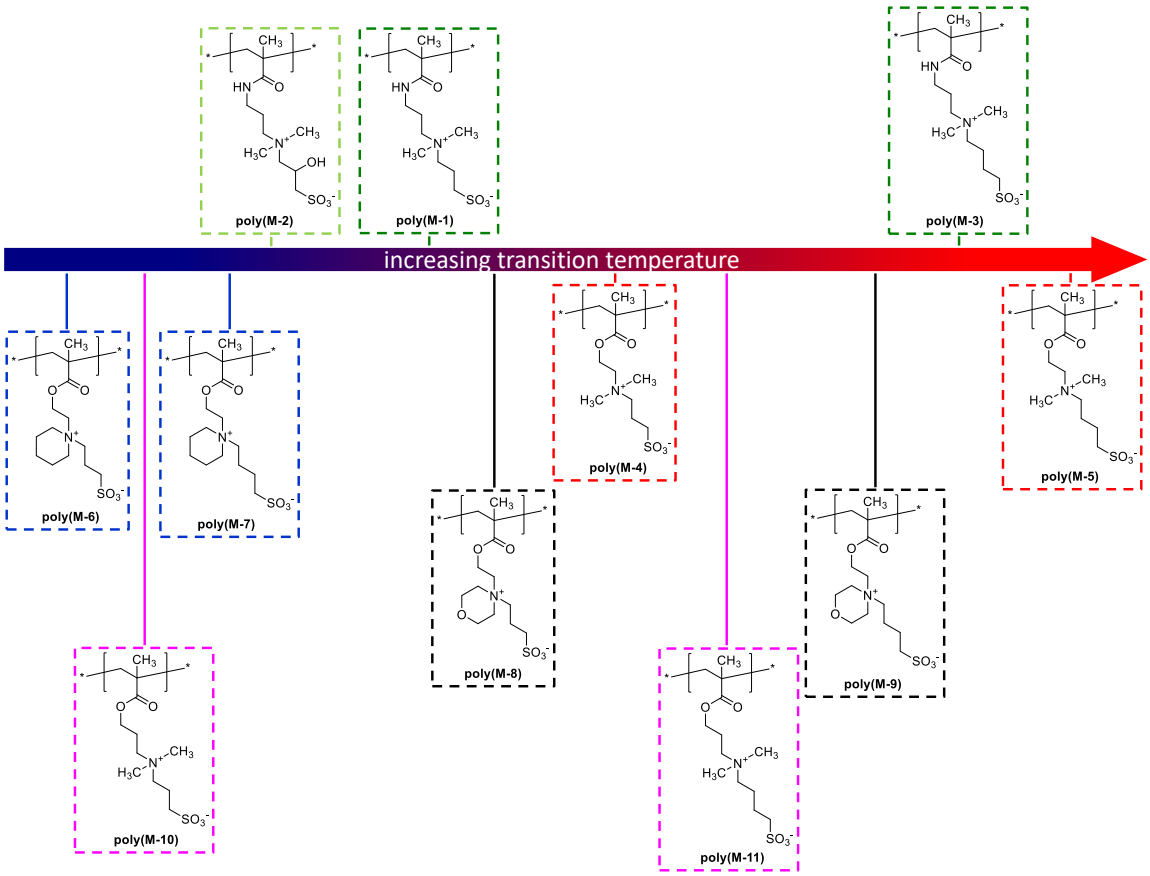

Figure 4.10. Order of poly(sulfobetaine)s according to their UCST-type transition temperature in H_2O. Above the arrow: methacrylamide-based poly(sulfobetaine)s, below the arrow: methacrylate-based poly(sulfobetaine)s. Temperature increase from left to right. Frame color indicates homolog structures with different spacer group between the cationic and anionic moieties.

The first variation of the chemical structure is the type of the polymerizable moiety. For the polymers with the same zwitterionic side chain, methacrylamide-based poly(sulfobetaine)s exhibit higher UCST-type transition temperatures than their methacrylate analogs (compare: green vs. magenta). The second possibility is

the variation of the distance between the polymer backbone and the ammonium group. Here, extension of the distance from 2 to 3 methylene units decreases the UCST-type transition temperatures (compare: red vs. magenta). The third option is the variation of the substituent on the ammonium group. Poly(sulfobetaine)s with dimethyl substituents show higher UCST-type transition temperatures than their analogs, bearing morpholine or piperidine rings (compare: red vs. black and red vs. blue). Counterintuitively, the poly(sulfobetaine)s bearing a morpholine ring exhibit higher UCST-type transition temperatures than the ones bearing a piperidine ring (compare: black vs. blue). The forth opportunity is the variation of the spacer group between the cationic and the anionic moieties. The UCST-type transition temperatures increase with spacer length from 3 to 4 methylene units. Moreover, modification the spacer group of 3 methylene units with a hydroxyl group decreases the UCST-type transition temperature in H_2O (green vs. light green).

4.3 Non-ionic poly(*N*-isopropylmethacrylamide)

The hydrophilic character of **poly(M-12)** ("**poly(NIPMAM)**") and **poly(M-13)** ("**poly(NIPAM)**") in various aqueous media was investigated by determining the LCST-type transition temperatures, since these polymers will be used to synthesize block copolymers. In the turbidimetric studies of solutions of **poly(M-12)** and **poly(M-13)** in both H_2O and D_2O (see in the appendix **Figure A.58**), the clouding transitions were all sharp and curves were highly reproducible. The hysteresis between the LCST-type transitions of **poly(M-12)** for heating and cooling runs was ≈ 5 °C (see in the appendix **Figure A.59**). **Table 4.5** summarizes the derived LCST-type transition temperatures.

Table 4.5. LCST-type transition of 5 wt% aqueous solutions of **poly(M-12)** and **poly(M-13)**.

sample	LCST-type transition [°C]	
	in H_2O	in D_2O
poly(M-12)$_{180}$ [a)]	42	43
poly(M-12)$_{40}$	26	28
poly(M-12)$_{45}$	28	30
poly(M-12)$_{65}$	32	33
poly(M-12)$_{195}$	39	40
poly(M-13)$_{195}$	27	28

[a)] using **CTA-1**.

As already known, the LCST-type transition temperature is higher for **poly(M-12)** than for **poly(M-13)** and only weakly sensitive to the presence of inorganic salts. The LCST-type transition temperature of **poly(M-12)** increase with molar mass for the polymers in H_2O[180] as well as in D_2O. The H-D-effect of 1 °C is marginal. Control experiments were performed with samples made with the unlabeled RAFT agent **CTA-1**, thus producing a polymer bearing a carboxyl group instead of the bulky 2-(naphthalimido)ethyl end group. The LCST-type transition temperature of this non-labeled polymer (**poly(M-12)$_{180}$**) is few degrees higher than the ones of its labeled analog (**Table 4.5**). This finding is consistent to the result found for the labeled **poly(M-13)** ("**poly(NIPAM**"), showing an LCST-type transition temperature below the typically observed value 32 °C[48, 56, 65, 171]. This finding suggests that the hydrophobic chromophore somehow supports the collapse of the polymer chains, and therefore decreasing the LCST-type transition temperature. As expected, the LCST-type transition temperatures of **poly(M-12)** decrease with increasing concentration at least up to 50 g·L^{-1}, approaching a minimum value. The concentration dependent evolution of LCST-type transition temperatures of fluorophore-labeled **poly(M-12)** is shown in **Figure 4.11**.

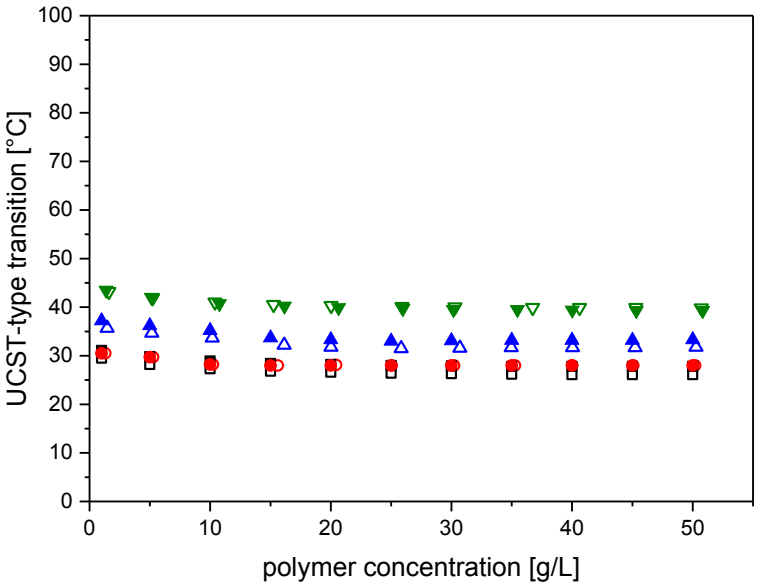

Figure 4.11. Concentration dependent evolution of LCST-type transition temperatures in aqueous solution of **poly(M-12)$_{40}$**: (▫) = in H_2O and (■) = in D_2O, **poly(M-12)$_{45}$**: (○) = in H_2O and (●) = in D_2O, **poly(M-12)$_{65}$**: (△) = in H_2O and (▲) = in D_2O, and **poly(M-12)$_{195}$**: (▽) = in H_2O and (▼) = in D_2O.

5 Twofold switchable block copolymers

5.1 Synthesis of the block copolymers

Generally, the fluorophore functionalized sulfobetaine homopolymers were utilized as macro-RAFT agents (**m-CTA**) for the synthesis of block copolymers **poly(monomer 1)$_v$-*block*-(monomer 2)$_w$**, with *v* and *w* being the number average degree of polymerization that was theoretically calculated using **equation 3.2**. Polymerizations were conducted in TFE at 30 wt% to establish homogeneous polymerization conditions for both the non-ionic monomer (**M-12** and **M-13**) and the **m-CTA**, using the azo initiator V-501. The ratio of monomer to **m-CTA** in the reaction mixtures was 100 : 1, 400 : 1, or 600 : 1, while the ratio between **m-CTA** and V-501 was kept constant as 5 : 1 (see **chapter 7.6**). The results of the polymerizations are summarized in **Table 5.1** – **5.3**.

Table 5.1. Analytical data for block copolymers made from methacrylamide-based poly(sulfobetaine)s (**poly(M-1** – **poly(M-3)**) and **poly(M-12)** ("**poly(NIPMAM)**").

sample		M_n [kg·mol^{-1}]		
	con-version [a]	theo-retical	by ^{1}H NMR [b]	by UV-vis (via R-group) [c]
poly(M-1)$_{85}$-*block*-(M-12)$_{100}$	0.33	42	46	39
poly(M-1)$_{170}$-*block*-(M-12)$_{160}$	0.40	71	61	57
poly(M-1)$_{280}$-*block*-(M-12)$_{85}$	0.21	93	87	87
poly(M-1)$_{500}$-*block*-(M-12)$_{145}$	0.36	165	156	151
poly(M-2)$_{80}$-*block*-(M-12)$_{160}$	0.27	47	51	45
poly(M-2)$_{115}$-*block*-(M-12)$_{155}$	0.26	55	59	52
poly(M-2)$_{235}$-*block*-(M-12)$_{175}$	0.29	95	98	92
poly(M-2)$_{505}$-*block*-(M-12)$_{145}$	0.24	174	177	171
poly(M-3)$_{40}$-*block*-(M-12)$_{190}$	0.48	37	31	32
poly(M-3)$_{50}$-*block*-(M-12)$_{155}$	0.39	36	34	35
poly(M-3)$_{80}$-*block*-(M-12)$_{115}$	0.29	39	36	32
poly(M-3)$_{245}$-*block*-(M-12)$_{105}$	0.26	88	83	86
poly(M-3)$_{425}$-*block*-(M-12)$_{110}$	0.27	144	143	143

[a] conversions were determined by ^{1}H NMR analysis of the crude reaction mixtures. [b] determined by comparing the integrals of signals of the poly(sulfobetaine) with the integrals of the signals of the **poly(M-12)**; and assuming that the DP_n of the poly(sulfobetaine)s are unchanged after polymerization with **M-12**. [c] calculated from the maximum absorbance in TFE, using the corrected extinction coefficients $\varepsilon_{\lambda max3}$ (corresponding to the poly(sulfobetaine)) of **Table 3.2** derived in TFE for **CTA-3**.

Table 5.2. Analytical data for block copolymers made from methacrylate-based poly(sulfobetaine)s (**poly(M-4** – **poly(M-11)**) and **poly(M-12)** ("**poly(NIPMAM)**").

sample		M_n [kg·mol^{-1}]		
	con-version [a)]	theo-retical	by ^{1}H NMR [b)]	by UV-vis (via R-group) [c)]
poly(M-4)$_{85}$-*block*-(M-12)$_{80}$	0.20	35	37	39
poly(M-4)$_{270}$-*block*-(M-12)$_{60}$	0.15	84	79	77
poly(M-4)$_{575}$-*block*-(M-12)$_{60}$	0.15	168	170	163
poly(M-4)$_{585}$-*block*-(M-12)$_{70}$	0.16	172	181	185
poly(M-4)$_{585}$-*block*-(M-12)$_{145}$	0.24	182	185	190
poly(M-5)$_{50}$-*block*-(M-12)$_{190}$	0.32	39	41	50
poly(M-5)$_{80}$-*block*-(M-12)$_{190}$	0.31	47	48	61
poly(M-5)$_{95}$-*block*-(M-12)$_{190}$	0.32	53	56	68
poly(M-5)$_{280}$-*block*-(M-12)$_{200}$	0.33	109	110	140
poly(M-6)$_{95}$-*block*-(M-12)$_{180}$	0.30	53	53	49
poly(M-6)$_{250}$-*block*-(M-12)$_{180}$	0.30	101	102	94
poly(M-6)$_{330}$-*block*-(M-12)$_{185}$	0.31	127	127	119
poly(M-6)$_{485}$-*block*-(M-12)$_{180}$	0.30	173	174	166
poly(M-7)$_{82}$-*block*-(M-12)$_{145}$	0.24	46	46	41
poly(M-7)$_{250}$-*block*-(M-12)$_{145}$	0.24	102	102	93
poly(M-7)$_{420}$-*block*-(M-12)$_{145}$	0.24	159	159	142
poly(M-7)$_{500}$-*block*-(M-12)$_{140}$	0.23	185	185	165
poly(M-8)$_{65}$-*block*-(M-12)$_{145}$	0.21	38	38	44
poly(M-8)$_{95}$-*block*-(M-12)$_{145}$	0.21	48	48	45
poly(M-8)$_{230}$-*block*-(M-12)$_{145}$	0.20	90	92	100
poly(M-8)$_{585}$-*block*-(M-12)$_{140}$	0.25	207	201	211
poly(M-9)$_{85}$-*block*-(M-12)$_{190}$	0.32	54	54	55
poly(M-9)$_{260}$-*block*-(M-12)$_{190}$	0.32	112	112	114
poly(M-9)$_{430}$-*block*-(M-12)$_{190}$	0.32	169	169	177
poly(M-9)$_{520}$-*block*-(M-12)$_{190}$	0.32	199	199	204

sample		M_n [kg·mol^{-1}]		
	con-version [a)]	theo-retical	by ^{1}H NMR [b)]	by UV-vis (via R-group) [c)]
poly(M-10)$_{75}$-*block*-(M-12)$_{190}$	0.31	47	46	52
poly(M-10)$_{295}$-*block*-(M-12)$_{190}$	0.31	112	111	118
poly(M-10)$_{480}$-*block*-(M-12)$_{190}$	0.31	166	165	175
poly(M-10)$_{585}$-*block*-(M-12)$_{190}$	0.31	196	193	210
poly(M-11)$_{100}$-*block*-(M-12)$_{205}$	0.33	57	56	61
poly(M-11)$_{290}$-*block*-(M-12)$_{205}$	0.34	117	112	125
poly(M-11)$_{480}$-*block*-(M-12)$_{205}$	0.34	174	174	189
poly(M-11)$_{540}$-*block*-(M-12)$_{205}$	0.34	192	191	216

[a)] conversions were determined by ^{1}H NMR analysis of the crude reaction mixtures. [b)] determined by comparing the integrals of signals of the poly(sulfobetaine) with the integrals of the signals of the **poly(M-12)**; and assuming that the DP_n of the poly(sulfobetaine)s are unchanged after polymerization with **M-12**. [c)] calculated from the maximum absorbance in TFE, using the corrected extinction coefficients $\varepsilon_{\lambda max3}$ (corresponding to the poly(sulfobetaine)) of **Table 3.2** derived in TFE for **CTA-3**.

Table 5.3. Analytical data for block copolymers made from poly(sulfobetaine)s and **poly(M-13)** ("**poly(NIPAM)**"), and for block copolymers using **poly(M-12)** ("**poly(NIPMAM)**") as **m-CTA**.

sample		M_n [kg·mol^{-1}]		
	con-version [a)]	theo-retical	by ^{1}H NMR [b)]	by UV-vis (via R-group) [c)]
poly(M-1)$_{430}$-*block*-(M-13)$_{200}$	1.00	150	149	152
poly(M-3)$_{80}$-*block*-(M-13)$_{100}$	1.00	36	38	32
poly(M-3)$_{80}$-*block*-(M-13)$_{400}$	1.00	70	71	72
poly(M-4)$_{270}$-*block*-(M-13)$_{200}$	1.00	99	99	97
poly(M-12)$_{195}$-*block*-(M-1)$_{385}$	0.64	138	128	147
poly(M-12)$_{195}$-*block*-(M-3)$_{15}$	0.16	30	31	32
poly(M-12)$_{195}$-*block*-(M-3)$_{30}$	0.31	34	34	35
poly(M-12)$_{195}$-*block*-(M-4)$_{530}$	0.88	173	172	188

[a)] conversions were determined by ^{1}H NMR analysis of the crude reaction mixtures. [b)] determined by comparing the integrals of signals of the poly(sulfobetaine) with the integrals of the signals of the **poly(M-13)**; and assuming that the DP_n of the poly(sulfobetaine)s or **poly(M-12)** are unchanged after chain extension. [c)] calculated from the maximum absorbance in TFE, using the corrected extinction coefficients $\varepsilon_{\lambda max3}$ (corresponding to the poly(sulfobetaine)) of **Table 3.2** derived in TFE for **CTA-3**.

The ^{1}H NMR spectrum of the block copolymer **poly(M-3)$_{80}$-*block*-(M-12)$_{115}$** taken at 25 °C superposes the characteristic peaks of **poly(M-3)** (**Figure 5.1a**) and of **poly(M-12)** (**Figure 5.1b**), as shown in **Figure 5.1c**. In the spectra, the signal at 3.8 – 4.0 ppm is typical for **poly(M-12)** (signal Q in **Figure 5.1b**) corresponding to one proton. This signal is well resolved from the broad signal complex at 2.8 – 3.6 ppm that is characteristic for **poly(M-3)** (signal E+G+I+H+L in **Figure 5.1a**) corresponding to 14 protons. It is assumed that the DP_n of the poly(sulfobetaine)s are unchanged after polymerization with the non-ionic monomers. Accordingly, the experimental M_n^{NMR} values for the block copolymers were determined by comparing the integrals of signals of the poly(sulfobetaine) with the integrals of the signals of the **poly(M-12)** or **poly(M-13)**, respectively. The experimental estimated M_n^{NMR} values are in good agreement with the theoretically expected molar masses M_n^{theo}.

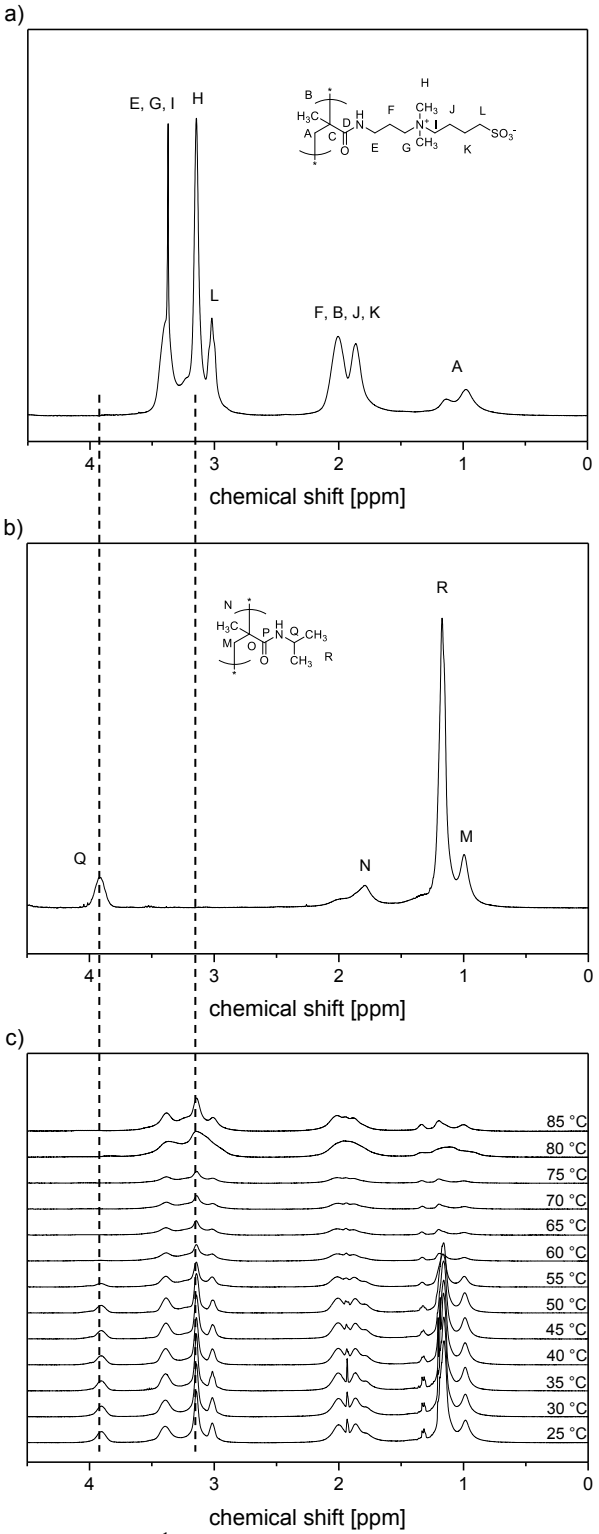

Figure 5.1. ^{1}H NMR spectra. a) **Poly(M-3)$_{80}$** in dilute aqueous NaCl (0.9 g·L^{-1}) in D_2O at 25 °C, b) **poly(12)$_{195}$** at 25 °C, and c) **poly(M-3)$_{80}$-*block*-(M-12)$_{115}$** in D_2O (5 wt%) at different temperature (25 – 85 °C).

As expected, ^{1}H NMR end group analysis becomes impossible for the block copolymers due to the small number of end groups to be quantified and the poor signal-to-noise ratio (**Figure 5.2a**). Thus, the intense signal of the naphthalimide chromophore in UV-vis spectrum (**Figure 5.2b**) was used to characterize the molar masses. When utilizing the corrected $\varepsilon_{\lambda max3}$ in TFE of **CTA-3**, theoretically expected and observed molar masses are in good agreement (**Table 5.1** – **5.3**), as typical for a well-behaved RAFT polymerization. Also, by virtue of the 4-dimethylamino-naphthalimide end group, the polymers are all strongly fluorescent.

Concerning thermal properties, TGA of the block copolymers shows the onset of decomposition accompanied by mass loss at ~300 °C. For block copolymers containing **poly(M-12)**, DSC measurements show a thermal transition at ~175 °C (glass-transition temperature: T_g), while DSC measurements of block copolymers containing **poly(M-13)** show thermal transition at about 135 °C (T_g).

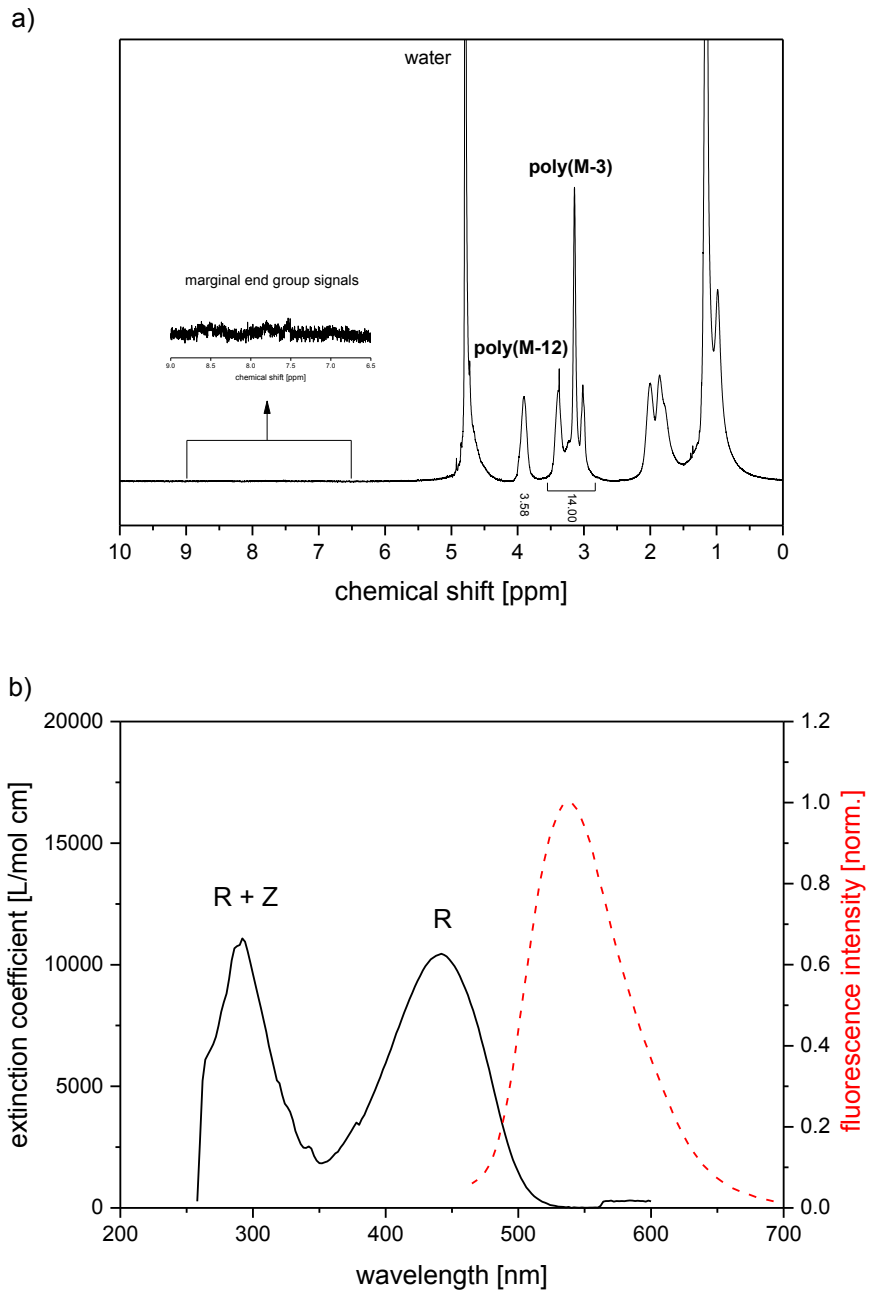

Figure 5.2. End group analysis of block copolymer of **poly(M-3)$_{40}$-*block*-(M-12)$_{190}$**. a) ^{1}H NMR spectrum in dilute aqueous NaCl (0.9 g·L^{-1}) in D_2O, inset: magnification of the vanishing end group signals between 6.5 and 9.0 ppm. b) Optical spectroscopy in TFE: absorbance (——) and fluorescence emission spectra (------), excitation at 442 nm. "R" indicates the absorbance bands of the naphthalimide chromophore, "Z" indicates the absorbance band of the trithiocarbonate moiety.

5.2 "Schizophrenic" behavior of block copolymers

As for the homopolymers, the turbidity of aqueous solutions of the block copolymers was studied in the dependence on the temperature. The derived UCST- and LCST-type transition temperatures at 5 wt% in both H_2O and D_2O are summarized in **Table 5.4** – **5.6**.

Table 5.4. Transition temperatures of 5 wt% in H_2O and in D_2O of block copolymers made from methacrylamide-based poly(sulfobetaine)s (**poly(M-1** – **poly(M-3)**) and **poly(M-12)** ("**poly(NIPMAM)**").

sample	UCST-type transition [°C]		LCST-type transition [°C]	
	in H_2O	in D_2O	in H_2O	in D_2O
poly(M-1)$_{85}$-*block*-(M-12)$_{100}$	<0	4	49	48
poly(M-1)$_{170}$-*block*-(M-12)$_{160}$	13	15	47	48
poly(M-1)$_{280}$-*block*-(M-12)$_{85}$	17	25	49	47
poly(M-1)$_{500}$-*block*-(M-12)$_{145}$	24	31	48	49
poly(M-2)$_{80}$-*block*-(M-12)$_{160}$	<0	7	47	47
poly(M-2)$_{115}$-*block*-(M-12)$_{155}$	7	22	48	48
poly(M-2)$_{235}$-*block*-(M-12)$_{175}$	11	27	46	46
poly(M-2)$_{505}$-*block*-(M-12)$_{145}$	32	49	48	48
poly(M-3)$_{40}$-*block*-(M-12)$_{190}$	35	38	43	43
poly(M-3)$_{50}$-*block*-(M-12)$_{155}$	40	44	44	44
poly(M-3)$_{80}$-*block*-(M-12)$_{115}$	49	53	45	45
poly(M-3)$_{245}$-*block*-(M-12)$_{105}$	>100	>100	49	49
poly(M-3)$_{425}$-*block*-(M-12)$_{110}$	>100	>100	49	49

Table 5.5. Transition temperatures of 5 wt% in H_2O and in D_2O of block copolymers made from methacrylate-based poly(sulfobetaine)s (**poly(M-4** – **poly(M-11)**) and **poly(M-12)** ("**poly(NIPMAM)**").

sample	UCST-type transition [°C]		LCST-type transition [°C]	
	in H_2O	in D_2O	in H_2O	in D_2O
poly(M-4)$_{85}$-*block*-(M-12)$_{80}$	19	27	45	44
poly(M-4)$_{270}$-*block*-(M-12)$_{60}$	54	57	47	46
poly(M-4)$_{575}$-*block*-(M-12)$_{60}$	56	64	48	47
poly(M-4)$_{585}$-*block*-(M-12)$_{70}$	63	68	45	44
poly(M-4)$_{585}$-*block*-(M-12)$_{145}$	62	68	48	50
poly(M-5)$_{50}$-*block*-(M-12)$_{190}$	<0	<0	42	42
poly(M-5)$_{80}$-*block*-(M-12)$_{190}$	<0	<0	43	43
poly(M-5)$_{95}$-*block*-(M-12)$_{190}$	<0	<0	42	42
poly(M-5)$_{280}$-*block*-(M-12)$_{200}$	<0	<0	42	42
poly(M-6)$_{95}$-*block*-(M-12)$_{180}$	<0	<0	43	43
poly(M-6)$_{250}$-*block*-(M-12)$_{180}$	<0	<0	43	44
poly(M-6)$_{330}$-*block*-(M-12)$_{185}$	<0	<0	43	43
poly(M-6)$_{485}$-*block*-(M-12)$_{180}$	<0	<0	44	44
poly(M-7)$_{82}$-*block*-(M-12)$_{145}$	<0	17	45	45
poly(M-7)$_{250}$-*block*-(M-12)$_{145}$	4	28	45	45
poly(M-7)$_{420}$-*block*-(M-12)$_{145}$	11	36	45	45
poly(M-7)$_{500}$-*block*-(M-12)$_{140}$	15	40	45	45
poly(M-8)$_{65}$-*block*-(M-12)$_{145}$	<0	14	45	45
poly(M-8)$_{95}$-*block*-(M-12)$_{145}$	21	31	45	45
poly(M-8)$_{230}$-*block*-(M-12)$_{145}$	35	45	44	45
poly(M-8)$_{585}$-*block*-(M-12)$_{140}$	45	54	44	44
poly(M-9)$_{85}$-*block*-(M-12)$_{190}$	70	75	42	42
poly(M-9)$_{260}$-*block*-(M-12)$_{190}$	88	94	42	42
poly(M-9)$_{430}$-*block*-(M-12)$_{190}$	>100	>100	42	42
poly(M-9)$_{520}$-*block*-(M-12)$_{190}$	>100	>100	42	42

sample	UCST-type transition [°C]		LCST-type transition [°C]	
	in H_2O	in D_2O	in H_2O	in D_2O
poly(M-10)$_{75}$-*block*-(M-12)$_{190}$	<0	<0	42	42
poly(M-10)$_{295}$-*block*-(M-12)$_{190}$	<0	8	42	43
poly(M-10)$_{480}$-*block*-(M-12)$_{190}$	<0	12	42	43
poly(M-10)$_{585}$-*block*-(M-12)$_{190}$	<0	14	42	43
poly(M-11)$_{100}$-*block*-(M-12)$_{205}$	<0	<0	45	45
poly(M-11)$_{290}$-*block*-(M-12)$_{205}$	57	64	45	45
poly(M-11)$_{480}$-*block*-(M-12)$_{205}$	69	75	45	45
poly(M-11)$_{540}$-*block*-(M-12)$_{205}$	90	96	45	45

Table 5.6. Transition temperatures of 5 wt% in H_2O and in D_2O of block copolymers made from poly(sulfobetaine)s and **poly(M-13)** ("**poly(NIPAM)**"), and for block copolymers using **poly(M-12)** ("**poly(NIPMAM)**") as **m-CTA**.

sample	UCST-type transition [°C]		LCST-type transition [°C]	
	in H_2O	in D_2O	in H_2O	in D_2O
poly(M-1)$_{430}$-*block*-(M-13)$_{200}$	22	29	33	34
poly(M-3)$_{80}$-*block*-(M-13)$_{100}$	n.d. [a)]	n.d. [a)]	31	32
poly(M-3)$_{80}$-*block*-(M-13)$_{400}$	n.d. [a)]	n.d. [a)]	33	33
poly(M-4)$_{270}$-*block*-(M-13)$_{200}$	n.d. [a)]	n.d. [a)]	30	31
poly(M-12)$_{195}$-*block*-(M-1)$_{385}$	25	34	48	48
poly(M-12)$_{195}$-*block*-(M-3)$_{15}$	8	18	41	42
poly(M-12)$_{195}$-*block*-(M-3)$_{30}$	18	25	43	44
poly(M-12)$_{195}$-*block*-(M-4)$_{530}$	76	87	46	47

[a)] LCST-type transition was too pronounced and therefore UCST-type transition cannot be reliably determined.

As expected, solutions of certain block copolymers are turbid at low as well as at high temperatures, while being clear at intermediate temperatures, i.e., showing a dissolved intermediate regime[8] (**Figure 5.3a**). In contrast, the solutions of other block copolymers are turbid at all temperatures, i.e., they exhibit an insoluble intermediate regime (**Figure 5.3b**). Furthermore, in some cases, the UCST-type transition temperature is below 0 °C. Accordingly, the various block copolymers prepared open access to two types of "schizophrenic" systems depending on the relative positions of the UCST- and LCST-type transitions.

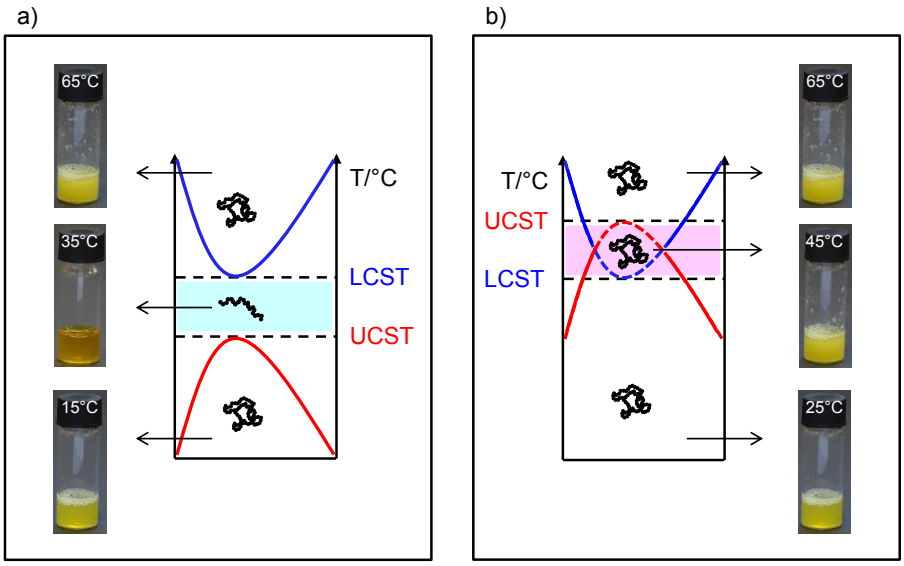

Figure 5.3. Schematic phase behavior of "schizophrenic" block copolymers depending on the relative positions of the individual blocks' phase transitions; (——) and (——) show the binodal lines of the UCST- and LCST-type transitions of the individual blocks, while (------) and (------) indicate the hypothetical continuations of the respective binodal lines in the overlap regime: a) polymers show a dissolved intermediate regime (exemplified with photographs of **poly(M-3)$_{40}$-*block*-(M-12)$_{190}$**), b) polymers show an insoluble intermediate regime (exemplified with photographs of **poly(M-3)$_{245}$-*block*-(M-12)$_{105}$**).

5.2.1 Block copolymers showing a dissolved intermediate regime

Different from the behavior of the poly(sulfobetaine) homopolymers, the block copolymers do not precipitate at low temperature even though the solutions are turbid. This means that these solutions are at least metastable at ambient conditions by virtue of the non-ionic blocks **poly(M-12)** or **poly(M-13)**, respectively. Increasing the temperature, the block copolymers cross the UCST-type transition and pass through a dissolved regime, before the LCST-type transition occurs as exemplified in **Figure 5.4**. As seen in the DLS measurements, the block copolymers precipitate at high temperatures (above the LCST-type transition) after a certain time. Note that turbidity and DLS measurements are in good agreement, demonstrating that the block copolymers show twofold switchable transitions.

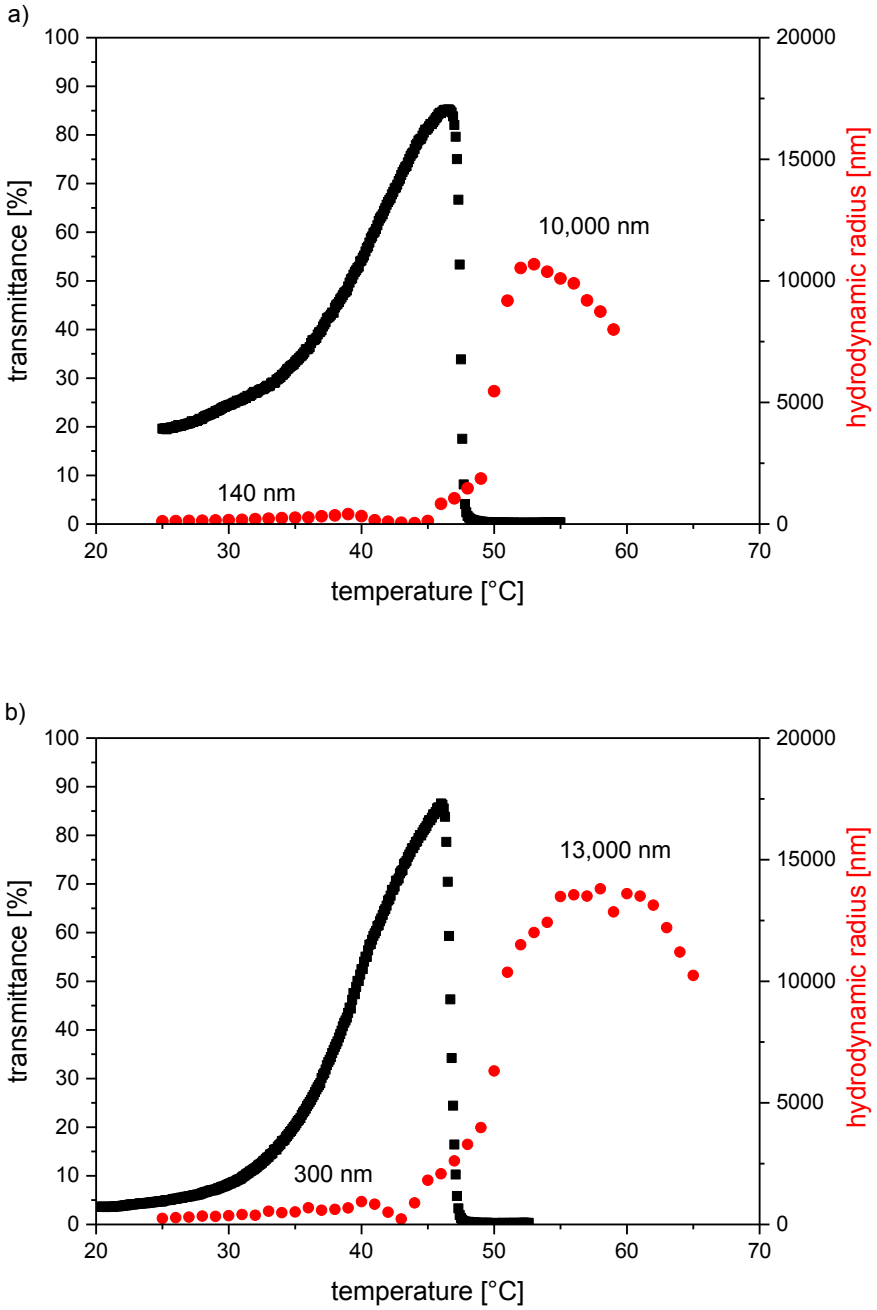

Figure 5.4. Heating run of turbidity and DLS measurements of 1 wt% solutions in H_2O of block copolymers a) **poly(M-3)$_{80}$-*block*-(M-12)$_{115}$** and b) **poly(M-11)$_{290}$-*block*-(M-12)$_{205}$**.

The cryo-SEM images **poly(M-3)$_{80}$-*block*-(M-12)$_{115}$** at 25 °C show aggregates with a diameter of 250 – 280 nm. Though keeping in mind that sample preparation may modify the polymer self-assembly, it is noted that these values are in good agreement with the DLS result (280 nm).

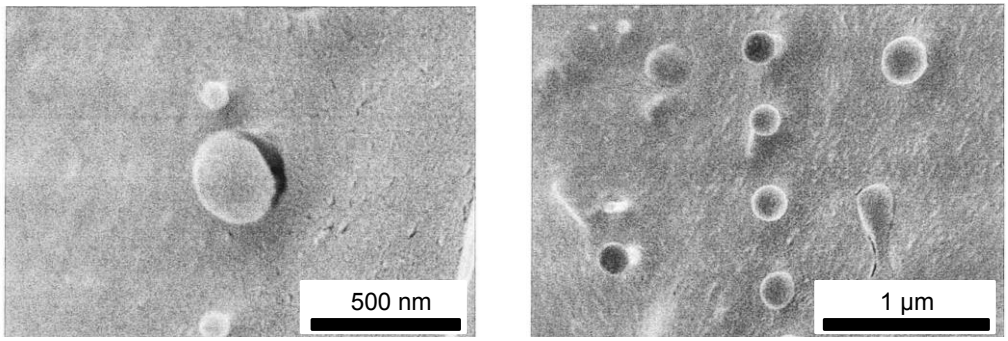

Figure 5.5. Cryo-SEM images of the block copolymer **poly(M-3)$_{80}$-*block*-(M-12)$_{115}$** (1 wt% solution in H_2O at 25 °C).

5.2.2 Block copolymers showing an insoluble intermediate regime

Amid the various samples studied, a second type of "schizophrenic" block copolymers is found. These copolymers exhibit an insoluble intermediate regime. As seen in **Figure 5.6** for **poly(M-3)$_{80}$-*block*-(M-12)$_{115}$** and **poly(M-11)$_{290}$-*block*-(M-12)$_{205}$**, the transmittance of the polymer solutions starts to increase when approaching the UCST-type transition. But before the clearing point is reached, the LCST-type transition occurs. This result suggests a scenario, where the UCST is equal or higher than the LCST. Also, there are samples, which are turbid from 0 °C to 100 °C (transmittance ≈ 0 %), indicating a higher UCST than LCST.

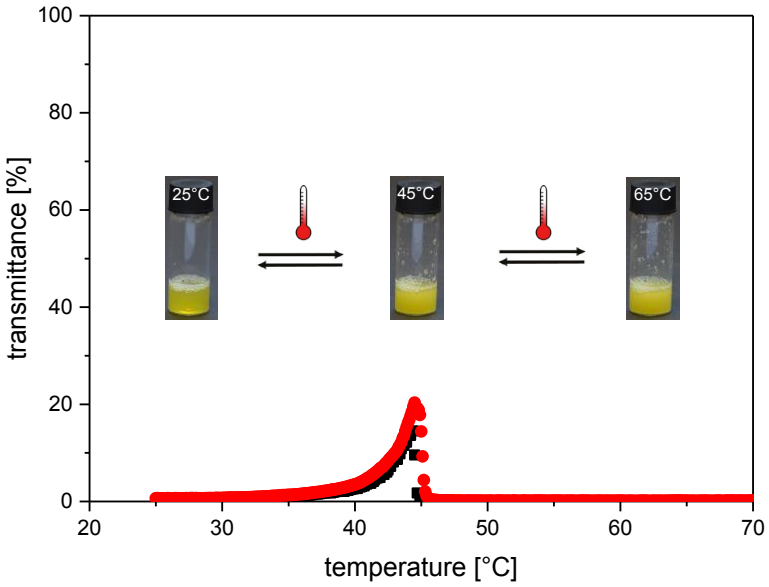

Figure 5.6. Turbidity measurements (heating run) of 5 wt% solutions in H_2O of (■) = **poly(M-3)$_{80}$-*block*-(M-12)$_{115}$** and (●) = **poly(M-11)$_{290}$-*block*-(M-12)$_{205}$**.

The fluorescent 4-dimethylaminonaphthalimide end group was used as probe to investigate the "schizophrenic" switching of block copolymers showing an insoluble intermediate regime. Since the chromophore is very sensitive to the polarity of its surrounding, the formation of aggregates below the UCST-type transition and above the LCST-type transition should affect its spectroscopic properties (for instance λ_{PL} and intensity) (**Figure 5.7**).

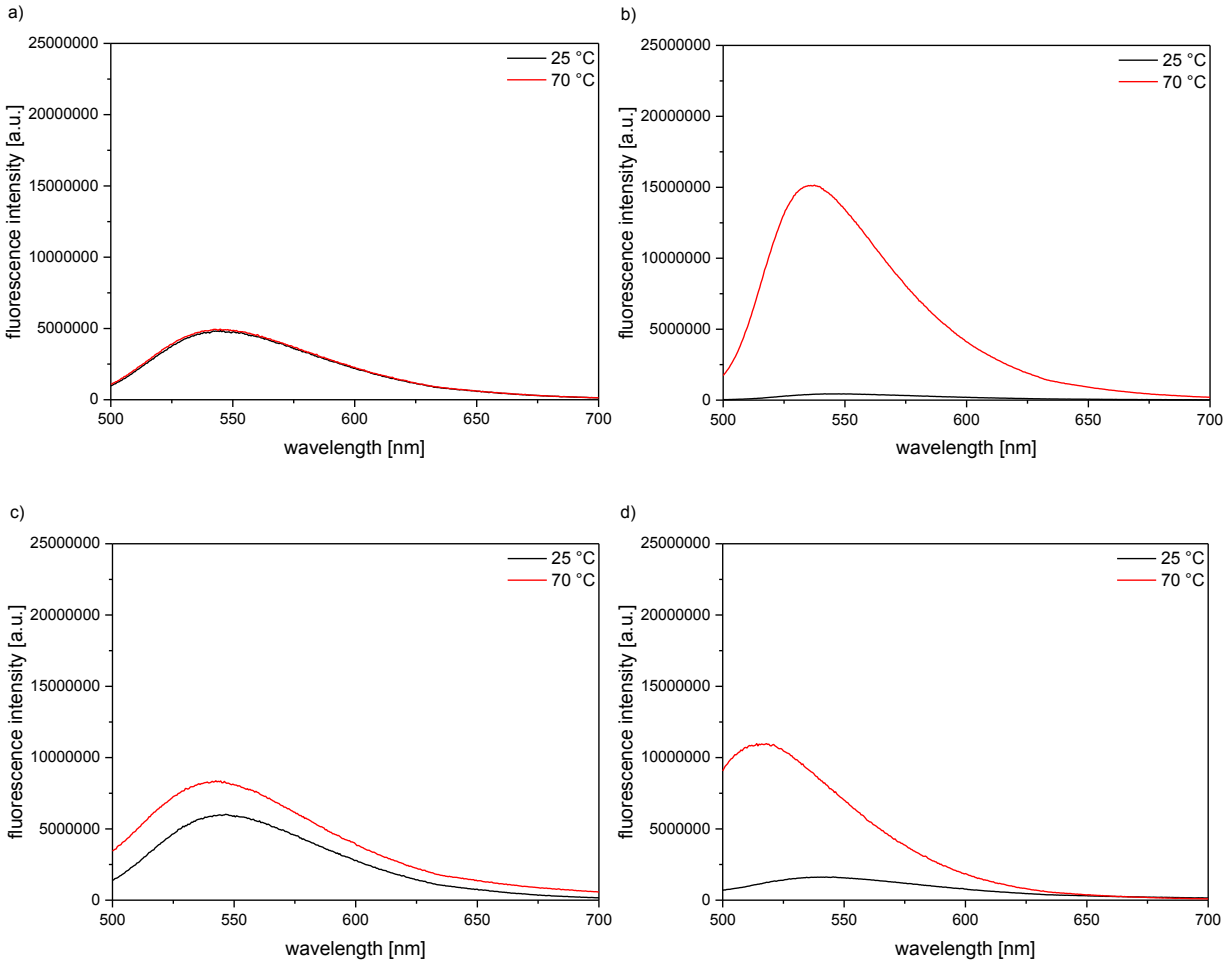

Figure 5.7. Fluorescence spectra of 1.5 wt% solutions in H_2O at 25 °C and 70 °C of homopolymers and block copolymers. a) **Poly(M-11)$_{290}$**, b) **poly(M-12)$_{195}$**, c) **poly(M-11)$_{290}$-*block*-(M-12)$_{205}$**, and d) **poly(M-12)$_{195}$-*block*-(M-4)$_{530}$**.

In aqueous solution, the reference homopolymer **poly(M-11)$_{290}$** emits at 544 nm above as well as below the UCST-type transition, where the polymer forms aggregates. In contrast, the reference homopolymer **poly(M-12)$_{195}$** emits at 546 nm below the LCST-type transition and emits at 536 nm above the LCST-type transition, where the polymer is collapsed (**Figure 5.7a-b**). These results suggest that the poly(sulfobetaine) **poly(M-11)$_{290}$** forms apparently polar aggregates with a similar polarity and affinity of the chromophore to the solvent H_2O. In contrast, the non-ionic **poly(M-12)$_{195}$** forms nonpolar aggregates, which preferentially accumulate the probe and strongly affect the λ_{PL} (which decreases) and the intensity (which increases). Also, these findings support the assumption that the chromophore hinders the poly(sulfobetaine)s from collapsing (lowering the UCST-type transition). In

contrast, the chromophore supports the non-ionic polymers to collapse (lowering the LCST-type transition).

The block copolymers made from the two parent homopolymers show as well the spectral shift with changing temperature (**Figure 5.7c-d**), which indicates a transfer of the fluorescent probe from a hydrophilic environment to a more hydrophobic surrounding when increasing the temperature from 25 °C to 70 °C. This can be explained by the formation of hydrophobic microdomains in the aggregates formed by the non-ionic **poly(M-12)** above its LCST transition. Note that the sequence of the blocks within the copolymers has a great impact on the spectral shift. The block copolymer **poly(M-11)$_{290}$-*block*-(M-12)$_{205}$**, where the chromophore is attached to the poly(sulfobetaine) block, shows a small shift of λ_{PL} (4 nm) and also a small increase of fluorescence intensity only. In contrast, the block copolymer **poly(M-12)$_{195}$-*block*-(M-4)$_{530}$**, where the chromophore is attached to the non-ionic block, shows a much more pronounced shift of λ_{PL} (26 nm) as well as a strong increase of fluorescence intensity. These findings support the assumption that the non-ionic block preferentially accumulates the chromophore, even when separated by the poly(sulfobetaine) block. Apparently, the effect on the spectral shift is strongly affected by the inherent environment of the chromophore.

5.3 Inverting the position of UCST- and LCST-type transitions

The relative positions of the UCST- and LCST-type phase transitions can be modulated by the polymer concentration and by the addition of salt (**Figure 5.8**). This modulation of thermoresponsive behavior of the block copolymers enables a switching between all superstructures depending on the combination of "stimuli" (compare **Figure 5.9** and **5.10**).

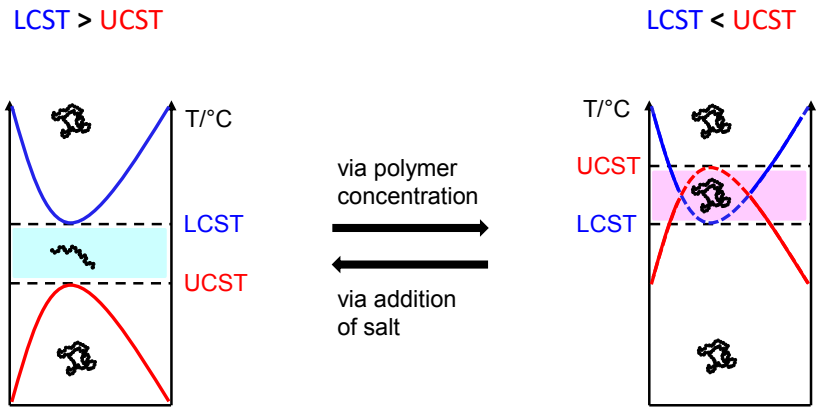

Figure 5.8. Inversion of relative positions of UCST and LCST. (——) and (——) show the binodal lines of the UCST- and LCST-type transitions of the individual blocks, while (------) and (------) indicate the hypothetical continuations of the respective binodal lines in the overlap regime.

5.3.1 Inverting the position of transitions via polymer concentration

As for the homopolymers, turbidity measurements of polymer solutions in H_2O at different concentrations were performed for the block copolymers (**Figure 5.9**). The UCST-type transition temperature increases with polymer concentration, while the LCST-type transition temperature slightly decreases. These observations were

already found for the homopolymers. Note that the lower LCST-type transition temperature of the non-ionic block in the copolymer compared to the parent homopolymer reference can be attributed to the shorter length of **poly(M-12)** within the block copolymer. Furthermore, the strong decrease of UCST-type transition temperature of the zwitterionic block in the copolymer compared to the parent homopolymer reference may be attributed to two major effects, namely, to the reduced content of the poly(sulfobetaine) when comparing homo- and block copolymer solutions of the same polymer mass fraction, and to the presumed influence of the hydrophilic **poly(M-12)** on the UCST-type transition temperature.

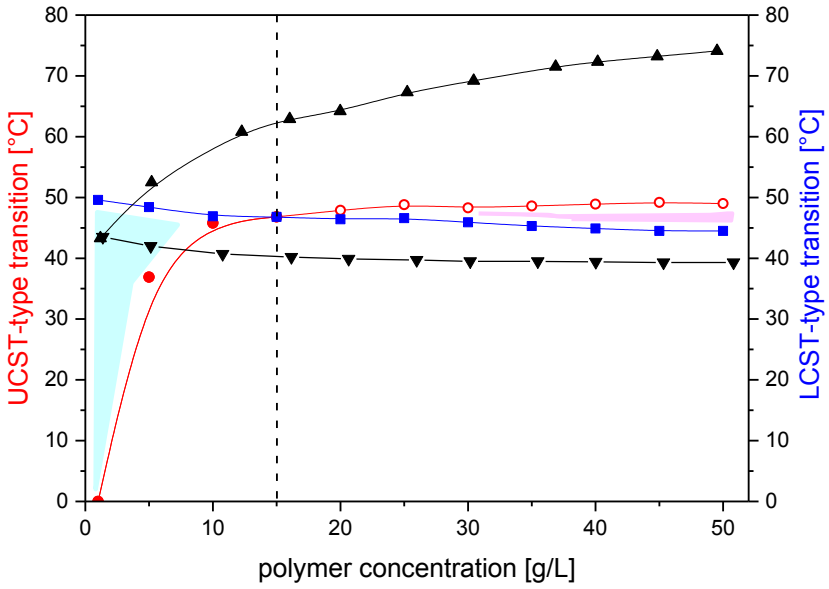

Figure 5.9. Turbidity of polymer solutions in H_2O of (—▲—) **poly(M-3)$_{80}$** (cooling run), (—▼—) **poly(M-12)$_{195}$** (heating run) and (—●— /—■—) **poly(M-3)$_{80}$-*block*-(M-12)$_{115}$** (heating run) at different polymer concentration. (—○—) UCST-type transition was estimated via extrapolation of the turbidity curves. Below 1.5 wt%: molecularly dissolved regime (cyan) and above 1.5 wt%: insoluble regime (magenta).

In this case, the block copolymer exhibits twofold switchable transitions. Depending on the polymer concentration, such block copolymers pass through a molecularly dissolved regime (below 1.5 wt%) or an insoluble regime (above 1.5 wt%). As a common feature, it is expected that core and corona of the aggregates

are turned inside-out, which is known as "schizophrenic" behavior.[9] See also in the appendix (**Figure A.60**) for an example showing only a molecularly dissolved intermediate regime.

5.3.2 Inverting the position of transitions via addition of salt

Turbidity measurements of solutions in H_2O containing NaCl were performed for the block copolymers. The modulation of the thermoresponsive behavior via electrolyte-sensitivity is shown in **Figure 5.10** for the example of **poly(M-3)$_{80}$-*block*-(M-12)$_{115}$**. As observed for the homopolymers, the UCST-type transition of the block copolymer decreases already by the addition of small amounts of salt, whereas the LCST-type transition is only affected at higher salt concentration. In this particular case, an insoluble regime is observed for intermediate temperatures at lower salt concentration, but a molecularly dissolved regime is found at higher salt concentration. Thus, an inversion of the relative position of UCST- and LCST-type transitions was realized by addition of salt (NaCl), superposing the thermo-responsiveness and the ion-sensitivity of poly(sulfobetaine)s. See also in the appendix (**Figure A.61**) for an example of the effect of added salt on a block copolymer showing only a molecularly dissolved intermediate regime.

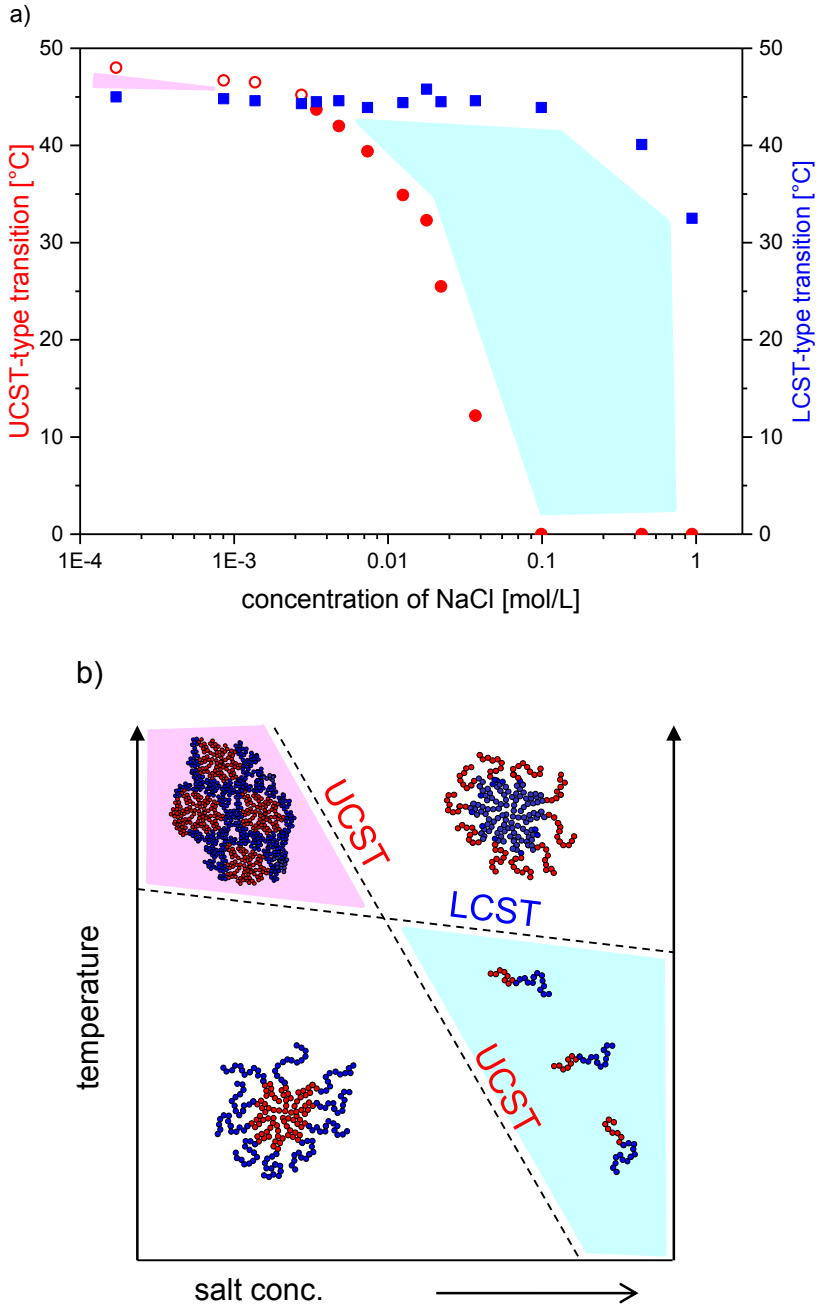

Figure 5.10. a) Turbidity of 5 wt% solutions of **poly(M-3)$_{80}$-*block*-(M-12)$_{115}$** in H_2O containing NaCl. (○) UCST-type transition was estimated via extrapolation of the turbidity curves. b) Schematic illustration of the modulation of thermoresponsive behavior via electrolyte-sensitivity.

6 Summary and conclusion

Two series of mostly new zwitterionic methacrylamide and methacrylate monomers were synthesized in good to excellent yields. They could be smoothly polymerized by reversible addition-fragmentation chain transfer (RAFT) polymerization in homogeneous solution in trifluoroethanol (TFE), without affecting the tacticity compared to the standard radical polymerization process. The RAFT method enabled well-controlled polymerization behavior as well as the facile incorporation of functional end groups, here, such bearing a fluorescent label, into the polymers.

The poly(sulfobetaine)s prepared are thermo-responsive in aqueous solution, exhibiting an UCST-type coil-to-globule phase transition, in dependence on the polyzwitterions' molar mass and concentration. The chemical structure of the poly(sulfobetaine) strongly affects the phase transition temperature, too, without following an obvious logic. For the polymers with the same zwitterionic side chain, methacrylamide-based poly(sulfobetaine)s exhibit higher UCST-type transition temperatures than their methacrylate analogs. The extension of the distance between polymerizable unit and zwitterionic group from 2 to 3 methylene units decreases the UCST-type transition temperatures. Methacrylate-based poly(sulfobetaine)s derived from aliphatic ammonium cations show higher UCST-type transition temperatures than their analogs featuring cyclic ammonium cations. Counterintuitively for the latter, the poly(sulfobetaine)s bearing a morpholine ring exhibit higher UCST-type transition temperatures than the ones bearing a piperidine ring. The UCST-type transition temperatures increase with spacer length separating the cationic and anionic moieties from 3 to 4 methylene units. Moreover, the incorporation of a hydroxyl group into a spacer group of 3 methylene units decreases the UCST

transition temperature in H_2O. Noteworthy, the cloud points in H_2O and D_2O differ substantially for all polymer series, whereby the strength of the effect depends sensitively on the detailed chemical structure of the polyzwitterion. This must be taken into account for interpreting studies of such polyzwitterions using deuterated solvents (such as ^1H NMR or neutron scattering experiments).

In agreement with the well-known "anti-polyelectrolyte" effect reported for other polyzwitterions, the solubility of newly synthesized poly(sulfobetaine)s in water is very sensitive to the addition of inorganic salts. Mostly salting-in effects are observed. The effectivity of salts in modulating the UCST-type transition temperatures can be correlated with the empirical Hofmeister series. Still, the UCST-type transition temperatures of the various polymers show characteristic differences in their detailed behavior upon salt addition. The salt effects still await understanding; clearly, will affect not only the use of such polymers in responsive systems, but also in all potential applications in biological or environmental systems that inherently contain low molar mass electrolytes. In any case, the findings show that apparently small variations of sulfobetaine structure can effectively modulate the phase transition temperature of these polyzwitterions in specific aqueous environments.

Using fluorophore functionalized poly(sulfobetaine)s as macro-RAFT agents, the non-ionic monomer **M-12** ("**NIPMAM**") was used to synthesize water-soluble block copolymers. As **poly(NIPMAM)** undergoes an LCST-type transition, these block copolymers with two hydrophilic blocks exhibit twofold thermoresponsive behavior in water, showing so-called "schizophrenic" behavior: this constellation induces a structure inversion of the solvophobic aggregates formed. Depending on the relative positions of the UCST- and LCST-type transitions, the block copolymers show either a molecularly dissolved or an insoluble state at intermediate temperatures. Moreover, the relative positions of UCST- and LCST-type transitions can be inverted by the polymer concentration or by the addition of low molar mass salts. Noteworthy, at low temperature, the poly(sulfobetaine) block forms polar aggregates that are kept in solution by the **poly(NIPMAM)** block, whereas at high temperature, the **poly(NIPMAM)** block forms hydrophobic aggregates that are kept in solution by the

poly(sulfobetaine) block. In this way, aggregates were prepared in water, which switch reversibly their “inside” to the “outside”, and vice versa.

7 Experimental part

7.1 Chemicals

Table 7.1. Utilized materials.

chemical	formula	CAS	purity	supplier
acetic acid	$C_2H_4O_2$	64-19-7	99.7 %	Aldrich
acetone	C_3H_6O	67-64-1	99.9 %	Aldrich
acetonitrile	C_2H_3N	75-05-8	99.8 %	Aldrich
mixed bed resin	-	100915-96-6	-	Aldrich
ammonium sulfate	$H_8N_2O_4S$	7783-20-2	99.5 %	Fluka
4,4´-azobis(4-cyanopentanoic acid) (V-501)	$C_{12}H_{16}N_4O_4$	2638-94-0	99 %	Wako
benzene	C_6H_6	71-43-2	99.8 %	Fluka
4-bromo-1,8-naphthalic anhydride	$C_{12}H_5BrO_3$	81-86-7	95 %	Aldrich
1,4-butane sultone	$C_4H_8O_3S$	1633-83-6	99+ %	Acros
calcium hydride	CaH_2	7789-78-8	95 %	Fluka
carbon disulfide	CS_2	75-15-0	99.9 %	Aldrich
chloroform	$CHCl_3$	67-66-3	99 %	Aldrich
chloroform-d	$CDCl_3$	865-49-6	99.8 atom% D	Armar

Chemical	formula	CAS	purity	supplier
3-chloro-2-hydroxy-1-propane sulfonic acid sodium-salt (CHPSNa)	$C_3H_6ClNaO_4S$	126-83-0	95 %	Raschig
4-chloro-1,8-naphthalic anhydride	$C_{12}H_5ClO_3$	4053-08-1	95 %	Fluka
deuterium oxide	D_2O	7789-20-2	99.9 atom% D	Armar
2,6-di-*tert*-butyl-4-methylphenol (BHT)	$C_{15}H_{24}O$	128-37-0	>99 %	Fluka
dichloromethane	CH_2Cl_2	75-09-2	99.8 %	Avantor
dichloromethane-d_2	CD_2Cl_2	1665-00-5	99.9 atom% D	Armar
N,N'-dicyclohexyl-carbodiimide (DCC)	$C_{13}H_{22}N_2$	538-75-0	99 %	Aldrich
diethyl ether	$C_4H_{10}O$	60-29-7	99.8 %	ChemSolute
N,N-dimethylacetamide	C_4H_9NO	127-19-5	99+ %	Aldrich
2-(dimethylamino)ethyl methacrylate	$C_8H_{15}NO_2$	2867-47-2	98 %	Aldrich
3-dimethylamino-1-propanol	$C_5H_{13}NO$	3179-63-3	98 %	Merck
3-(dimethylamino)-propionitrile	$C_5H_{10}N_2$	1738-25-6	98 %	Merck
N-(3-(dimethylamino)-propyl)methacrylamide (DMAPMA)	$C_9H_{18}N_2O$	5205-93-6	-	Evonik
4-(dimethylamino)-pyridine (DMAP)	$C_7H_{10}N_2$	1122-58-3	98 %	Fluka
dimethylformamide	C_3H_7NO	68-12-2	99.9 %	Roth
dimethyl sulfoxide	C_2H_6OS	67-68-5	99.5 %	Aldrich
ethanol	C_2H_6O	64-17-5	99.5 %	ChemSolute
ethanol amine	C_2H_7NO	141-43-5	99+ %	Aldrich
ethyl acetate	$C_4H_8O_2$	141-78-6	99.5 %	Merck

chemical	formula	CAS	purity	supplier
1-ethyl-3-methylimidazolium crotonic acid	$C_{10}H_{16}N_2O_2$	-	-	IAP (Dr. Bohrisch)
hexafluoroisopropanol	$C_3H_2F_6O$	920-66-1	99 %	Aldrich
n-hexane	C_6H_{14}	110-54-3	98.5 %	Merck
hydrochloric acid	HCl	7647-01-0	98 %	ChemSolute
hydrogen peroxide solution	H_2O_2	7722-84-1	33 %	Technical
hydroquinone	$C_6H_6O_2$	123-31-9	99 %	Aldrich
4-(2-hydroxyethyl)-morpholine	$C_6H_{13}NO_2$	622-40-2	99 %	Alfa Aesar
1-(2-hydroxyethyl)-piperidine	$C_7H_{17}NO$	3040-44-6	99 %	Alfa Aesar
inhibitor removers	-	306312	-	Aldrich
iodine	I_2	12190-71-5	-	Appli Chem
isoamyl alcohol	$C_5H_{12}O$	123-51-3	98 %	Amresco
N-isopropylacrylamide (**M-13**)	$C_6H_{11}NO$	2210-25-5	98 %	TCI
N-isopropylmethacryl-amide (**M-12**)	$C_7H_{13}NO$	13749-61-6	97 %	Aldrich
lithium aluminium hydride	AlH_4Li	16853-85-3	95 %	Aldrich
methyl methacrylate (**MMA**)	$C_5H_8O_2$	80-62-6	99 %	Aldrich
magnesium sulfate	$MgSO_4$	7487-88-9	99.5 %	Alfa Aesar
3-((3-methacrylamido-propyl)dimethyl-ammonio)propane-1-sulfonate (**M-1**)	$C_{12}H_{24}N_2O_4S$	5205-95-8	-	Raschig
methacryloyl chloride	C_4H_5ClO	920-46-7	97 %	Alfa Aesar

chemical	formula	CAS	purity	supplier
3-((2-(methacryloyloxy)-ethyl)dimethylammonio)-propane-1-sulfonate (**M-4**)	$C_{11}H_{21}NO_5S$	3637-26-1	-	Raschig
methanol	CH_4O	67-56-1	99.5 %	Avantor
methanol-d_4	CD_4O	811-98-3	99.9 atom% D	Armar
4-methoxybenzyl alcohol	$C_8H_{10}O_2$	105-13-5	98 %	Merck
4-methoxyphenol (MEHQ)	$C_7H_8O_2$	150-76-5	99.9 %	Acros
molecular sieve 4 Å	-	-	-	Roth
nitrobenzene	$C_6H_5NO_2$	98-95-3	99 %	Fluka
1-pentanol	$C_5H_{12}O$	13403-73-1	99+ %	Aldrich
2-phenylethyl bromide	C_8H_9Br	103-63-9	98 %	Alfa Aesar
2-phenylethanthiol	$C_8H_{10}S$	4410-99-5	98 %	Aldrich
phosphate buffered saline (PBS, clear)	-	P4417	-	Aldrich
potassium bromide	KBr	7758-02-3	99 %	Aldrich
potassium iodide	KI	7681-11-0	99.5 %	VK Labor
potassium phosphate	K_3PO_4	7778-53-2	99.9 %	Amresco
1,3-propanesultone	$C_3H_6O_3S$	1120-71-4	99 %	TCI
Sicapent®	O_5P_2	1314-56-3	-	Merck
sodium bromide	NaBr	7647-15-6	99 %	Aldrich
sodium chloride	NaCl	7647-14-5	99 %	ChemSolute
sodium hydride	NaH	7646-69-7	60.6 %	Alfa Aesar
sodium hydrogencarbonate	$NaHCO_3$	144-55-8	99 %	Roth
sodium hydroxide	NaOH	1310-73-2	-	ChemSolute
sodium sulfate	Na_2SO_4	7757-82-6	98.5 %	ChemSolute
sodium thiosulfate pentahydrate	$H_{10}Na_2O_8S_2$	10102-17-7	99.5 %	Merck

chemical	formula	CAS	purity	supplier
1,1,2,2-tetrachloroethane	$C_2H_2Cl_4$	79-34-5	98 %	Aldrich
tetrachloromethane	CCl_4	56-23-5	99 %	Aldrich
tetrahydrofuran	C_4H_8O	109-99-9	99.5 %	Acros
thiourea	CH_4N_2S	62-56-6	99+ %	Acros
toluene	C_7H_8	108-88-3	99.8 %	Merck
triethylamine	$C_6H_{15}N$	121-44-8	99 %	Acros
trifluoroacetic acid	$C_2HF_3O_2$	76-05-1	99 %	Aldrich
trifluoroethanol (TFE)	$C_2H_3F_3O$	75-89-8	99.8 %	Roth
trifluoroethanol-d_3	$C_2D_3F_3O$	77253-67-9	98 atom% D	Armar

Dichloromethane was dried over calcium hydride. Sodium hydride (NaH, 60.6 % in paraffin) was washed with dry *n*-hexane (stored over $LiAlH_4$) prior to use. Methacryloyl chloride was freshly distilled.[181] To remove inhibitors prior to use, **M-12** and **M-13** were crystallized from *n*-hexane, V-501 was crystallized in methanol, and **MMA** was passed through a column fitted with "inhibitor removers" (for removing hydroquinone and monomethyl ether hydroquinone). Deionized water was further purified by a Millipore Milli-Q Plus water purification system (resistivity 18 $M\Omega \cdot cm^{-1}$). Phosphate buffered saline was prepared according to the directions by Aldrich. All other chemicals were used as received.

7.2 Methods and calculations

Nuclear magnetic resonance (NMR) spectroscopy

^{1}H and ^{13}C NMR spectra, ^{1}H-^{1}H-Correlation Spectra (COSY), and ^{1}H-^{13}C-Hetero-nuclear Multiple Quantum Coherence spectra (HMQC) were recorded with a Bruker Avance 300 spectrometer (300 MHz and 75 MHz, respectively) and with a Bruker Avance 400 spectrometer (400 MHz and 125 MHz, respectively) at ambient temperature in deuterated solvents. ^{13}C NMR spectra were recorded in ^{1}H-broad band decoupling mode and in Attached Proton Test (APT) mode, respectively. Solvent signals were used as internal shift secondary reference. Approximate monomer conversions were determined via ^{1}H NMR spectra of the crude polymerization mixtures. Theoretically expected number average molar masses M_n^{theo} are calculated according to **equation 7.1**.

$$M_n^{theo} = \frac{c_{Mon,0} \cdot conversion \cdot M_{CRU}}{c_{CTA,0}} + M_{CTA} \qquad (\mathbf{7.1})$$

M_{CRU} = molar mass of the constitutional repeat unit
M_{CTA} = molar mass of the RAFT agent
$c_{Mon,0}$ = initial molar concentration of the monomer
$c_{CTA,0}$ = initial molar concentration of the RAFT agent

Molar masses were determined by end group analysis, comparing the integrals of signals characteristic for the Z- or R-group, respectively, with the integrals of the signals of the constitutional repeat unit (**equation 7.2**).[150]

$$M_n^{NMR} = \frac{\frac{N_{H(polymer)}}{N_{H(monomer)}}}{\frac{N_{H(end-group)}}{N_{H(end-group)}(theo.)}} \cdot M_{CRU} + M_{CTA} \qquad (\mathbf{7.2})$$

Gel permeation chromatography (GPC)

Measurements were conducted at two different systems. Both Spectra-System apparatuses were equipped with detectors SEC-3010 from WGE Dr. Bures (UV and refractive index) and with a set of PolarGel columns (Guard 8.0 x 50 mm and PolarGel L 300 x 7.5 mm) from Polymer Laboratory. For all measurements, flow rate was 1 $mL \cdot min^{-1}$ and calibration standard was PMMA from Polymer Standards Service. The differences of the two GPC systems were eluent and temperature. Thus, measurements in dimethylformamide + 0.1 % LiBr as eluent were performed at 50 °C, whereas measurements in tetrahydrofuran as eluent were performed at 30 °C.

Ultraviolet-visible (UV-vis) spectroscopy

Absorption spectra were recorded by a Perkin Elmer UV/Vis/NIR Spectrometer Lambda 19 and by a Varian Cary 50 Scan UV-vis spectrophotometer. The Cary 50 is equipped with Peltier element to control the temperature of the sample cell. Optical silica cuvettes with an optical path length d = 1 cm were used.

For the determination of extinction coefficients ε, 5 to 12 individual samples were prepared. Extinction coefficients of RAFT agents at maximum absorbance wavelengths λ_{max} (π-π*-transition) in various solvents were determined by linear regression of the absorbance with concentration data. Values of λ_{max} were reproducible within ±1 nm.

Number average molar masses of the polymers were determined by end group analysis using the corrected $\varepsilon_{\lambda max3}$ ($L \cdot mol^{-1} \cdot cm^{-1}$) in TFE (see **Table 3.2**), assuming that every polymer chain carries one naphthalimide chromophore moiety. The molar concentration of the naphthalimide chromophore, and thus of the polymer, in a diluted solution was calculated using the Lambert-Beer law (**equation 7.3**). The molar masses of the polymers were calculated via **equation 7.4**.

$$c = \frac{A}{d \cdot \varepsilon} \qquad (\mathbf{7.3})$$

$$M_n^{UV} = \frac{m}{c \cdot V} = \frac{m \cdot \varepsilon \cdot d}{A \cdot V} \quad (7.4)$$

M_n^{UV} = number average molar mass calculated from UV-data
c = molar concentration of the polymer in $mol \cdot L^{-1}$
A = absorbance of the sample
d = path length of the cell in cm
ε = extinction coefficient in $L \cdot mol^{-1} \cdot cm^{-1}$
m = mass of the polymer in g
V = volume of the solvent in L

Fluorescence spectroscopy

Fluorescence spectra were recorded by a Perkin Elmer Luminescence Spectrometer LS 50 B (for measurements at 25 °C) and by a Horiba FluoroMax-3 (for temperature dependent measurements). Optical silica cuvettes with an optical path length d = 1 cm were utilized. Excitation wavelength was 442 nm, slit width was varied from 2 – 10 nm. The FluoroMax-3 apparatus, equipped with a thermostated cell holder, was used at slit width of 2 nm.

Mass spectrometry

High resolution mass spectra (HR-MS) were recorded with a Thermo Scientific ESI-Q-TOFmicro (Quadropol – Time of Flight). Electrospray ionization (ESI) and water as solvent was chosen as method.

Elemental analysis

Measurements were carried out using a Vario ELIII microanalyzer from Elementar Analysensysteme (Germany, Hanau).

Fourier transform-infrared (FT-IR) spectroscopy

FT-IR spectra were recorded in a N_2 purged atmosphere with a Thermo Nicolet Nexus FT-IR spectrometer equipped with an attenuated total reflection (ATR) Smart Endurance element, or the spectra were taken from KBr pellets using a FT-IR spectrometer IFS 66/s from Bruker.

Thermogravimetric analysis (TGA)

Measurements were conducted under N_2 atmosphere with a Mettler Toledo TGA/SDTA 851^e or a Netzsch TG 209 F1 apparatus, in the temperature range from 25 °C to 900 °C with a heating rate of 10 $K \cdot min^{-1}$.

Differential scanning calorimetry (DSC)

Analyses were performed with a Mettler Toledo DSC 822^e at N_2 atmosphere. Method was set as follows: first and third cycle with heating and cooling rates of 10 $K \cdot min^{-1}$, second cycle with heating and cooling rates of 30 $K \cdot min^{-1}$, while the temperature range is set as 25 – 250 °C.

Turbidimetry

Cloud points were determined by turbidimetry using a Varian Cary 50 Scan UV-vis spectrophotometer, equipped with a single cell Peltier thermostated cell holder, using 1 cm x 1 cm optical silica cuvettes. Measurements with the Cary 50 were performed at a wavelength of 800 nm and with heating and cooling rates of 0.5 $K \cdot min^{-1}$. Aqueous polymer solutions of various concentrations were prepared in D_2O, in Millipore water, or aqueous salt solutions. The cloud point was taken as the temperature where the normalized transmittance of the solution in the cooling runs reached 95 % (relative %).

Dynamic light scattering (DLS)

Size determination of polymers in aqueous solution was performed with Malvern Instrument High Performance Particle Sizer and Zetasizer Nano Series equipped with a He-Ne laser (λ = 633 nm) and a thermoelectric Peltier element for temperature control. Measurements were conducted at scattering angle θ = 173° (backscattering detection mode). Aqueous polymer solutions were prepared in Millipore water using 1 cm x 1 cm optical silica cuvettes. Temperature *vs*. size trend was performed with 12 individual runs per temperature and the data are given over arithmetic averages of all runs. Temperature steps of 1 °C and equilibration time of 2 min were chosen.

7.3 Synthesis of RAFT agents

7.3.1 Synthesis of benzyl-labeled RAFT agent

Synthesis of 4-cyano-4-(((phenethylthio)carbonothioyl)thio)pentanoic acid (CTA-1)

The trithiocarbonate RAFT agent 4-cyano-4-(((phenethylthio)carbonothioyl)thio) pentanoic acid (**CTA-1**) was synthesized as described by Semsarilar et al.[145]

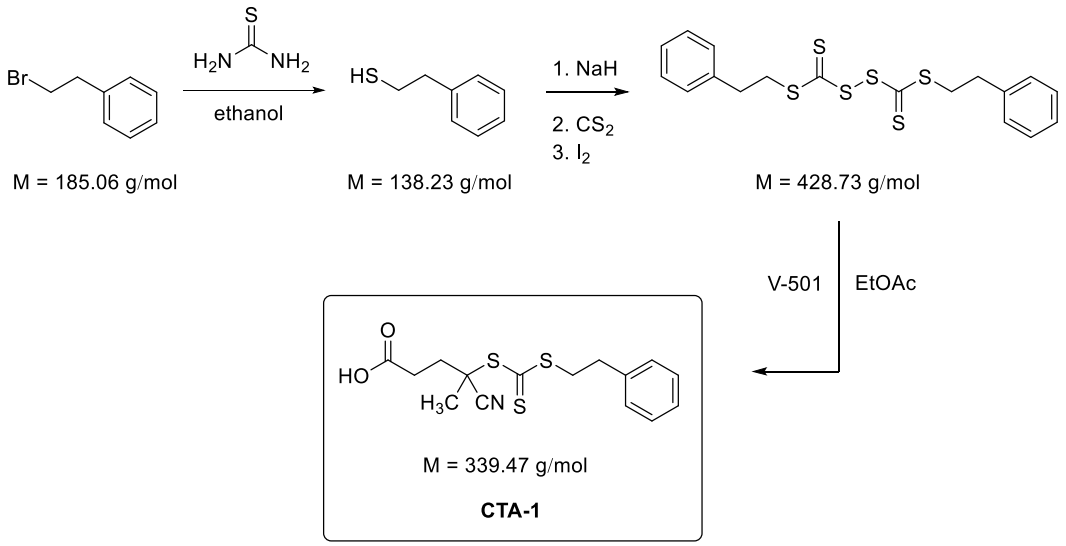

Step 1[182]: 2-Phenylethyl bromide (18.6 g, 0.1 mol) and thiourea (1.1 eq., 8.4 g, 0.11 mol) were dissolved in ethanol (5 ml). After purging with N_2, the suspension was heated to 80 °C and refluxed for 6 h. The thiourea dissolved after ~30 min. The reaction mixture was allowed to cool down to room temperature and stirred for 2 days. During that time, a white solid precipitated. 5 N NaOH (60 ml, purged with N_2) was added dropwise to the mixture, resulting in a cloudy and pinkish suspension which was refluxed for another 2 h. At this stage, the mixture cleared up and an oil phase began to separate. Subsequently, 2 N HCl (100 ml, purged with N_2) was added dropwise to the reaction flask, resulting in a white precipitate which was filtered off. Organic and water phase were extracted with diethyl ether (40 ml, 4 times). The combined organic phases were dried over sodium sulfate and filtrated. Subsequently, after removal of the solvent, the product was purified by ball tube distillation

(T = 60 °C, p = 0.1 mbar). The pure 2-phenylethanethiol was obtained as colorless oil (yield 10.7 g, 78 %).

Step 2: Sodium hydride (1.1 eq., 3.52 g, 0.09 mol) was washed with dry *n*-hexane (20 ml, 2 times) in order to remove the paraffin (to deactivate small amounts of NaH in *n*-hexane, the washing solvent was mixed with 2-propanol) and subsequently mixed with dry diethyl ether (150 ml). 2-Phenylethanethiol (10.70 g, 0.08 mol) was added dropwise to the suspension of NaH and diethyl ether, resulting in a strong H_2 formation and a white precipitate. When the H_2 formation ceased after 2 h, carbon disulfide (CS_2, 1.1 eq., 5.20 ml, ρ = 1.26 g·ml^{-1}, 0.09 mol) was added resulting in new H_2 formation of 30 min due to the release of encapsulated NaH which subsequently reacted with unconverted 2-phenylethanethiol. Subsequently, I_2 (10.20 g, 0.04 mol) was added in small portions and the yellow-brown suspension was allowed to stir for 1 h followed by filtration. The progress of reaction was followed by thin layer chromatography (TLC) (eluent: *n*-hexane:ethyl acetate (10/1 v/v), R_f: 0.60). Water saturated with sodium thiosulfate pentahydrate (200 ml) was poured in the reaction flask. The organic phase was separated, washed and extracted with water (200 ml, 2 times). After drying over Na_2SO_4, removing the solvent and drying in vacuum, *bis*-(2-phenylethane sulfanylthiocarbonyl) disulfide was obtained as orange solid (yield 8.78 g, 53 %).

Step 3: *Bis*-(2-phenylethane sulfanylthiocarbonyl) disulfide (4.260 g, 0.010 mol) was dissolved in ethyl acetate (100 ml). After purging with N_2, 4,4'-azobis (4-cyanopentanoic acid) (V-501, 4.200 g, 0.015 mol) was added and the yellow-orange mixture was refluxed for 20 h. The progress of reaction was followed by TLC (eluent: *n*-hexane:ethyl acetate (10/1 v/v), R_f: 0). Afterwards, most of the solvent was removed. The residue was washed with diethyl ether and water (100 ml, 5 times). After drying over Na_2SO_4 and evaporating the residual solvent, the residue was purified via gradient flash chromatography (eluent: *n*-hexane:ethyl acetate (1/0, 10/1, 1/1 v/v R_f: 0.12). Pure 4-cyano-4-(((phenethylthio)carbonothioyl)thio) pentanoic acid (**CTA-1**) was obtained as yellow-orange oil (yield 4.00 g, 59 %).

^{1}H NMR (300 MHz, CD_3OD, 298 K): δ (ppm) = 1.84 (s, 3H, -C-CH_3), 2.30 – 2.62 (m, 4H, -$(CH_2)_2$-COO-, 2.96 (t, *J* = 7.7 Hz, 2H, -CH_2-S-), 3.60 (t, *J* = 7.7 Hz, 2H, aryl-CH_2-), 7.12 – 7.32 (m, 5H, =CH- phenyl).

^{13}C NMR (75 MHz, $CDCl_3$, 298 K): δ (ppm) = 24.5 (-C-$\underline{C}H_3$), 29.4 (-C-$\underline{C}H_2$-COO-), 33.3 (-$\underline{C}H_2$-C-COO-), 33.8 (-$\underline{C}H_2$-S-), 37.8 (aryl-$\underline{C}H_2$-), 46.2 (-S-$\underline{C}$-CN), 118.6 (-$\underline{C}$N), 126.6, 128.4, and 128.5 (=$\underline{C}$H- phenyl), 138.9 (=$\underline{C}$- phenyl), 177.0 (-$\underline{C}$OO-), 216.3 (-$\underline{C}$=S).

UV-vis absorbance maxima: in chloroform (λ_{max} = 295 nm; ε_{295} = $1.23 \cdot 10^4$ $L \cdot mol^{-1} \cdot cm^{-1}$), in ethanol ($\lambda_{max}$ = 301 nm; ε_{301} = $1.03 \cdot 10^4$ $L \cdot mol^{-1} \cdot cm^{-1}$), and in trifluoroethanol (λ_{max} = 306 nm; ε_{306} = $1.14 \cdot 10^4$ $L \cdot mol^{-1} \cdot cm^{-1}$).

7.3.2 Synthesis of methoxybenzyl-labeled RAFT agent

Synthesis of 4-methoxybenzyl 4-cyano-4-(((phenethylthio)carbonothioyl)thio) pentanoate (CTA-2)

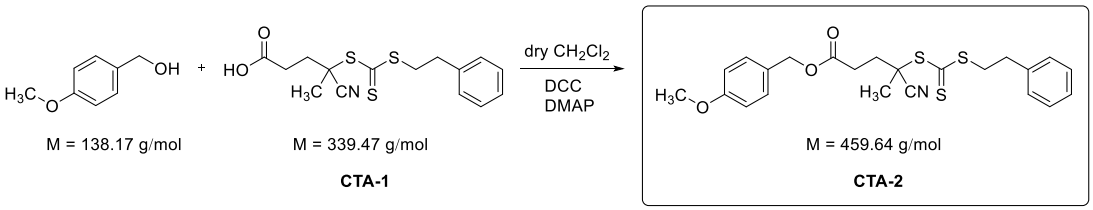

The esterification of **CTA-1** with 4-methoxybenzyl alcohol was carried out using the Steglich procedure.[183] **CTA-1** (1.66 g, $4.9 \cdot 10^{-3}$ mol) and 4-methoxybenzyl alcohol (1.2 eq., 0.81 g, $3.9 \cdot 10^{-3}$ mol) were dissolved in dry dichloromethane (7 ml, 1.00 g alcohol requires 10 ml solvent). After purging the mixture with N_2, the clear solution was cooled down to 0 °C in an ice bath. Meanwhile, N,N'-dicyclohexyl-carbodiimide (DCC, 1.5 eq., 1.52 g, $7.3 \cdot 10^{-3}$ mol) and 4-dimethylaminopyridine (DMAP, 5 mol% of DCC, 0.05 g, $3.7 \cdot 10^{-4}$ mol) were dissolved in dry dichloromethane (3 ml) and subsequently added dropwise to the reaction mixture.

Precipitation of dicyclohexylurea was observed. The resulting suspension was allowed to stir for 15 min at 0 °C, before it was stirred for the next 5 days at room temperature. The progress of reaction was followed by TLC (eluent: *n*-hexane:ethyl acetate (1/1 v/v), R_f: 0.96). After diluting the suspension by dichloromethane (20 ml) and filtrating off the byproduct, the solvent was evaporated to give a viscous yellow oil. The dilution-filtration-evaporation step was repeated 2 times to completely remove dicyclohexylurea. The residue was diluted by ethyl acetate (1 ml) and purified via gradient flash chromatography (eluent: *n*-hexane:ethyl acetate (2/1 v/v R_f: 0.65, 1/1 v/v). Pure labeled trithiocarbonate RAFT agent 4-methoxybenzyl 4-cyano-4-(((phenethylthio)carbonothioyl)thio)pentanoate (**CTA-2**) was isolated as viscous yellow oil (yield 1.32 g, 59 %).

^{1}H NMR (300 MHz, CD_2Cl_2, 298 K): δ (ppm) = 1.75 (s, 3H, -C-CH_3), 2.30 – 2.60 (m, 4H, -$(CH_2)_2$-COO-, 2.89 (t, *J* = 7.7 Hz, 2H, -CH_2-S-), 3.51 (t, *J* = 7.7 Hz, 2H, aryl-CH_2-), 3.70 (s, 3H, -O-CH_3), 4.99 (s, 2H, -COO-CH_2-), 6.83 (dd, 2H, *J* = 8.7 Hz, =CH- methoxyphenyl (C3, C5)), 7.10 – 7.30 (m, 7H, =CH- phenyl), =CH- methoxyphenyl (C2, C6)).

^{13}C NMR (75 MHz, CD_2Cl_2, 298 K): δ (ppm) = 29.7 (-C-$\underline{C}H_3$), 35.4 (-C-$\underline{C}H_2$-COO-), 39.2 (-$\underline{C}H_2$-C-COO-), 39.6 (-$\underline{C}H_2$-S-), 43.6 (aryl-$\underline{C}H_2$-), 58.9 (-S-$\underline{C}$-CN), 60.5 (-O-$\underline{C}H_3$), 72.3 (COO-$\underline{C}H_2$-), 119.5 (=$\underline{C}$H- methoxyphenyl, (C3, C5)), 124.8 (-$\underline{C}$N), 132.3 and 134.2 (=$\underline{C}$H- phenyl), 133.6 (=$\underline{C}$- phenyl), 135.8 (=$\underline{C}$H- methoxyphenyl, (C2, C6)), 145.1 (=$\underline{C}$- methoxyphenyl, (C1, C4)), 177.4 ($\underline{C}$OO-), 223.3 (-$\underline{C}$=S).

HR-MS (ESI): calculated: 459.1000 $[M]^+$; found: 460.1068 $[M+H]^+$.

Elemental analysis ($C_{23}H_{25}NO_3S_3$, M_r = 459.64): calculated: C = 60.10 %, H = 5.48 %, N = 3.05 %, S = 20.93 %; found: C = 60.18 %, H = 5.47 %, N = 3.05 %, S = 19.90 %.

FT-IR (selected bands, cm^{-1}): 2932 ν(CH_2), 2230 ν(CN), 1729 ν(OC=O), 1612, 1514 ν(C=C_{aryl}), 1246 ν(C=S).

UV-vis absorbance maxima: in chloroform (λ_{max} = 296 nm; ε_{296} = $1.23 \cdot 10^4$ $L \cdot mol^{-1} \cdot cm^{-1}$), in ethanol ($\lambda_{max}$ = 302 nm; ε_{302} = $1.04 \cdot 10^4$ $L \cdot mol^{-1} \cdot cm^{-1}$), and in trifluoroethanol (λ_{max} = 307 nm; ε_{307} = $1.14 \cdot 10^4$ $L \cdot mol^{-1} \cdot cm^{-1}$).

7.3.3 Synthesis of fluorophore-labeled RAFT agent

Synthesis of 4-dimethylamino-*N*-2-hydroxyethyl-1,8-naphthalimide (I-1)

The fluorophore intermediate 4-dimethylamino-*N*-2-hydroxyethyl-1,8-naphthalimide (**I-1**) is synthesized as described by Inal et al.[143]

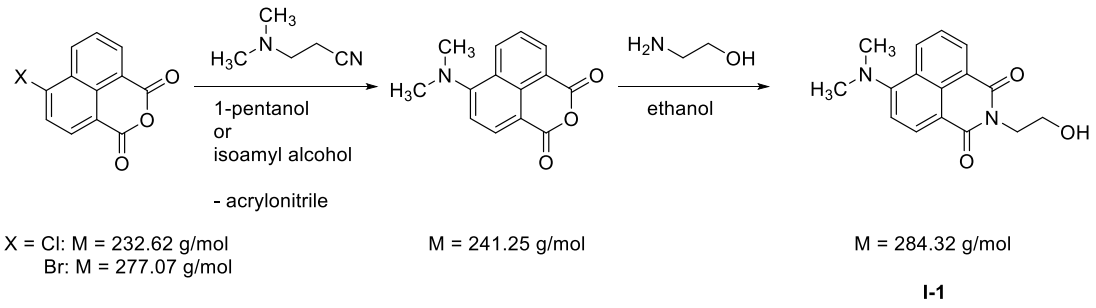

Step 1: 4-chloro-1,8-naphthalic anhydride (15.00 g, $6.4 \cdot 10^{-2}$ mol) was mixed with 1-pentanol (450 ml). The suspension was purged with N_2 and heated to 140 °C to dissolve 4-chloro-1,8-naphthalic anhydride. Strong gas (acrylonitrile) formation was observed after adding 3-(dimethylamino)propionitrile (4 eq., 29.0 ml, ρ = 0.87 $g \cdot ml^{-1}$, 0.26 mol) dropwise within 10 min to the solution. Subsequently, the reaction mixture was continuously stirred at 140 °C for 18 h before it was cooled to room temperature resulting in the formation of an orange-yellow precipitate. After filtering off and washing thoroughly with water (80 ml), 4-dimethylamino-1,8-naphthalic anhydride was dried in vacuum over Sicapent® at 65 °C for 24 h. Golden-yellow needles were obtained after recrystallization in 1-pentanol (450 ml) (yield 11.77 g, 76 %, m.p. = 198 – 200 °C).

This intermediate was also successfully synthesized with 4-bromo-1,8-naphthalic anhydride (5.54 g, $2.0 \cdot 10^{-2}$ mol) and 3-(dimethylamino)propionitrile (4 eq., 9.0 ml, $\rho = 0.87$ g·ml^{-1}, $8.0 \cdot 10^{-2}$ mol) in isoamyl alcohol (140 ml) (yield 3.72 g, 77 %) or with 4-bromo-1,8-naphthalic anhydride (1.11 g, $4.0 \cdot 10^{-3}$ mol) and 3-(dimethylamino) propionitrile (4 eq., 1.8 ml, $\rho = 0.87$ g·ml^{-1}, $1.6 \cdot 10^{-2}$ mol) in 1-pentanol (28 ml) (yield 0.76 g, 79 %). While synthesis with 4-chloro-1,8-naphthalic anhydride (0.93 g, $4.0 \cdot 10^{-3}$ mol) and 3-(dimethylamino)propionitrile (4 eq., 1.8 ml, $\rho = 0.87$ g·ml^{-1}, $1.6 \cdot 10^{-2}$ mol) in isoamyl alcohol (28 ml) gave a yield of only 0.13 g (13 %).

Step 2: 4-dimethylamino-1,8-naphthalic anhydride (3.59 g, $1.5 \cdot 10^{-2}$ mol) and ethanolamine (1.3 eq., 1.0 ml, $\rho = 1.01$ g·ml^{-1}, $1.9 \cdot 10^{-2}$ mol) were mixed in ethanol (140 ml). The resulting suspension was refluxed for 26 h, in the meantime 4-dimethylamino-1,8-naphthalic anhydride dissolved (at ~78 °C). The progress of the reaction was followed by TLC (eluent: chloroform:methanol (9/1 v/v), R_f: 0.52). The solvent was removed to give an orange oil, which was then diluted by chloroform and extracted with water (100 ml, 3 times) to remove the excess of ethanolamine. Subsequently, the organic phase was dried over Na_2SO_4. After removal of the solvent and drying in vacuum, pure 4-dimethylamino-*N*-2-hydroxyethyl-1,8-naphthalimide (**I-1**) was obtained as orange solid (yield 4.08 g, 99 %, m.p. >300 °C).

^{1}H NMR (300 MHz, $CDCl_3$, 298 K): δ (ppm) = 3.09 (s, 6H, -N-$(CH_3)_2$), 3.95 (t, *J* = 5.3 Hz, 2H, (-N-CH_2-), 4.41 (t, *J* = 5.3 Hz, 2H, -CH_2-OH), 7.07 (d, *J* = 8.3 Hz, 1H, =CH- naphthyl (C3)), 7.60 (t, *J* = 7.3 Hz, 1H, =CH- naphthyl (C6)), 8.40 (dd, *J* = 8.3, 7.3 Hz, 2H, =CH- naphthyl (C2, C7)), 8.50 (d, *J* = 7.3 Hz, 1H, =CH- naphthyl (C5)).

^{13}C NMR (75 MHz, $CDCl_3$, 298 K): δ (ppm) = 42.7 (-N-$\underline{C}H_2$-), 44.9 (-N-$(\underline{C}H_3)_2$), 62.0 ($\underline{C}H_2$-OH), 113.1 (=$\underline{C}$H- naphthyl (C3)), 114.3 (=$\underline{C}$- naphthyl (C1)), 122.6 (=$\underline{C}$- naphthyl (C9)), 124.7 (=$\underline{C}$- naphthyl (C8)), 130.3 (=$\underline{C}$- naphthyl (C10)), 131.2 (=$\underline{C}$H- naphthyl (C6)), 131.4 (=$\underline{C}$H- naphthyl (C5)), 132.9 (=$\underline{C}$H- naphthyl (C7)), 157.1 (=$\underline{C}$H- naphthyl (C2)), 164.9 (-$\underline{C}$ON-), 165.4 (=$\underline{C}$H- naphthyl (C4)).

FT-IR (selected bands, cm^{-1}): 3476 ν(OH), 2960 ν(CH_3), 1682 ν(NC=O), 1631 ν(NC=O), 1582 1585 ν(C=C_{aryl}).

UV-vis absorbance maxima: in chloroform (λ_{max} = 420 nm; ε_{420} = $1.11 \cdot 10^4$ $L \cdot mol^{-1} \cdot cm^{-1}$), in ethanol ($\lambda_{max}$ = 260, 288, and 418 nm; $\varepsilon_{418} = 0.98 \cdot 10^4$ $L \cdot mol^{-1} \cdot cm^{-1}$), and in trifluoroethanol (λ_{max} = 258, 286, and 444 nm; $\varepsilon_{444} = 1.98 \cdot 10^4$ $L \cdot mol^{-1} \cdot cm^{-1}$).

Fluorescence emission maxima: in chloroform (λ_{PL} = 505 nm), in ethanol (λ_{PL} = 529 nm), in trifluoroethanol (λ_{PL} = 542 nm), and in water (λ_{PL} = 546 nm).

Synthesis of 2-(6-(dimethylamino)-1,3-dioxo-1H-benzo[de]isoquinolin-2(3H)-yl) ethyl 4-cyano-4-(((phenethyl-thio)carbonothioyl)thio)pentanoate (CTA-3)

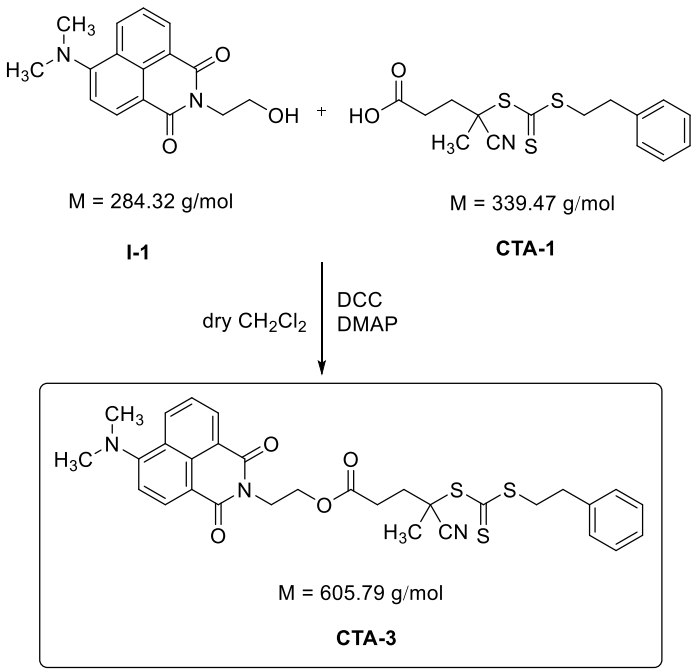

The synthesis of 2-(6-(dimethylamino)-1,3-dioxo-1H-benzo[de]isoquinolin-2(3H)-yl)ethyl 4-cyano-4-(((phenethylthio)carbonothioyl)thio)pentanoate (**CTA-3**) was carried out by esterification according to Steglich's procedure.[183] In a typical procedure, **CTA-1** (2.63 g, $7.7 \cdot 10^{-3}$ mol) and **I-1** (1.2 eq., 2.62 g, $9.2 \cdot 10^{-3}$ mol) were dissolved in dry dichloromethane (16 ml, 1.00 g alcohol requires 10 ml solvent). The

reaction mixture was purged with N_2 and cooled to 0 °C, and a solution of DCC (1.5 eq., 2.46 g, $1.2 \cdot 10^{-2}$ mol) and DMAP (5 mol% of DCC, 0.08 g, $6.0 \cdot 10^{-4}$ mol) in dry dichloromethane (10 ml) was added dropwise. Precipitation of dicyclohexylurea was observed. The resulting suspension was stirred for 15 min at 0 °C, and subsequently stirred for 48 h at room temperature. The progress of reaction was followed by TLC (eluent: *n*-hexane:ethyl acetate (1/1 v/v), R_f: 0.50, R_f of starting materials: 0.16). The suspension was diluted by dichloromethane (50 ml) and the precipitate was filtered off. The precipitate is dried to afford a viscous orange oil. The crude product was dissolved in ethyl acetate (3 ml), and filtered once more. After evaporating the solvent, the residue was purified via flash chromatography (eluent: *n*-hexane:ethyl acetate (1/1 v/v), R_f: 0.50). Pure fluorophore-labeled 2-(6-(dimethylamino)-1,3-dioxo-1H-benzo[de]isoquinolin-2(3H)-yl)ethyl 4-cyano-4-(((phenethylthio)carbonothioyl)thio)pentanoate (**CTA-3**) was obtained as highly viscous orange oil (yield 4.40 g, 72 %).

^{1}H NMR (300 MHz, CD_3OD, 298 K): δ (ppm) = 1.35 (s, 3H, -C-CH_3), 1.80 – 2.10 (m, 4H, $(CH_2)_2$-COO-, 2.50 (t, *J* = 7.7 Hz, 2H, -CH_2-S-), 2.64 (s, 6H, -N-$(CH_3)_2$), 3.09 (t, *J* = 7.7 Hz, 2H, aryl-CH_2-), 3.95 (m, 4H, -COO-$(CH_2)_2$-), 6.65 (d, *J* = 8.3 Hz, 1H, =CH- naphthyl (C3)), 6.70 – 6.90 (m, 5H, =CH- phenyl), 7.19 (t, *J* = 7.3 Hz, 1H, =CH- naphthyl (C6)), 7.99 (dd, *J* = 8.3, 7.3 Hz, 2H, =CH- naphthyl (C2, C7)), 8.05 (d, *J* = 7.3 Hz, 1H, =CH- naphthyl (C5)).

^{13}C NMR (75 MHz, $CDCl_3$, 298 K): δ (ppm) = 24.5 (-C-$\underline{C}H_3$), 29.6 (-$\underline{C}H_2$-COO-), 33.6 ($\underline{C}H_2$-C-COO-), 33.9 (-$\underline{C}H_2$-S-), 37.7 (aryl-$\underline{C}H_2$-), 38.5 (-$\underline{C}$-CN), 44.6 (-N-($\underline{C}H_3)_2$), 46.4 (COO-C-$\underline{C}H_2$-N-), 62.2 (-COO-$\underline{C}H_2$-C-N-), 113.1 (=$\underline{C}$H- naphthyl (C3)), 114.3 (-$\underline{C}$N), 118.8 (=$\underline{C}$- naphthyl (C1)), 122.5 (=$\underline{C}$- naphthyl (C9)), 124.7 (=$\underline{C}$H- naphthyl (C6)), 125.0 (=$\underline{C}$- naphthyl (C8)), 126.6 (=$\underline{C}$H- phenyl (C4)), 128.3 (=$\underline{C}$H- phenyl (C2, C3, C5, C6)), 128.5 (=$\underline{C}$- naphthyl (C10)), 130.1 (=$\underline{C}$H- naphthyl (C5)), 131.2 (=$\underline{C}$H- naphthyl (C7)), 132.6 (=$\underline{C}$H- naphthyl (C2)), 139.0 (=$\underline{C}$- phenyl (C1)), 156.9 (=$\underline{C}$- naphthyl (C4)), 163.8 (-$\underline{C}$ON-), 164.4 ($\underline{C}$ON-), 171.1 (-$\underline{C}$OO-), 216.5 (-$\underline{C}$=S).

HR-MS (ESI): calculated: 605.1500 $[M]^+$; found: 606.1574 $[M+H]^+$.

Elemental analysis ($C_{31}H_{31}N_3O_4S_3$, M_r = 605.79): calculated: C = 61.46 %, H = 5.16 %, N = 6.94 %, S = 15.88 %; found: C = 61.34 %, H = 5.16 %, N = 6.72 %, S = 15.08 %.

FT-IR (selected bands, cm^{-1}): 2960 ν(CH_3), 2230 ν(CN), 1739 ν(OC=O), 1692 ν(NC=O), 1654 ν(NC=O), 1585 ν(C=C_{aryl}).

UV-vis absorbance maxima: in chloroform (λ_{max} = 420 nm, ε_{420} = $1.19 \cdot 10^4$ $L \cdot mol^{-1} \cdot cm^{-1}$), in ethyl acetate ($\lambda_{max}$ = 259, 288, and 409 nm; ε_{409} = $1.14 \cdot 10^4$ $L \cdot mol^{-1} \cdot cm^{-1}$), in dimethylacetamide (λ_{max} = 292, and 423 nm; ε_{423} = $0.81 \cdot 10^4$ $L \cdot mol^{-1} \cdot cm^{-1}$), in dimethylformamide (λ_{max} = 290, and 423 nm; ε_{423} = $1.71 \cdot 10^4$ $L \cdot mol^{-1} \cdot cm^{-1}$), in ethanol ($\lambda_{max}$ = 259, 290, and 422 nm; ε_{422} = $1.08 \cdot 10^4$ $L \cdot mol^{-1} \cdot cm^{-1}$), in trifluoroethanol ($\lambda_{max}$ = 258, 290, and 444 nm; ε_{444} = $1.30 \cdot 10^4$ $L \cdot mol^{-1} \cdot cm^{-1}$), in water (sparingly soluble; λ_{max} = 258, 297, and 447 nm), and in 1-ethyl-3-methylimidazolium crotonic acid (sparingly soluble; λ_{max} = 432 nm).

Fluorescence emission maxima: in chloroform (λ_{PL} = 502 nm), in ethyl acetate (λ_{PL} = 509 nm), in dimethylacetamide (λ_{PL} = 528 nm), in dimethylformamide (λ_{PL} = 529 nm), in ethanol (λ_{PL} = 525 nm), in trifluoroethanol (λ_{PL} = 539 nm), in water (sparingly soluble; λ_{PL} = 546 nm), and in 1-ethyl-3-methylimidazolium crotonic acid (sparingly soluble; λ_{PL} = 520 nm).

7.4 Synthesis of sulfobetaine monomers

7.4.1 Synthesis of methacrylamide sulfobetaines

Synthesis of 2-hydroxy-3-((3-methacrylamidopropyl)dimethylammonio)propane-1-sulfonate (M-2)

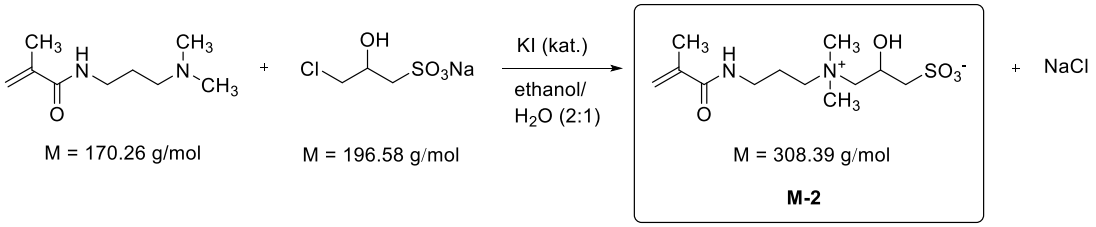

For the synthesis of 2-hydroxy-3-((3-methacrylamidopropyl)dimethylammonio) propane-1-sulfonate (**M-2**), the approach reported by Zhu et al. was adapted.[184] *N*-(3-(dimethylamino)propyl)methacrylamide (DMAPMA, 1.72 g, 0.01 mol), 3-chloro-2-hydroxy-1-propane sulfonic acid sodium-salt (CHPSNa, 1.0 eq., 1.97 g, 0.01 mol), potassium iodide (0.02 g, 1 mol%), and a few milligrams of 2,6-di-*tert*-butyl-4-methylphenol (BHT) were dissolved in a mixture of ethanol (7 ml) and water (3 ml). After purging with N_2, the mixture (pH = 9) was refluxed while stirring for 96 h. After cooling, water (50 ml) was added to the mixture, resulting in a small amount of white precipitate (side product) which was removed by filtration. The filtrate was passed through a column filled with adequate amount (~20 ml) of mixed bed ion exchanger (capacity: 0.55 meq·ml^{-1} for cation and anion). A small amount of hydroquinone was added and the solution was freeze-dried. Crystallization of the residue from acetonitrile yielded monomer 2-hydroxy-3-((3-methacrylamidopropyl) dimethylammonio)propane-1-sulfonate (**M-2**) as colorless powder (yield 2.40 g, 77 %, m.p. = 125 – 128 °C).

^{1}H NMR (300 MHz, D_2O, 298 K): δ (ppm) = 1.94 (s, 3H, =C-CH_3), 2.09 (m, 2H, -CON-C-CH_2-), 3.15 (d, 2H, *J* = 5.7 Hz, -CH_2-SO_3^-), 3.2 (s, 6H, -N^+-$(CH_3)_2$), 3.38 (t, 2H, *J* = 6.5 Hz, -CON-CH_2-), 3.4 – 3.7 (m, 4H, -CH_2-N^+-CH_2-), 4.66 (m, 1H, -CH-OH), 5.48 (s, 1H, CH=C-CON- (trans)), 5.72 (s, 1H, CH=C-CON- (cis)).

^{13}C NMR (75 MHz, D_2O, 298 K): δ (ppm) = 18.0 (CH_2=C-<u>C</u>H_3), 22.8 (-CON-C-<u>C</u>H_2-), 36.6 (-CON-<u>C</u>H_2-), 52.2 (-N^+-(<u>C</u>H_3)$_2$), 55.6 (-<u>C</u>H_2-SO_3^-), 63.1 (-<u>C</u>H-OH), 63.8 (-<u>C</u>H_2-N^+-), 67.4 (-N^+-<u>C</u>H_2-CHOH-), 121.7 (=<u>C</u>H_2), 139.3 (=<u>C</u>-CON-), 172.4 (-<u>C</u>ON-).

HR-MS (ESI): calculated: 308.1400 $[M]^+$; found: 309.1480 $[M+H]^+$.

Elemental analysis ($C_{12}H_{24}N_2O_5S$, M_r = 308.39): calculated: C = 46.74 %, H = 7.84 %, N = 9.08 %, S = 10.40 %; found: C = 46.55 %, H = 7.90 %, N = 9.10 %, S = 10.22 %.

FT-IR (selected bands, cm^{-1}): 3500 ν(OH), 3341 ν(NH), 3042 ν(N^+-CH_3), 2973 ν(CH_3), 1658 ν(amide I), 1617 ν(C=C), 1537 ν(amide II), 1202 $\nu_{as}(SO_3^-)$, 1041 $\nu_s(SO_3^-)$.

Synthesis of 4-((3-methacrylamidopropyl)dimethylammonio)butane-1-sulfonate (M-3)

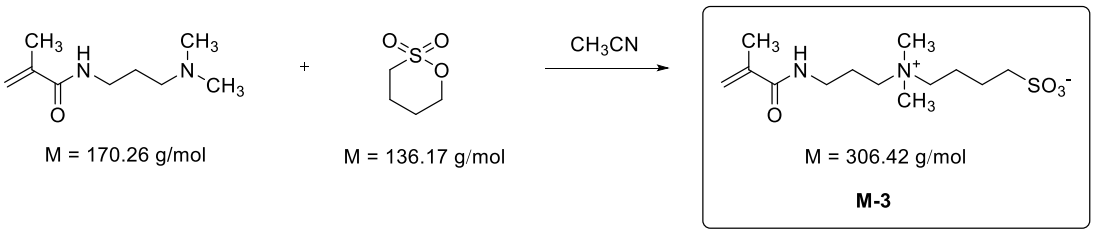

In a typical procedure adapted from Dong et al.[185], DMAPMA (85.3 g, 0.50 mol) and 1,4-butane sultone (1.1 eq., 56 ml, ρ = 1.33 $g \cdot ml^{-1}$, 0.55 mol) in acetonitrile (150 ml) were stirred at room temperature. After 1 h, a white solid began to precipitate. After 24 h, the precipitate was filtered off, washed with dry ethyl acetate, and dried in vacuum, to give the pure monomer 4-((3-methacrylamidopropyl) dimethylammonio)butane-1-sulfonate (**M-3**) as colorless powder (yield 142.0 g, 93 %, m.p. = 103 – 112 °C).

^{1}H NMR (300 MHz, D_2O, 298 K): δ (ppm) = 1.82 – 2.08 (m, 9H, -CH_2-C-SO_3^-, -N^+-C-CH_2-, =C-CH_3, -CON-C-CH_2-), 2.99 (t, *J* = 7.3 Hz, 2H, -CH_2-SO_3^-), 3.10 (s, 6H, -N^+-$(CH_3)_2$), 3.30 – 3.40 (m, 6H, -CON-CH_2- and -CH_2-N^+-CH_2-), 5.51 (s, 1H, CH=C-CON- (trans)), 5.75 (s, 1H, CH=C-CON- (cis)).

^{13}C NMR (75 MHz, D_2O, 298 K): δ (ppm) = 19.2 (CH_2=C-$\underline{C}H_3$), 22.4 and 22.6 (-N^+-C-$\underline{C}H_2$-$\underline{C}H_2$-), 23.8 (-CON-C-$\underline{C}H_2$-), 37.8 (-CON-$\underline{C}H_2$-), 51.5 (-$\underline{C}H_2$-SO_3^-), 52.3 (-N^+-$(\underline{C}H_3)_2$), 63.3 (-$\underline{C}H_2$-N^+-), 64.9 (-N^+-$\underline{C}H_2$-), 122.9 (=$\underline{C}H_2$), 140.4 (=$\underline{C}$-CON-), 173.5 (-$\underline{C}$ON-).

HR-MS (ESI): calculated: 306.1600 $[M]^+$; found: 307.1680 $[M+H]^+$.

Elemental analysis ($C_{13}H_{26}N_2O_4S$, M_r = 306.42): calculated: C = 50.96 %, H = 8.55 %, N = 9.14 %, S = 10.46 %; found: C = 50.73 %, H = 8.52 %, N = 9.02 %, S = 10.51 %.

FT-IR (selected bands, cm^{-1}): 3487 ν(NH), 3029 ν(N^+-CH_3), 2975 ν(CH_3), 1655 ν(amide I), 1605 ν(C=C), 1546 ν(amide II), 1194 $\nu_{as}(SO_3^-)$, 1042 $\nu_s(SO_3^-)$.

7.4.2 Synthesis of methacrylate sulfobetaines

Synthesis of 4-((2-(methacryloyloxy)ethyl)dimethylammonio)butane-1-sulfonate (M-5)

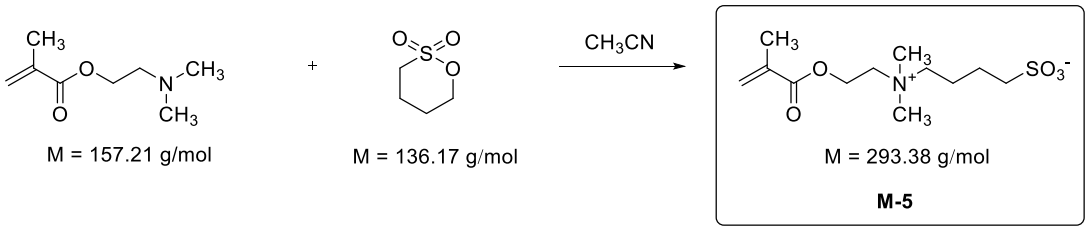

4-((2-(methacryloyloxy)ethyl)dimethylammonio)butane-1-sulfonate (**M-5**) was synthesized analogously to **M-3**. 2-(Dimethylamino)ethyl methacrylate (1.60 g, 0.01 mol) and 1,4-butane sultone (3 eq., 4.12 g, 0.03 mol) were dissolved in

acetonitrile (7.5 ml) and stirred at room temperature. After 1 h, a white solid began to precipitate which was filtered off after 24 h. The precipitate was washed with dry acetonitrile (to deactivate the unreacted 1,4-butane sultone, the washing solvent was mixed with saturated NaOH solution). Drying in vacuum gave the pure monomer 4-((2-(methacryloyloxy)ethyl)dimethylammonio)butane-1-sulfonate (**M-5**) as colorless crystals (yield 2.00 g, 68 %, fine needles m.p. = 179 °C).

^{1}H NMR (300 MHz, D_2O, 298 K): δ (ppm) = 1.72 – 2.10 (m, 7H, -CH_2-CH_2-C-SO_3^-, =C-CH_3), 2.99 (t, *J* = 7.5 Hz, 2H, -CH_2-SO_3^-), 3.21 (s, 6H, -N^+-$(CH_3)_2$), 3.45 (m, 2H, -N^+-CH_2-), 3.81 (m, 2H, -COO-C-CH_2-N^+-), 4.66 (t, 2H, *J* = 4.6 Hz, -COO-CH_2-), 5.81 (s, 1H, CH=C-COO- (trans)), 6.18 (s, 1H, CH=C-COO- (cis)).

^{13}C NMR (75 MHz, D_2O, 298 K): δ (ppm) = 18.3 (-C-$\underline{C}H_3$), 22.0 and 22.1 (-$\underline{C}H_2$-$\underline{C}H_2$-C-SO_3^-), 51.0 (-C-$\underline{C}H_2$-SO_3^-), 52.3 (-N^+-$(\underline{C}H_3)_2$), 59.4 (-COO-$\underline{C}H_2$-), 63.4 (-COO-C-$\underline{C}H_2$-), 65.7 (-N^+-$\underline{C}H_2$-), 128.7 (=$\underline{C}H_2$), 136.2 (=$\underline{C}$-COO-), 169.4 (-$\underline{C}$OO-).

HR-MS (ESI): calculated: 293.1300 $[M]^+$; found: 316.1164 $[M+Na]^+$.

Elemental analysis ($C_{12}H_{23}NO_5S$, M_r = 293.38): calculated: C = 49.13 %, H = 7.90 %, N = 4.77 %, S = 10.93 %; found: C = 49.03 %, H = 7.95 %, N = 4.80 %, S = 10.92 %.

FT-IR (selected bands, cm^{-1}): 3033 ν(N^+-CH_3), 2960 ν(CH_3), 1713 ν(C=O), 1636 ν(C=C), 1169 $\nu_{as}(SO_3^-)$, 1035 $\nu_s(SO_3^-)$.

Synthesis of 3-(1-(2-(methacryloyloxy)ethyl)piperidin-1-ium-1-yl)propane-1-sulfonate (M-6)

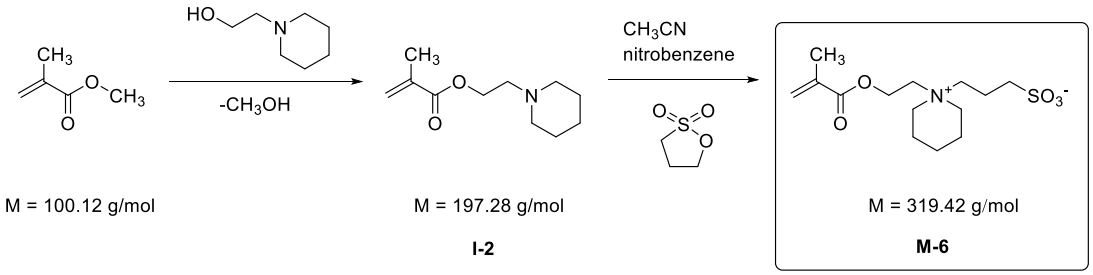

Step 1[‡]: The intermediate 2-(piperidin-1-yl)ethyl methacrylate (**I-2**) was adapted from Bette et al.[186]: 2-(piperidin-1-yl)ethan-1-ol (32.8 g, 0.5 mol), methyl methacrylate (4 eq., 200.0 g, 2.0 mol), 4-methoxyphenol (0.2 g, $1.6 \cdot 10^{-3}$ mol), and potassium phosphate (2.2 g, $1.0 \cdot 10^{-2}$ mol) were refluxed at 300 mbar for 6 h and left over night at room temperature. After addition of more methyl methacrylate (50 ml), the reaction mixture was refluxed for 2 h, before the excess of methyl methacrylate was distilled off under reduced pressure (T = 100 °C, p = 19 mbar). The pure intermediate 2-(piperidin-1-yl)ethyl methacrylate (**I-2**) was obtained after ball tube distillation (T = 130 °C, p ~ 0.01 mbar) as colorless oil (yield 41.0 g, 84 %).

^{1}H NMR (300 MHz, CD_2Cl_2, 298 K): δ (ppm) = 1.35 – 1.60 (m, 6H, -CH_2-piperidine (C3, C4, C5)), 1.92 (s, 3H, =C-CH_3), 2.40 (m, 4H, -CH_2-N-CH_2-piperidine (C2, C6)), 2.59 (t, *J* = 6.0 Hz, 2H, -COO-C-CH_2-), 4.20 (t, *J* = 6.0 Hz, 2H, -COO-CH_2-), 5.54 (s, 1H, CH=C-COO- (trans)), 6.05 (s, 1H, CH=C-COO- (cis)).

Step 2: The synthesis of 3-(1-(2-(methacryloyloxy)ethyl)piperidin-1-ium-1-yl)propane-1-sulfonate (**M-6**) was adapted from Köberle et al.[29] **I-2** (9.86 g, 0.05 mol), 1,3-propanesultone (1.2 eq., 6.72 g, 0.06 mol), and nitrobenzene (0.1 ml) were dissolved in acetonitrile (30 wt%, 73 ml) and refluxed for 7 days. The reaction mixture was cooled to room temperature and a white solid precipitated (side product). After filtration, removal of solvent, and drying in vacuum, the crude product was diluted in acetonitrile. Pure 3-(1-(2-(methacryloyloxy)ethyl)piperidin-1-

[‡] Dr. Michael Päch is acknowledged for the kind gift of the intermediate.

ium-1-yl)propane-1-sulfonate (**M-6**) was obtained as colorless powder by precipitation in diethyl ether (yield 15.10 g, 94 %, m.p. = 188 – 193 °C).

^{1}H NMR (300 MHz, D_2O, 298 K): δ (ppm) = 1.60 – 2.30 (m, 11H, -CH_2-CH_2-CH_2- piperidine (C4, C3, C5)), =C-CH_3, -CH_2-C-SO_3^-), 3.00 (t, *J* = 7.2 Hz, 2H, -CH_2-SO_3^-), 3.40 – 3.54 (t, *J* = 5.6 Hz, 4H, -CH_2-N^+-CH_2- piperidine (C2, C6), 3.54 – 3.68 (m, 2H, -N^+-CH_2-, 3.80 – 3.90 (m, 2H, -COO-C-CH_2-N^+-), 4.64 (t, 2H, *J* = 4.6 Hz, -COO-CH_2-), 5.80 (s, 1H, CH=C-COO- (trans)), 6.17 (s, 1H, CH=C-COO- (cis)).

^{13}C NMR (75 MHz, D_2O, 298 K): δ (ppm) = 18.2 (-$\underline{C}H_2$-C-SO_3^-), 18.3 (-C-$\underline{C}H_3$), 20.3 ($\underline{C}H_2$-C-$\underline{C}H_2$- piperidine (C3, C5)), 21.5 (-C-$\underline{C}H_2$-C- piperidine (C4)), 48.2 (-$\underline{C}H_2$-SO_3^-), 57.8 (-COO-C-$\underline{C}H_2$-), 58.3 (-N^+-$\underline{C}H_2$-), 58.9 (-COO-$\underline{C}H_2$-), 61.3 (-$\underline{C}H_2$-N^+-$\underline{C}H_2$- piperidine (C2, C6)), 128.7 (=$\underline{C}H_2$), 136.2 (=$\underline{C}$-COO-), 169.5 (-$\underline{C}$OO-).

HR-MS (ESI): calculated: 319.1500 $[M]^+$; found: 320.1524 $[M+H]^+$.

Elemental analysis ($C_{14}H_{25}NO_5S$, M_r = 319.42): calculated: C = 52.64 %, H = 7.89 %, N = 4.39 %, S = 10.04 %; found: C = 52.77 %, H = 7.97 %, N = 4.39 %, S = 10.04 %.

FT-IR (selected bands, cm^{-1}): 3022 ν(N^+-CH_2), 2961 ν(CH_3), 1722 ν(C=O), 1637 ν(C=C), 1155 $\nu_{as}(SO_3^-)$, 1034 $\nu_s(SO_3^-)$.

Synthesis of 4-(1-(2-(methacryloyloxy)ethyl)piperidin-1-ium-1-yl)butane-1-sulfonate (M-7)

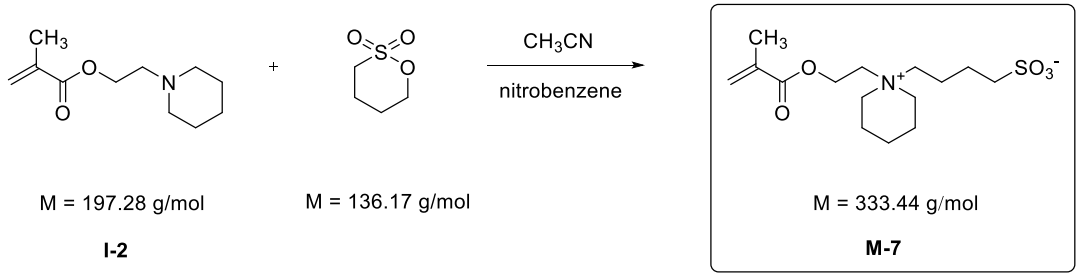

M = 197.28 g/mol

I-2

M = 136.17 g/mol

M = 333.44 g/mol

M-7

The synthesis of 4-(1-(2-(methacryloyloxy)ethyl)piperidin-1-ium-1-yl)butane-1-sulfonate (**M-7**) was performed analogously to the synthesis of **M-6** (reaction step 2): **I-2** (1.58 g, $7.5 \cdot 10^{-3}$ mol), 1,4-butane sultone (1.02 eq., 1.08 g, $7.7 \cdot 10^{-3}$ mol), and nitrobenzene (0.1 ml) were dissolved in acetonitrile (100 ml) and refluxed for 7 days. White solid was precipitated during the removal of the solvent. The crude product was washed with dry acetonitrile and dried in vacuum to give the pure monomer 4-(1-(2-(methacryloyloxy)ethyl)piperidin-1-ium-1-yl)butane-1-sulfonate (**M-7**) as colorless powder (yield 1.93 g, 77 %, m.p. = 253 – 264 °C).

^{1}H NMR (400 MHz, D_2O, 298 K): δ (ppm) = 1.60 – 2.00 (m, 13H, -CH_2-CH_2-CH_2- piperidine (C4, C3, C5)), -CH_2-CH_2-C-SO_3^-, =C-CH_3), 2.95 (t, *J* = 7.2 Hz, 2H, -CH_2-SO_3^-), 3.38 – 3.70 (m, 6H, -CH_2-N^+-CH_2- piperidine (C2, C6), -N^+-CH_2-), 3.80 (t, 2H, *J* = 4.6 Hz, COO-C-CH_2-N^+-), 4.60 (t, 2H, *J* = 4.6 Hz, -COO-CH_2-), 5.78 (s, 1H, CH=C-COO- (trans)), 6.14 (s, 1H, CH=C-COO- (cis)).

^{13}C NMR (125 MHz, D_2O, 298 K): δ (ppm) = 18.3 (-C-$\underline{C}H_3$), 20.3 (-$\underline{C}H_2$-C-$\underline{C}H_2$- piperidine (C3, C5)), 21.0 (-C-$\underline{C}H_2$-C- piperidine (C4)), 21.6 (-$\underline{C}H_2$-C-SO_3^-), 22.3 (-$\underline{C}H_2$-C-C-SO_3^-), 51.1 (-$\underline{C}H_2$-SO_3^-), 57.7 (-COO-C-$\underline{C}H_2$-), 58.9 (-COO-$\underline{C}H_2$-), 59.8 (-N^+-$\underline{C}H_2$-), 61.3 (-$\underline{C}H_2$-N^+-$\underline{C}H_2$- piperidine (C2, C6)), 128.7 (=$\underline{C}H_2$), 136.2 (=$\underline{C}$-COO-), 169.6 (-$\underline{C}$OO-).

HR-MS (ESI): calculated: 333.1600 $[M]^+$; found: 334.1673 $[M+H]^+$.

Elemental analysis ($C_{15}H_{27}NO_5S$, M_r = 333.44): calculated: C = 54.03 %, H = 8.16 %, N = 4.20 %, S = 9.61 %; found: C = 54.40 %, H = 8.10 %, N = 4.20 %, S = 9.92 %.

FT-IR (selected bands, cm^{-1}): 3010 $\nu(N^+\text{-}CH_2)$, 2967 $\nu(CH_3)$, 1712 $\nu(C{=}O)$, 1627 $\nu(C{=}C)$, 1160 $\nu_{as}(SO_3^-)$, 1035 $\nu_s(SO_3^-)$.

Synthesis of 3-(4-(2-(methacryloyloxy)ethyl)morpholino-4-ium)propane-1-sulfonate (M-8)

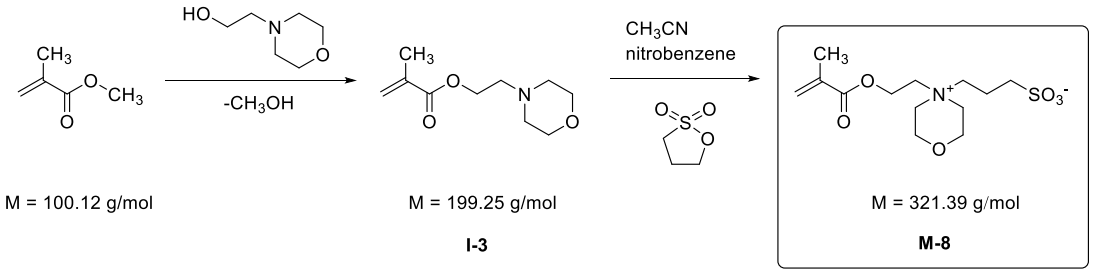

Step 1[§]: The synthesis of the intermediate 2-morpholinoethyl methacrylate (**I-3**) was performed analogously to the synthesis of **I-2**. 2-Morpholinoethan-1-ol (32.8 g, 0.25 mol), methyl methacrylate (4 eq., 100.0 g, 1.0 mol), 4-methoxyphenol (0.1 g, $8.0 \cdot 10^{-4}$ mol), and potassium phosphate (1.1 g, $5.1 \cdot 10^{-3}$ mol) were refluxed at 300 mbar for 6 h and left over night at room temperature. After addition of more methyl methacrylate (50 ml), the reaction mixture was refluxed for 2 h, before the excess of methyl methacrylate was distilled off under reduced pressure (T = 100 °C, p = 19 mbar). The intermediate 2-morpholinoethyl methacrylate (**I-3**) was obtained after ball tube distillation (T = 130 °C, p ~ 0.01 mbar) as colorless oil (yield 36.8 g, 80 %).

^{1}H NMR (300 MHz, CD_2Cl_2, 298 K): δ (ppm) = 1.92 (s, 3H, =C-CH_3), 2.48 (m, 4H, -CH_2-N-CH_2- piperidine (C2, C6)), 2.64 (t, *J* = 5.8 Hz, 2H, -COO-C-CH_2-),

[§] Dr. Michael Päch is acknowledged for the kind gift of the intermediate.

3.64 (m, 4H, -CH_2-O-CH_2- piperidine (C3, C5)), 4.24 (t, J = 5.8 Hz, 2H, COO-CH_2), 5.56 (s, 1H, CH=C-COO- (trans)), 6.06 (s, 1H, CH=C-COO- (cis)).

Step 2: The synthesis of 3-(4-(2-(methacryloyloxy)ethyl)morpholino-4-ium) propane-1-sulfonate (**M-8**) was analogous to the synthesis of **M-6**. The intermediate **I-3** (13.2 g, 0.07 mol), 1,3-propanesultone (1.0 eq., 8.9 g, 0.07 mol), and nitrobenzene (0.1 ml) were dissolved in acetonitrile (30 wt%, 75 ml) and refluxed for 7 days. The monomer 3-(4-(2-(methacryloyloxy)ethyl)morpholino-4-ium)propane-1-sulfonate (**M-8**) was obtained as colorless powder by precipitation in diethyl ether (yield 15.10 g, 94 %, m.p. = 190 – 195 °C).

^{1}H NMR (300 MHz, D_2O, 298 K): δ (ppm) = 1.95 (s, 3H, =C-CH_3), 2.26 (m, 2H, -CH_2-C-SO_3^-), 3.01 (t, J = 7.2 Hz, 2H, -CH_2-SO_3^-), 3.60 – 3.80 (m, 6H, -CH_2-N^+-CH_2- morpholine (C2, C6), -N^+-CH_2-), 3.96 – 4.20 (m, 6H, -COO-C-CH_2-N^+-, -CH_2-O-CH_2- morpholine (C3, C5)), 4.68 (t, 2H, J = 4.0 Hz, -COO-CH_2-), 5.80 (s, 1H, CH=C-COO- (trans)), 6.15 (s, 1H, CH=C-COO- (cis)).

^{13}C NMR (75 MHz, D_2O, 298 K): δ (ppm) = 18.2 (-$\underline{C}H_2$-C-SO_3^-), 18.3 (-C-$\underline{C}H_3$), 48.0 ($\underline{C}H_2$-SO_3^-), 53.2 (-N^+-$\underline{C}H_2$-), 58.8 (-COO-$\underline{C}H_2$-), 59.9 (-$\underline{C}H_2$-N^+-$\underline{C}H_2$- morpholine (C2, C6)), 61.1 (-$\underline{C}H_2$-O-$\underline{C}H_2$- morpholine (C3, C5)), 64.8 (-COO-C-$\underline{C}H_2$-), 128.7 (=$\underline{C}H_2$), 136.0 (=$\underline{C}$-COO-), 169.4 (-$\underline{C}$OO-).

HR-MS (ESI): calculated: 321.1200 $[M]^+$; found: 322.1319 $[M+H]^+$.

Elemental analysis ($C_{13}H_{23}NO_6S$, M_r = 321.39): calculated: C = 48.58 %, H = 7.21 %, N = 4.36 %, S = 9.98 %; found: C = 48.60 %, H = 7.21 %, N = 4.34 %, S = 9.94 %.

FT-IR (selected bands, cm^{-1}): 3020 ν(N^+-CH_2), 2962 ν(CH_3), 1723 ν(C=O), 1636 ν(C=C), 1156 ν_{as}(SO_3^-), 1033 ν_s(SO_3^-).

Synthesis of 4-(4-(2-(methacryloyloxy)ethyl)morpholino-4-ium)butane-1-sulfonate (M-9)

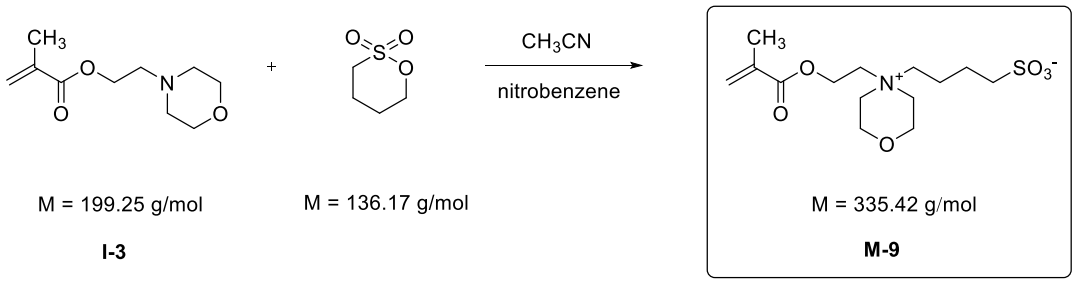

M = 199.25 g/mol

I-3

M = 136.17 g/mol

M = 335.42 g/mol

M-9

The monomer 4-(4-(2-(methacryloyloxy)ethyl)morpholino-4-ium)butane-1-sulfonate (**M-9**) was synthesized analogously to the synthesis of **M-7**. Thus, intermediate **I-3** (1.52 g, $7.5 \cdot 10^{-3}$ mol), 1,4-butane sultone (1.02 eq., 1.05 g, $7.7 \cdot 10^{-3}$ mol), and nitrobenzene (0.1 ml) were dissolved in acetonitrile (100 ml) and refluxed for 7 days. 4-(4-(2-(methacryloyloxy)ethyl)morpholino-4-ium)butane-1-sulfonate (**M-9**) was collected by filtration as colorless powder (yield 2.00 g, 80 %, m.p. = 255 – 266 °C).

^{1}H NMR (400 MHz, D_2O, 298 K): δ (ppm) = 1.75 – 2.00 (m, 7H, -CH_2-CH_2-C-SO_3^-, =C-CH_3), 2.97 (t, *J* = 7.4 Hz, 2H, -CH_2-SO_3^-), 3.55 – 3.72 (m, 6H, -CH_2-N^+-CH_2- morpholine (C2, C6), -N^+-CH_2-), 3.99 (t, 2H, *J* = 3.9 Hz, -COO-C-CH_2-N^+-), 4.10 (m, 4H, -CH_2-O-CH_2- morpholine (C3, C5)), 4.65 (t, 2H, *J* = 3.5 Hz, -COO-CH_2-), 5.79 (s, 1H, CH=C-COO- (trans)), 6.14 (s, 1H, CH=C-COO- (cis)).

^{13}C NMR (125 MHz, D_2O, 298 K): δ (ppm) = 18.3 (-C-$\underline{C}H_3$), 20.9 (-$\underline{C}H_2$-C-C-SO_3^-), 22.1 ($\underline{C}H_2$-C-SO_3^-), 51.0 (-$\underline{C}H_2$-SO_3^-), 58.2 (-COO-C-$\underline{C}H_2$-), 58.8 (-COO-$\underline{C}H_2$-), 59.8 (-$\underline{C}H_2$-N^+-$\underline{C}H_2$- morpholine (C2, C6)), 60.2 (-N^+-$\underline{C}H_2$-), 61.1 ($\underline{C}H_2$-O-$\underline{C}H_2$- morpholine (C3, C5)), 128.8 (=$\underline{C}H_2$), 136.3 (=$\underline{C}$-COO-), 169.5 (-$\underline{C}$OO-).

HR-MS (ESI): calculated: 335.1400 $[M]^+$; found: 336.1465 $[M+H]^+$.

Elemental analysis ($C_{14}H_{25}NO_6S$, M_r = 335.42): calculated: C = 50.13 %, H = 7.51 %, N = 4.18 %, S = 9.56 %; found: C = 50.08 %, H = 7.49 %, N = 4.19 %, S = 9.53 %.

FT-IR (selected bands, cm^{-1}): 3008 $\nu(N^+-CH_2)$, 2968 $\nu(CH_3)$, 1715 $\nu(C=O)$, 1629 $\nu(C=C)$, 1171 $\nu_{as}(SO_3^-)$, 1030 $\nu_s(SO_3^-)$.

Synthesis of 3-((3-(methacryloyloxy)propyl)dimethylammonio)propane-1-sulfonate (M-10)

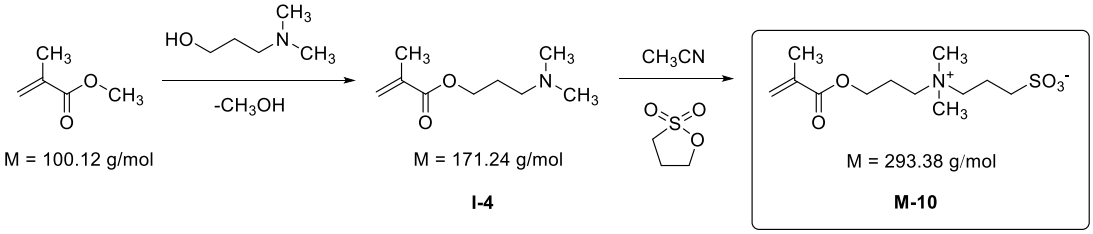

Step 1: The typical procedure of transesterification via azeotrope removal of methanol at 300 mbar with molecular sieve 4 Å was inspired by the patent of Bette et al.[186]: 3-(dimethylamino)propan-1-ol (20.52 g, 0.2 mol), methyl methacrylate (4 eq., 80.15 g, 0.8 mol), hydroquinone (0.11 g, 350 ppm), and potassium phosphate (0.86 g, 2.0 mol% based on 3-(dimethylamino)propan-1-ol) were stirred in a 250 ml 3-neck round-bottom flask, equipped with a thermometer and a pressure-equalizing dropping funnel which was filled with sufficient molecular sieve 4 Å (8.5 ml of methanol has to be removed). The vacuum was regulated to 300 mbar. Subsequently, the suspension was heated to 80 °C and the first distillation drops occurred at 64 °C (azeotrope of methanol and methyl methacrylate). After 5 h, unreacted methyl methacrylate was distilled off under reduced pressure (T = 25 °C, p = 19 mbar) and the residue was filtered. Hydroquinone was added to the crude product before it was purified by ball tube distillation (T = 50 – 75 °C, p = 0.25 mbar) to give the colorless intermediate 3-(dimethylamino)propyl methacrylate (**I-4**) (yield 24.05 g, 70 %).

This intermediate was also synthesized analogously to the approach described by Itoh[187] (starting material was methacryloyl chloride) to give a yield of 20.30 g (60 %).

^{1}H NMR (300 MHz, $CDCl_3$, 298 K): δ (ppm) = 1.66 – 1.86 (m, 5H, -CH_2-C-N-, =C-CH_3), 2.10 (s, 6H, -N-$(CH_3)_2$), 2.23 (t, 2H, *J* = 7.4 Hz, -CH_2-N-), 4.07 (t, *J* = 6.5 Hz, 2H, -COO-CH_2-), 5.42 (s, 1H, CH=C-COO- (trans)), 5.97 (s, 1H, CH=C-COO- (cis)).

^{13}C NMR (75 MHz, $CDCl_3$, 298 K): δ (ppm) = 18.3 (=C-$\underline{C}H_3$), 27.0 (-COO-C-$\underline{C}H_2$-), 45.4 (-N-$(\underline{C}H_3)_2$), 56.3 (-$\underline{C}H_2$-N-$(CH_3)_2$), 63.0 (-COO-$\underline{C}H_2$-), 125.1 (=$\underline{C}H_2$), 136.5 (=$\underline{C}$-COO-), 173.5 (-$\underline{C}$OO-).

HR-MS (ESI): calculated: 171.1300 $[M]^+$; found: 171.1480 $[M+H]^+$.

Elemental analysis ($C_9H_{17}NO_2$, M_r = 171.24): calculated: C = 63.13 %, H = 10.01%, N = 8.18 %; found: C = 63.18 %, H = 10.02 %, N = 8.20 %.

FT-IR (selected bands, cm^{-1}): 2949 ν(CH_3), 1717 ν(C=O), 1637 ν(C=C).

Step 2: The synthesis of 3-((3-(methacryloyloxy)propyl)dimethylammonio) propane-1-sulfonate (**M-10**) was performed analogously to the synthesis of **M-3**. **I-4** (1.76 g, 0.01 mol) and 1,3-propane sultone (3 eq., 4.15 g, 0.03 mol) were dissolved in acetonitrile (7 ml) and stirred at room temperature for 1 h. The pure monomer 3-((3-(methacryloyloxy)propyl)dimethylammonio)propane-1-sulfonate (**M-10**) was obtained as colorless crystals (yield 2.61 g, 90 %, fine needles m.p. = 165 °C).

^{1}H NMR (300 MHz, D_2O, 298 K): δ (ppm) = 1.95 (s, 3H, =C-CH_3), 2.15 – 2.35 (m, 4H, COO-C-CH_2-, -CH_2-C-SO_3^-), 3.01 (t, *J* = 7.1 Hz, 2H, -CH_2-SO_3^-), 3.17 (s, 6H, -N^+-$(CH_3)_2$), 3.45 – 3.60 (m, 4H, -CH_2-N^+-CH_2-), 4.31 (t, 2H, *J* = 5.8 Hz, -COO-CH_2-), 5.76 (s, 1H, CH=C-COO- (trans)), 6.17 (s, 1H, CH=C-COO- (cis)).

^{13}C NMR (75 MHz, D_2O, 298 K): δ (ppm) = 18.3 (-C-$\underline{C}H_3$), 19.1 (-$\underline{C}H_2$-C-SO_3^-), 22.7 (COO-C-$\underline{C}H_2$-), 48.2 (-$\underline{C}H_2$-SO_3^-), 51.7 (-N^+-$(\underline{C}H_3)_2$), 62.3 (-N^+-$\underline{C}H_2$-), 62.8 (-COO-$\underline{C}H_2$-), 63.2 (-$\underline{C}H_2$-N^+-), 128.0 (=$\underline{C}H_2$), 136.7 (=$\underline{C}$-COO-), 170.5 (-$\underline{C}$OO-).

HR-MS (ESI): calculated: 293.1300 $[M]^+$; found: 316.1181 $[M+Na]^+$.

Elemental analysis ($C_{12}H_{23}NO_5S$, M_r = 293.38): calculated: C = 49.13 %, H = 7.90 %, N = 4.77 %, S = 10.93 %; found: C = 49.00 %, H = 7.81 %, N = 4.78 %, S = 10.90 %.

FT-IR (selected bands, cm^{-1}): 3041 $\nu(N^+-CH_3)$, 2972 $\nu(CH_3)$, 1708 $\nu(C=O)$, 1627 $\nu(C=C)$, 1189 $\nu_{as}(SO_3^-)$, 1037 $\nu_s(SO_3^-)$.

Synthesis of 4-((3-(methacryloyloxy)propyl)dimethylammonio)butane-1-sulfonate (M-11)

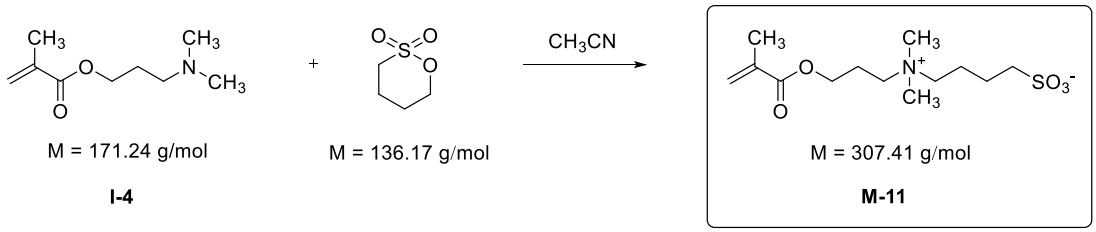

Synthesis of monomer 4-((3-(methacryloyloxy)propyl)dimethylammonio)butane-1-sulfonate (**M-11**) was performed as described for **M-3**. Intermediate **I-4** (3.42 g, 0.02 mol) and 1,4-butane sultone (3 eq., 8.16 g, 0.06 mol) were dissolved in acetonitrile (15 ml) and stirred at room temperature for 6 h. After filtering, washing with dry acetonitrile, and drying in vacuum, the pure monomer 4-((3-(methacryloyloxy)propyl)dimethylammonio)butane-1-sulfonate (**M-11**) was obtained as colorless crystals (yield 4.80 g, 80 %, fine needles m.p. = 173 °C).

^{1}H NMR (300 MHz, D_2O, 298 K): δ (ppm) = 1.70 – 2.40 (m, 9H, $-CH_2-CH_2-C-SO_3^-$), $=C-CH_3$, $COO-C-CH_2-$), 2.99 (t, *J* = 7.4 Hz, 2H, $-CH_2-SO_3^-$), 3.13 (s, 6H, $-N^+-(CH_3)_2$), 3.30 – 3.60 (m, 4H, $-CH_2-N^+-CH_2-$), 4.31 (t, 2H, *J* = 5.8 Hz, $-COO-CH_2-$), 5.77 (s, 1H, CH=C-COO- (trans)), 6.17 (s, 1H, CH=C-COO- (cis)).

^{13}C NMR (75 MHz, D_2O, 298 K): δ (ppm) = 18.3 ($C-\underline{C}H_3$), 21.9 ($\underline{C}H_2-C-C-SO_3^-$), 22.1 ($\underline{C}H_2-C-SO_3^-$), 22.7 ($COO-C-\underline{C}H_2-$), 51.0 ($-\underline{C}H_2-SO_3^-$), 51.7 ($-N^+-(\underline{C}H_3)_2$), 62.2

(-$\underline{C}H_2$-N^+-), 62.8 (-COO-$\underline{C}H_2$-), 64.4 (-N^+-$\underline{C}H_2$-), 128.0 (=$\underline{C}H_2$), 136.0 (=$\underline{C}$-COO-), 169.4 (-$\underline{C}$OO-).

HR-MS (ESI): calculated: 307.1500 $[M]^+$; found: 330.1338 $[M+Na]^+$.

Elemental analysis ($C_{13}H_{25}NO_5S$, M_r = 307.41): calculated: C = 50.79 %, H = 8.20 %, N = 4.56 %, S = 10.43 %; found: C = 50.80 %, H = 8.22 %, N = 4.55 %, S = 10.44 %.

FT-IR (selected bands, cm^{-1}): 3031 $\nu(N^+$-$CH_3)$, 2956 $\nu(CH_3)$, 1715 ν(C=O), 1636 ν(C=C), 1171 $\nu_{as}(SO_3^-)$, 1034 $\nu_s(SO_3^-)$.

7.5 Synthesis of homopolymers

7.5.1 Kinetic studies of RAFT polymerizations

A typical RAFT polymerization of all monomers with fluorophore-labeled **CTA-3** for preliminary kinetic studies is described in the following.

The monomer 3-((3-methacrylamidopropyl)dimethylammonio)propane-1-sulfonate (**M-1**, 18.50 g, $6.0 \cdot 10^{-2}$ mol), **CTA-3** (0.39 g, $6.3 \cdot 10^{-4}$ mol), and 4,4'-azobis(4-cyanopentanoic acid) (V-501, 0.04 g, $1.3 \cdot 10^{-4}$ mol) were dissolved in trifluoroethanol (TFE, 30 wt%, 33 ml) for the preparation of 14 aliquot samples. The yellow reaction mixture was purged with N_2 for 30 min and subsequently polymerized at 75 °C. After predefined reaction times (0.00, 0.25, 0.50, 0.75, 1.00, 1.25, 1.50, 1.75, 2.00, 2.50, 3.00, 4.00, and 19.00 h), small samples (1 - 2 ml) were withdrawn with a syringe under N_2 to avoid intrusion of O_2. The sample was rapidly cooled, and a small amount of the crude product was submitted to ^{1}H NMR for conversion determination. The other residual part of the sample was precipitated into methanol (dissolution in TFE and precipitation into methanol was repeated 3 times),

the polymer was isolated, and dried in vacuum to give a hygroscopic amorphous yellow solid.

The polymers of *N*-isopropylmethacrylamide (**M-12**) and methyl methacrylate (**MMA**) were precipitated into diethyl ether, resulting in amorphous yellow solids. All purified homopolymers were characterized by ^{1}H NMR, UV-vis, and GPC.

Table 7.2. Reaction conditions for the kinetic experiments of RAFT polymerization at 75 °C, using RAFT agent **CTA-3** and initiator V-501. The molar ratio Mon : **CTA-3** : V-501 was 100 : 1 : 0.2. Monomer concentration was 30 wt%.

monomer	solvent	$V_{solvent}$ [ml]	m_{Mon} [g]	m_{CTA-3} [g]	m_{V-501} [g]
M-1	TFE	33	18.5	0.39	0.040
M-2	TFE	30	16.3	0.32	0.030
M-3	TFE	27	15.0	0.29	0.028
M-4	TFE	24	13.0	0.28	0.028
M-5	TFE	27	15.0	0.30	0.030
M-6	TFE	23	12.5	0.25	0.023
M-7	TFE	18	10.0	0.18	0.017
M-8	TFE	21	12.0	0.23	0.021
M-9	TFE	26	15.0	0.27	0.025
M-10	TFE	27	15.0	0.30	0.030
M-11	TFE	27	15.0	0.30	0.027
M-12	TFE	17	10.5	0.68	0.046
MMA	TFE	28	15.0	0.91	0.084
MMA	benzene	61	15.0	0.91	0.084

7.5.2 RAFT polymerization of sulfobetaine monomers

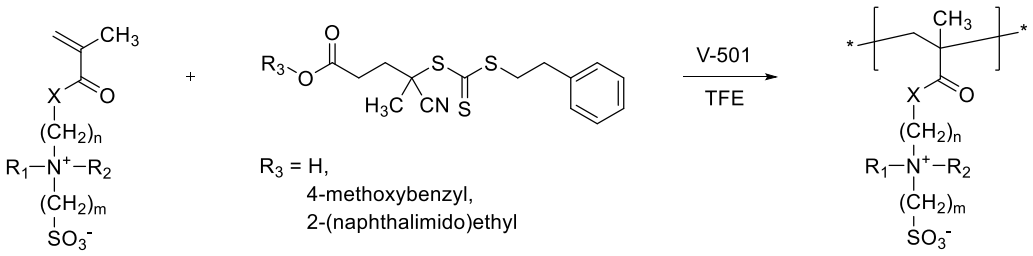

sulfobetaine **CTA** **poly(sulfobetaine)**

R_3 = H,
4-methoxybenzyl,
2-(naphthalimido)ethyl

X = NH, O
n = 2, 3
m = 3, 4, C_3-OH

R_1, R_2 = CH_3,
ring : piperidine,
morpholine

All RAFT polymerizations of sulfobetaine monomers were performed as described in the following.

In a typical procedure, sulfobetaine monomer, RAFT agent and initiator V-501 were dissolved in TFE. The yellow mixture was purged with N_2 for 30 min and subsequently polymerized for a given timespan at 75 °C. After precipitation into methanol (dissolution in TFE and precipitation into methanol was repeated 3 times), the polymer was isolated and dried in vacuum. Polymers were obtained as hygroscopic amorphous yellow solid.

Purified homopolymers were characterized by ^{1}H NMR, UV-vis, fluorescence, and IR spectroscopies, as well as by TGA, DSC, turbidimetry, and DLS. The individual samples are named **poly(monomer)$_n$**, with *n* being the number average degree of polymerization that was theoretically calculated using **equation 7.1** (conversions were shown in **chapter 4.1**).

RAFT polymerization of sulfobetaine M-1

Exemplarily, **M-1** (5.000 g, $1.7 \cdot 10^{-2}$ mol), **CTA-3** (0.018 g, $2.9 \cdot 10^{-3}$ mol), and V-501 (0.002 g, $5.8 \cdot 10^{-6}$ mol) were dissolved in trifluoroethanol (10 ml) and purged with N_2. The reaction mixture was polymerized at 75 °C for 15 h yielding **poly(M-1)$_{500}$** (yield 3.100 g, 62 %). TGA (the onset of decomposition): 290 °C. DSC: no thermal transition.

^{1}H NMR (300 MHz, in dilute aqueous NaCl (9.0 g·L^{-1}) in D_2O, 298 K): δ (ppm) = 0.8 – 1.9 (broad 5H, -CH_3 and -CH_2- on/in backbone), 1.9 – 2.3 (4H, -CH_2-C-N^+-C-CH_2-), 2.9 – 3.0 (2H, -CH_2-SO_3^-), 3.0 – 3.3 (6H, -N^+-$(CH_3)_2$), 3.3 – 3.6 (6H, -CH_2-N^+-CH_2-, -CON-CH_2-).

FT-IR (selected bands, cm^{-1}): 3446 ν(NH), 1645 ν(amide I), 1539 ν(amide II), 1195 $\nu_{as}(SO_3^-)$, 1043 $\nu_s(SO_3^-)$.

UV-vis absorbance maxima: in trifluoroethanol (λ_{max} = 260, 294, and 442 nm), and in water (λ_{max} = 258, 297, and 447 nm).

Fluorescence emission maxima: in trifluoroethanol (λ_{PL} = 537 nm), and in water (λ_{PL} = 546 nm).

Table 7.3. Reaction conditions for the RAFT polymerization of **M-1** in TFE at 75 °C, using different RAFT agents and initiator V-501. Monomer concentration was 30 wt%.

sample	RAFT agent	molar ratio M-1 : CTA : V-501	m_{M-1} [g]	m_{CTA} [g]	m_{V-501} [g]	t [h]
poly(M-1)$_{85}$	CTA-1	100 : 1 : 0.2	5.0	0.057	0.009	2.5
poly(M-1)$_{405}$	CTA-1	600 : 1 : 0.2	5.0	0.010	0.002	15.0
poly(M-1)$_{40}$	CTA-2	100 : 1 : 0.2	5.0	0.079	0.010	2.5
poly(M-1)$_{495}$	CTA-2	600 : 1 : 0.2	5.0	0.013	0.002	15.0
poly(M-1)$_{85}$	CTA-3	100 : 1 : 0.2	18.5	0.382	0.036	2.5
poly(M-1)$_{170}$	CTA-3	200 : 1 : 0.2	2.5	0.028	0.003	5.0
poly(M-1)$_{280}$	CTA-3	300 : 1 : 0.2	5.0	0.035	0.003	7.5
poly(M-1)$_{500}$	CTA-3	600 : 1 : 0.2	5.0	0.018	0.002	15.0

RAFT polymerization of sulfobetaine M-2

Exemplarily, **M-2** (1.000 g, $3.3 \cdot 10^{-3}$ mol), **CTA-3** (0.003 g, $5.6 \cdot 10^{-6}$ mol), and V-501 (0.001 g, $1.1 \cdot 10^{-6}$ mol) were dissolved in trifluoroethanol (2 ml) and purged with N_2. The reaction mixture was polymerized at 75 °C for 18 h yielding **poly(M-2)$_{460}$** (yield 0.600 g, 60 %). TGA (the onset of decomposition): 290 °C. DSC: no thermal transition.

^{1}H NMR (300 MHz, in dilute aqueous NaCl (0.9 g·L^{-1}) in D_2O, 298 K): δ (ppm) = 0.6 – 2.1 (7H, -CH_3 and -CH_2- on/in backbone, -CON-C-CH_2-), 2.8 – 3.7 (14H, CON-CH_2-C-CH_2-$N^+(CH_3)_2$-CH_2-C-CH_2-SO_3^-), 4.5 – 4.6 (1H, -CH-OH).

FT-IR (selected bands, cm^{-1}): 3446 ν(NH), 1645 ν(amide I), 1539 ν(amide II), 1195 $\nu_{as}(SO_3^-)$, 1043 $\nu_s(SO_3^-)$.

UV-vis absorbance maxima: in trifluoroethanol (λ_{max} = 260, 294, and 442 nm), and in water (λ_{max} = 258, 297, and 447 nm).

Fluorescence emission maxima: in trifluoroethanol (λ_{PL} = 537 nm), and in water (λ_{PL} = 546 nm).

Table 7.4. Reaction conditions for the RAFT polymerization of **M-2** in TFE at 75 °C, using RAFT agent **CTA-3** and initiator V-501. Monomer concentration was 30 wt%.

sample	molar ratio M-2 : CTA-3 : V-501	m_{M-2} [g]	m_{CTA-3} [g]	m_{V-501} [g]	t [h]
poly(M-2)$_{70}$	100 : 1 : 0.2	1.6	0.030	0.003	3
poly(M-2)$_{80}$	100 : 1 : 0.2	1.6	0.030	0.003	19
poly(M-2)$_{115}$	300 : 1 : 0.2	5.0	0.016	0.002	18
poly(M-2)$_{235}$	300 : 1 : 0.2	1.0	0.007	0.001	9
poly(M-2)$_{460}$	600 : 1 : 0.2	1.0	0.003	0.001	18
poly(M-2)$_{505}$	600 : 1 : 0.2	1.0	0.003	0.001	18

RAFT polymerization of sulfobetaine M-3

Exemplarily, **M-3** (5.000 g, $1.6 \cdot 10^{-2}$ mol), **CTA-3** (0.100 g, $1.6 \cdot 10^{-4}$ mol), and V-501 (0.009 g, $3.0 \cdot 10^{-5}$ mol) were dissolved in trifluoroethanol (9 ml) and purged with N_2. The reaction mixture was polymerized at 75 °C for 18 h yielding **poly(M-3)$_{80}$** (yield 3.100 g, 62 %). TGA (the onset of decomposition): 310 °C. DSC: no thermal transition.

^{1}H NMR (300 MHz, in dilute aqueous NaCl (0.9 g·L^{-1}) in D_2O, 298 K): δ (ppm) = 0.6 – 1.2 (broad 5H, -CH_3 and -CH_2- on/in backbone), 1.6 – 2.1 (6H, -CH_2-C-N^+-C-CH_2-CH_2-), 2.8 – 3.0 (2H, -CH_2-SO_3^-), 3.0 – 3.1 (6H, -N^+-$(CH_3)_2$), 3.2 – 3.4 (6H, -CH_2-N^+-CH_2-, CON-CH_2-).

FT-IR (selected bands, cm^{-1}): 3446 ν(NH), 1645 ν(amide I), 1539 ν(amide II), 1195 $\nu_{as}(SO_3)$, and 1043 $\nu_s(SO_3)$.

UV-vis absorbance maxima: in trifluoroethanol (λ_{max} = 262, 299, and 444 nm), and in water (λ_{max} = 256, 288, and 441 nm).

Fluorescence emission maxima: in trifluoroethanol (λ_{PL} = 538 nm), and in water (λ_{PL} = 549 nm).

Table 7.5. Reaction conditions for the RAFT polymerization of **M-3** in TFE at 75 °C, using RAFT agent **CTA-3** and initiator V-501. Monomer concentration was 30 wt%.

sample	molar ratio M-3 : CTA-3 : V-501	m_{M-3} [g]	m_{CTA-3} [g]	m_{V-501} [g]	t [h]
poly(M-3)$_{40}$	100 :1 : 0.2	5	0.100	0.009	0.75
poly(M-3)$_{50}$	100 : 1 : 0.2	5	0.100	0.009	1.00
poly(M-3)$_{80}$	100 : 1 : 0.2	5	0.100	0.009	2.50
poly(M-3)$_{245}$	300 : 1 : 0.2	5	0.030	0.003	7.50
poly(M-3)$_{425}$	600 : 1 : 0.2	5	0.017	0.002	15.00

RAFT polymerization of sulfobetaine M-4

Exemplarily, **M-4** (5.000 g, $1.8 \cdot 10^{-2}$ mol), **CTA-3** (0.018 g, $3.0 \cdot 10^{-5}$ mol), and V-501 (0.002 g, $6.0 \cdot 10^{-6}$ mol) were dissolved in trifluoroethanol (9 ml) and purged with N_2. The reaction mixture was polymerized at 75 °C for 15 h yielding **poly(M-4)$_{575}$** (yield 4.200 g, 84 %). TGA (the onset of decomposition): 305 °C. DSC: no thermal transition.

^{1}H NMR (400 MHz, in dilute aqueous NaCl (0.9 g·L^{-1}) in D_2O, 298 K): δ (ppm) = 0.6 – 2.5 (broad 7H, -CH_3 and -CH_2- on/in backbone, -CH_2-C-SO_3^-), 2.9 – 3.1 (2H, -CH_2-SO_3^-), 3.2 – 3.4 (6H, -N^+-$(CH_3)_2$), 3.6 – 4.0 (4H, -CH_2-N^+-CH_2-), 4.4 – 4.7 (2H, -COO-CH_2-).

FT-IR (selected bands in cm^{-1}): 3039 $\nu(N^+-CH_3)$, 2977 $\nu(CH_2)$, 1740 $\nu(C=O)$, 1173 $\nu_{as}(SO_3^-)$, 1036 $\nu_s(SO_3^-)$.

UV-vis absorbance maxima: in trifluoroethanol (λ_{max} = 266, 296, and 444 nm), and in water (λ_{max} = 254, 283, and 430 nm).

Fluorescence emission maxima: in trifluoroethanol (λ_{PL} = 537 nm), and in water (λ_{PL} = 548 nm).

Table 7.6. Reaction conditions for the RAFT polymerization of **M-4** in TFE at 75 °C, using RAFT agent **CTA-3** and initiator V-501. Monomer concentration was 30 wt%.

sample	molar ratio M-4 : CTA-3 : V-501	m_{M-4} [g]	m_{CTA-3} [g]	m_{V-501} [g]	t [h]
poly(M-4)$_{85}$	100 : 1 : 0.2	5	0.109	0.010	2.5
poly(M-4)$_{270}$	300 : 1 : 0.2	5	0.036	0.003	7.5
poly(M-4)$_{575}$	600 : 1 : 0.2	5	0.018	0.002	15.0
poly(M-4)$_{585}$	600 : 1 : 0.2	5	0.018	0.002	15.0

RAFT polymerization of sulfobetaine M-5

Exemplarily, **M-5** (1.000 g, $3.4 \cdot 10^{-3}$ mol), **CTA-3** (0.026 g, $4.3 \cdot 10^{-5}$ mol), and V-501 (0.002 g, $8.5 \cdot 10^{-6}$ mol) were dissolved in trifluoroethanol (2 ml) and purged with N_2. The reaction mixture was polymerized at 75 °C for 2 h yielding **poly(M-5)$_{80}$** (yield 0.960 g, 96 %). TGA (the onset of decomposition): 295 °C. DSC: no thermal transition.

^{1}H NMR (300 MHz, in dilute aqueous NaCl (0.9 $g \cdot L^{-1}$) in D_2O, 298 K): δ (ppm) = 0.5 – 2.5 (broad 9H, $-CH_3$ and $-CH_2-$ on/in backbone, $-CH_2-CH_2-C-SO_3^-$), 2.8 – 3.1 (2H, $CH_2-SO_3^-$), 3.1 – 3.4 (6H, $-N^+-(CH_3)_2$), 3.4 – 4.0 (4H, $-CH_2-N^+-CH_2-$), 4.4 – 5.0 (2H, $-COO-CH_2-$).

FT-IR (selected bands in cm^{-1}): 3030 $\nu(N^+-CH_3)$, 2967 $\nu(CH_2)$, 1724 $\nu(C=O)$, 1146 $\nu_{as}(SO_3^-)$, 1035 $\nu_s(SO_3^-)$.

UV-vis absorbance maxima: in trifluoroethanol (λ_{max} = 260, 306, and 444 nm), and in water (λ_{max} = 252, 296, and 436 nm).

Fluorescence emission maxima: in trifluoroethanol (λ_{PL} = 539 nm), and in water (λ_{PL} = 545 nm).

Table 7.7. Reaction conditions for the RAFT polymerization of **M-5** in TFE at 75 °C, using RAFT agent **CTA-3** and initiator V-501. Monomer concentration was 30 wt%.

sample	molar ratio M-5 : CTA-3 : V-501	m_{M-5} [g]	m_{CTA-3} [g]	m_{V-501} [g]	t [h]
poly(M-5)$_{50}$	50 : 1 : 0.2	1	0.041	0.004	2
poly(M-5)$_{80}$	80 : 1 : 0.2	1	0.026	0.002	2
poly(M-5)$_{95}$	100 : 1 : 0.2	2	0.041	0.004	2
poly(M-5)$_{282}$	300 : 1 : 0.2	1	0.007	0.001	6

RAFT polymerization of sulfobetaine M-6

Exemplarily, **M-6** (1.000 g, $3.2 \cdot 10^{-3}$ mol), **CTA-3** (0.003 g, $5.4 \cdot 10^{-6}$ mol), and V-501 (0.001 g, $1.1 \cdot 10^{-6}$ mol) were dissolved in trifluoroethanol (2 ml) and purged with N_2. The reaction mixture was polymerized at 75 °C for 18 h yielding **poly(M-6)$_{485}$** (yield 0.810 g, 81 %). TGA (the onset of decomposition): 295 °C. DSC: no thermal transition.

^{1}H NMR (400 MHz, in dilute aqueous NaCl (0.9 $g \cdot L^{-1}$) in D_2O, 298 K): δ (ppm) = 0.5 – 2.5 (broad 13H, $-CH_3$ and $-CH_2-$ on/in backbone, $-CH_2-CH_2-CH_2-$ piperidine (C4, C3, C5), $CH_2-C-SO_3^-$), 2.8 – 3.1 (2H, $-CH_2-SO_3^-$), 3.1 – 4.0 (8H,

-CH_2-N^+-CH_2- piperidine (C2, C6), -N^+-CH_2-, -COO-C-CH_2-), 4.6 – 4.7 (2H, -COO-CH_2-).

FT-IR (selected bands in cm^{-1}): 3002 $\nu(N^+-CH_3)$, 2968 $\nu(CH_2)$, 1728 $\nu(C=O)$, 1162 $\nu_{as}(SO_3^-)$, 1034 $\nu_s(SO_3^-)$.

UV-vis absorbance maxima: in trifluoroethanol (λ_{max} = 268, 286, and 442 nm), and in water (λ_{max} = 258, 288, and 439 nm).

Fluorescence emission maxima: in trifluoroethanol (λ_{PL} = 534 nm), and in water (λ_{PL} = 532 nm).

Table 7.8. Reaction conditions for the RAFT polymerization of **M-6** in TFE at 75 °C, using RAFT agent **CTA-3** and initiator V-501. Monomer concentration was 30 wt%.

sample	**molar ratio**	$\mathbf{m_{M-6}}$	$\mathbf{m_{CTA-3}}$	$\mathbf{m_{V-501}}$	**t**
	M-6 : CTA-3 : V-501	**[g]**	**[g]**	**[g]**	**[h]**
poly(M-6)$_{95}$	100 : 1 : 0.2	2.5	0.049	0.005	19
poly(M-6)$_{250}$	600 : 1 : 0.2	1.0	0.003	0.001	18
poly(M-6)$_{330}$	400 : 1 : 0.2	1.0	0.005	0.001	12
poly(M-6)$_{485}$	600 : 1 : 0.2	1.0	0.003	0.001	18

RAFT polymerization of sulfobetaine M-7

Exemplarily, **M-7** (1.900 g, $5.7 \cdot 10^{-3}$ mol), **CTA-3** (0.006 g, $9.5 \cdot 10^{-6}$ mol), and V-501 (0.001 g, $1.9 \cdot 10^{-6}$ mol) were dissolved in trifluoroethanol (4 ml) and purged with N_2. The reaction mixture was polymerized at 75 °C for 15 h yielding **poly(M-7)$_{500}$** (yield 1.600 g, 83 %). TGA (the onset of decomposition): 290 °C. DSC: no thermal transition.

^{1}H NMR (300 MHz, in dilute aqueous NaCl (0.9 g·L^{-1}) in D_2O, 298 K): δ (ppm) = 0.5 – 2.5 (broad 15H, -CH_3 and -CH_2- on/in backbone, -CH_2-CH_2-CH_2- piperidine (C4, C3, C5), CH_2-CH_2-C-SO_3^-), 2.8 – 3.1 (2H, -CH_2-SO_3^-), 3.1 – 4.0 (8H, -CH_2-N^+-CH_2- piperidine (C2, C6), -N^+-CH_2-, -COO-C-CH_2-), 4.4 – 4.7 (2H, -COO-CH_2-).

FT-IR (selected bands in cm^{-1}): 3027 ν(N^+-CH_3), 2951 ν(CH_2), 1724 ν(C=O), 1170 $\nu_{as}(SO_3^-)$, 1034 $\nu_s(SO_3^-)$.

UV-vis absorbance maxima: in trifluoroethanol (λ_{max} = 262, 305, and 439 nm), and in water (λ_{max} = 260, 296, and 444 nm).

Fluorescence emission maxima: in trifluoroethanol (λ_{PL} = 534 nm), and in water (λ_{PL} = 537 nm).

Table 7.9. Reaction conditions for the RAFT polymerization of **M-7** in TFE at 75 °C, using RAFT agent **CTA-3** and initiator V-501. Monomer concentration was 30 wt%.

sample	molar ratio M-7 : CTA-3 : V-501	m_{M-7} [g]	m_{CTA-3} [g]	m_{V-501} [g]	t [h]
poly(M-7)$_{80}$	100 : 1 : 0.2	1.0	0.018	0.002	2.5
poly(M-7)$_{250}$	300 : 1 : 0.2	1.0	0.006	0.001	7.5
poly(M-7)$_{420}$	500 : 1 : 0.2	1.0	0.004	0.001	12.5
poly(M-7)$_{500}$	600 : 1 : 0.2	1.9	0.006	0.001	15.0

RAFT polymerization of sulfobetaine M-8

Exemplarily, **M-8** (1.000 g, $3.1 \cdot 10^{-3}$ mol), **CTA-3** (0.019 g, $3.1 \cdot 10^{-5}$ mol), and V-501 (0.002 g, $6.2 \cdot 10^{-6}$ mol) were dissolved in trifluoroethanol (2 ml) and purged with N_2. The reaction mixture was polymerized at 75 °C for 2.75 h yielding **poly(M-8)$_{95}$** (yield 0.960 g, 96 %). TGA (the onset of decomposition): 280 °C. DSC: no thermal transition.

^{1}H NMR (300 MHz, in dilute aqueous NaCl (0.9 g·L^{-1}) in D_2O, 298 K): δ (ppm) = 0.5 – 2.5 (broad 7H, -CH_3 and -CH_2- on/in backbone, -CH_2-C-SO_3^-), 2.8 – 3.3 (2H, -CH_2-SO_3^-), 3.3 – 4.4 (12H, -CH_2-CH_2-N^+-CH_2-CH_2- morpholine (C2, C3, C5, C6), -CH_2-N^+-CH_2-), 4.4 – 4.7 (2H, -COO-CH_2-).

FT-IR (selected bands in cm^{-1}): 3021 ν(N^+-CH_3), 2951 ν(CH_2), 1726 ν(C=O), 1172 $\nu_{as}(SO_3^-)$, 1036 $\nu_s(SO_3^-)$.

UV-vis absorbance maxima: in trifluoroethanol (λ_{max} = 269, 310, and 444 nm), and in water (λ_{max} = 254, 295, and 444 nm).

Fluorescence emission maxima: in trifluoroethanol (λ_{PL} = 537 nm), and in water (λ_{PL} = 547 nm).

Table 7.10. Reaction conditions for the RAFT polymerization of **M-8** in TFE at 75 °C, using RAFT agent **CTA-3** and initiator V-501. Monomer concentration was 30 wt%.

sample	molar ratio M-8 : CTA-3 : V-501	m_{M-8} [g]	m_{CTA-3} [g]	m_{V-501} [g]	t [h]
poly(M-8)$_{65}$	100 : 1 : 0.2	2	0.038	0.004	19.00
poly(M-8)$_{95}$	100 : 1 : 0.2	1	0.019	0.002	2.75
poly(M-8)$_{230}$	300 : 1 : 0.2	1	0.006	0.001	9.00
poly(M-8)$_{585}$	600 : 1 : 0.2	1	0.003	0.001	18.00

RAFT polymerization of sulfobetaine M-9

Exemplarily, **M-9** (1.000 g, $3.0 \cdot 10^{-3}$ mol), **CTA-3** (0.018 g, $3.0 \cdot 10^{-5}$ mol), and V-501 (0.002 g, $6.0 \cdot 10^{-6}$ mol) were dissolved in trifluoroethanol (2 ml) and purged with N_2. The reaction mixture was polymerized at 75 °C for 3 h yielding **poly(M-9)$_{85}$** (yield 0.700 g, 70 %). TGA (the onset of decomposition): 250 °C. DSC: no thermal transition.

^{1}H NMR (400 MHz, in dilute aqueous NaCl (0.9 g·L^{-1}) in D_2O, 298 K): δ (ppm) = 0.5 – 2.5 (broad 9H, -CH_3 and -CH_2- on/in backbone, -CH_2-CH_2-C-SO_3^-), 2.8 – 3.3 (2H, CH_2-SO_3^-), 3.3 – 4.4 (12H, -CH_2-CH_2-N^+-CH_2-CH_2- morpholine (C2, C3, C5, C6), -CH_2-N^+-CH_2-), 4.4 – 4.7 (2H, -COO-CH_2-).

FT-IR (selected bands in cm^{-1}): 3011 ν(N^+-CH_3), 2967 ν(CH_2), 1724 ν(C=O), 1169 $\nu_{as}(SO_3^-)$, 1035 $\nu_s(SO_3^-)$.

UV-vis absorbance maxima: in trifluoroethanol (λ_{max} = 263, 306, and 442 nm), and in water (λ_{max} = 260, 295, and 444 nm).

Fluorescence emission maxima: in trifluoroethanol (λ_{PL} = 534 nm), and in water (λ_{PL} = 541 nm).

Table 7.11. Reaction conditions for the RAFT polymerization of **M-9** in TFE at 75 °C, using RAFT agent **CTA-3** and initiator V-501. Monomer concentration was 30 wt%.

sample	molar ratio M-9 : CTA-3 : V-501	m_{M-9} [g]	m_{CTA-3} [g]	m_{V-501} [g]	t [h]
poly(M-9)$_{85}$	100 : 1 : 0.2	1.0	0.018	0.002	3.0
poly(M-9)$_{260}$	300 : 1 : 0.2	1.0	0.006	0.001	9.0
poly(M-9)$_{430}$	500 : 1 : 0.2	1.0	0.004	0.001	15.0
poly(M-9)$_{520}$	600 : 1 : 0.2	1.4	0.004	0.001	18.0

RAFT polymerization of sulfobetaine M-10

Exemplarily, **M-10** (2.000 g, $6.8 \cdot 10^{-3}$ mol), **CTA-3** (0.007 g, $1.1 \cdot 10^{-5}$ mol), and V-501 (0.001 g, $2.3 \cdot 10^{-6}$ mol) were dissolved in trifluoroethanol (4 ml) and purged with N_2. The reaction mixture was polymerized at 75 °C for 12 h yielding **poly(M-10)$_{585}$** (yield 1.900 g, 95 %). TGA (the onset of decomposition): 295 °C. DSC: no thermal transition.

^{1}H NMR (300 MHz, in dilute aqueous NaCl (0.9 g·L^{-1}) in D_2O, 298 K): δ (ppm) = 0.5 – 2.5 (broad 9H, -CH_3 and -CH_2- on/in backbone, -CH_2-C-SO_3^-, -COO-C-CH_2-), 2.9 – 3.1 (2H, CH_2-SO_3^-), 3.1 – 3.4 (6H, -N^+-$(CH_3)_2$), 3.4 – 3.8 (4H, -CH_2-N^+-CH_2-), 3.9 – 4.3 (2H, -COO-CH_2-).

FT-IR (selected bands in cm^{-1}): 3036 ν(N^+-CH_3), 2966 ν(CH_2), 1720 ν(C=O), 1150 $\nu_{as}(SO_3^-)$, 1033 $\nu_s(SO_3^-)$.

UV-vis absorbance maxima: in trifluoroethanol (λ_{max} = 263, 307, and 445 nm), and in water (λ_{max} = 254, 296, and 444 nm).

Fluorescence emission maxima: in trifluoroethanol (λ_{PL} = 538 nm), and in water (λ_{PL} = 545 nm).

Table 7.12. Reaction conditions for the RAFT polymerization of **M-10** in TFE at 75 °C, using RAFT agent **CTA-3** and initiator V-501. Monomer concentration was 30 wt%.

sample	molar ratio M-10 : CTA-3 : V-501	$m_{M\text{-}10}$ [g]	$m_{CTA\text{-}3}$ [g]	$m_{V\text{-}501}$ [g]	t [h]
poly(M-10)$_{75}$	100 : 1 : 0.2	1	0.027	0.002	2
poly(M-10)$_{295}$	300 : 1 : 0.2	1	0.007	0.001	6
poly(M-10)$_{480}$	500 : 1 : 0.2	1	0.004	0.001	10
poly(M-10)$_{585}$	600 : 1 : 0.2	2	0.007	0.001	12

RAFT polymerization of sulfobetaine M-11

Exemplarily, **M-11** (5.000 g, $1.6 \cdot 10^{-2}$ mol), **CTA-3** (0.099 g, $1.6 \cdot 10^{-4}$ mol), and V-501 (0.009 g, $3.3 \cdot 10^{-5}$ mol) were dissolved in trifluoroethanol (9 ml) and purged with N_2. The reaction mixture was polymerized at 75 °C for 19 h yielding **poly(M-11)$_{100}$** (yield 4.900 g, 98 %). TGA (the onset of decomposition): 300 °C. DSC: no thermal transition.

^{1}H NMR (300 MHz, in dilute aqueous NaCl (0.9 g·L^{-1}) in D_2O, 298 K): δ (ppm) = 0.5 – 2.5 (broad 11H, -CH_3 and -CH_2- on/in backbone, -CH_2-CH_2-C-SO_3^-, -COO-C-CH_2-), 2.9 – 3.1 (2H, -CH_2-SO_3^-), 3.1 – 3.3 (6H, -N^+-$(CH_3)_2$), 3.3 – 3.6 (4H, -CH_2-N^+-CH_2-), 3.9 – 4.3 (2H, COO-CH_2-).

FT-IR (selected bands in cm^{-1}): 3033 ν(N^+-CH_3), 2967 ν(CH_2), 1722 ν(C=O), 1165 $\nu_{as}(SO_3^-)$, 1034 $\nu_s(SO_3^-)$.

UV-vis absorbance maxima: in trifluoroethanol (λ_{max} = 264, 306, and 449 nm), and in water (λ_{max} = 256, 285, and 447 nm).

Fluorescence emission maxima: in trifluoroethanol (λ_{PL} = 538 nm), and in water (λ_{PL} = 545 nm).

Table 7.13. Reaction conditions for the RAFT polymerization of **M-11** in TFE at 75 °C, using RAFT agent **CTA-3** and initiator V-501. Monomer concentration was 30 wt%.

sample	molar ratio M-11 : CTA-3 : V-501	$m_{M\text{-}11}$ [g]	$m_{CTA\text{-}3}$ [g]	$m_{V\text{-}501}$ [g]	t [h]
poly(M-11)$_{100}$	100 : 1 : 0.2	5.0	0.099	0.009	19
poly(M-11)$_{290}$	300 : 1 : 0.2	2.0	0.013	0.002	3
poly(M-11)$_{480}$	500 : 1 : 0.2	1.0	0.004	0.001	5
poly(M-11)$_{540}$	600 : 1 : 0.2	3.2	0.012	0.001	6

7.5.3 RAFT polymerization of non-ionic monomers

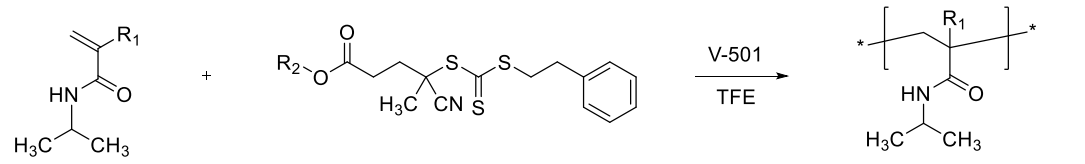

non-ionic monomer **CTA** **poly(non-ionic monomer)**

R_1 = H, CH_3 R_2 = H, 2-(naphthalimido)ethyl

In a typical procedure, *N*-isopropylmethacrylamide (**M-12**, 10.000 g, $7.9 \cdot 10^{-2}$ mol), **CTA-3** (0.119 g, $2.0 \cdot 10^{-4}$ mol), and V-501 (0.011 g, $3.9 \cdot 10^{-5}$ mol) were dissolved in TFE (18 ml). The yellow mixture was purged with N_2 for 30 min and subsequently polymerized at 75 °C for 16 h. After precipitation into diethyl ether (dissolution in TFE and precipitation into diethyl ether was repeated 3 times), the polymer was isolated and dried in vacuum. The homopolymer **poly(M-12)$_{195}$** was obtained as amorphous yellow solid (yield 5.100 g, 50 %).

Purified homopolymers were characterized by ^{1}H NMR, UV-vis, fluorescence, and IR spectroscopies, as well as by GPC, TGA, DSC, turbidimetry, and DLS. The individual samples are named **poly(monomer)$_n$**, with *n* being the number average degree of polymerization that was theoretically calculated using **equation 7.1** (conversions were shown in **chapter 4**).

TGA (the onset of decomposition): 280 °C. DSC: thermal transition at about 175 °C (T_g).

^{1}H NMR (400 MHz, CD_2Cl_2, 298 K): δ (ppm) = 0.5 – 2.6 (broad 11H, -CH_3 and -CH_2- on/in backbone, -N-C-$(CH_3)_2$), 3.8 – 4.0 (1H, -N-CH-).

FT-IR (selected bands in cm^{-1}): 3360 ν(NH), 2971 ν(CH_2), 1631 ν(amide I), and 1513 ν(amide II).

UV-vis absorbance maxima: in trifluoroethanol (λ_{max} = 260, 292, and 441 nm), and in water (λ_{max} = 263, 293, and 449 nm).

Fluorescence emission maxima: in trifluoroethanol (λ_{PL} = 538 nm), and in water (λ_{PL} = 544 nm).

Results of RAFT polymerization using **M-13** (yield: 0.500 g, 50 %): TGA (the onset of decomposition): 380 °C. DSC: thermal transition at about 130 °C (T_g) and at about 39 °C (recrystallization).

^{1}H NMR (300 MHz, CD_3OD, 298 K): δ (ppm) = 0.8 – 2.4 (broad 9H, -CH_2- and -CH- on/in backbone, -N-C-$(CH_3)_2$), 3.8 – 4.0 (1H, -N-CH-).

FT-IR (selected bands in cm^{-1}): 3279 ν(NH), 2972 ν(CH_2), 1641 ν(amide I), and 1539 ν(amide II).

UV-vis absorbance maxima: in trifluoroethanol (λ_{max} = 264, 302, and 442 nm), and in water (λ_{max} = 258, 298, and 446 nm).

Fluorescence emission maxima: in trifluoroethanol (λ_{PL} = 539 nm), and in water (λ_{PL} = 545 nm).

Table 7.14. Reaction conditions for the RAFT polymerization of **M-12** and **M-13** in TFE at 75 °C, using different RAFT agents and initiator V-501. The monomer concentration was 30 wt%.

sample	RAFT agent	molar ratio Mon : CTA : V-501	m_{Mon} [g]	m_{CTA} [g]	m_{V-501} [g]	t [h]
poly(M-12)$_{180}$	CTA-1	400 : 1 : 0.2	5.0	0.060	0.006	16
poly(M-12)$_{40}$	CTA-3	100 : 1 : 0.2	10.5	0.500	0.046	3
poly(M-12)$_{45}$	CTA-3	100 : 1 : 0.2	10.5	0.500	0.046	4
poly(M-12)$_{65}$	CTA-3	100 : 1 : 0.2	10.5	0.500	0.046	19
poly(M-12)$_{195}$	CTA-3	400 : 1 : 0.2	10.0	0.119	0.011	16
poly(M-13)$_{195}$	CTA-3	200 : 1 : 0.2	1.0	0.026	0.003	6

7.6 Synthesis of block copolymers

Synthesized homopolymers were utilized as macro-RAFT agents (**m-CTA**) for the synthesis of block copolymers. The synthesis of block copolymers via RAFT polymerization (route **A** or **B**) was conducted according a general procedure which is described in the following.

route **A**:

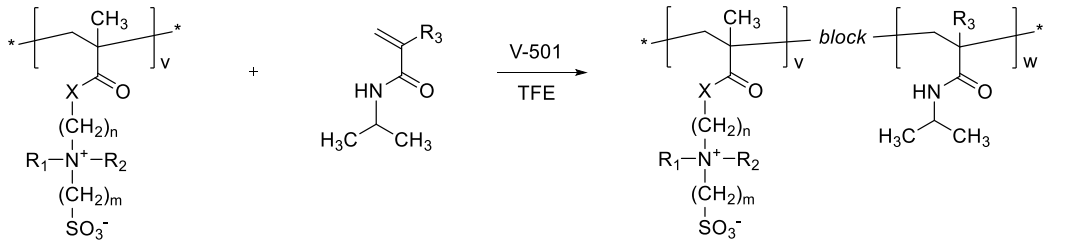

poly(sulfobetaine)$_v$ as **m-CTA** | **non-ionic monomer** | **poly(sulfobetaine)$_v$-*block*-(non-ionic monomer)$_w$**

X = NH, O; n = 2, 3; m = 3, 4, C_3-OH | R_1, R_2 = CH_3, ring : piperidine, morpholine | R_3 = H, CH_3 | v, w = number average degree of polymerization

route **B**:

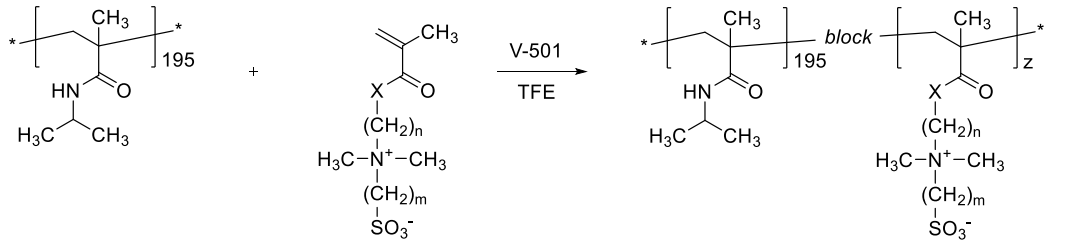

poly(M-12)$_{195}$ as **m-CTA** | **sulfobetaine** | **poly(M-12)$_{195}$-*block*-(sulfobetaine)$_z$**

X = NH, O; n = 2, 3; m = 3, 4 | z = number average degree of polymerization

In a typical procedure, **m-CTA**, monomer, and V-501 were dissolved in TFE. The yellow mixture was purged with N_2 for 30 min and subsequently polymerized for a given time at 75 °C. Due to the solubility in methanol, the block copolymer was then precipitated into diethyl ether (dissolution in TFE and precipitation into diethyl ether

was repeated 3 times), washed with dichloromethane, isolated, and dried in vacuum. The purified block copolymer was obtained as amorphous yellow solid.

Purified block copolymers were characterized by ^{1}H NMR, UV-vis, fluorescence, and IR spectroscopies, as well as by TGA, DSC, turbidimetry, and DLS. The individual samples are named **poly(monomer 1)$_v$-*block*-(monomer 2)$_w$** or **poly(M-12)$_{195}$-*block*-(sulfobetaine)$_z$**, with *v*, *w*, and *z* being the number average degree of polymerization that was theoretically calculated using **equation 7.1** (conversions were shown in **chapter 5.1**).

7.6.1 RAFT polymerization with poly(sulfobetaine) as macro-RAFT agent (route A)

RAFT polymerization of M-12 or M-13 using m-CTA poly(M-1)

Exemplarily, **poly(M-1)$_{500}$** (1.500 g, $1.0 \cdot 10^{-5}$ mol), **M-12** (0.520 g, $4.1 \cdot 10^{-3}$ mol), and V-501 (0.0006 g, $2.1 \cdot 10^{-6}$ mol) were dissolved in TFE (4 ml) and purged with N_2. The yellow reaction mixture was polymerized at 75 °C for 9 h yielding **poly(M-1)$_{500}$-*block*-(M-12)$_{145}$** (yield 1.070 g, 54 %).

^{1}H NMR (400 MHz, in dilute aqueous NaCl (9.0 g·L^{-1}) in D_2O, 298 K): δ (ppm) = 0.5 – 2.5 (broad 20H, -CH_3 and -CH_2- on/in backbone of **M-1** and **M-12**, -N-C-$(CH_3)_2$, -CH_2-C-N^+-C-CH_2-), 3.1 – 3.2 (2H, -CH_2-SO_3^-), 3.2 – 3.5 (6H, -N^+-$(CH_3)_2$), 3.5 – 3.8 (6H, -CH_2-N^+-CH_2, -CON-CH_2-), 3.9 – 4.1 (1H, -N-CH-).

FT-IR (selected bands, cm^{-1}): 3406 ν(NH), 3039 ν(N^+-CH_3), 2977 ν(CH_2), 1640 ν(amide I), 1532 ν(amide II), 1173 $\nu_{as}(SO_3^-)$, 1035 $\nu_s(SO_3^-)$.

UV-vis absorbance maxima: in trifluoroethanol (λ_{max} = 260, 290, and 440 nm), and in water (λ_{max} = 253, 285, and 440 nm).

Fluorescence emission maxima: in trifluoroethanol (λ_{PL} = 538 nm), and in water (λ_{PL} = 547 nm).

Table 7.15. Reaction conditions for the RAFT polymerization of **M-12** or **M-13** in TFE at 75 °C, using **m-CTA poly(M-1)** and initiator V-501. Monomer and **m-CTA** concentration was 30 wt%.

sample	molar ratio	m_{Mon}	$m_{m\text{-}CTA}$	$m_{V\text{-}501}$	t
	Mon : m-CTA : V-501	**[g]**	**[g]**	**[g]**	**[h]**
poly(M-1)$_{85}$-*block*-(M-12)$_{100}$	400 : 1 : 0.2	7.00	3.5	0.0077	9
poly(M-1)$_{170}$-*block*-(M-12)$_{160}$	400 : 1 : 0.2	0.50	0.5	0.0006	9
poly(M-1)$_{280}$-*block*-(M-12)$_{85}$	400 : 1 : 0.2	0.62	1.0	0.0007	9
poly(M-1)$_{500}$-*block*-(M-12)$_{145}$	400 : 1 : 0.2	0.52	1.5	0.0006	9
poly(M-1)$_{430}$-*block*-(M-13)$_{200}$	200 : 1 : 0.2	0.45	2.7	0.0010	24

RAFT polymerization of M-12 using m-CTA poly(M-2)

Exemplarily, **poly(M-2)$_{505}$** (1.000 g, $6.4 \cdot 10^{-6}$ mol), **M-12** (0.490 g, $3.9 \cdot 10^{-3}$ mol), and V-501 (0.0004 g, $1.3 \cdot 10^{-6}$ mol) were dissolved in TFE (3 ml) and purged with N_2. The yellow reaction mixture was polymerized at 75 °C for 96 h yielding **poly(M-2)$_{505}$-*block*-(M-12)$_{145}$** (yield 0.900 g, 60 %).

^{1}H NMR (400 MHz, in dilute aqueous NaCl (9.0 g·L^{-1}) in D_2O, 298 K): δ (ppm) = 0.5 – 2.5 (broad 18H, -CH_3 and -CH_2- on/in backbone of **M-2** and **M-12**, -N-C-$(CH_3)_2$, -CON-C-CH_2-), 2.8 – 3.8 (14H, -CON-CH_2-C-CH_2-$N^+(CH_3)_2$-CH_2-C-CH_2-SO_3^-), 3.9 – 4.1 (1H, -N-CH-), 4.5 – 4.6 (-CH-OH).

FT-IR (selected bands, cm^{-1}): 3401 ν(NH), 3031 ν(N^+-CH_3), 2969 ν(CH_2), 1639 ν(amide I), 1531 ν(amide II), 1172 $\nu_{as}(SO_3^-)$, 1035 $\nu_s(SO_3^-)$.

UV-vis absorbance maxima: in trifluoroethanol (λ_{max} = 260, 290, and 440 nm), and in water (λ_{max} = 254, 287, and 440 nm).

Fluorescence emission maxima: in trifluoroethanol (λ_{PL} = 537 nm), and in water (λ_{PL} = 546 nm).

Table 7.16. Reaction conditions for the RAFT polymerization of **M-12** in TFE at 75 °C, using **m-CTA poly(M-2)** and initiator V-501. Monomer and **m-CTA** concentration was 30 wt%.

sample	molar ratio	m_{M-12}	m_{m-CTA}	m_{V-501}	t
	M-12 : m-CTA : V-501	**[g]**	**[g]**	**[g]**	**[h]**
poly(M-2)$_{80}$-*block*-(M-12)$_{160}$	600 : 1 : 0.2	1.47	0.5	0.0011	96
poly(M-2)$_{115}$-*block*-(M-12)$_{155}$	600 : 1 : 0.2	1.08	0.5	0.0008	96
poly(M-2)$_{235}$-*block*-(M-12)$_{175}$	600 : 1 : 0.2	0.52	0.5	0.0004	96
poly(M-2)$_{505}$-*block*-(M-12)$_{145}$	600 : 1 : 0.2	0.49	1.0	0.0004	96

RAFT polymerization of M-12 or M-13 using m-CTA poly(M-3)

Exemplarily, **poly(M-3)$_{80}$** (1.500 g, $6.1 \cdot 10^{-5}$ mol), **M-12** (3.110 g, $2.4 \cdot 10^{-2}$ mol), and V-501 (0.0034 g, $1.2 \cdot 10^{-5}$ mol) were dissolved in TFE (8 ml) and purged with N_2. The yellow reaction mixture was polymerized at 75 °C for 90 h yielding **poly(M-1)$_{80}$-*block*-(M-12)$_{115}$** (yield 2.000 g, 42 %).

^{1}H NMR (300 MHz, in dilute aqueous NaCl (9.0 g·L^{-1}) in D_2O, 298 K): δ (ppm) = 0.5 – 2.5 (broad 22H, -CH_3 and -CH_2- on/in backbone of **M-3** and **M-12**, -N-C-$(CH_3)_2$, -CH_2-C-N^+-CH_2-CH_2-), 2.9 – 3.5 (14H, -CH_2-SO_3^-, -N^+-$(CH_3)_2$), -CH_2-N^+-CH_2, -CON-CH_2-), 3.8 – 4.0 (1H, -N-CH-).

FT-IR (selected bands, cm^{-1}): 3387 ν(NH), 2971 ν(N^+-CH_3), 2938 ν(CH_2), 1633 ν(amide I), 1523 ν(amide II), 1197 $\nu_{as}(SO_3^-)$, 1037 $\nu_s(SO_3^-)$.

UV-vis absorbance maxima: in trifluoroethanol (λ_{max} = 263, 292, and 442 nm), and in water (λ_{max} = 285 and 440 nm).

Fluorescence emission maxima: in trifluoroethanol (λ_{PL} = 538 nm), and in water (λ_{PL} = 538 nm).

Table 7.17. Reaction conditions for the RAFT polymerization of **M-12** or **M-13** in TFE at 75 °C, using **m-CTA poly(M-3)** and initiator V-501. Monomer and **m-CTA** concentration was 30 wt%.

sample	molar ratio	m_{Mon}	$m_{m\text{-}CTA}$	$m_{V\text{-}501}$	t
	Mon : m-CTA : V-501	**[g]**	**[g]**	**[g]**	**[h]**
poly(M-3)$_{40}$-*block*-(M-12)$_{190}$	400 : 1 : 0.2	1.97	0.5	0.0022	96
poly(M-3)$_{50}$-*block*-(M-12)$_{155}$	400 : 1 : 0.2	2.20	0.7	0.0024	96
poly(M-3)$_{80}$-*block*-(M-12)$_{115}$	400 : 1 : 0.2	3.11	1.5	0.0034	90
poly(M-3)$_{245}$-*block*-(M-12)$_{105}$	400 : 1 : 0.2	1.35	2.0	0.0015	90
poly(M-3)$_{425}$-*block*-(M-12)$_{110}$	400 : 1 : 0.2	0.78	2.0	0.0009	90
poly(M-3)$_{80}$-*block*-(M-13)$_{100}$	100 : 1 : 0.2	0.69	1.5	0.0034	5
poly(M-3)$_{80}$-*block*-(M-13)$_{400}$	400 : 1 : 0.2	1.11	0.6	0.0014	19

RAFT polymerization of M-12 or M-13 using m-CTA poly(M-4)

Exemplarily, **poly(M-4)$_{575}$** (2.000 g, $1.2 \cdot 10^{-5}$ mol), **M-12** (0.630 g, $5.0 \cdot 10^{-3}$ mol), and V-501 (0.0007 g, $2.5 \cdot 10^{-6}$ mol) were dissolved in TFE (5 ml) and purged with N_2. The yellow reaction mixture was polymerized at 75 °C for 40 h yielding **poly(M-4)$_{575}$-*block*-(M-12)$_{60}$** (yield 1.700 g, 65 %).

^{1}H NMR (400 MHz, in dilute aqueous NaCl (9.0 g·L^{-1}) in D_2O, 298 K): δ (ppm) = 0.5 – 2.5 (broad 18H, -CH_3 and -CH_2- on/in backbone of **M-4** and **M-12**, -N-C-$(CH_3)_2$, -CH_2-C-SO_3^-), 2.9 – 3.1 (2H, -CH_2-SO_3^-), 3.1 – 3.3 (6H, -N^+-$(CH_3)_2$), 3.5 – 4.1 (5H, -CH_2-N^+-CH_2-, N-CH-), 4.3 – 4.7 (2H, -COO-CH_2-).

FT-IR (selected bands, cm^{-1}): 3440 ν(NH), 3000 ν(N^+-CH_3), 2977 ν(CH_2), 1724 ν(C=O), 1650 ν(amide I), 1530 ν(amide II), 1172 $\nu_{as}(SO_3^-)$, 1036 $\nu_s(SO_3^-)$.

UV-vis absorbance maxima: in trifluoroethanol (λ_{max} = 286, 310, and 445 nm), and in water (λ_{max} = 290 and 445 nm).

Fluorescence emission maxima: in trifluoroethanol (λ_{PL} = 538 nm), and in water (λ_{PL} = 545 nm).

Table 7.18. Reaction conditions for the RAFT polymerization of **M-12** or **M-13** in TFE at 75 °C, using **m-CTA poly(M-4)** and initiator V-501. Monomer and **m-CTA** concentration was 30 wt%.

sample	molar ratio	m_{Mon}	$m_{m\text{-}CTA}$	$m_{V\text{-}501}$	t
	Mon : m-CTA : V-501	[g]	[g]	[g]	[h]
poly(M-4)$_{85}$-*block*-(M-12)$_{80}$	400 : 1 : 0.2	5.17	2.5	0.0057	9
poly(M-4)$_{270}$-*block*-(M-12)$_{60}$	400 : 1 : 0.2	1.34	2.0	0.0015	16
poly(M-4)$_{575}$-*block*-(M-12)$_{60}$	400 : 1 : 0.2	0.63	2.0	0.0007	40
poly(M-4)$_{585}$-*block*-(M-12)$_{70}$	400 : 1 : 0.2	0.62	2.0	0.0007	9
poly(M-4)$_{585}$-*block*-(M-12)$_{145}$	600 : 1 : 0.2	0.47	1.0	0.0004	96
poly(M-4)$_{270}$-*block*-(M-13)$_{200}$	200 : 1 : 0.2	0.60	2.0	0.0016	6

RAFT polymerization of M-12 using m-CTA poly(M-5)

Exemplarily, **poly(M-5)$_{80}$** (0.500 g, $2.2 \cdot 10^{-5}$ mol), **M-12** (1.640 g, $1.3 \cdot 10^{-2}$ mol), and V-501 (0.0012 g, $4.3 \cdot 10^{-6}$ mol) were dissolved in TFE (4 ml) and purged with N_2. The yellow reaction mixture was polymerized at 75 °C for 96 h yielding **poly(M-5)$_{80}$-*block*-(M-12)$_{185}$** (yield 0.900 g, 79 %).

^{1}H NMR (400 MHz, in dilute aqueous NaCl (9.0 g·L^{-1}) in D_2O, 298 K): δ (ppm) = 0.5 – 2.5 (broad 20H, -CH_3 and -CH_2- on/in backbone of **M-5** and **M-12**, -N-C-$(CH_3)_2$, -CH_2-CH_2-C-SO_3^-), 2.9 – 3.1 (2H, -CH_2-SO_3^-), 3.1 – 3.4 (6H, -N^+-$(CH_3)_2$), 3.4 – 4.0 (5H, -CH_2-N^+-CH_2-, -N-CH-), 4.4 – 4.5 (2H, -COO-CH_2-).

FT-IR (selected bands, cm^{-1}): 3358 ν(NH), 2974 $\nu(N^+\text{-}CH_3)$, 2939 $\nu(CH_2)$, 1727 ν(C=O), 1630 ν(amide I), 1520 ν(amide II), 1148 $\nu_{as}(SO_3^-)$, 1037 $\nu_s(SO_3^-)$.

UV-vis absorbance maxima: in trifluoroethanol (λ_{max} = 257, 293, and 446 nm), and in water (λ_{max} = 256, 292, and 446 nm).

Fluorescence emission maxima: in trifluoroethanol (λ_{PL} = 538 nm), and in water (λ_{PL} = 545 nm).

Table 7.19. Reaction conditions for the RAFT polymerization of **M-12** in TFE at 75 °C, using **m-CTA poly(M-5)** and initiator V-501. Monomer and **m-CTA** concentration was 30 wt%.

sample	molar ratio	$m_{M\text{-}12}$	$m_{m\text{-}CTA}$	$m_{V\text{-}501}$	t
	M-12 : m-CTA : V-501	**[g]**	**[g]**	**[g]**	**[h]**
poly(M-5)$_{50}$-*block*-(M-12)$_{190}$	600 : 1 : 0.2	2.65	0.5	0.0019	96
poly(M-5)$_{80}$-*block*-(M-12)$_{190}$	600 : 1 : 0.2	1.64	0.5	0.0012	96
poly(M-5)$_{95}$-*block*-(M-12)$_{190}$	600 : 1 : 0.2	2.71	1.0	0.0020	96
poly(M-5)$_{280}$-*block*-(M-12)$_{200}$	600 : 1 : 0.2	0.46	0.5	0.0003	96

RAFT polymerization of M-12 using m-CTA poly(M-6)

Exemplarily, **poly(M-6)$_{485}$** (0.500 g, $3.3\cdot10^{-6}$ mol), **M-12** (0.250 g, $2.0\cdot10^{-3}$ mol), and V-501 (0.0002 g, $7.0\cdot10^{-7}$ mol) were dissolved in TFE (2 ml) and purged with N_2. The yellow reaction mixture was polymerized at 75 °C for 96 h yielding **poly(M-6)$_{485}$-*block*-(M-12)$_{180}$** (yield 0.500 g, 67 %).

^{1}H NMR (400 MHz, in dilute aqueous NaCl (9.0 $g\cdot L^{-1}$) in D_2O, 298 K): δ (ppm) = 0.5 – 2.5 (broad 24H, $-CH_3$ and $-CH_2-$ on/in backbone of **M-6** and **M-12**, $-N\text{-}C\text{-}(CH_3)_2$, $-CH_2\text{-}CH_2\text{-}CH_2-$ piperidine (C4, C3, C5), $-CH_2\text{-}C\text{-}SO_3^-$), 2.8 – 3.1 (2H, $-CH_2\text{-}SO_3^-$), 3.1 – 4.0 (9H, $-CH_2\text{-}N^+\text{-}CH_2-$ piperidine (C2, C6), $-N^+\text{-}CH_2-$, $-COO\text{-}C\text{-}CH_2-$, -N-CH-), 4.6 – 4.7 (2H, $COO\text{-}CH_2-$).

FT-IR (selected bands, cm^{-1}): 3443 ν(NH), 3002 $\nu(N^+\text{-}CH_3)$, 2969 $\nu(CH_2)$, 1725 ν(C=O), 1642 ν(amide I), 1524 ν(amide II), 1173 $\nu_{as}(SO_3^-)$, 1036 $\nu_s(SO_3^-)$.

UV-vis absorbance maxima: in trifluoroethanol (λ_{max} = 263, 298, and 442 nm), and in water (λ_{max} = 231, 290, and 444 nm).

Fluorescence emission maxima: in trifluoroethanol (λ_{PL} = 534 nm), and in water (λ_{PL} = 532 nm).

Table 7.20. Reaction conditions for the RAFT polymerization of **M-12** in TFE at 75 °C, using **m-CTA poly(M-6)** and initiator V-501. Monomer and **m-CTA** concentration was 30 wt%.

sample	molar ratio	$m_{M\text{-}12}$	$m_{m\text{-}CTA}$	$m_{V\text{-}501}$	t
	M-12 : m-CTA : V-501	**[g]**	**[g]**	**[g]**	**[h]**
poly(M-6)$_{95}$-*block*-(M-12)$_{180}$	600 : 1 : 0.2	1.29	0.5	0.0009	96
poly(M-6)$_{250}$-*block*-(M-12)$_{180}$	600 : 1 : 0.2	0.49	0.5	0.0004	96
poly(M-6)$_{330}$-*block*-(M-12)$_{185}$	600 : 1 : 0.2	0.37	0.5	0.0003	96
poly(M-6)$_{485}$-*block*-(M-12)$_{180}$	600 : 1 : 0.2	0.25	0.5	0.0002	96

RAFT polymerization of M-12 using m-CTA poly(M-7)

Exemplarily, **poly(M-7)$_{500}$** (0.350 g, $2.8\cdot10^{-7}$ mol), **M-12** (0.160 g, $1.3\cdot10^{-3}$ mol), and V-501 (0.0001 g, $4.0\cdot10^{-7}$ mol) were dissolved in TFE (1 ml) and purged with N_2. The yellow reaction mixture was polymerized at 75 °C for 96 h yielding **poly(M-7)$_{500}$-*block*-(M-12)$_{140}$** (yield 0.500 g, 76 %).

^{1}H NMR (300 MHz, in dilute aqueous NaCl (9.0 $g\cdot L^{-1}$) in D_2O, 298 K): δ (ppm) = 0.5 – 2.5 (broad 26H, $\text{-}CH_3$ and $\text{-}CH_2\text{-}$ on/in backbone of **M-7** and **M-12**, $\text{-N-C-}(CH_3)_2$, $\text{-}CH_2\text{-}CH_2\text{-}CH_2\text{-}$ piperidine (C4, C3, C5), $\text{-}CH_2\text{-}CH_2\text{-C-}SO_3^-$), 2.8 – 3.1 (2H, $\text{-}CH_2\text{-}SO_3^-$), 3.1 – 4.0 (9H, $\text{-}CH_2\text{-}N^+\text{-}CH_2\text{-}$ piperidine (C2, C6), $\text{-}N^+\text{-}CH_2\text{-}$, $\text{-COO-C-}CH_2\text{-}$, -N-CH-), 4.4 – 4.7 (2H, $\text{-COO-}CH_2\text{-}$).

FT-IR (selected bands, cm^{-1}): 3443 ν(NH), 3002 $\nu(N^+\text{-}CH_3)$, 2969 $\nu(CH_2)$, 1725 ν(C=O), 1642 ν(amide I), 1524 ν(amide II), 1173 $\nu_{as}(SO_3^-)$, 1036 $\nu_s(SO_3^-)$.

UV-vis absorbance maxima: in trifluoroethanol (λ_{max} = 264, 300, and 446 nm), and in water (λ_{max} = 232, 289, and 444 nm).

Fluorescence emission maxima: in trifluoroethanol (λ_{PL} = 535 nm), and in water (λ_{PL} = 534 nm).

Table 7.21. Reaction conditions for the RAFT polymerization of **M-12** in TFE at 75 °C, using **m-CTA poly(M-7)** and initiator V-501. Monomer and **m-CTA** concentration was 30 wt%.

sample	molar ratio	$m_{M\text{-}12}$	$m_{m\text{-}CTA}$	$m_{V\text{-}501}$	t
	M-12 : m-CTA : V-501	**[g]**	**[g]**	**[g]**	**[h]**
poly(M-7)$_{82}$-*block*-(M-12)$_{145}$	600 : 1 : 0.2	1.37	0.50	0.0010	96
poly(M-7)$_{250}$-*block*-(M-12)$_{145}$	600 : 1 : 0.2	0.46	0.50	0.0003	96
poly(M-7)$_{420}$-*block*-(M-12)$_{145}$	600 : 1 : 0.2	0.27	0.50	0.0002	96
poly(M-7)$_{500}$-*block*-(M-12)$_{140}$	600 : 1 : 0.2	0.16	0.35	0.0001	96

RAFT polymerization of M-12 using m-CTA poly(M-8)

Exemplarily, **poly(M-8)$_{95}$** (0.300 g, $9.5\cdot10^{-6}$ mol), **M-12** (0.730 g, $5.7\cdot10^{-3}$ mol), and V-501 (0.0005 g, $2.0\cdot10^{-6}$ mol) were dissolved in TFE (2 ml) and purged with N_2. The yellow reaction mixture was polymerized at 75 °C for 96 h yielding **poly(M-8)$_{95}$-*block*-(M-12)$_{125}$** (yield 0.400 g, 39 %).

^{1}H NMR (400 MHz, in dilute aqueous NaCl (9.0 $g\cdot L^{-1}$) in D_2O, 298 K): δ (ppm) = 0.5 – 2.5 (broad 18H, $-CH_3$ and $-CH_2-$ on/in backbone of **M-8** and **M-12**, $-N\text{-}C\text{-}(CH_3)_2$, $-CH_2\text{-}C\text{-}SO_3^-$), 2.9 – 3.2 (2H, $-CH_2\text{-}SO_3^-$), 3.2 – 4.4 (13H, $-CH_2\text{-}CH_2\text{-}N^+\text{-}CH_2\text{-}CH_2-$ morpholine (C2, C3, C5, C6), $-CH_2\text{-}N^+\text{-}CH_2-$, -N-CH-), 4.4 – 4.7 (2H, $-COO\text{-}CH_2-$).

FT-IR (selected bands, cm^{-1}): 3448 ν(NH), 2972 $\nu(N^+\text{-}CH_3)$, 2939 $\nu(CH_2)$, 1726 ν(C=O), 1649 ν(amide I), 1528 ν(amide II), 1171 $\nu_{as}(SO_3^-)$, 1036 $\nu_s(SO_3^-)$.

UV-vis absorbance maxima: in trifluoroethanol (λ_{max} = 257, 295, and 446 nm), and in water (λ_{max} = 248, 288, and 441 nm).

Fluorescence emission maxima: in trifluoroethanol (λ_{PL} = 537 nm), and in water (λ_{PL} = 543 nm).

Table 7.22. Reaction conditions for the RAFT polymerization of **M-12** in TFE at 75 °C, using **m-CTA poly(M-8)** and initiator V-501. Monomer and **m-CTA** concentration was 30 wt%.

sample	molar ratio	$m_{M\text{-}12}$	$m_{m\text{-}CTA}$	$m_{V\text{-}501}$	t
	M-12 : m-CTA : V-501	**[g]**	**[g]**	**[g]**	**[h]**
poly(M-8)$_{65}$-*block*-(M-12)$_{145}$	600 : 1 : 0.2	1.05	0.3	0.0008	96
poly(M-8)$_{95}$-*block*-(M-12)$_{145}$	600 : 1 : 0.2	0.73	0.3	0.0005	96
poly(M-8)$_{230}$-*block*-(M-12)$_{145}$	600 : 1 : 0.2	0.41	0.4	0.0003	96
poly(M-8)$_{585}$-*block*-(M-12)$_{140}$	600 : 1 : 0.2	0.49	1.0	0.0004	96

RAFT polymerization of M-12 using m-CTA poly(M-9)

Exemplarily, **poly(M-9)$_{85}$** (0.500 g, $1.7\cdot10^{-5}$ mol), **M-12** (1.290 g, $5.7\cdot10^{-3}$ mol), and V-501 (0.0010 g, $3.4\cdot10^{-6}$ mol) were dissolved in TFE (3 ml) and purged with N_2. The yellow reaction mixture was polymerized at 75 °C for 96 h yielding **poly(M-9)$_{85}$-*block*-(M-12)$_{190}$** (yield 0.700 g, 39 %).

^{1}H NMR (400 MHz, in dilute aqueous NaCl (9.0 $g\cdot L^{-1}$) in D_2O, 298 K): δ (ppm) = 0.5 – 2.5 (broad 20H, $-CH_3$ and $-CH_2-$ on/in backbone of **M-9** and **M-12**, $-N-C-(CH_3)_2$, $-CH_2-CH_2-C-SO_3^-$), 2.9 – 3.2 (2H, $-CH_2-SO_3^-$), 3.2 – 4.4 (13H, $-CH_2-CH_2-N^+-CH_2-CH_2-$ morpholine (C2, C3, C5, C6), $-CH_2-N^+-CH_2-$, -N-CH-), 4.4 – 4.7 (2H, $-COO-CH_2-$).

FT-IR (selected bands, cm^{-1}): 3439 ν(NH), 3011 $\nu(N^+\text{-}CH_3)$, 2967 $\nu(CH_2)$, 1724 ν(C=O), 1649 ν(amide I), 1528 ν(amide II), 1169 $\nu_{as}(SO_3^-)$, 1035 $\nu_s(SO_3^-)$.

UV-vis absorbance maxima: in trifluoroethanol (λ_{max} = 263, 306, and 442 nm), and in water (λ_{max} = 260, 295, and 444 nm).

Fluorescence emission maxima: in trifluoroethanol (λ_{PL} = 534 nm), and in water (λ_{PL} = 541 nm).

Table 7.23. Reaction conditions for the RAFT polymerization of **M-12** in TFE at 75 °C, using **m-CTA poly(M-9)** and initiator V-501. Monomer and **m-CTA** concentration was 30 wt%.

sample	molar ratio	$m_{M\text{-}12}$	$m_{m\text{-}CTA}$	$m_{V\text{-}501}$	t
	M-12 : m-CTA : V-501	**[g]**	**[g]**	**[g]**	**[h]**
poly(M-9)$_{85}$-*block*-(M-12)$_{190}$	600 : 1 : 0.2	1.29	0.5	0.0010	96
poly(M-9)$_{260}$-*block*-(M-12)$_{190}$	600 : 1 : 0.2	0.44	0.5	0.0003	96
poly(M-9)$_{430}$-*block*-(M-12)$_{190}$	600 : 1 : 0.2	0.26	0.5	0.0002	96
poly(M-9)$_{520}$-*block*-(M-12)$_{190}$	600 : 1 : 0.2	0.22	0.5	0.0002	96

RAFT polymerization of M-12 using m-CTA poly(M-10)

Exemplarily, **poly(M-10)$_{585}$** (1.000 g, $5.8\cdot10^{-6}$ mol), **M-12** (0.440 g, $3.5\cdot10^{-3}$ mol), and V-501 (0.0003 g, $1.2\cdot10^{-6}$ mol) were dissolved in TFE (2.5 ml) and purged with N_2. The yellow reaction mixture was polymerized at 75 °C for 96 h yielding **poly(M-10)$_{585}$-*block*-(M-12)$_{190}$** (yield 0.910 g, 63 %).

^{1}H NMR (300 MHz, in dilute aqueous NaCl (9.0 $g\cdot L^{-1}$) in D_2O, 298 K): δ (ppm) = 0.5 – 2.5 (broad 20H, $-CH_3$ and $-CH_2-$ on/in backbone of **M-10** and **M-12**, $-N\text{-}C\text{-}(CH_3)_2$, $-CH_2\text{-}C\text{-}SO_3^-$, $-COO\text{-}C\text{-}CH_2-$), 2.9 – 3.1 (2H, $-CH_2\text{-}SO_3^-$), 3.1 – 3.4 (6H, $-N^+\text{-}(CH_3)_2$), 3.4 – 3.7 (4H, $-CH_2\text{-}N^+\text{-}CH_2-$), 3.7 – 4.3 (3H, N-CH-, $COO\text{-}CH_2-$).

FT-IR (selected bands, cm^{-1}): 3439 ν(NH), 3033 $\nu(N^+\text{-}CH_3)$, 2967 $\nu(CH_2)$, 1717 ν(C=O), 1650 ν(amide I), 1528 ν(amide II), 1163 $\nu_{as}(SO_3^-)$, 1034 $\nu_s(SO_3^-)$.

UV-vis absorbance maxima: in trifluoroethanol (λ_{max} = 266, 297, and 447 nm), and in water (λ_{max} = 259, 290, and 444 nm).

Fluorescence emission maxima: in trifluoroethanol (λ_{PL} = 539 nm), and in water (λ_{PL} = 545 nm).

Table 7.24. Reaction conditions for the RAFT polymerization of **M-12** in TFE at 75 °C, using **m-CTA poly(M-10)** and initiator V-501. Monomer and **m-CTA** concentration was 30 wt%.

sample	molar ratio	$m_{M\text{-}12}$	$m_{m\text{-}CTA}$	$m_{V\text{-}501}$	t
	M-12 : m-CTA : V-501	**[g]**	**[g]**	**[g]**	**[h]**
poly(M-10)$_{75}$-*block*-(M-12)$_{190}$	600 : 1 : 0.2	1.69	0.5	0.0012	96
poly(M-10)$_{295}$-*block*-(M-12)$_{190}$	600 : 1 : 0.2	0.44	0.5	0.0003	96
poly(M-10)$_{480}$-*block*-(M-12)$_{190}$	600 : 1 : 0.2	0.27	0.5	0.0002	96
poly(M-10)$_{585}$-*block*-(M-12)$_{190}$	600 : 1 : 0.2	0.44	1.0	0.0003	96

RAFT polymerization of M-12 using m-CTA poly(M-11)

Exemplarily, **poly(M-11)$_{100}$** (0.300 g, $9.6\cdot10^{-6}$ mol), **M-12** (0.730 g, $6.0\cdot10^{-3}$ mol), and V-501 (0.0005 g, $2.0\cdot10^{-6}$ mol) were dissolved in TFE (10 ml) and purged with N_2. The yellow reaction mixture was polymerized at 75 °C for 96 h yielding **poly(M-11)$_{100}$-*block*-(M-12)$_{205}$** (yield 0.500 g, 50 %).

^{1}H NMR (400 MHz, in dilute aqueous NaCl (9.0 $g\cdot L^{-1}$) in D_2O, 298 K): δ (ppm) = 0.5 – 2.5 (broad 22H, $-CH_3$ and $-CH_2-$ on/in backbone of **M-11** and **M-12**, $-N\text{-}C\text{-}(CH_3)_2$, $-CH_2\text{-}CH_2\text{-}C\text{-}SO_3^-$, $-COO\text{-}C\text{-}CH_2-$), 2.9 – 3.1 (2H, $-CH_2\text{-}SO_3^-$), 3.1 – 3.3 (6H, $-N^+\text{-}(CH_3)_2$), 3.3 – 3.6 (4H, $-CH_2\text{-}N^+\text{-}CH_2-$), 3.8 – 4.2 (3H, -N-CH-, $-COO\text{-}CH_2-$).

FT-IR (selected bands, cm^{-1}): 3457 ν(NH), 3103 $\nu(N^{+}\text{-}CH_3)$, 2976 $\nu(CH_2)$, 1721 ν(C=O), 1637 ν(amide I), 1518 ν(amide II), 1171 $\nu_{as}(SO_3^{-})$, 1037 $\nu_{s}(SO_3^{-})$.

UV-vis absorbance maxima: in trifluoroethanol (λ_{max} = 260, 293, and 445 nm), and in water (λ_{max} = 257, 287, and 442 nm).

Fluorescence emission maxima: in trifluoroethanol (λ_{PL} = 538 nm), and in water (λ_{PL} = 545 nm).

Table 7.25. Reaction conditions for the RAFT polymerization of **M-12** in TFE at 75 °C, using **m-CTA poly(M-11)** and initiator V-501. Monomer and **m-CTA** concentration was 30 wt%.

sample	**molar ratio**	$\mathbf{m_{M\text{-}12}}$	$\mathbf{m_{m\text{-}CTA}}$	$\mathbf{m_{V\text{-}501}}$	**t**
	M-12 : m-CTA : V-501	**[g]**	**[g]**	**[g]**	**[h]**
poly(M-11)$_{100}$-*block*-(M-12)$_{205}$	600 : 1 : 0.2	0.73	0.3	0.0005	96
poly(M-11)$_{290}$-*block*-(M-12)$_{205}$	600 : 1 : 0.2	0.84	1.0	0.0006	96
poly(M-11)$_{480}$-*block*-(M-12)$_{205}$	600 : 1 : 0.2	0.26	0.5	0.0002	96
poly(M-11)$_{540}$-*block*-(M-12)$_{205}$	600 : 1 : 0.2	0.23	0.5	0.0002	96

7.6.2 RAFT polymerization with poly(M-12)$_{195}$ as macro-RAFT agent (route B)

RAFT polymerization of different sulfobetaines using m-CTA poly(M-12)$_{195}$

Exemplarily, **poly(M-12)$_{195}$** (0.720 g, 2.9·10^{-5} mol), **M-1** (5.000 g, 1.7·10^{-2} mol), and V-501 (0.0016 g, 5.8·10^{-6} mol) were dissolved in TFE (10 ml) and purged with N_2. The yellow reaction mixture was polymerized at 75 °C for 15 h yielding **poly(M-12)$_{195}$-*block*-(M-1)$_{385}$** (yield 3.000 g, 53 %).

^{1}H NMR (400 MHz, in dilute aqueous NaCl (9.0 g·L^{-1}) in D_2O, 298 K): δ (ppm) = 0.5 – 2.5 (broad 20H, -CH_3 and -CH_2- on/in backbone of **M-12** and **M-1**, -N-C-$(CH_3)_2$, -CH_2-C-N^+-C-CH_2-), 2.9 – 3.1 (2H, -CH_2-SO_3^-), 3.1 – 3.3 (6H, -N^+-$(CH_3)_2$), 3.3 – 3.6 (6H, -CH_2-N^+-CH_2, -CON-CH_2-), 3.8 – 4.0 (1H, -N-CH-).

FT-IR (selected bands, cm^{-1}): 3419 ν(NH), 3041 ν(N^+-CH_3), 2969 ν(CH_2), 1635 ν(amide I), 1539 ν(amide II), 1174 $\nu_{as}(SO_3^-)$, 1035 $\nu_s(SO_3^-)$.

UV-vis absorbance maxima: in trifluoroethanol (λ_{max} = 270, 298, and 442 nm), and in water (λ_{max} = 258, 293, and 440 nm).

Fluorescence emission maxima: in trifluoroethanol (λ_{PL} = 537 nm), and in water (λ_{PL} = 540 nm).

Results of RAFT polymerization of **M-3** using **poly(M-12)$_{195}$** (yield 0.8 g, 73 % and 1 g, 91 %):

^{1}H NMR (300 MHz, in dilute aqueous NaCl (9.0 g·L^{-1}) in D_2O, 298 K): δ (ppm) = 0.5 – 2.5 (broad 22H, -CH_3 and -CH_2- on/in backbone of **M-3** and **M-12**, -N-C-$(CH_3)_2$, -CH_2-C-N^+-CH_2-CH_2-), 2.9 – 3.5 (14H, -CH_2-SO_3^-, -N^+-$(CH_3)_2$), -CH_2-N^+-CH_2, -CON-CH_2-), 3.8 – 4.0 (1H, -N-CH-).

FT-IR (selected bands, cm^{-1}): 3388 ν(NH), 2970 ν(N^+-CH_3), 2939 ν(CH_2), 1632 ν(amide I), 1522 ν(amide II), 1198 $\nu_{as}(SO_3^-)$, 1038 $\nu_s(SO_3^-)$.

UV-vis absorbance maxima: in trifluoroethanol (λ_{max} = 263, 293, and 441 nm), and in water (λ_{max} = 284 and 440 nm).

Fluorescence emission maxima: in trifluoroethanol (λ_{PL} = 538 nm), and in water (λ_{PL} = 539 nm).

Results of polymerization of **M-4** using **poly(M-12)$_{195}$** (yield 3.700 g, 65 %):

^{1}H NMR (400 MHz, in dilute aqueous NaCl (9.0 g·L^{-1}) in D_2O, 298 K): δ (ppm) = 0.5 – 2.5 (broad 18H, -CH_3 and -CH_2- on/in backbone of **M-4** and **M-12**, -N-C-$(CH_3)_2$, -CH_2-C-SO_3^-), 2.9 – 3.1 (2H, -CH_2-SO_3^-), 3.1 – 3.4 (6H, -N^+-$(CH_3)_2$), 3.5 – 4.1 (5H, -CH_2-N^+-CH_2-, N-CH-), 4.3 – 4.7 (2H, -COO-CH_2-).

FT-IR (selected bands, cm^{-1}): 3440 ν(NH), 3002 ν(N^+-CH_3), 2976 ν(CH_2), 1723 ν(C=O), 1650 ν(amide I), 1531 ν(amide II), 1172 $\nu_{as}(SO_3^-)$, 1035 $\nu_s(SO_3^-)$.

UV-vis absorbance maxima: in trifluoroethanol (λ_{max} = 302 and 444 nm), and in water (λ_{max} = 298 and 445 nm).

Fluorescence emission maxima: in trifluoroethanol (λ_{PL} = 539 nm), and in water (λ_{PL} = 545 nm).

Table 7.26. Reaction conditions for the RAFT polymerization of different sulfobetaine monomers in TFE at 75 °C, using **m-CTA poly(M-12)$_{195}$** and initiator V-501. Monomer and **m-CTA** concentration was 30 wt%.

sample	molar ratio	m_{Mon}	$m_{m\text{-}CTA}$	$m_{V\text{-}501}$	t
	Mon : m-CTA : V-501	[g]	[g]	[g]	[h]
poly(M-12)$_{195}$-*block*-(M-1)$_{385}$	600 : 1 : 0.2	5.0	0.72	0.0016	15
poly(M-12)$_{195}$-*block*-(M-3)$_{15}$	100 : 1 : 0.2	0.6	0.50	0.0011	19
poly(M-12)$_{195}$-*block*-(M-3)$_{30}$	100 : 1 : 0.2	0.6	0.50	0.0011	96
poly(M-12)$_{195}$-*block*-(M-4)$_{530}$	600 : 1 : 0.2	5.0	0.74	0.0017	15

Selbstständigkeitserklärung

Hiermit erkläre ich, dass ich die vorliegende Arbeit selbstständig und mit der angegebenen Literatur, sowie Hilfsmittel angefertigt habe. Diese Arbeit wurde an keiner anderen Hochschule eingereicht.

Potsdam, Viet Hildebrand, geb. Hoang

SELBSTSTÄNDIGKEITSERKLÄRUNG

Appendix

NMR spectra

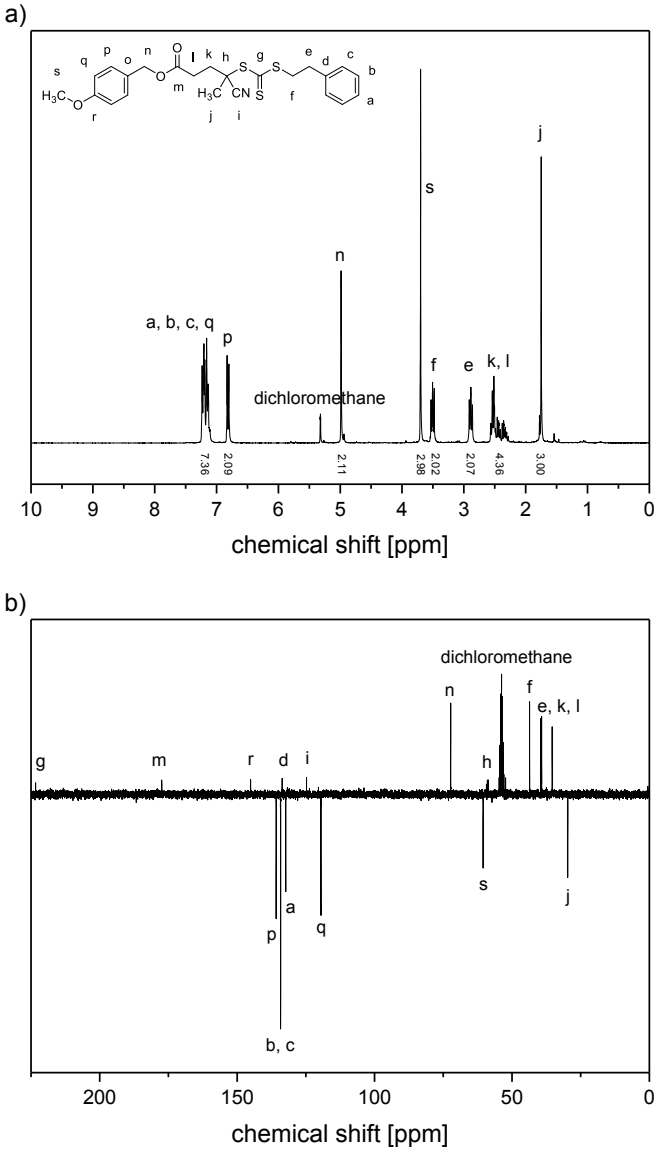

Figure A.1. a) ^{1}H and b) ^{13}C (APT) NMR spectra of **CTA-2** in CD_2Cl_2.

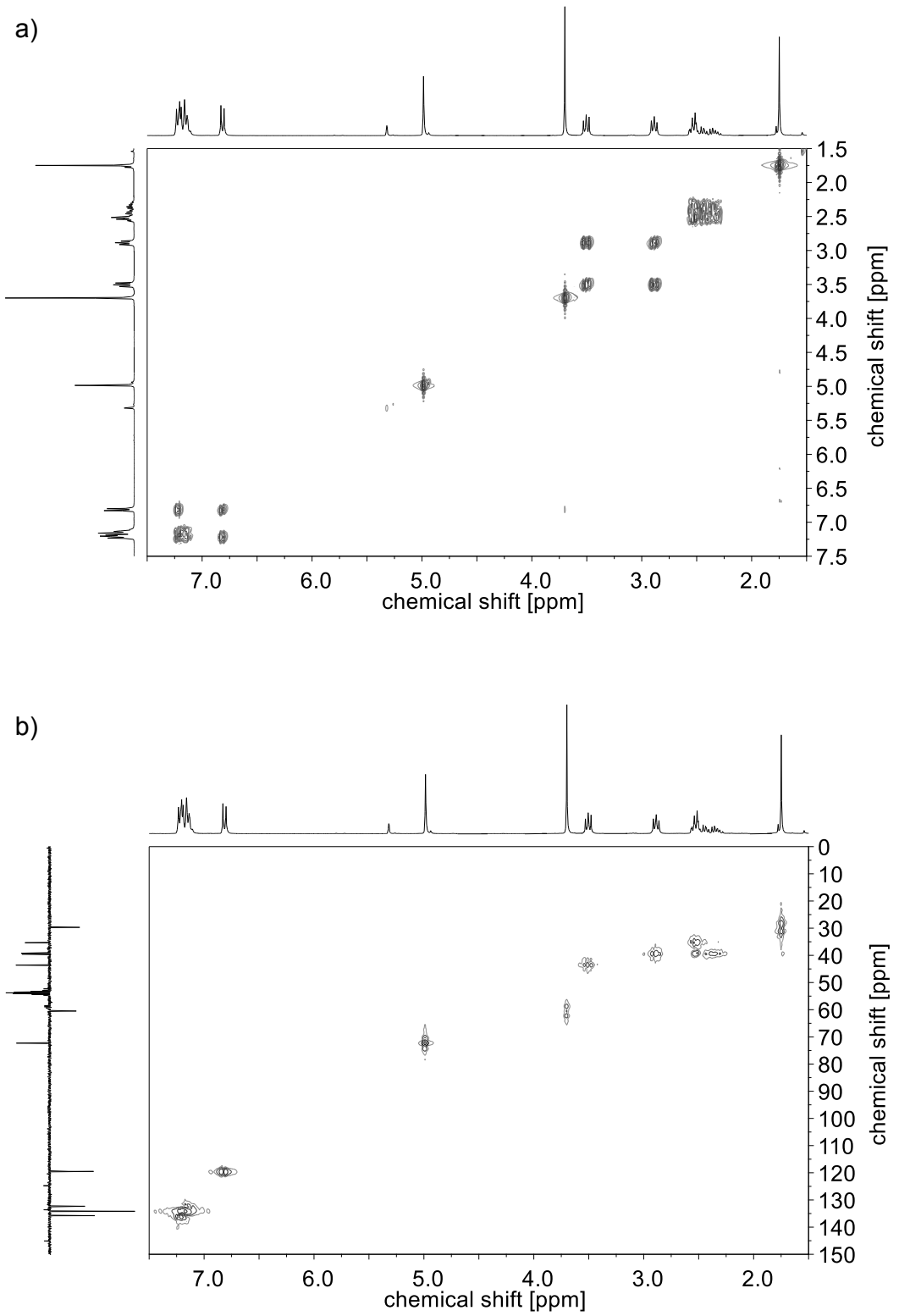

Figure A.2. a) ^{1}H-^{1}H-COSY and b) ^{1}H-^{13}C-HMQC NMR spectra of **CTA-2** in CD_2Cl_2.

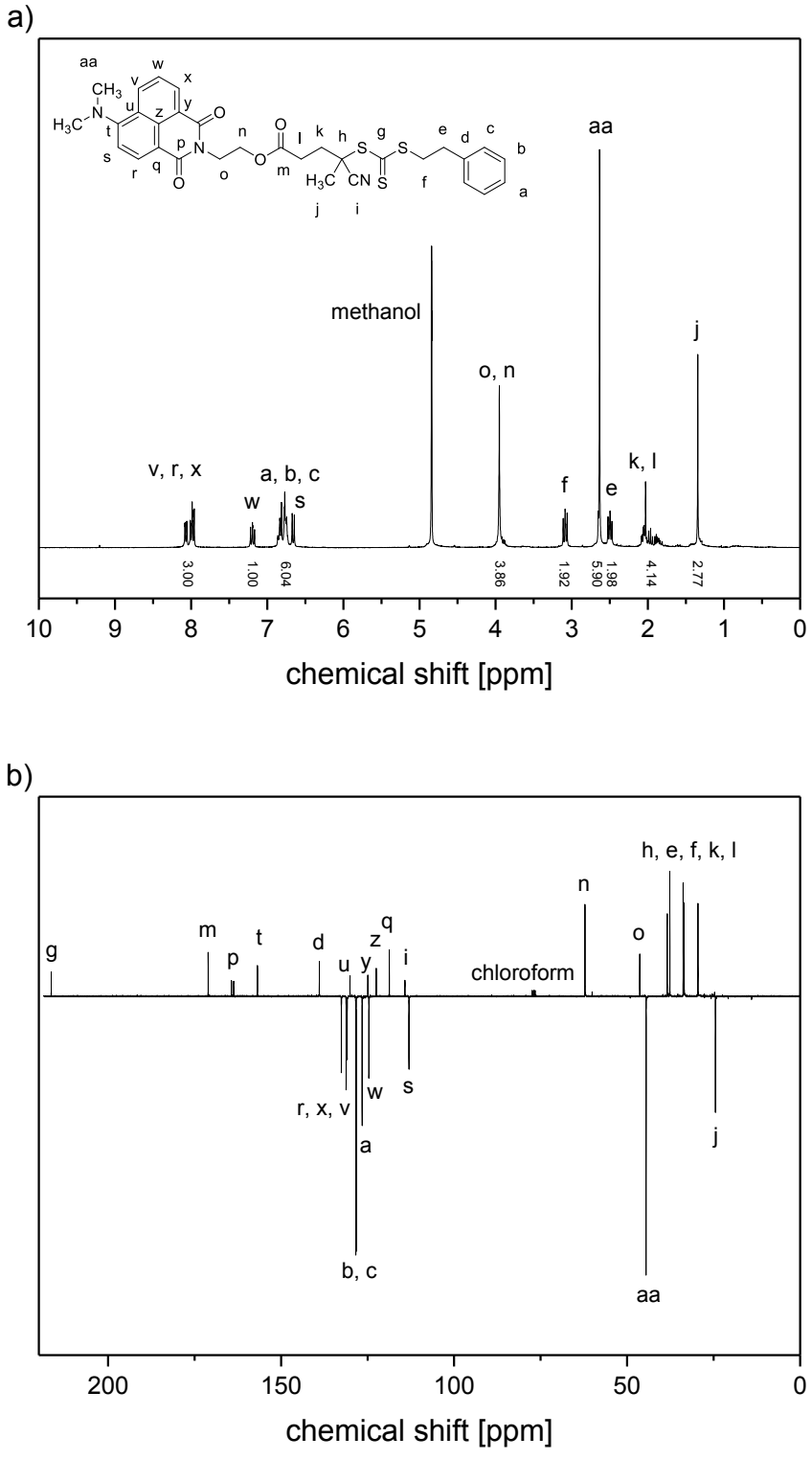

Figure A.3. a) ^{1}H (in CD_3OD) and b) ^{13}C (APT, in $CDCl_3$) NMR spectra of **CTA-3**.

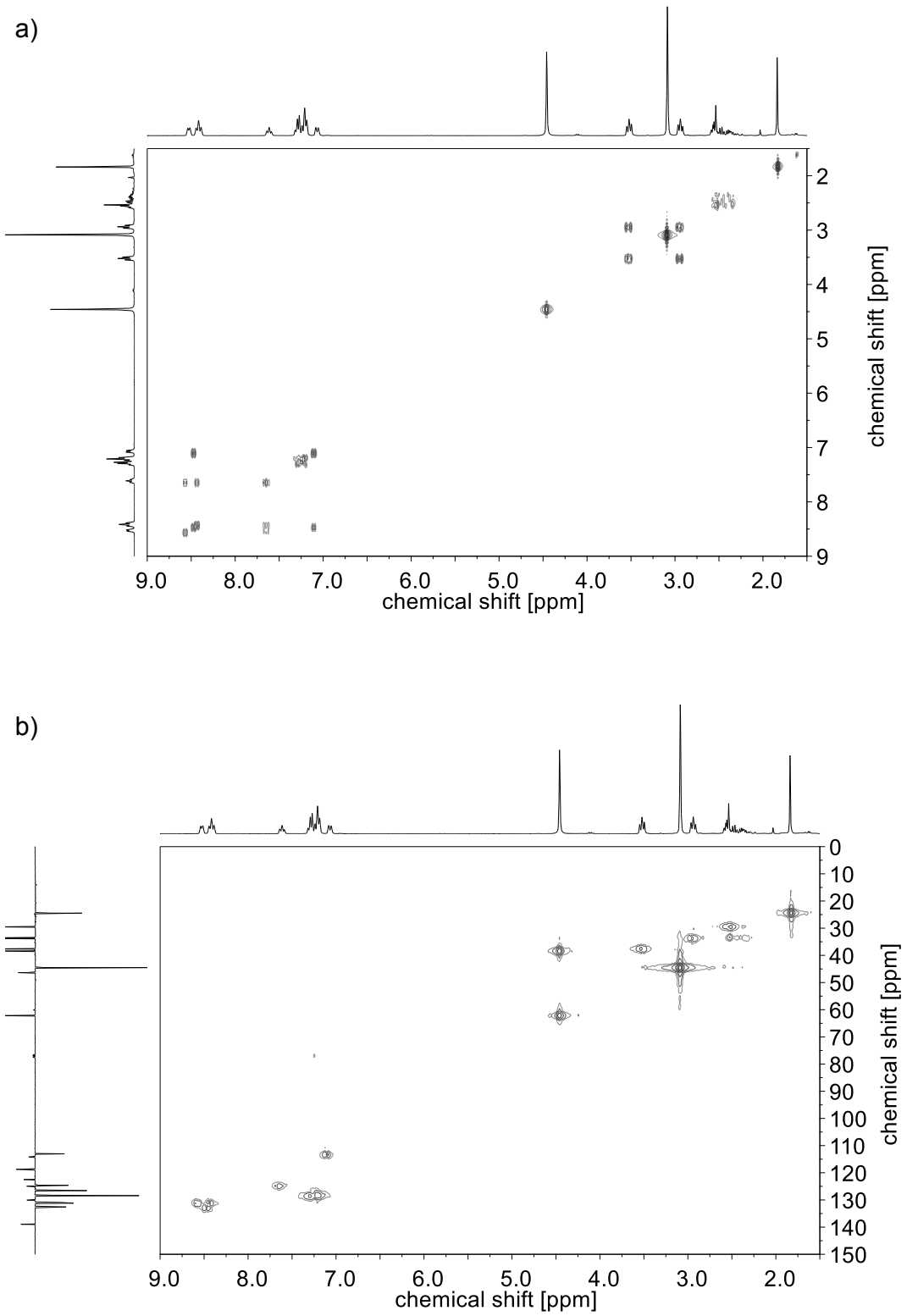

Figure A.4. a) ^{1}H-^{1}H-COSY and b) ^{1}H-^{13}C-HMQC NMR spectra of **CTA-3** (in $CDCl_3$).

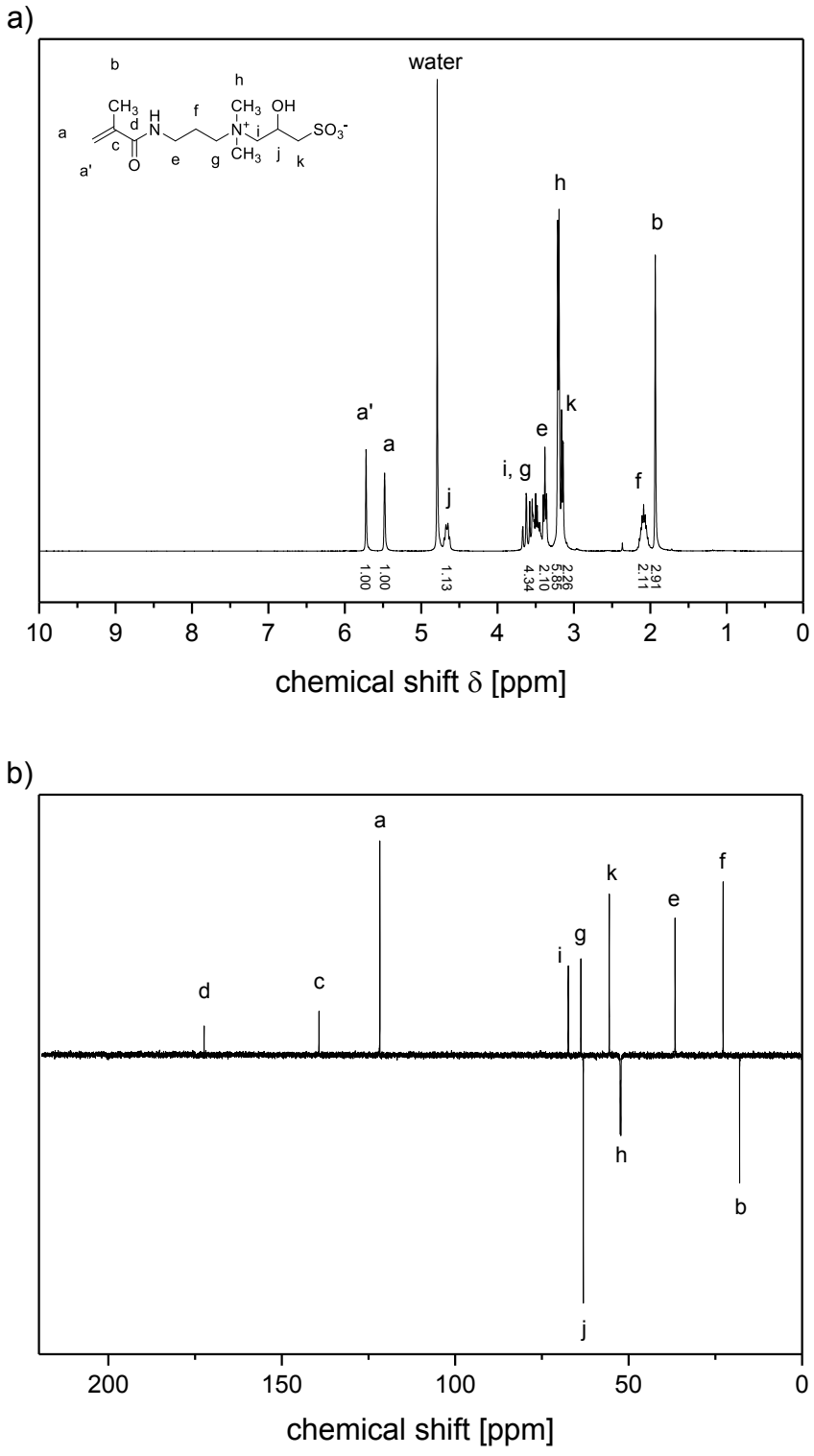

Figure A.5. a) ^{1}H and b) ^{13}C (APT) NMR spectra of **M-2** in D_2O.

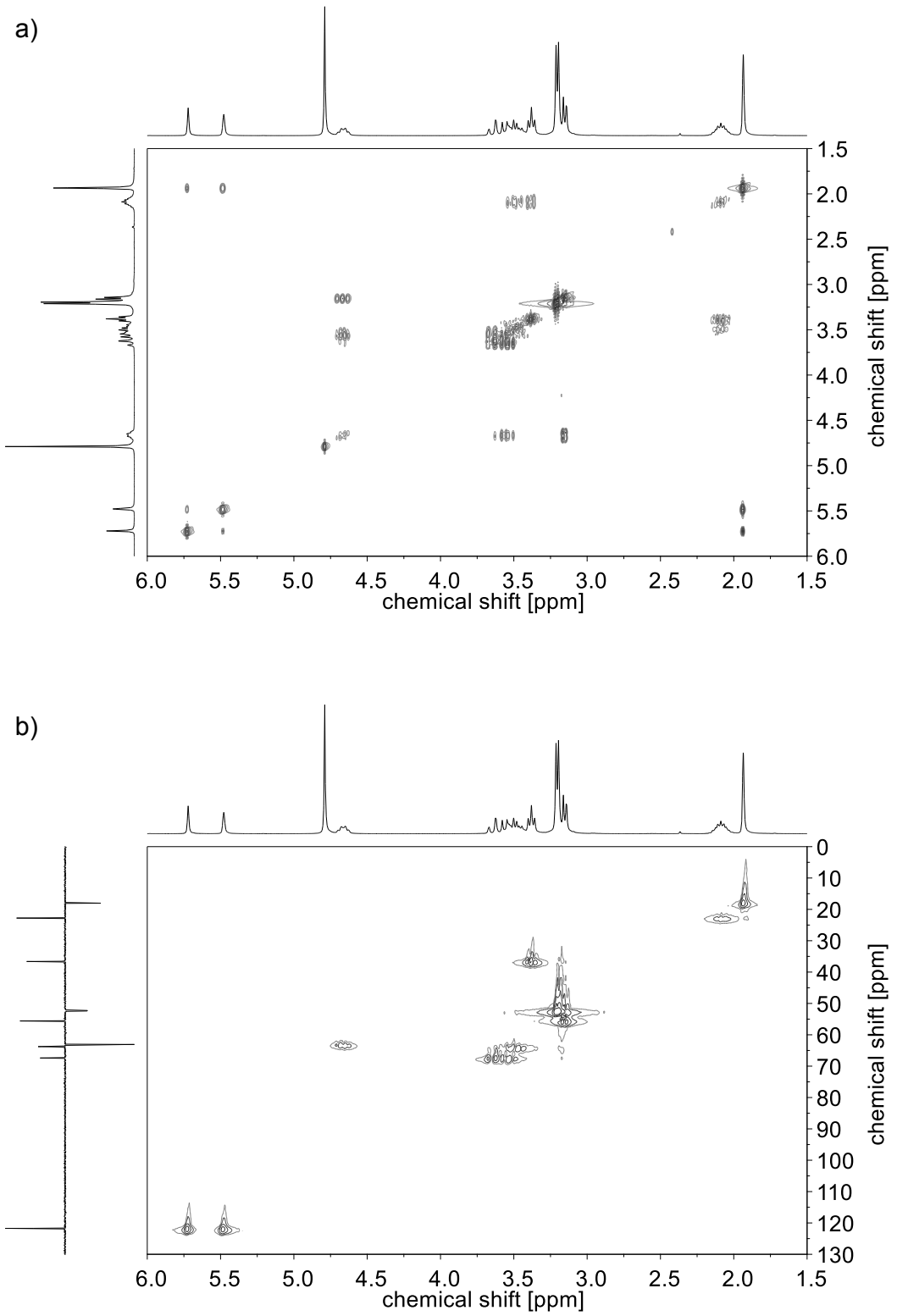

Figure A.6. a) ^{1}H-^{1}H-COSY and b) ^{1}H-^{13}C-HMQC NMR spectra of **M-2** in D_2O.

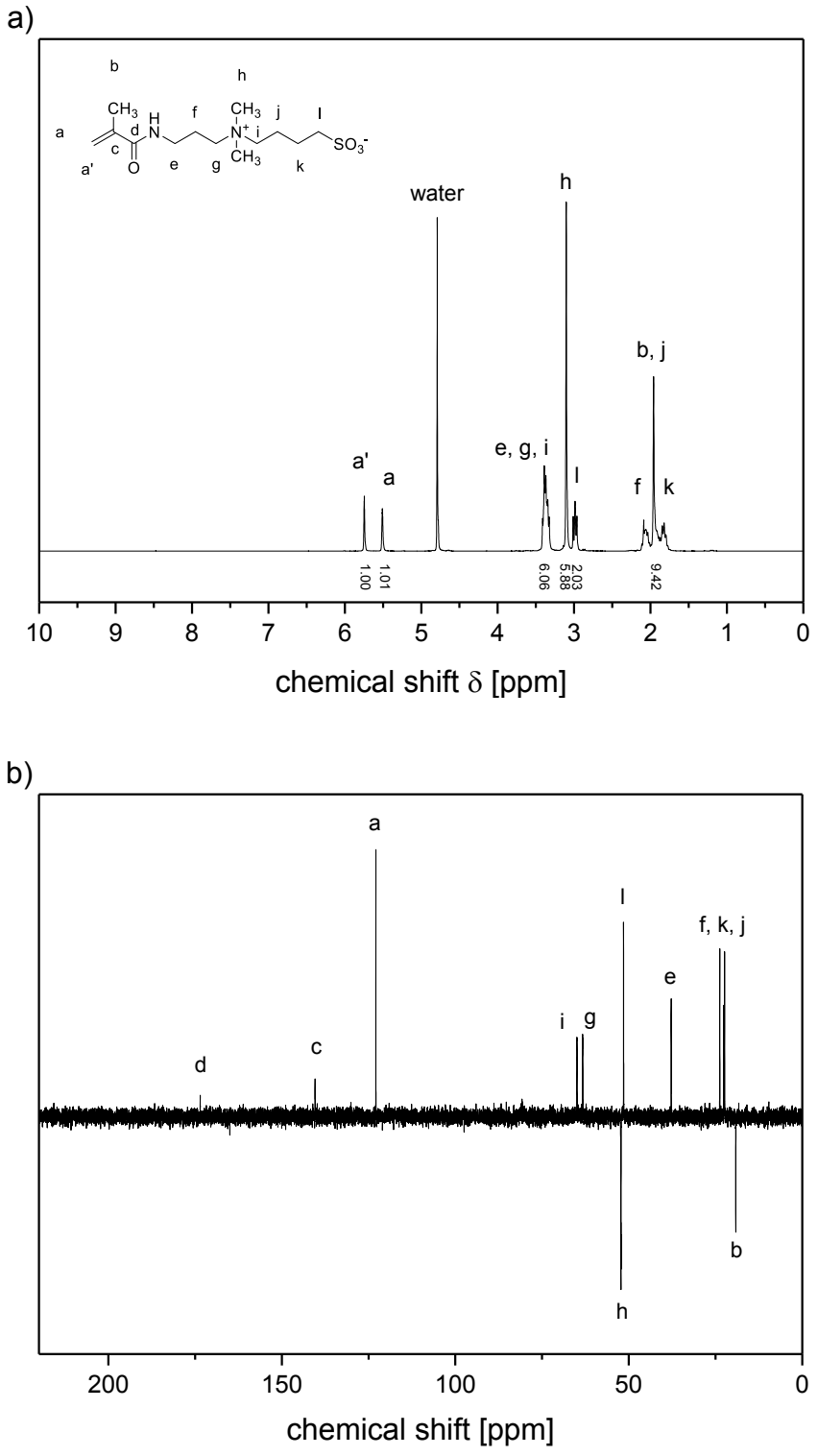

Figure A.7. a) ^{1}H and b) ^{13}C (APT) NMR spectra of **M-3** in D_2O.

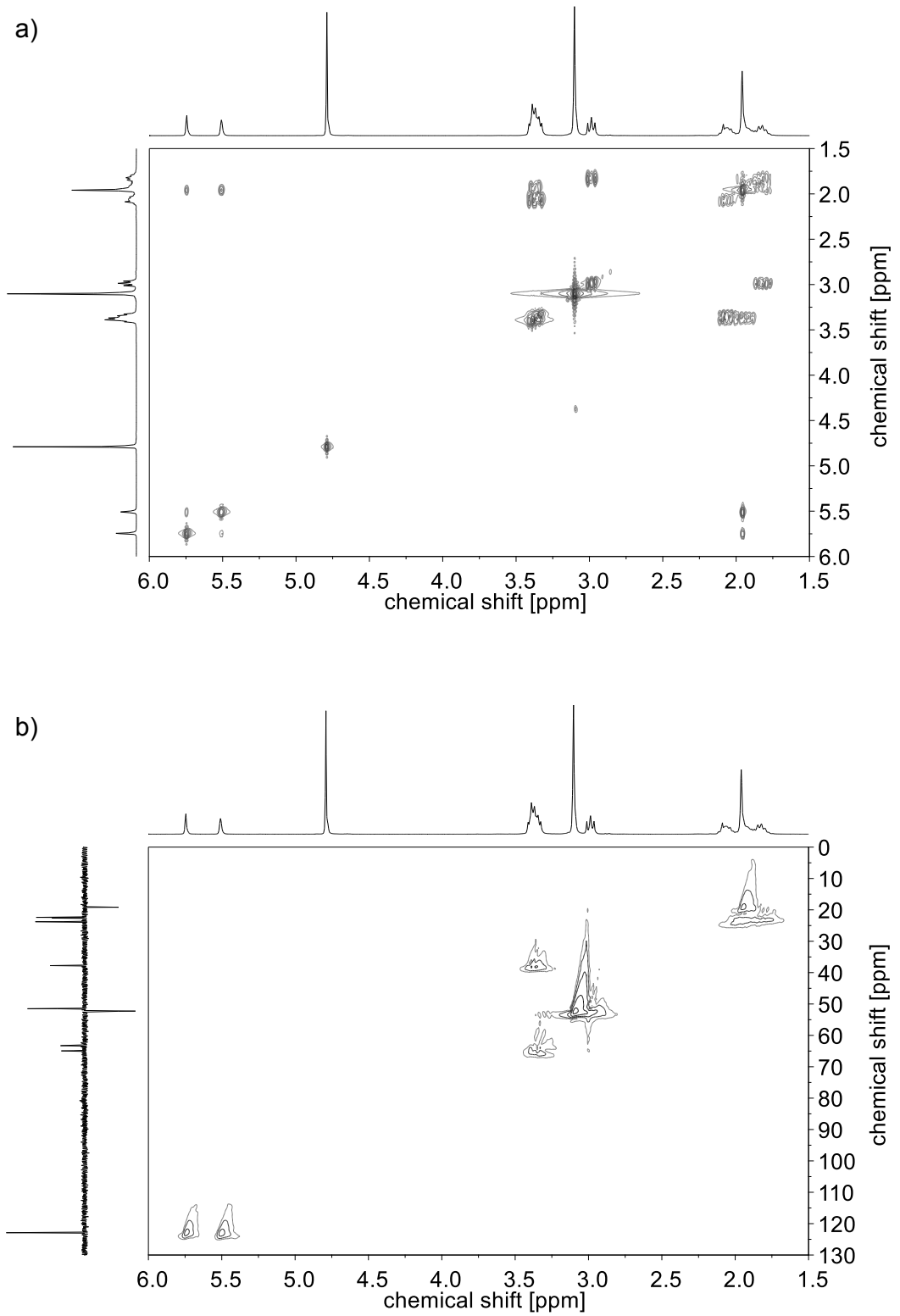

Figure A.8. a) ^{1}H-^{1}H-COSY and b) ^{1}H-^{13}C-HMQC NMR spectra of **M-3** in D_2O.

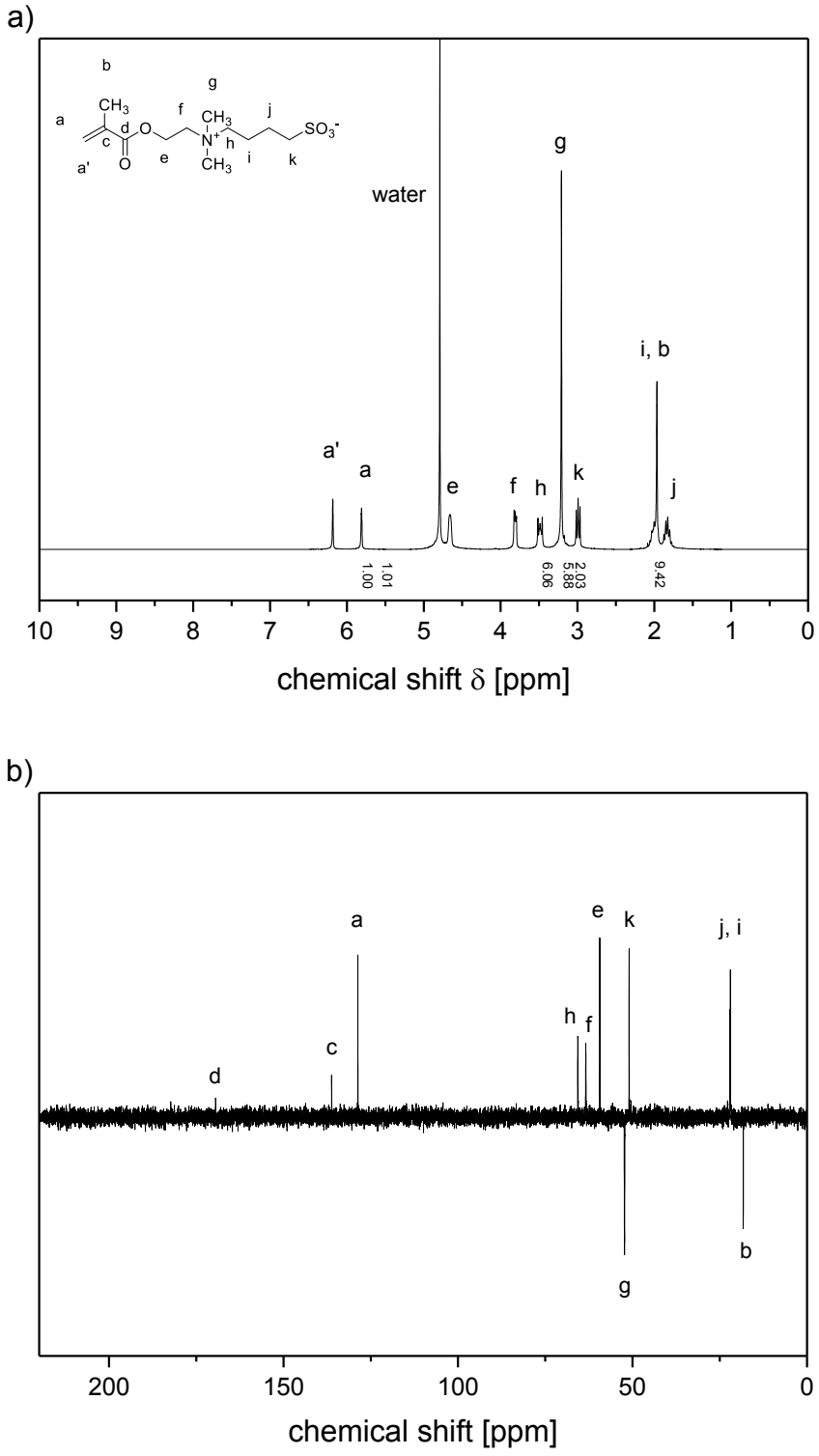

Figure A.9. a) ^{1}H and b) ^{13}C (APT) NMR spectra of **M-5** in D_2O.

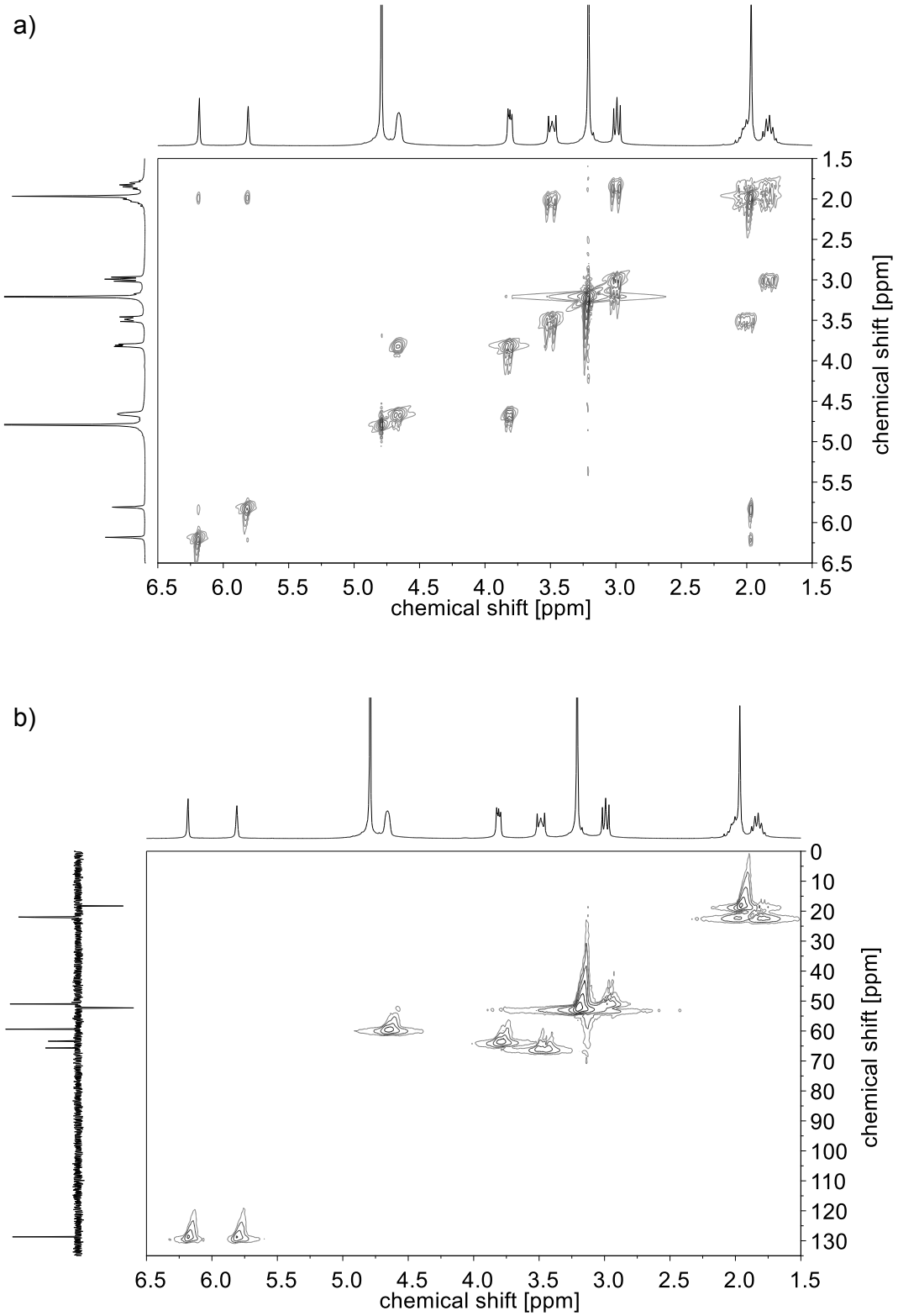

Figure A.10. a) ^{1}H-^{1}H-COSY and b) ^{1}H-^{13}C-HMQC NMR spectra of **M-5** in D_2O.

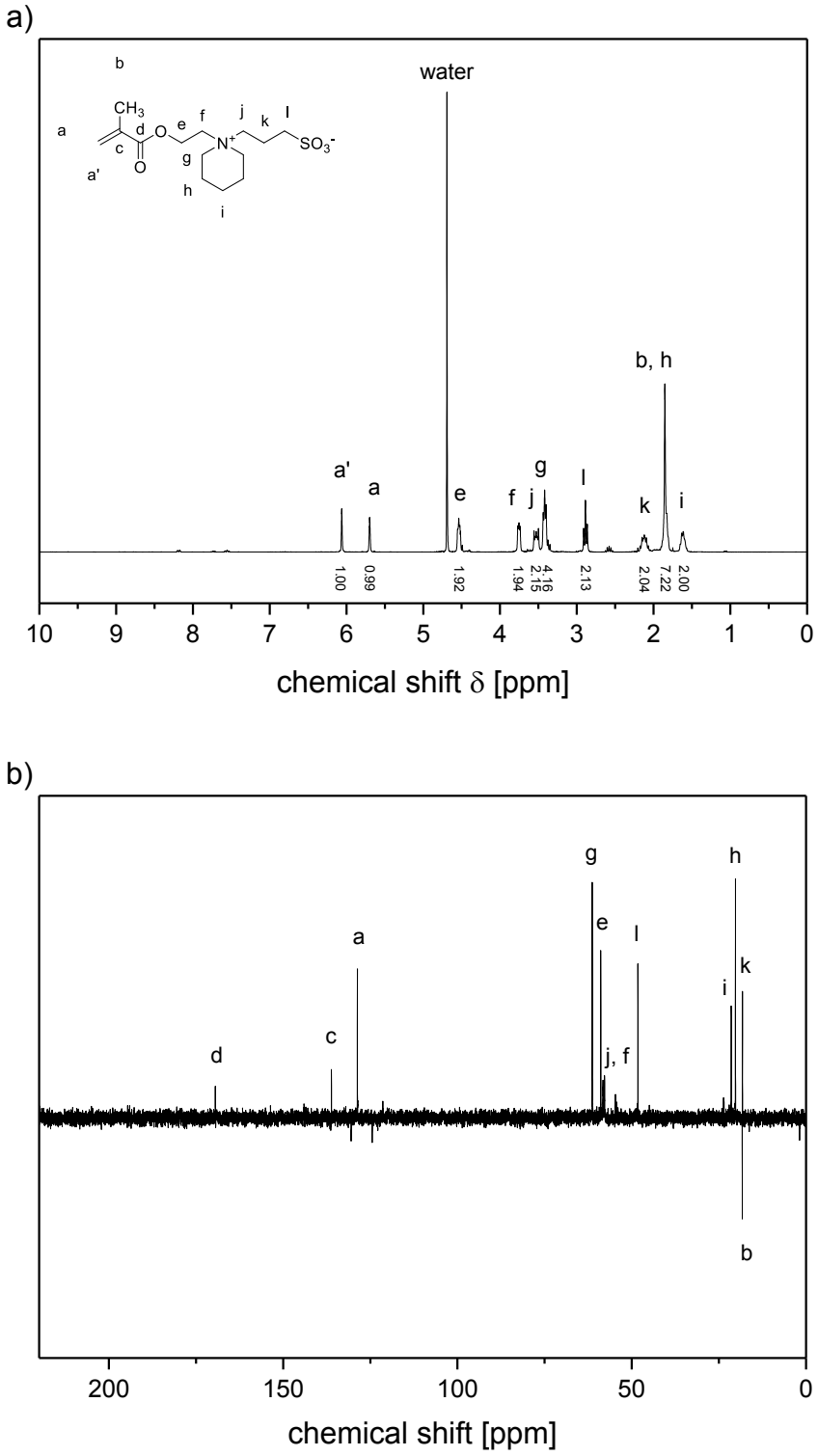

Figure A.11. a) ^{1}H and b) ^{13}C (APT) NMR spectra of **M-6** in D_2O.

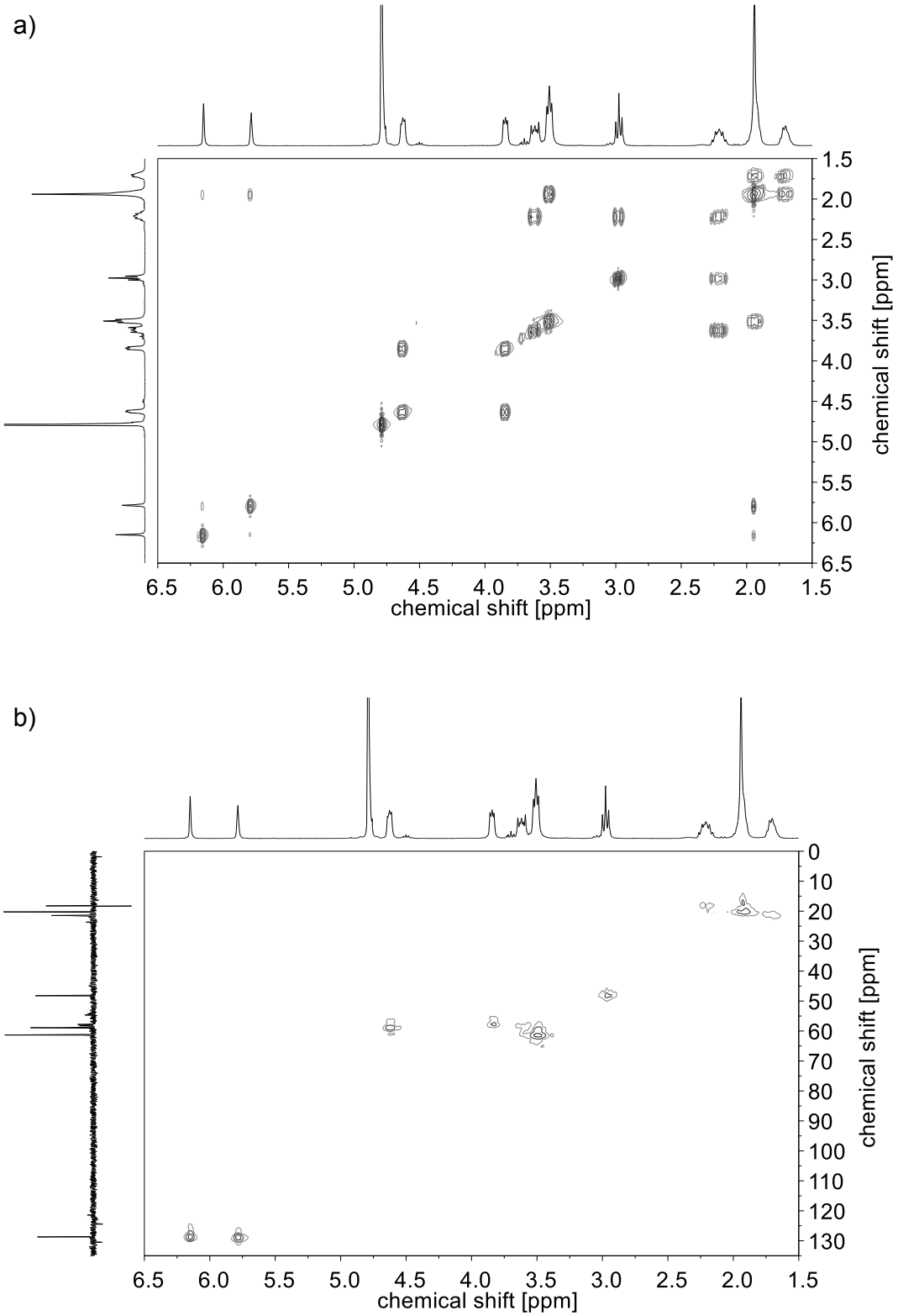

Figure A.12. a) ^{1}H-^{1}H-COSY and b) ^{1}H-^{13}C-HMQC NMR spectra of **M-6** in D_2O.

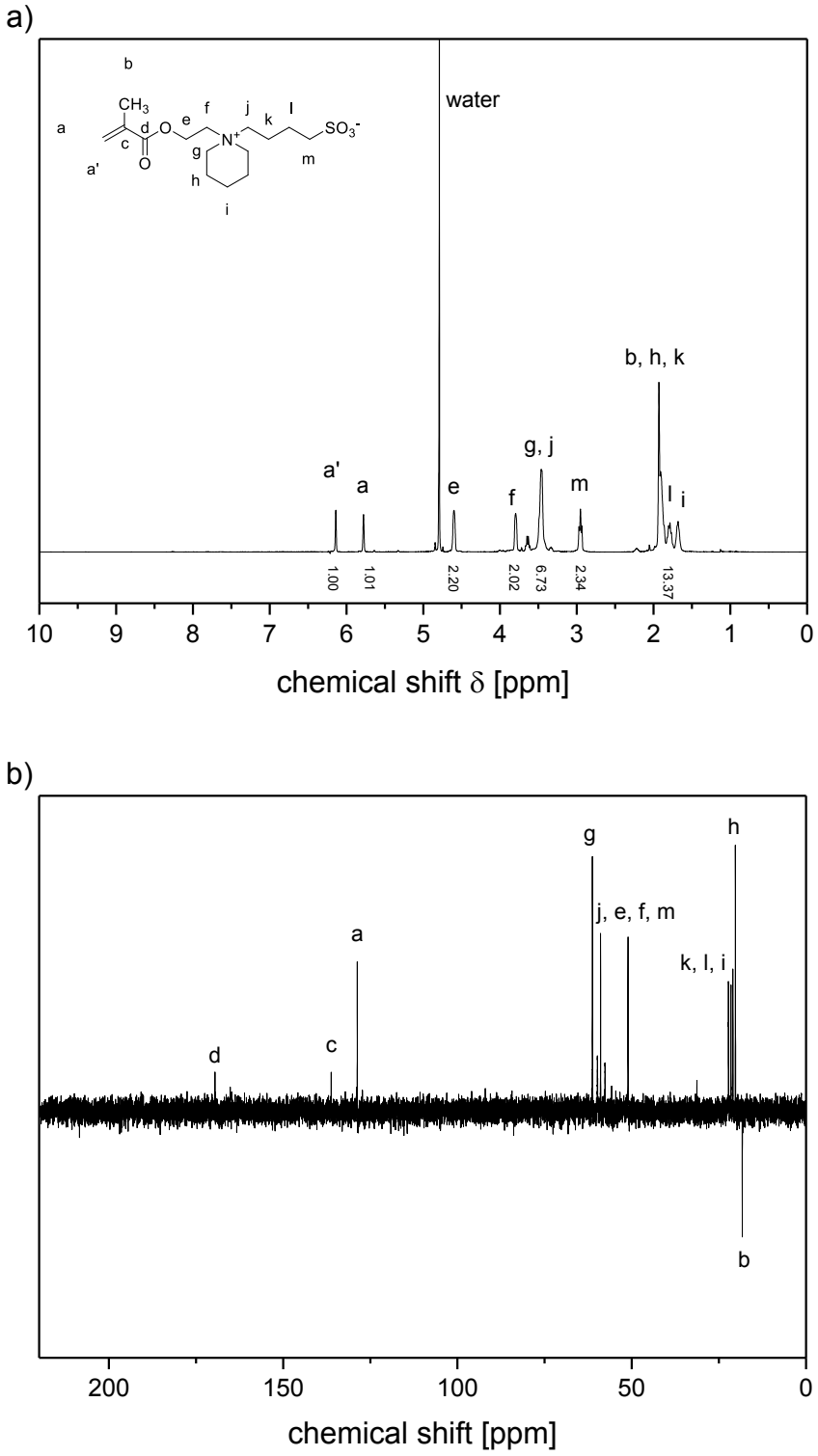

Figure A.13. a) ^{1}H and b) ^{13}C (APT) NMR spectra of **M-7** in D_2O.

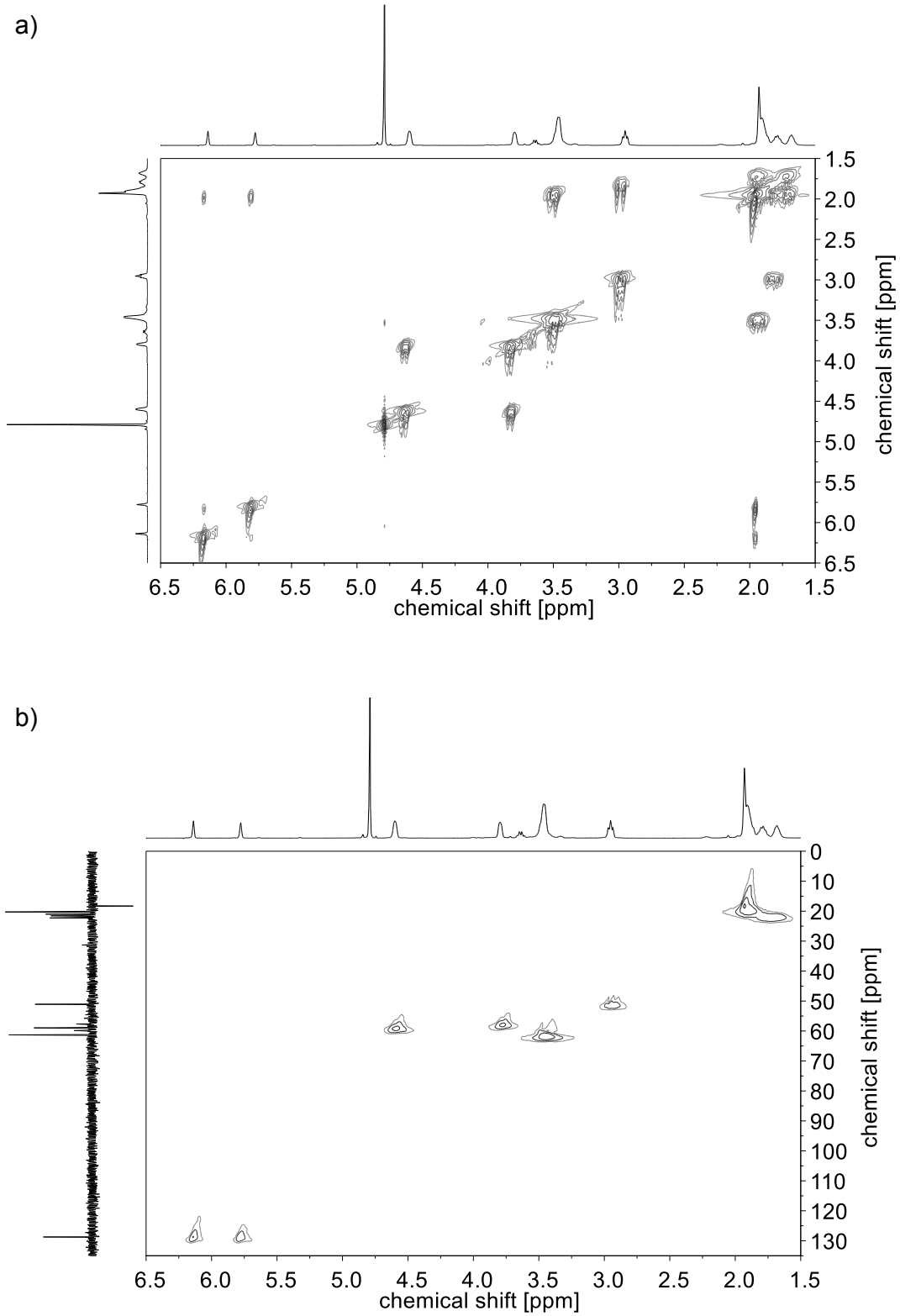

Figure A.14. a) ^{1}H-^{1}H-COSY and b) ^{1}H-^{13}C-HMQC NMR spectra of **M-7** in D_2O.

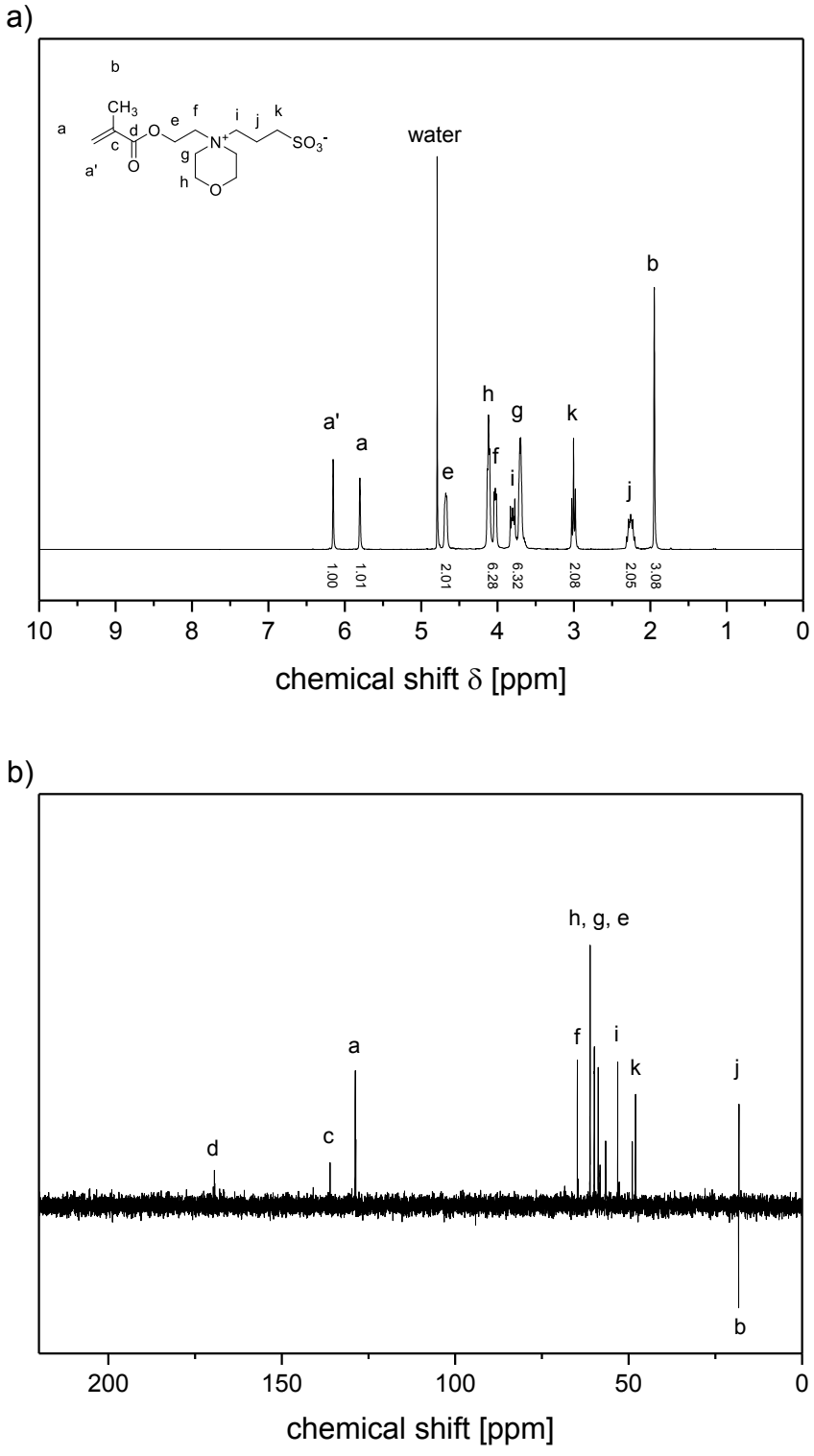

Figure A.15. a) ^{1}H and b) ^{13}C (APT) NMR spectra of **M-8** in D_2O.

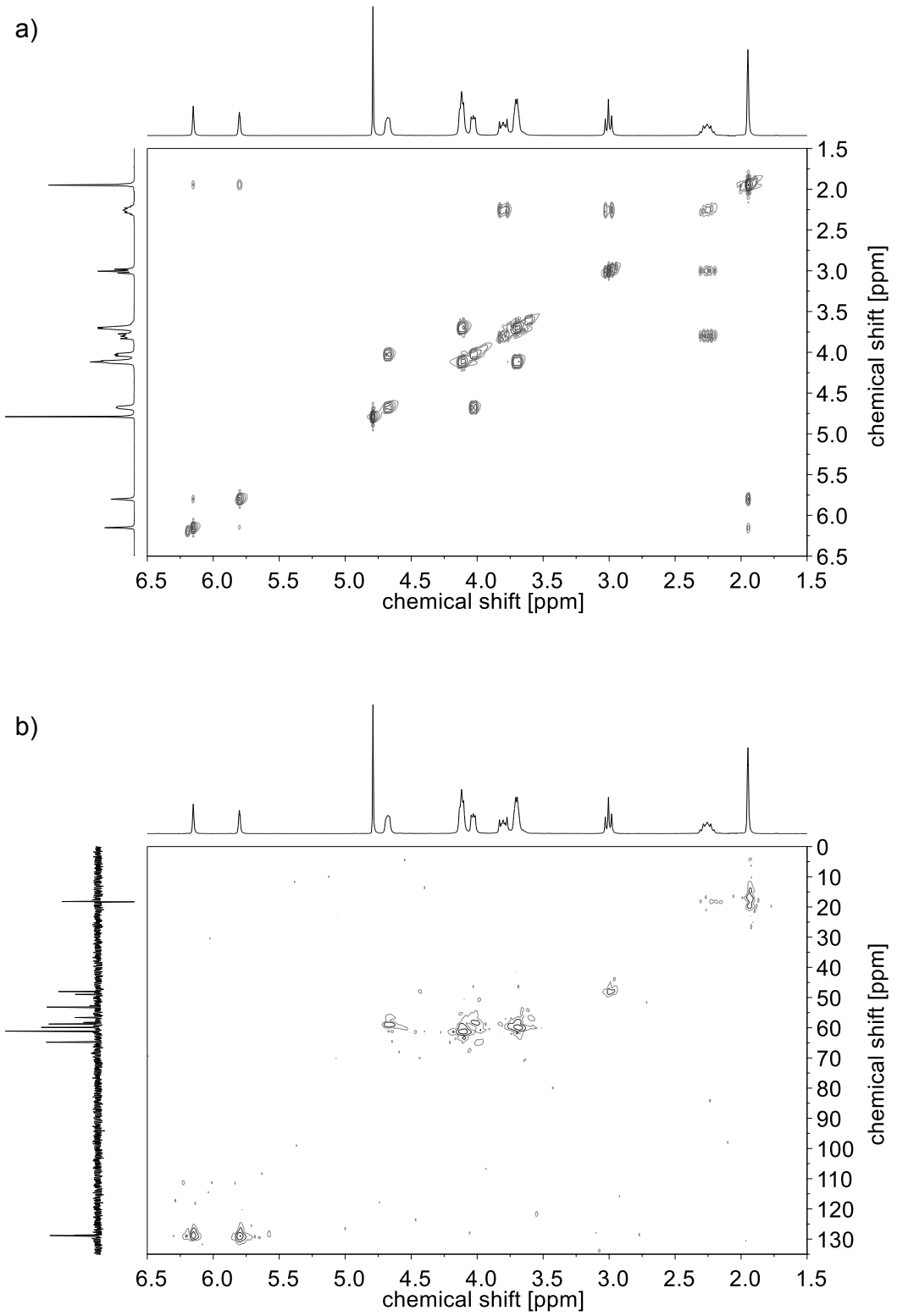

Figure A.16. a) ^{1}H-^{1}H-COSY and b) ^{1}H-^{13}C-HMQC NMR spectra of **M-8** in D_2O.

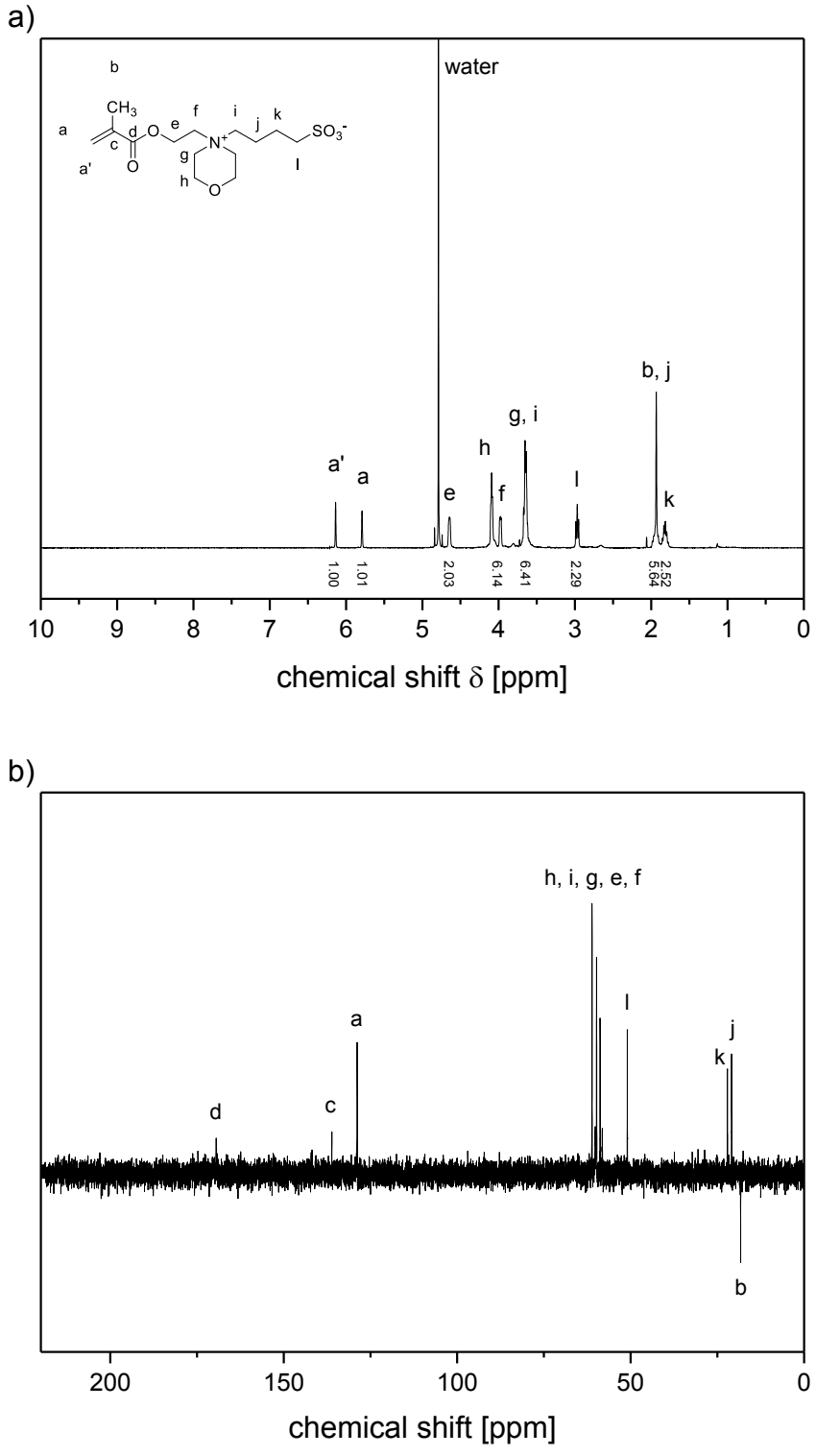

Figure A.17. a) ^{1}H and b) ^{13}C (APT) NMR spectra of **M-9** in D_2O.

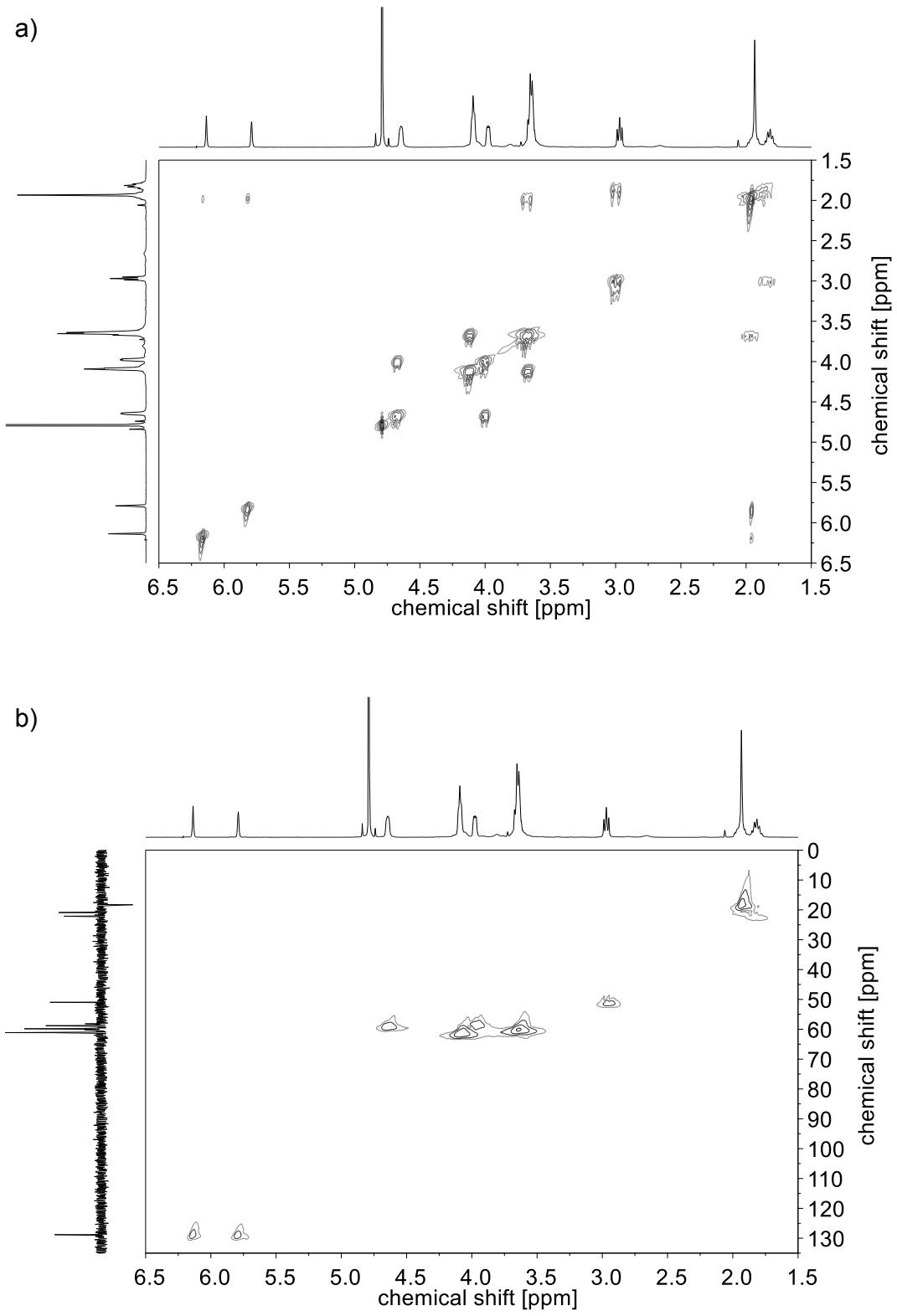

Figure A.18. a) ^{1}H-^{1}H-COSY and b) ^{1}H-^{13}C-HMQC NMR spectra of **M-9** in D_2O.

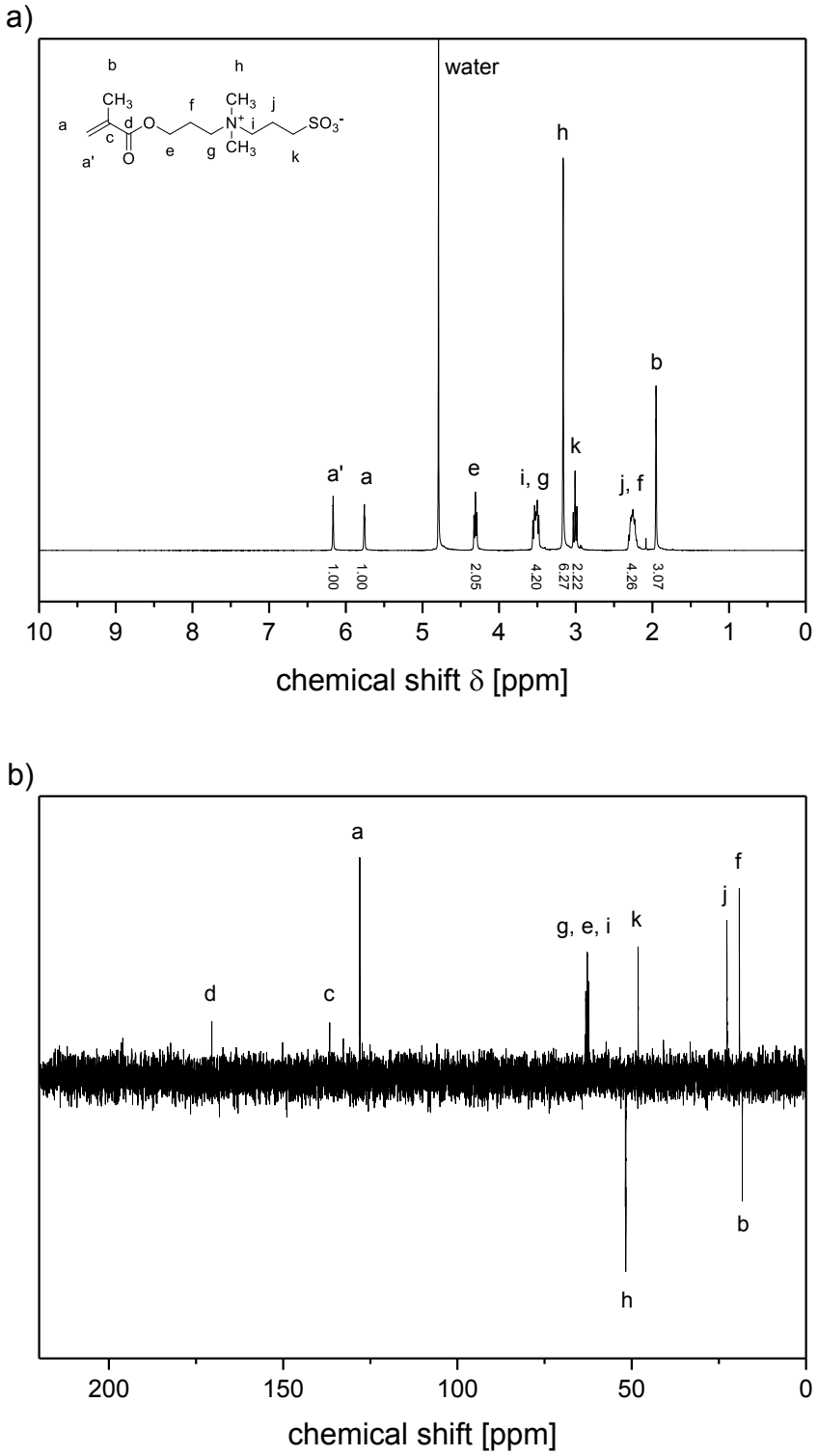

Figure A.19. a) ^{1}H and b) ^{13}C (APT) NMR spectra of **M-10** in D_2O.

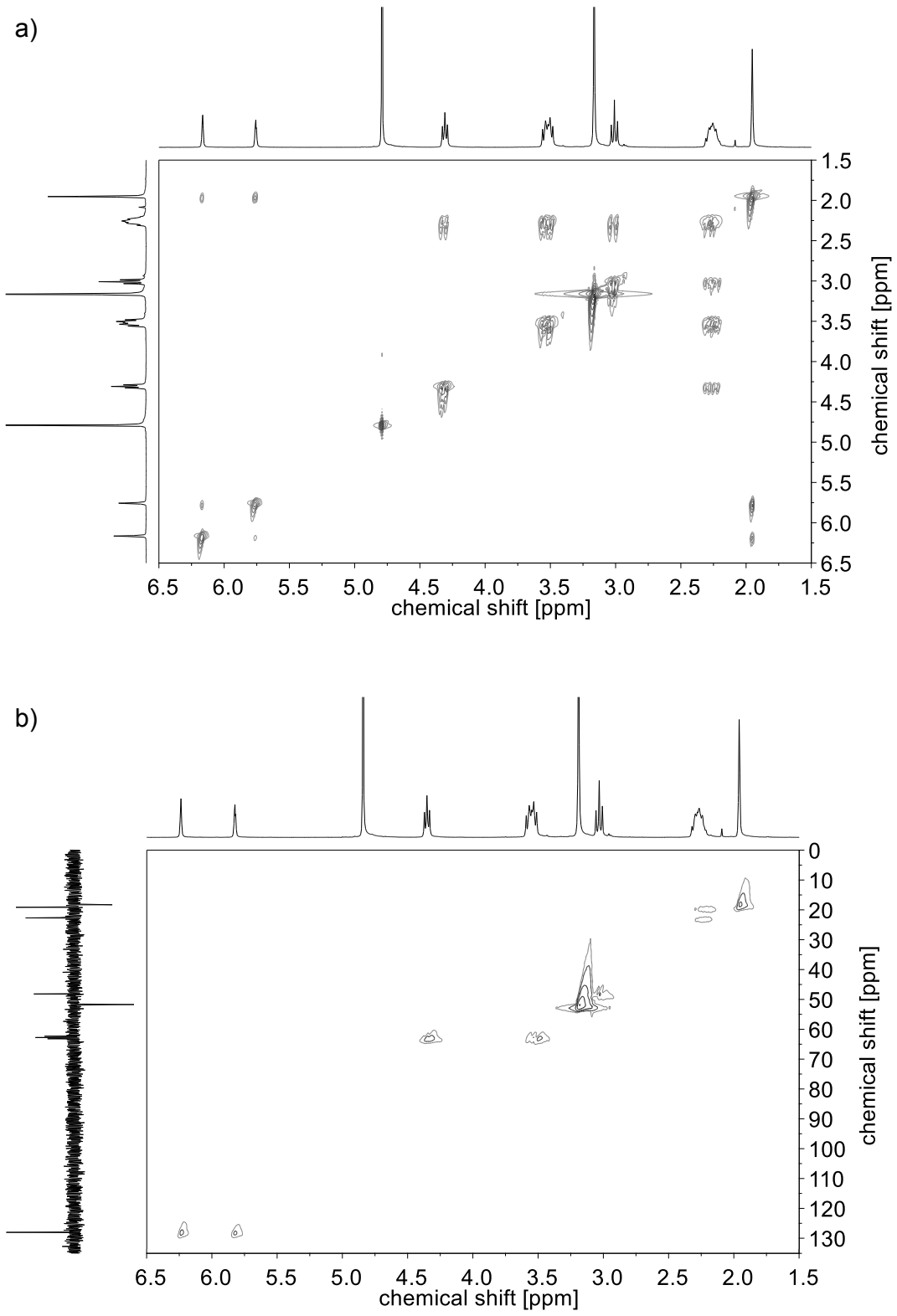

Figure A.20. a) ^{1}H-^{1}H-COSY and b) ^{1}H-^{13}C-HMQC NMR spectra of **M-10** in D_2O.

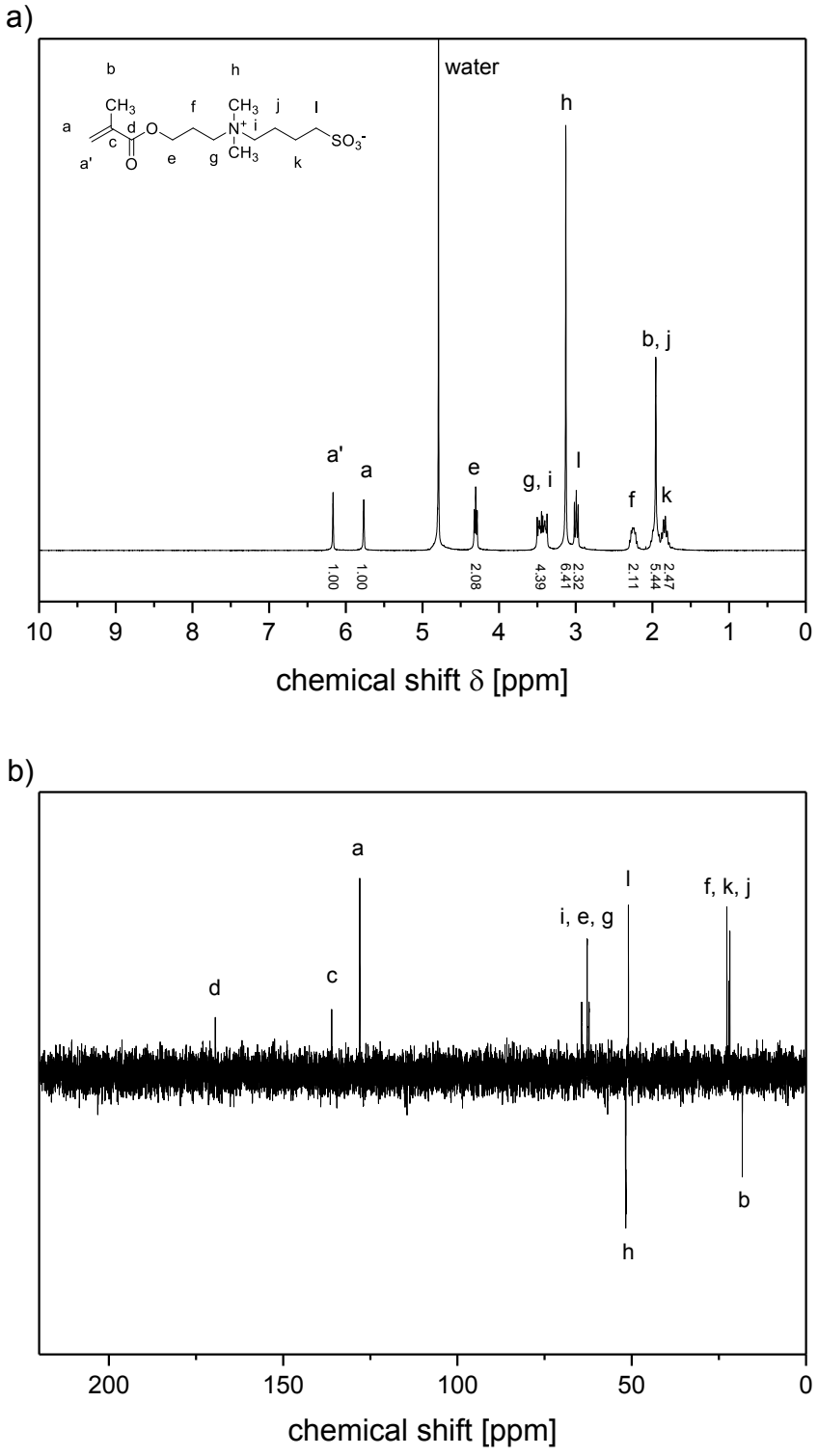

Figure A.21. a) ^{1}H and b) ^{13}C (APT) NMR spectra of **M-11** in D_2O.

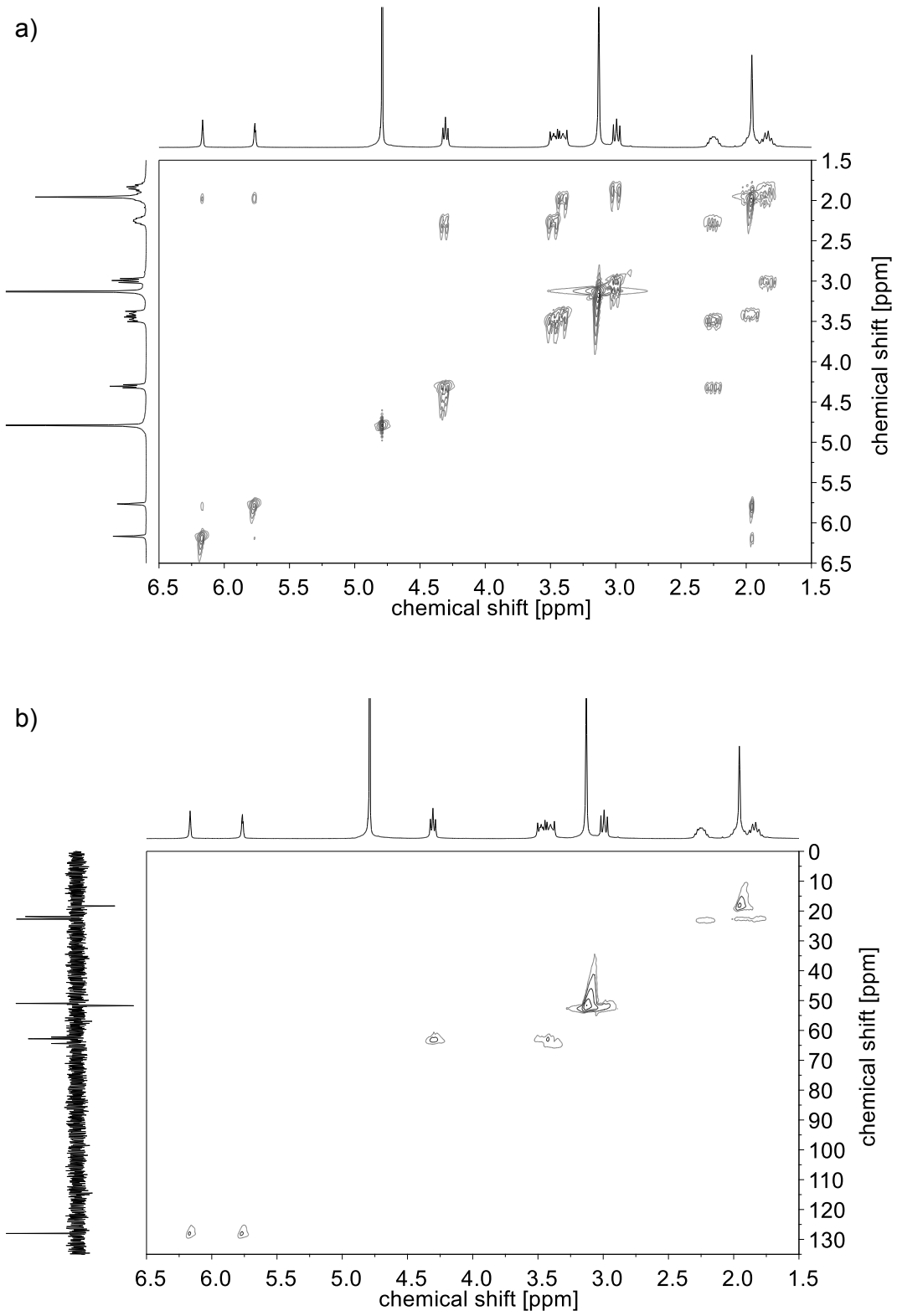

Figure A.22. a) ^{1}H-^{1}H-COSY and b) ^{1}H-^{13}C-HMQC NMR spectra of **M-11** in D_2O.

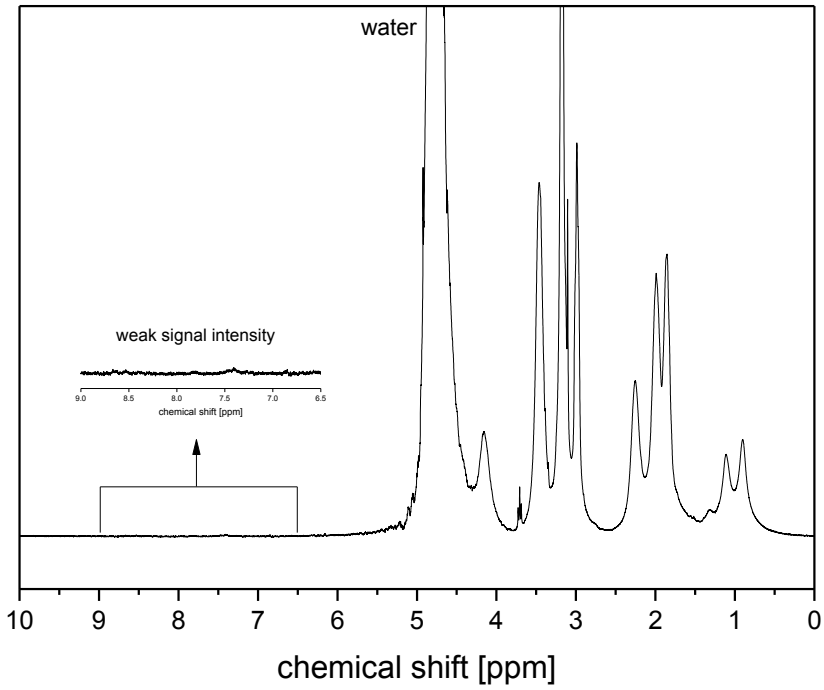

Figure A.23. Limits of end group analysis by ^{1}H NMR, exemplified for **poly(M-11)$_{290}$**. ^{1}H NMR spectrum in D_2O, inset shows the barely visible weak signals of the Z- and R-groups between 6.5 and 9.0 ppm.

IR spectra

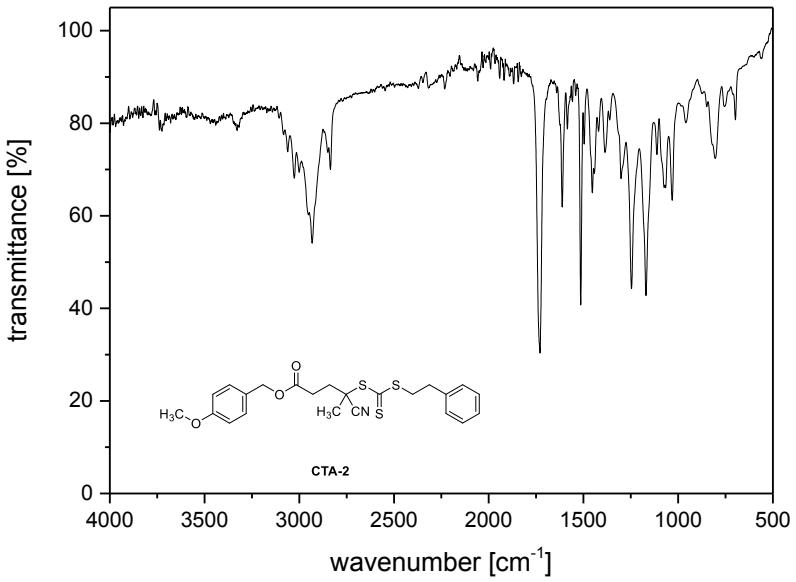

Figure A.24. IR spectrum of **CTA-2**.

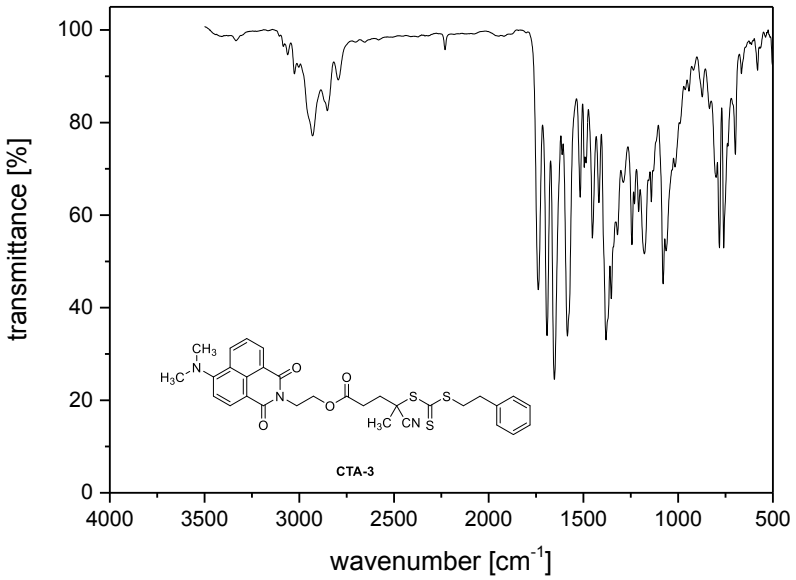

Figure A.25. IR spectrum of **CTA-3**.

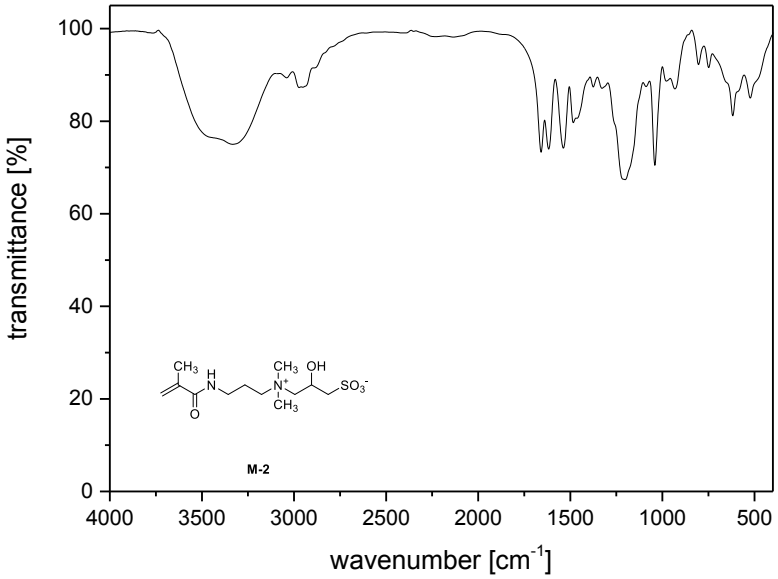

Figure A.26. IR spectrum of **M-2**.

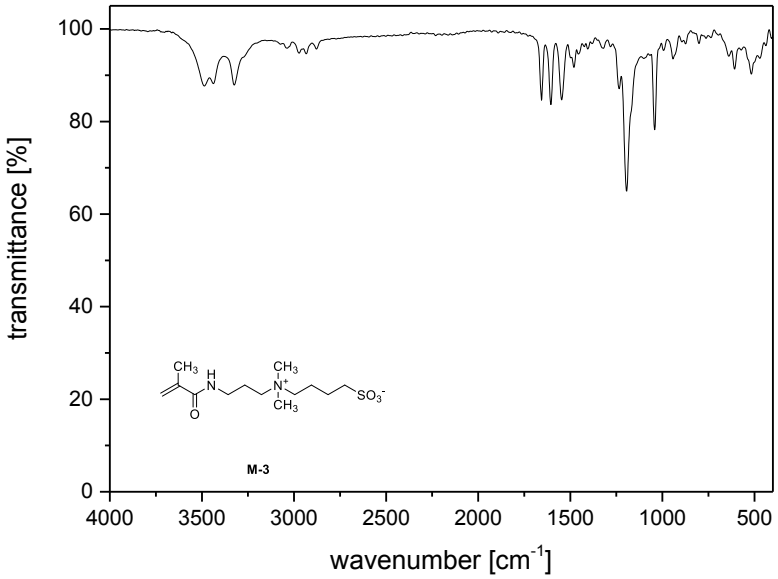

Figure A.27. IR spectrum of **M-3**.

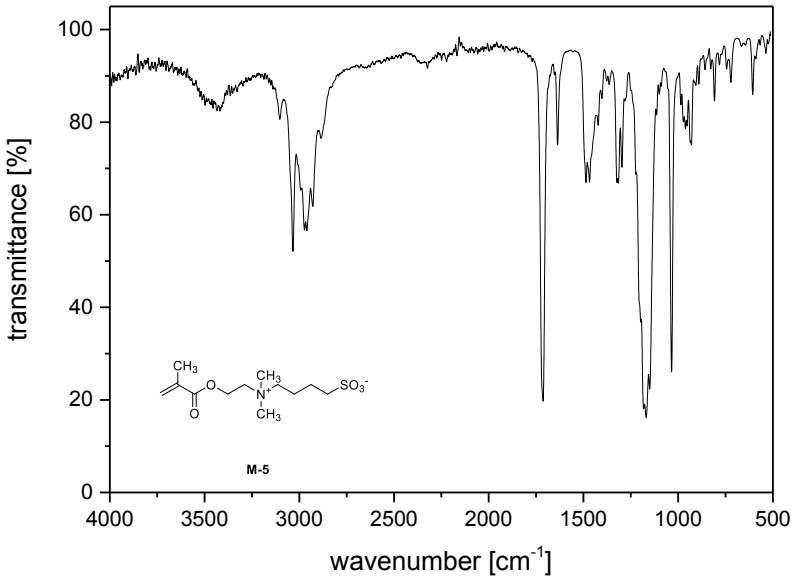

Figure A.28. IR spectrum of **M-5**.

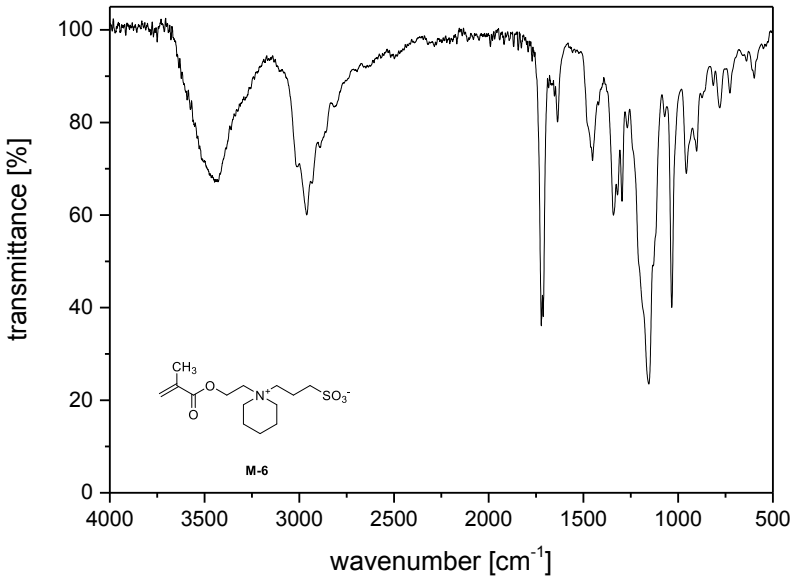

Figure A.29. IR spectrum of **M-6**.

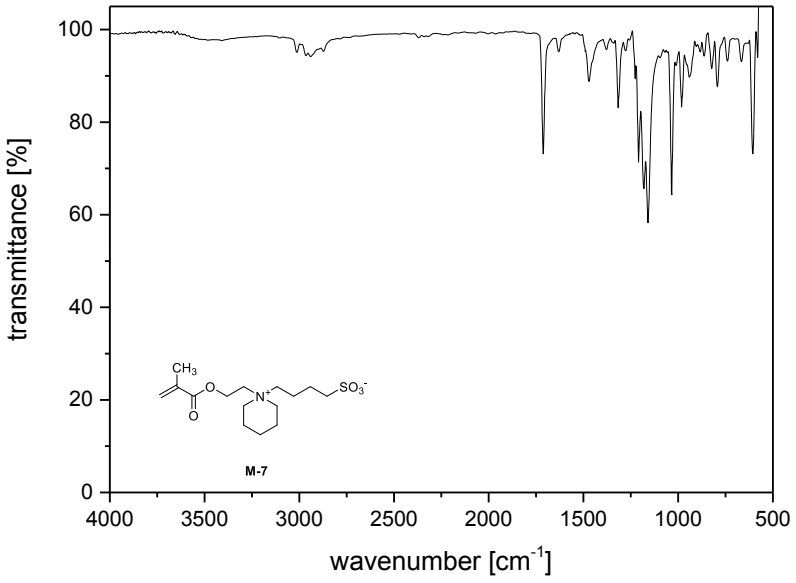

Figure A.30. IR spectrum of **M-7**.

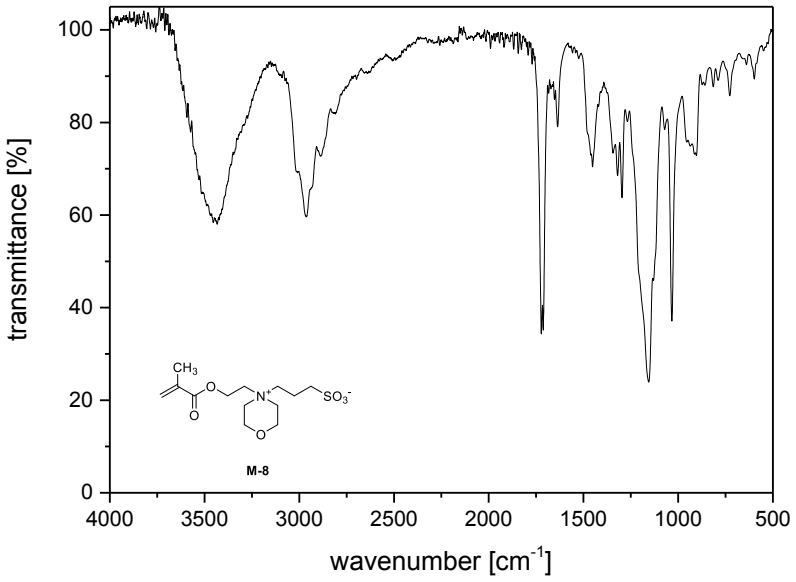

Figure A.31. IR spectrum of **M-8**.

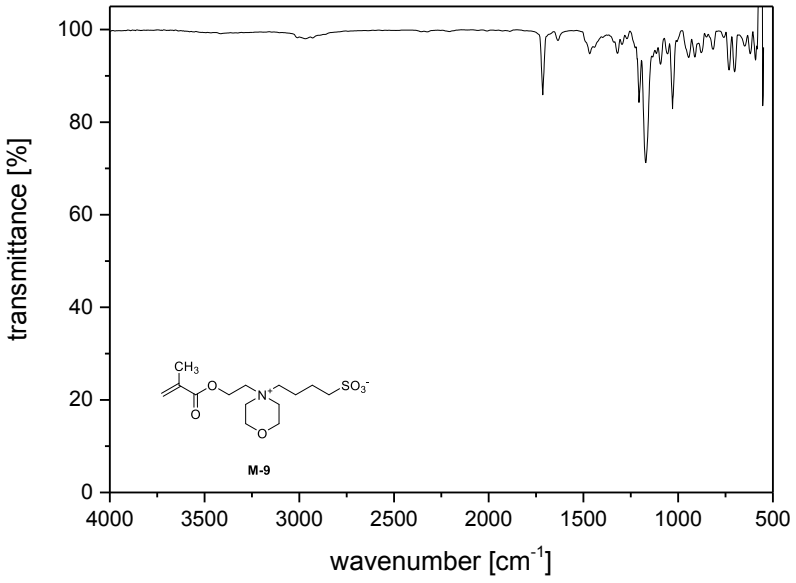

Figure A.32. IR spectrum of **M-9**.

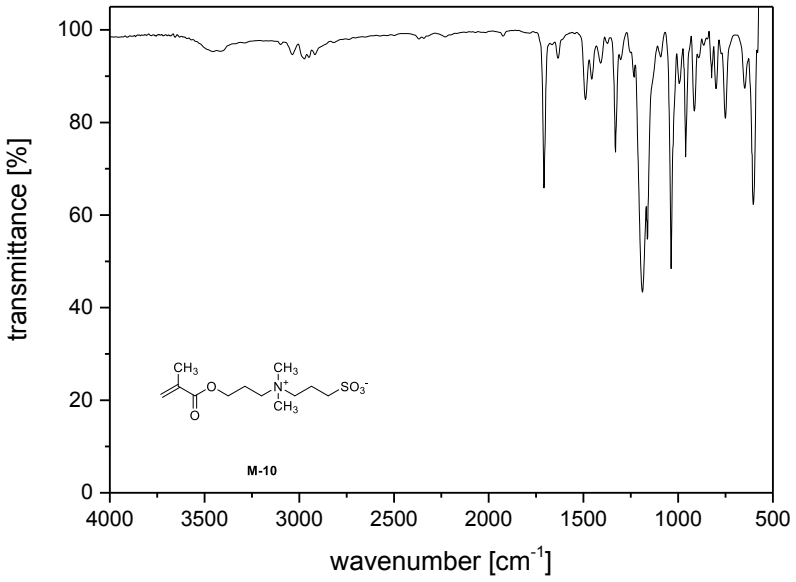

Figure A.33. IR spectrum of **M-10**.

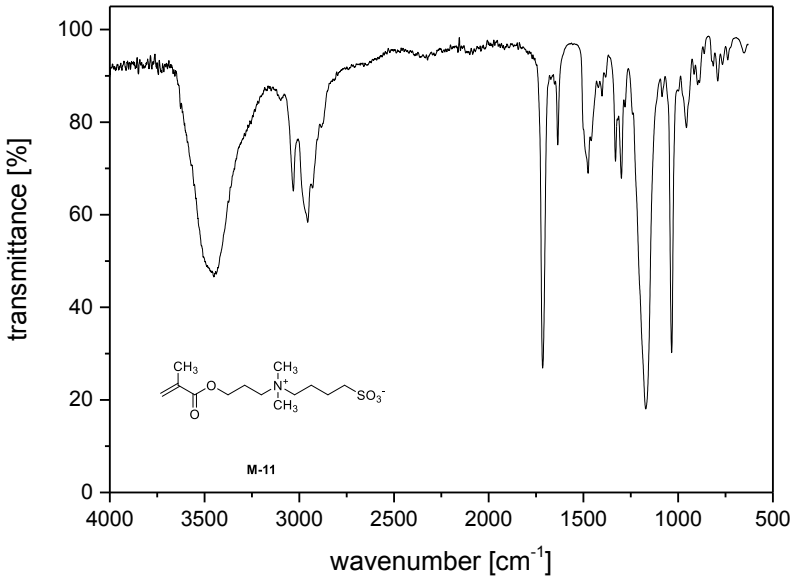

Figure A.34. IR spectrum of **M-11**.

UV-vis and fluorescence spectra

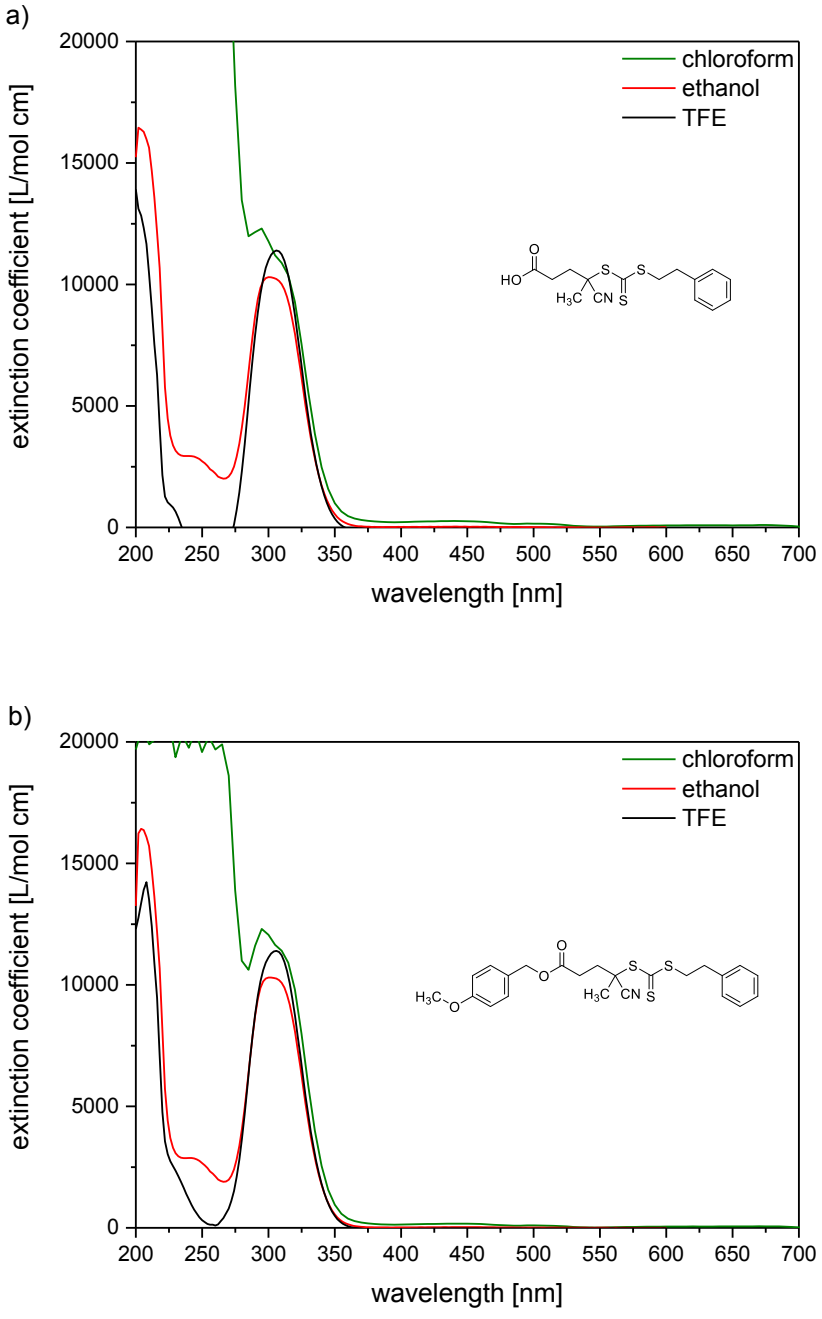

Figure A.35. UV-vis absorbance spectra in various solvents of a) **CTA-1** and b) **CTA-2**. TFE = trifluoroethanol.

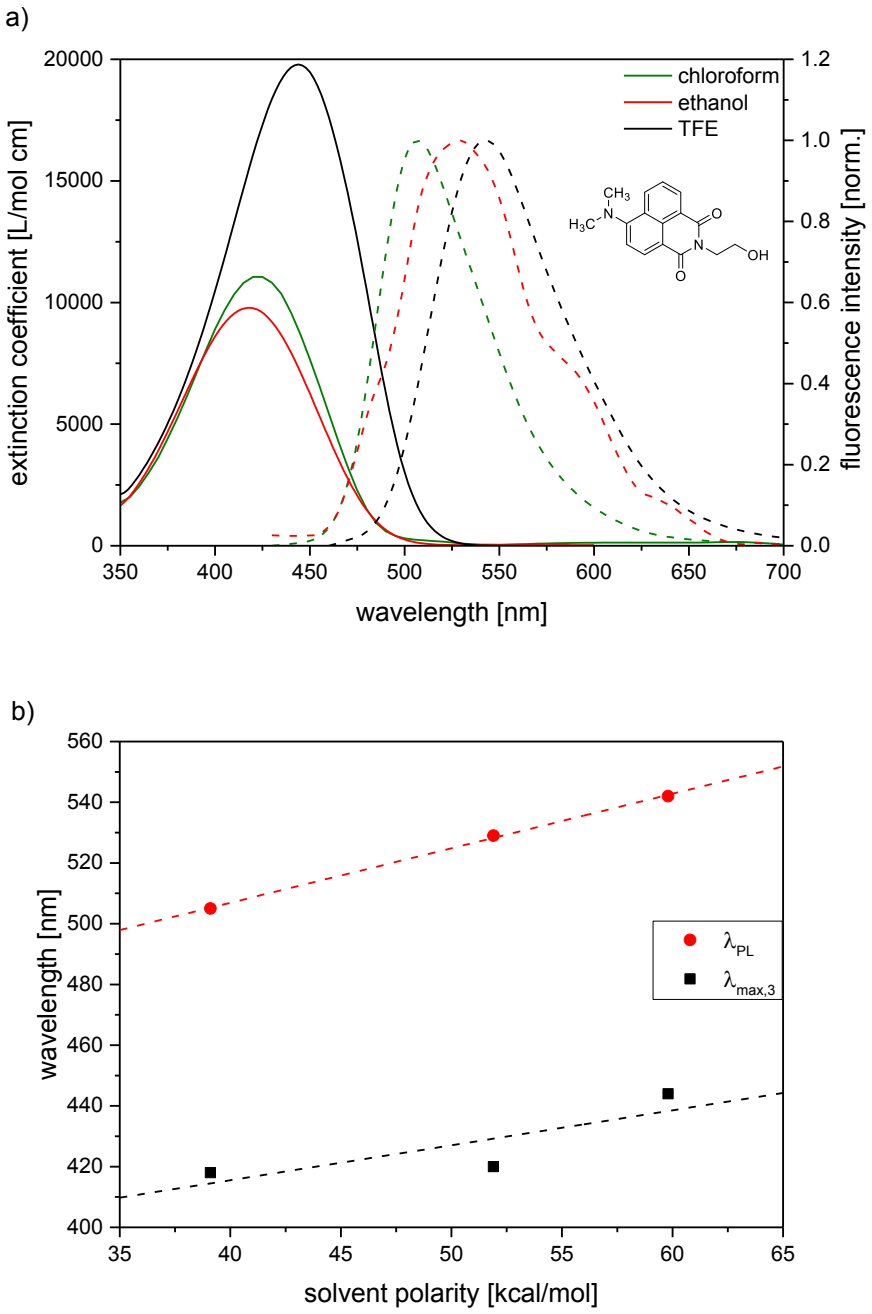

Figure A.36. a) UV-vis absorbance spectra (solid lines) and normalized fluorescence emission spectra (dashed lines) of **I-1** in various solvents. Excitation at maximum absorbance wavelength. b) Evolution of λ_{PL} (●) and $\lambda_{max,3}$ (■) with empirical solvent polarity $E_T(30)$ parameter[147] (dashed line = linear regression). Increasing solvent polarity from left to right. TFE = trifluoroethanol.

Gel permeation chromatography

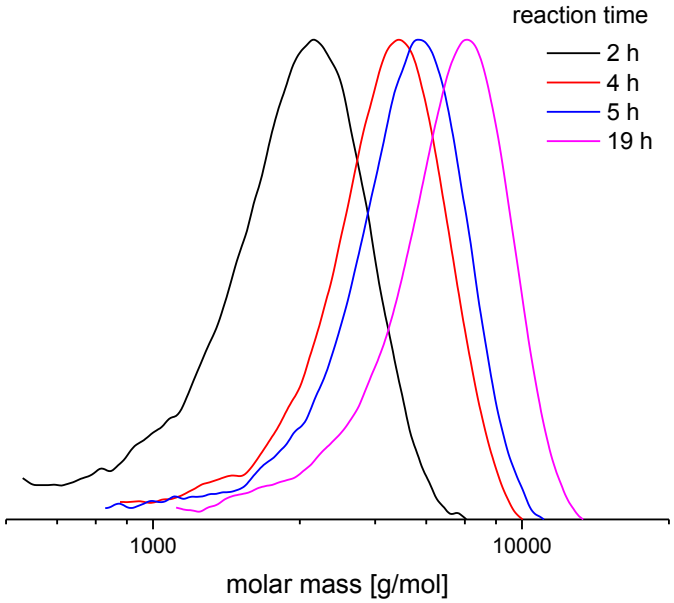

Figure A.37. Selected elugrams of the crude products of kinetic experiments of **M-12** in TFE (RI detector). From left to right: increasing reaction time and conversion. For all curves: Đ = 1.2.

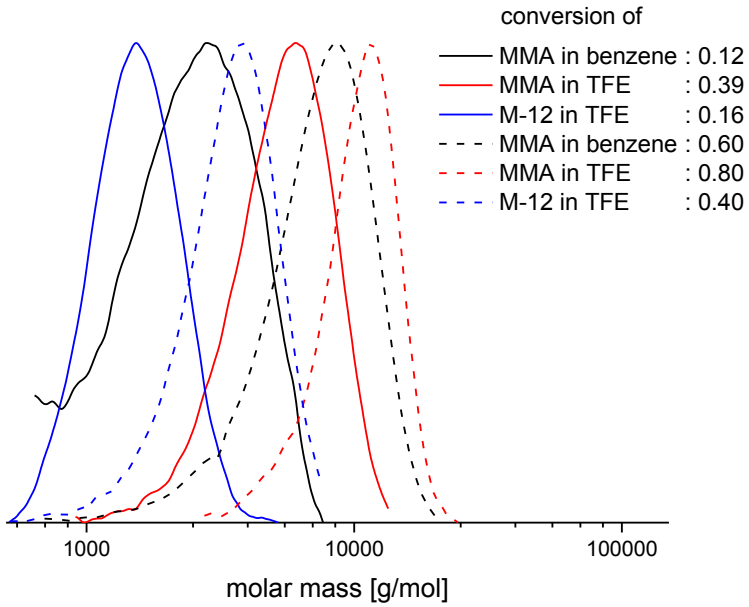

Figure A.38. Selected elugrams of purified polymers. Conversion of **MMA** in benzene: 0.12 (——); 0.60 (------), of **MMA** in TFE: 0.39 (——); 0.80 (------), and of **M-12** in TFE: 0.16 (——); 0.40 (------). Polymerization times were 1 h (bold lines) and 3 h (dashed lines).

Figures

Monomers

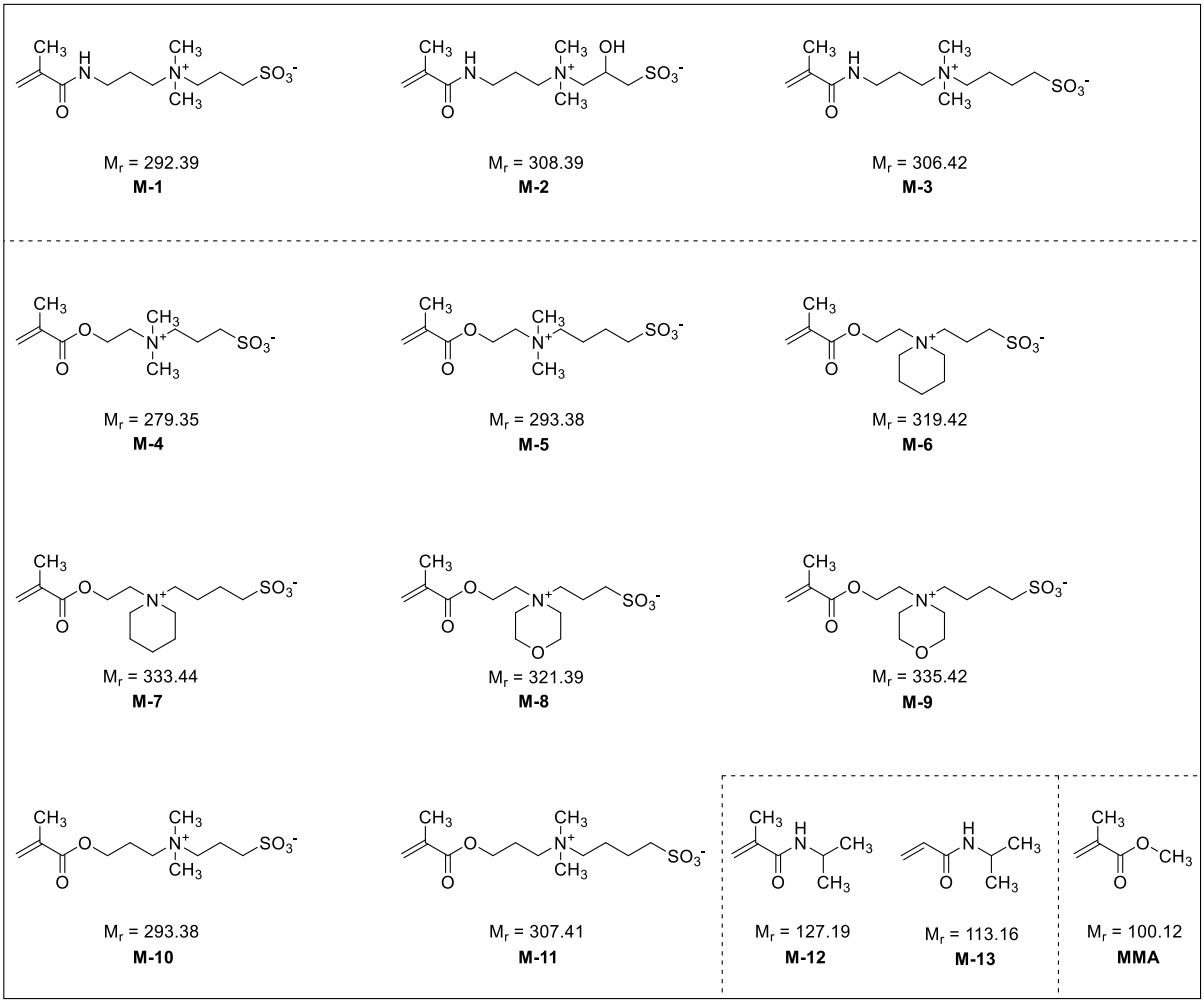

RAFT agents

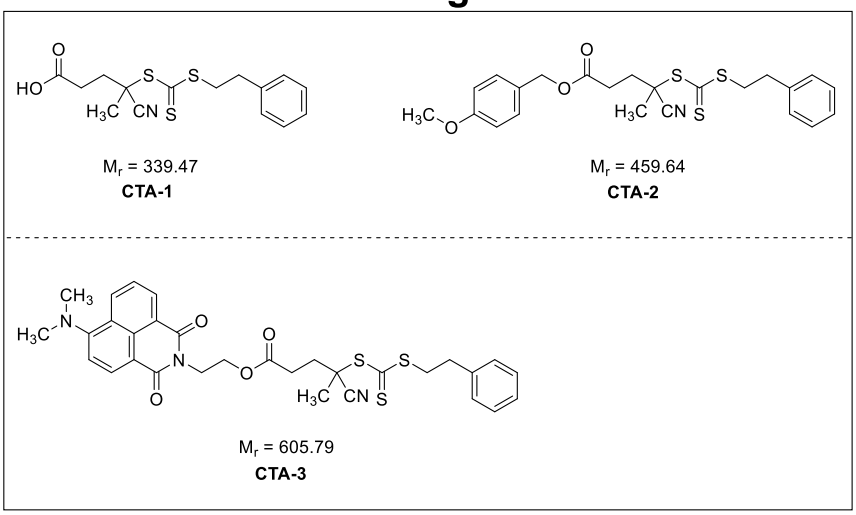

Initiator

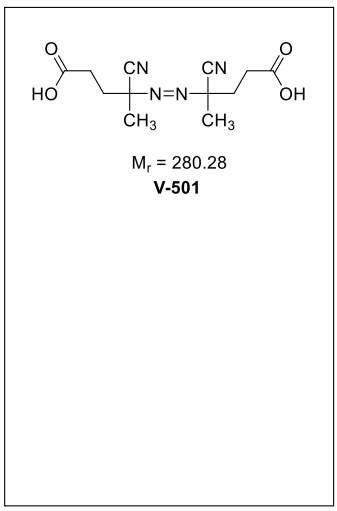

Figure A.39. Overview of monomers, RAFT agents, and initiator used in this study.

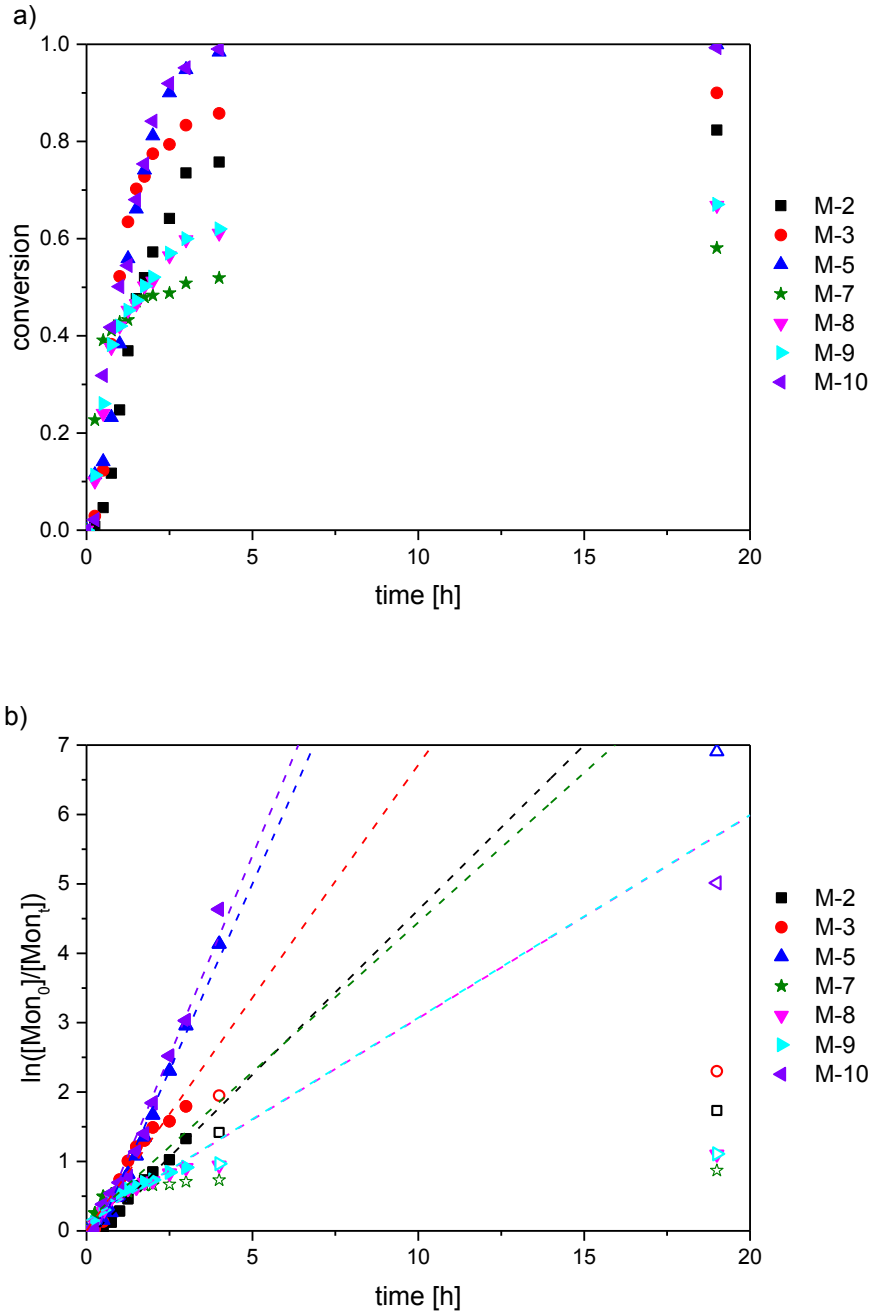

Figure A.40. Evolution of kinetic experiments of sulfobetaines in TFE. a) Conversion with time and b) pseudo-first-order kinetic behavior of **M-2** (■), **M-3** (●), **M-5** (▲), **M-7** (★), **M-8** (▼), **M-9** (▶), and **M-10** (◀). The data of **M-2** (□), **M-3** (○), **M-5** (△), **M-7** (☆), **M-8** (▽), **M-9** (▷), and **M-10** (◁) were not plotted. Polymerizations at 75 °C, using **CTA-3** and V-501. The molar ratio Mon : **CTA-3** : V-501 was 100 : 1 : 0.2. The monomer concentration was 30 wt%.

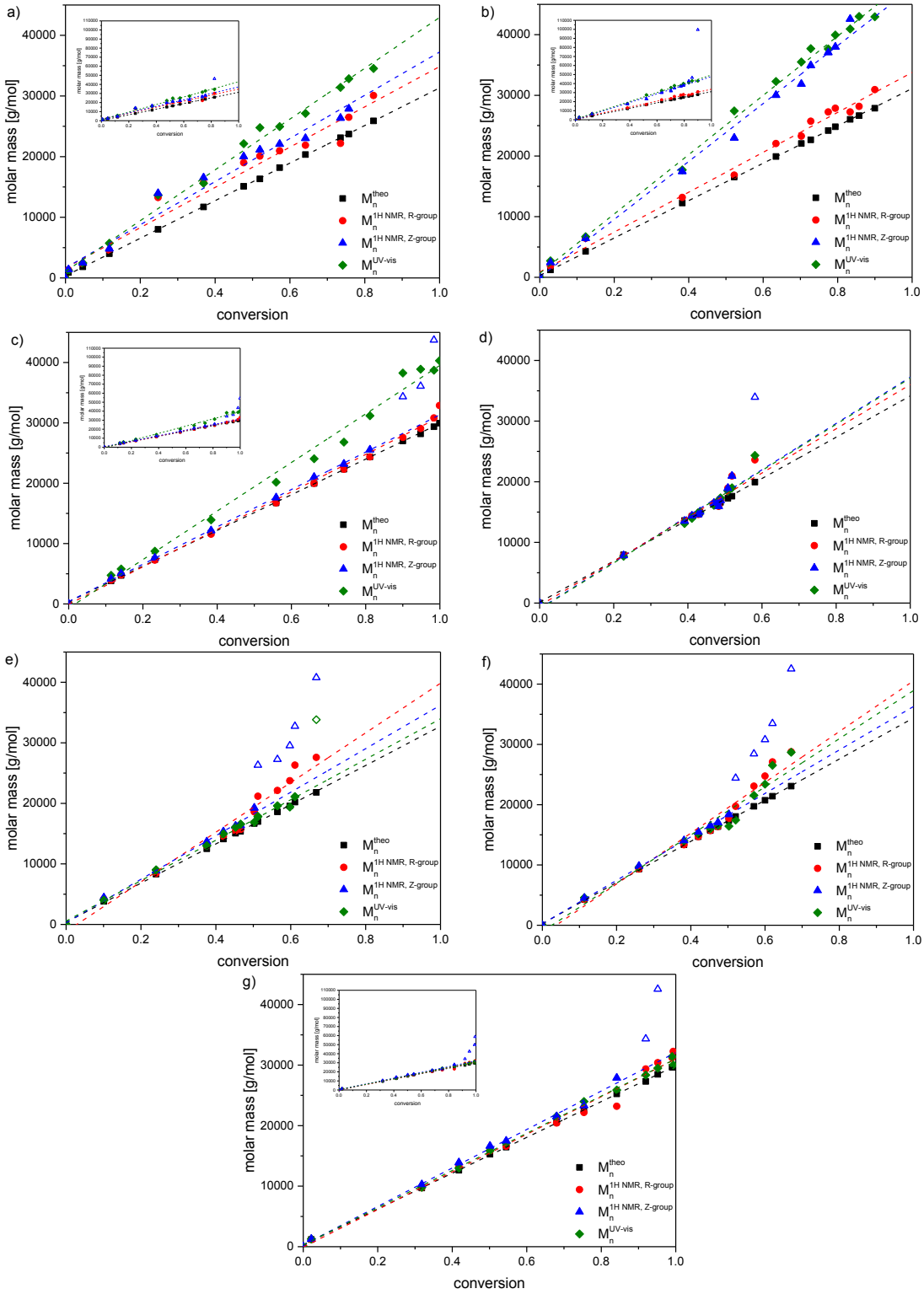

Figure A.41. Dependence of molar mass on conversion of the RAFT polymerization of a) **M-2**, b) **M-3**, c) **M-5**, d) **M-7**, e) **M-8**, f) **M-9**, and g) **M-10** in TFE. Molar masses: theoretical (■), NMR (R-group) (●), NMR (Z-group) (▲), and UV-vis (R-group) (◆). (△), (◇) Data were not used for fitting. UV-vis in TFE using ε at λ_{max3}. Polymerizations at 75 °C, using **CTA-3** and V-501. Inset illustrates the complete data set.

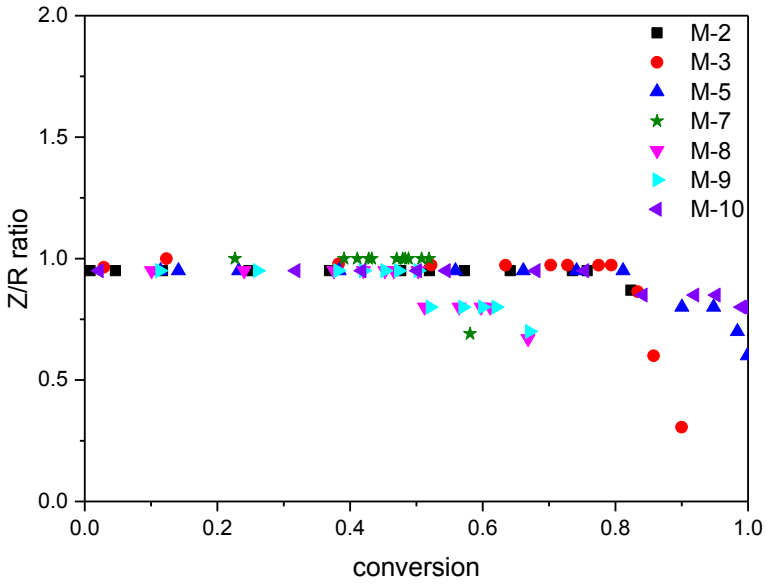

Figure A.42. End group preservation in polymerization of monomers **M-2** (■), **M-3** (●), **M-5** (▲), **M-7** (★), **M-8** (▼), **M-9** (▶), and **M-10** (◀).

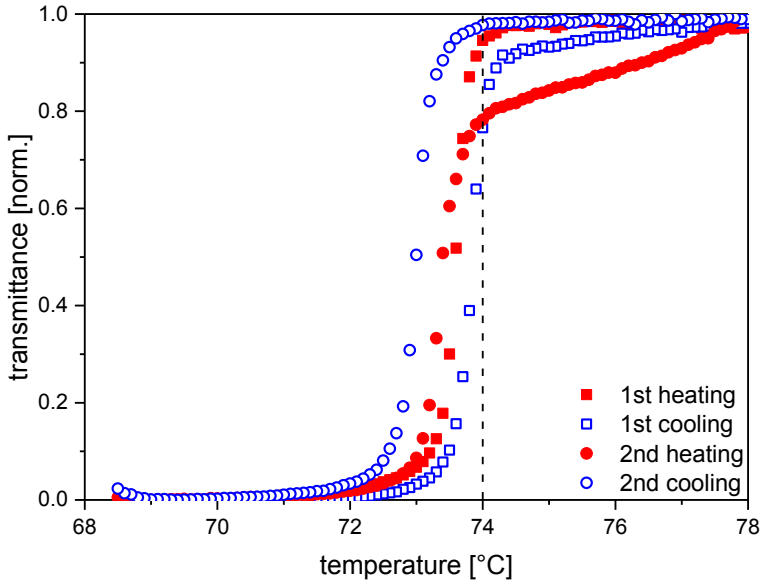

Figure A.43. Reproducibility of turbidimetry using the example of **poly(M-3)$_{80}$** (5 wt% in H_2O).

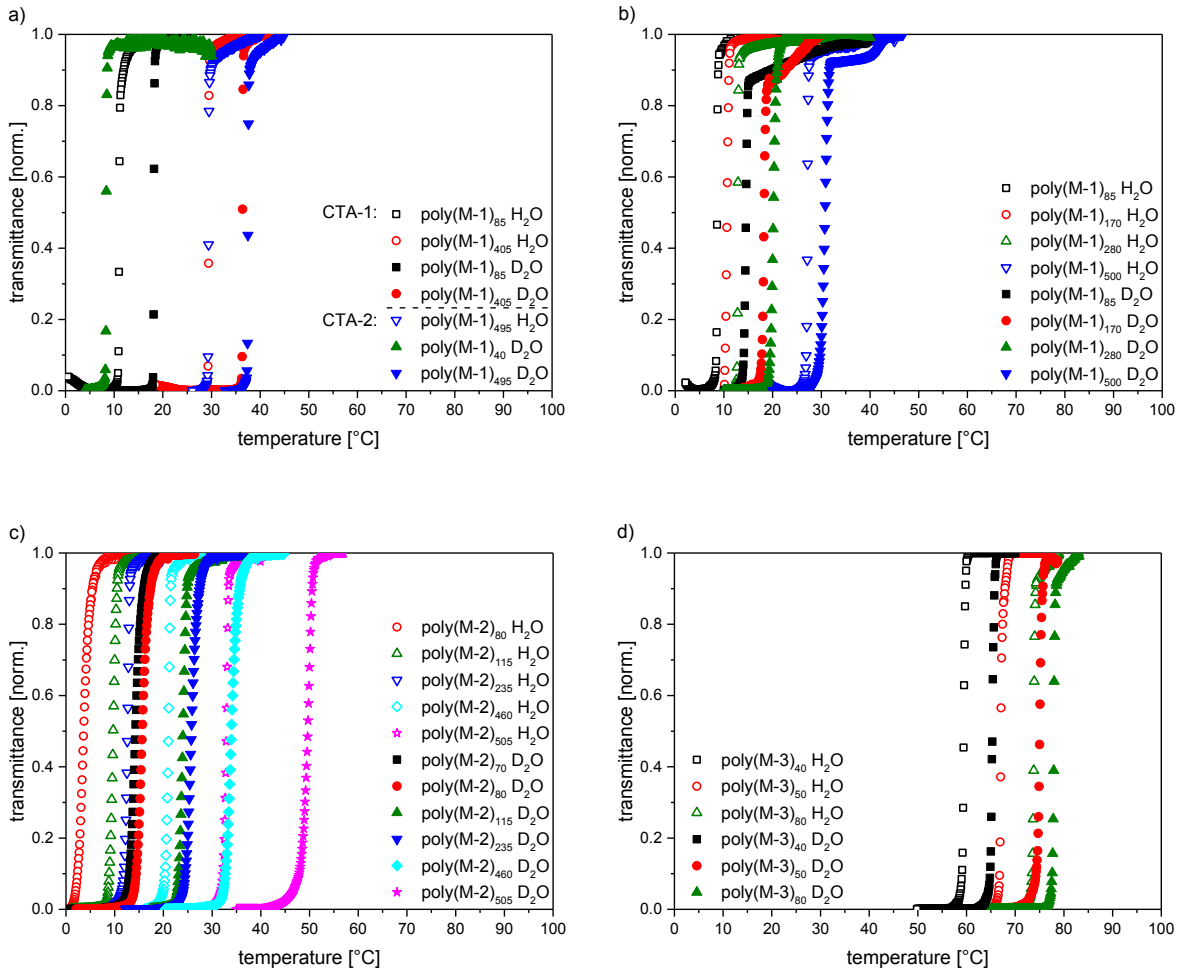

Figure A.44. Temperature dependent turbidity (cooling runs) of 5 wt% aqueous solutions of methacrylamide-based poly(sulfobetaine)s in H_2O (open symbols) and D_2O (close symbols). a) **Poly(M-1)** using **CTA-1** and **CTA-2**; the phase transition of **poly(M-1)$_{40}$** in H_2O is below 0 °C, b) **poly(M-1)** using **CTA-3**, c) **poly(M-2)** using **CTA-3**; the phase transition of **poly(M-2)$_{70}$** in H_2O is below 0 °C, and d) **poly(M-3)** using **CTA-3**; the phase transitions of **poly(M-3)$_{245}$** and **poly(M-3)$_{425}$** in H_2O and in D_2O are above 100 °C.

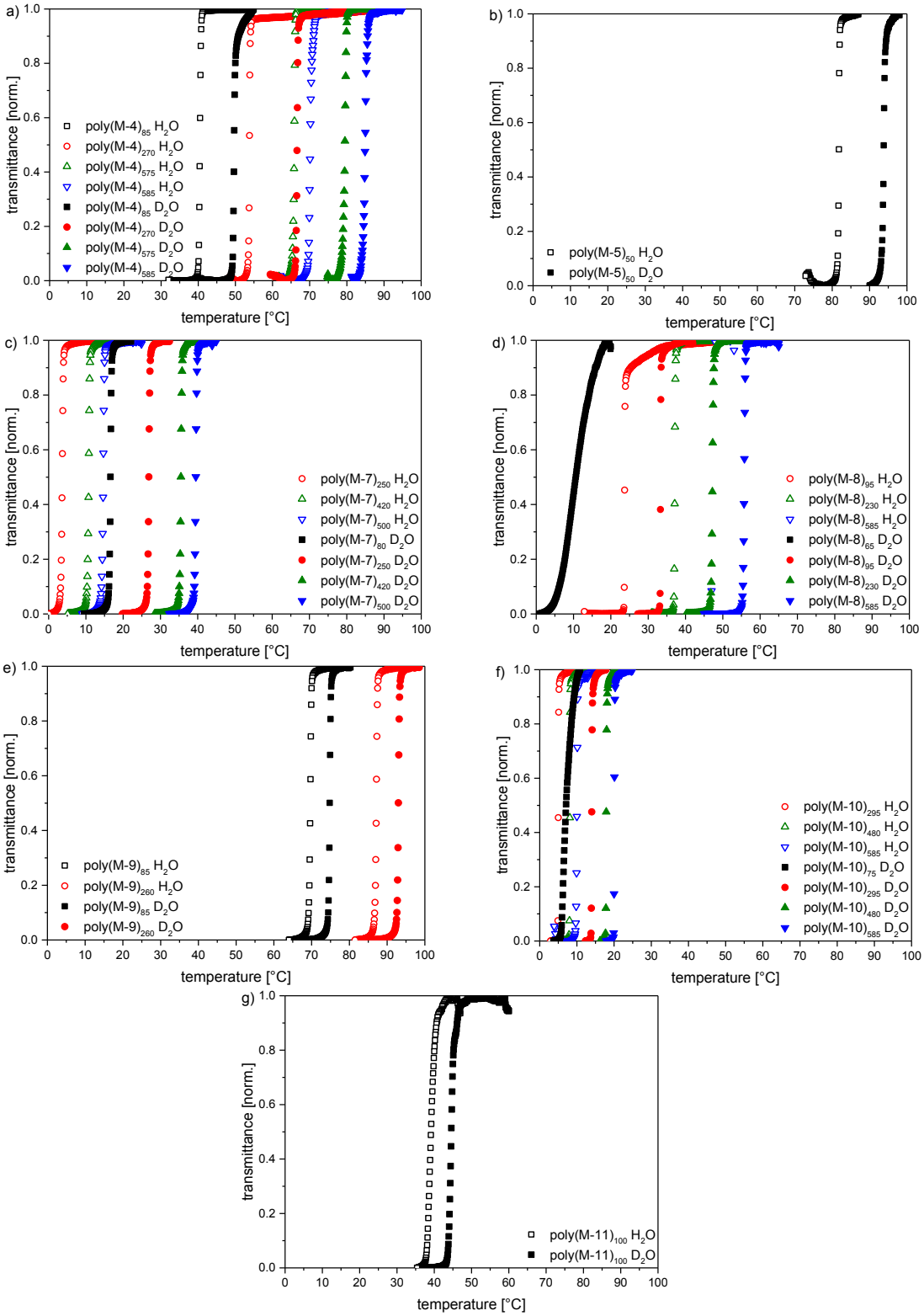

Figure A.45. Temperature dependent turbidity (cooling runs) of 5 wt% aqueous solutions of methacrylate-based poly(sulfobetaine)s in H_2O (open symbols) and D_2O (close symbols). RAFT agent was **CTA-3**. a) **Poly(M-4)**, b) **poly(M-5)**, c) **poly(M-7)**, d) **poly(M-8)**, e) **poly(M-9)**, f) **poly(M-10)**, g) **poly(M-11)**. The phase transition of **poly(M-6)** in H_2O and D_2O is below 0 °C.

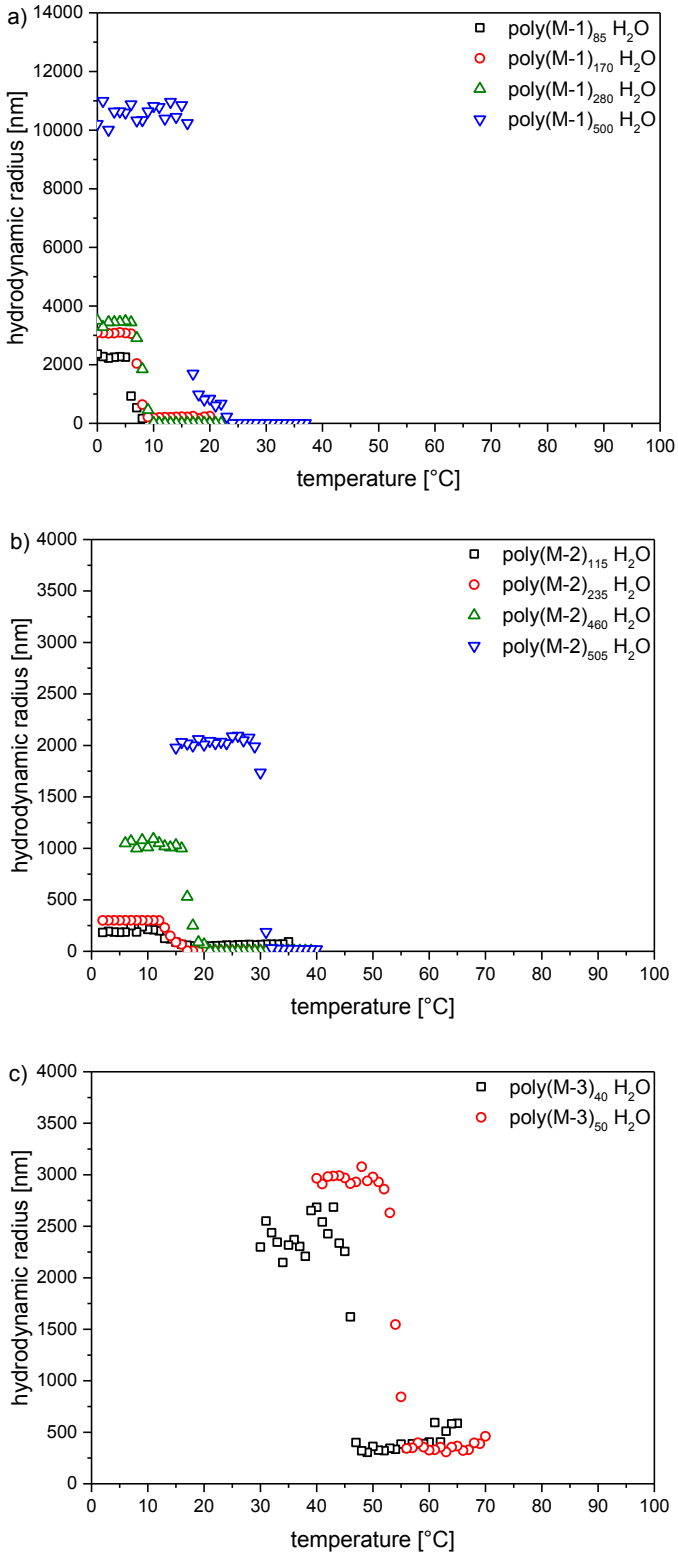

Figure A.46. DLS measurements (cooling runs) of 1 wt% solutions of methacrylamide-based poly(sulfobetaine)s in H_2O. a) **Poly(M-1)**, b) **poly(M-2)**, and c) **poly(M-3)**.

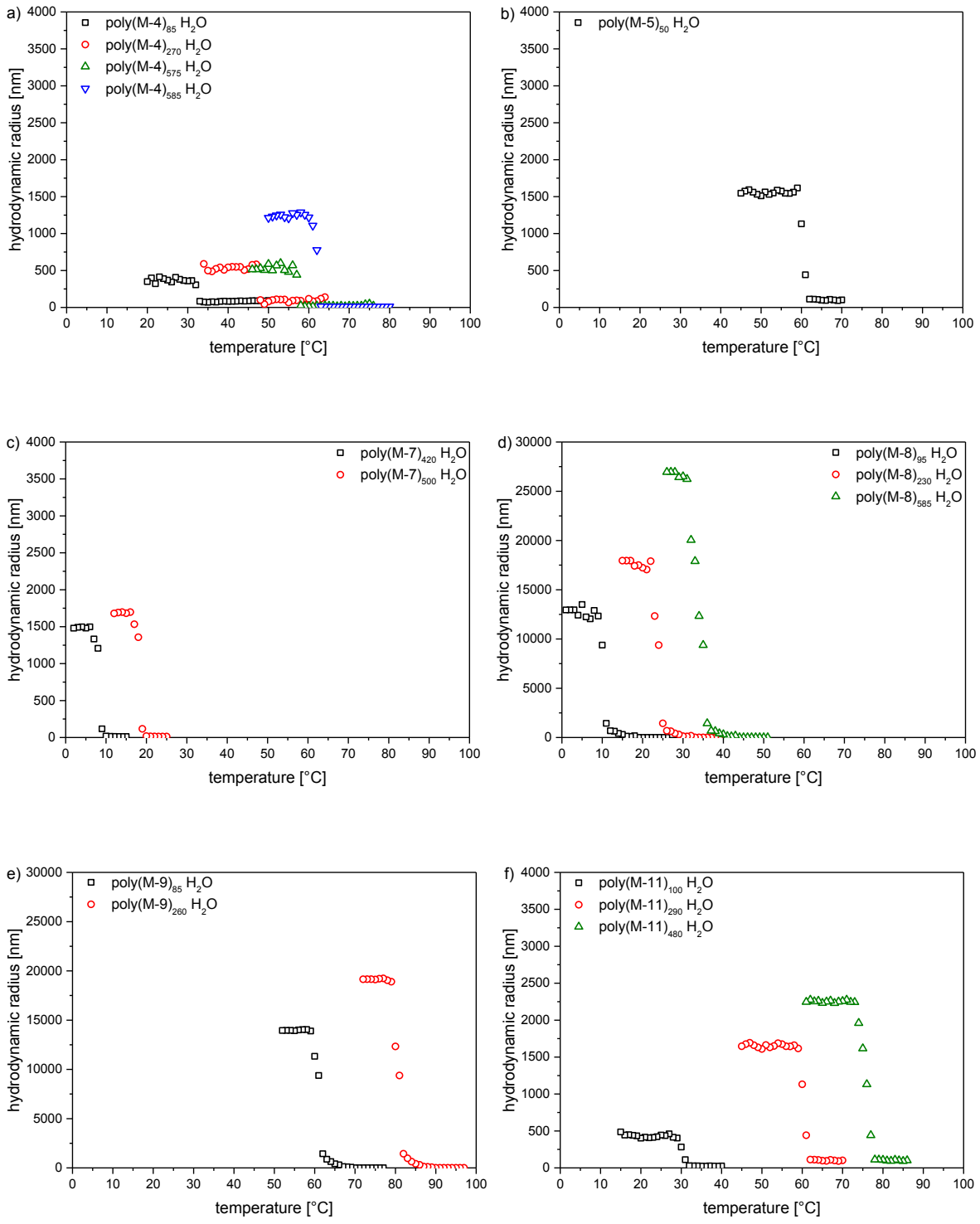

Figure A.47. DLS measurements (cooling runs) of 1 wt% solutions of methacrylate-based poly(sulfobetaine)s in H_2O. a) **Poly(M-4)**, b) **poly(M-5)**, c) **poly(M-7)**, d) **poly(M-8)**, e) **poly(M-9)**, f) **poly(M-11)**. The phase transitions of **poly(M-6)** and **poly(M-10)** in H_2O (at 1 wt%) is below 0 °C.

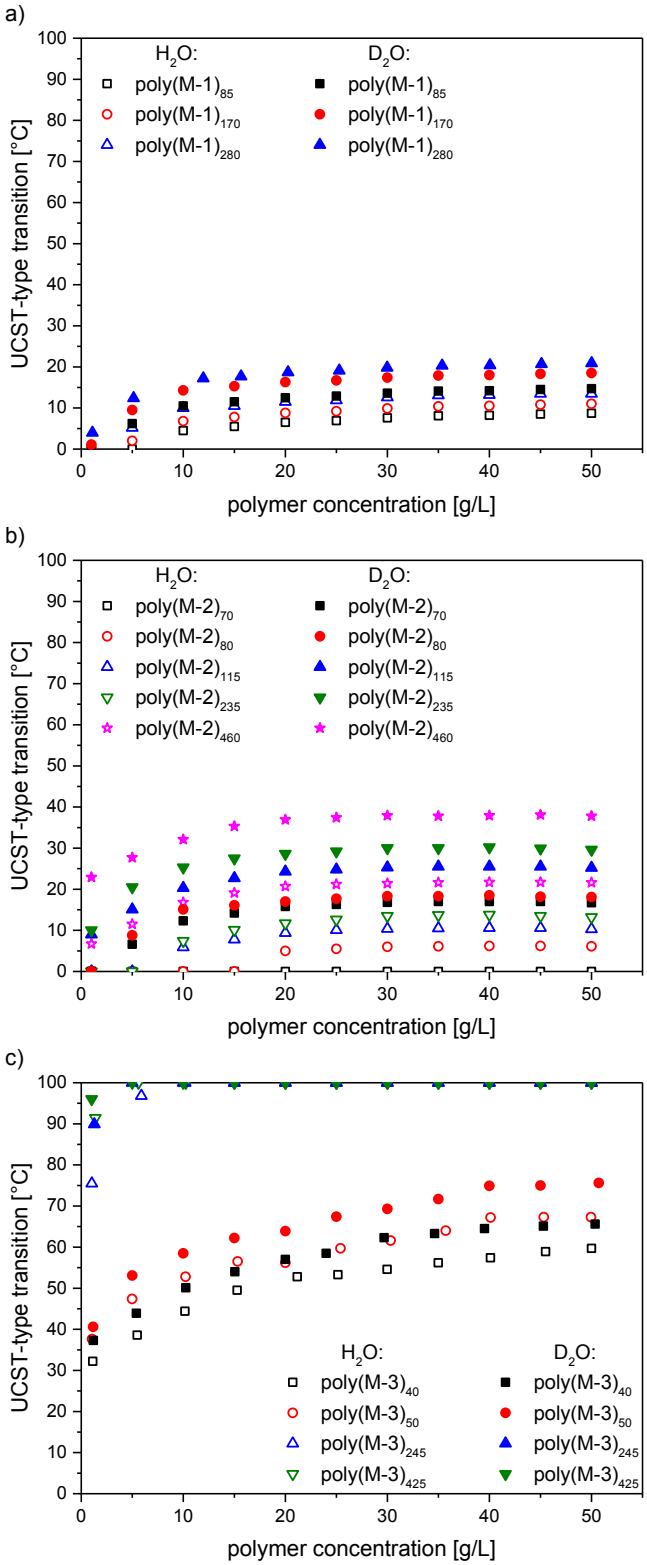

Figure A.48. Concentration dependent evolution of UCST-type transition temperatures in H_2O (open symbols) and D_2O (close symbols) of a) **poly(M-1)**, b) **poly(M-2)**, and **poly(M-3)**.

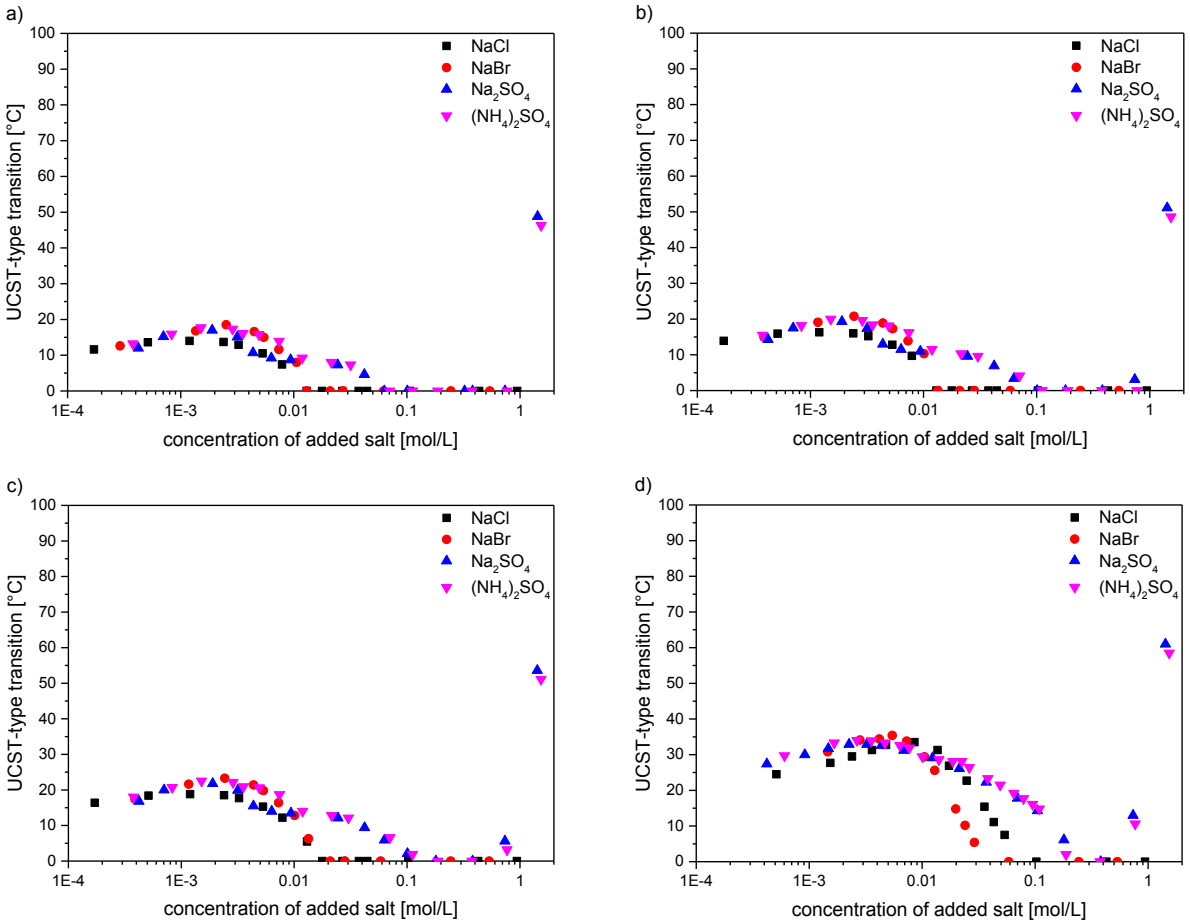

Figure A.49. Evolution of UCST-type transition temperatures in 5 wt% aqueous solution containing inorganic salts of **poly(M-1)** series. In H_2O: a) **poly(M-1)$_{85}$**, b) **poly(M-1)$_{270}$**, and c) **poly(M-1)$_{280}$** and in D_2O: d) **poly(M-1)$_{280}$**. (■) = NaCl, (●) = NaBr, (▲) = Na_2SO_4, and (▼) = $(NH_4)_2SO_4$.

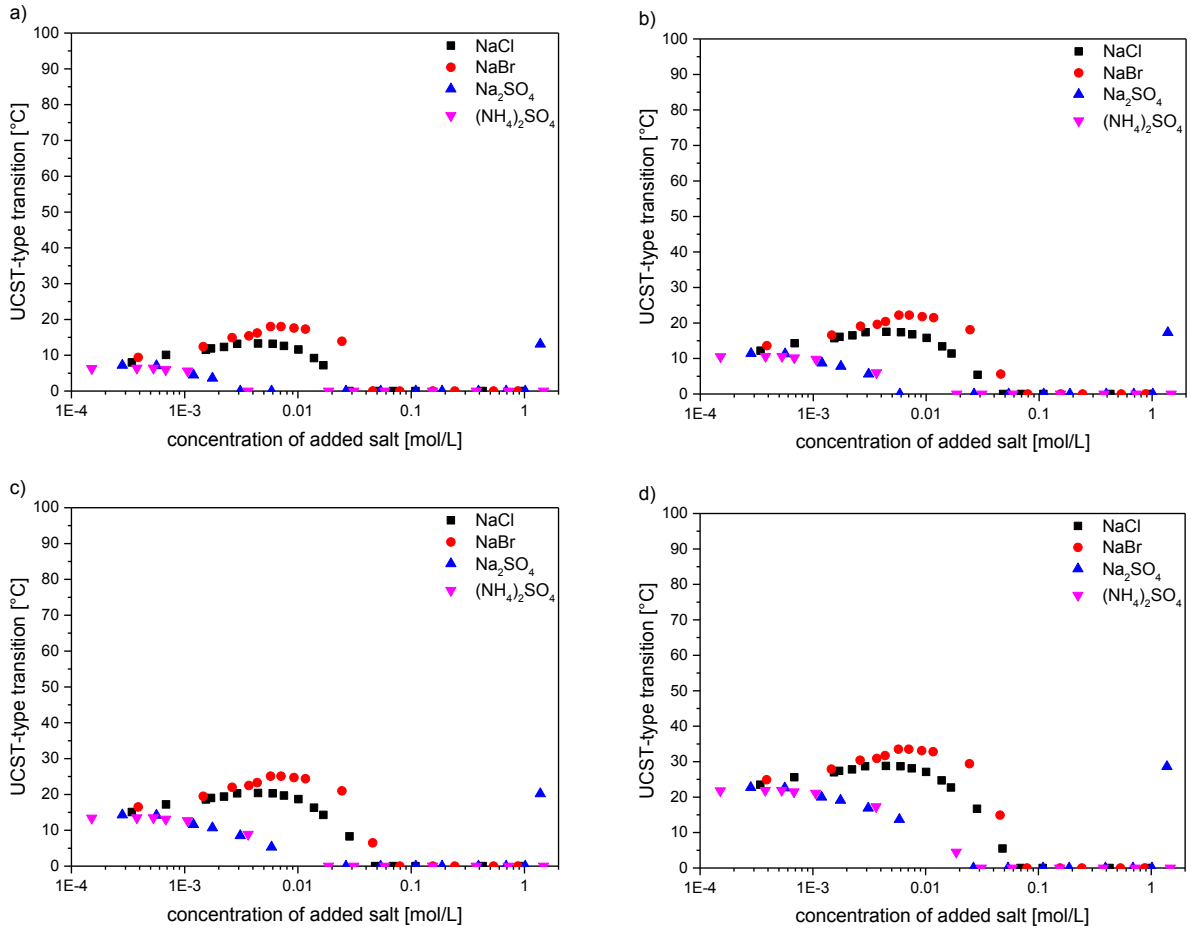

Figure A.50. Evolution of UCST-type transition temperatures in 5 wt% H_2O containing inorganic salts of **poly(M-2)** series. a) **Poly(M-2)$_{80}$**, b) **poly(M-2)$_{115}$**, c) **poly(M-2)$_{235}$**, and d) **poly(M-2)$_{460}$**. (■) = NaCl, (●) = NaBr, (▲) = Na_2SO_4, and (▼) = $(NH_4)_2SO_4$.

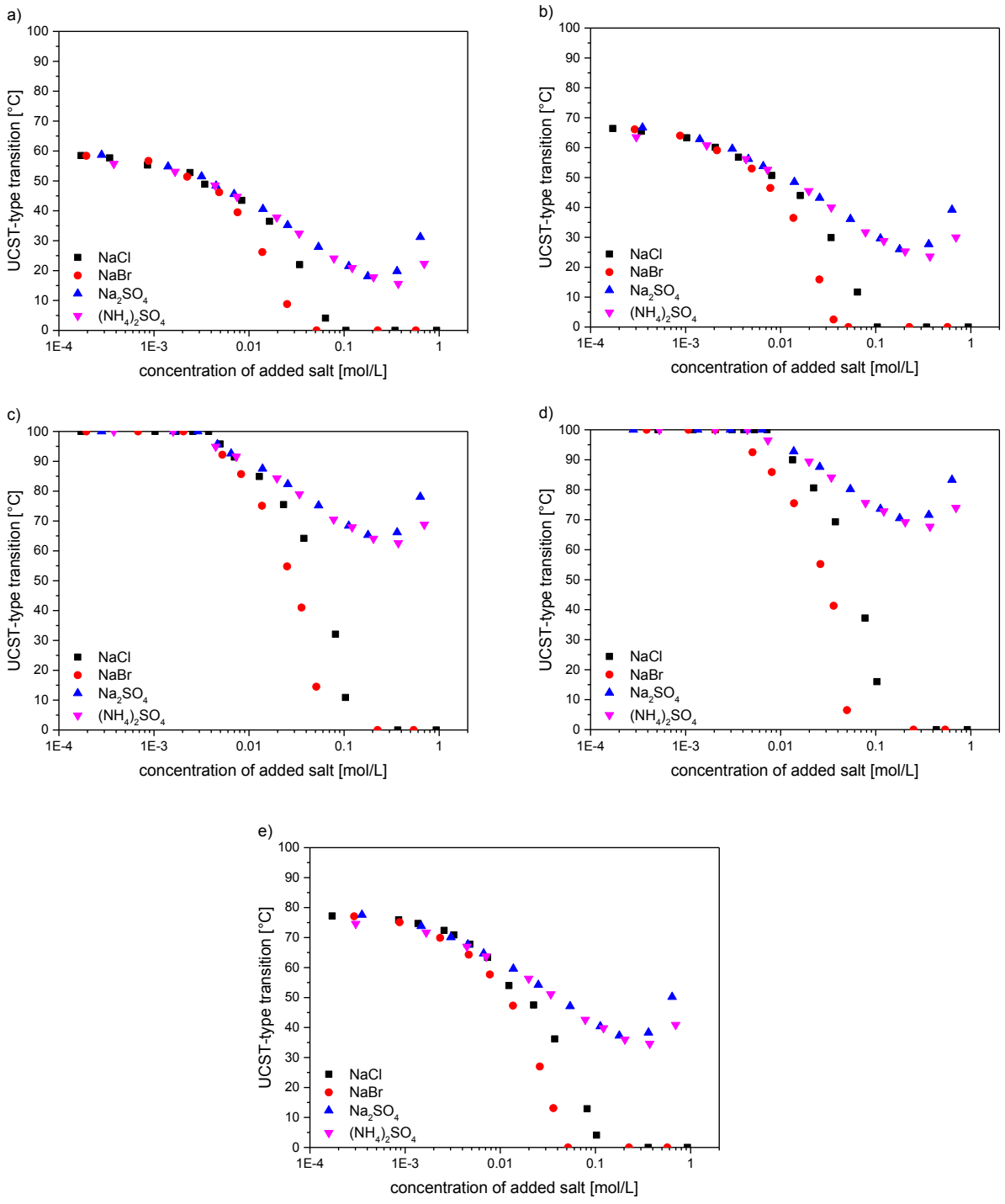

Figure A.51. Evolution of UCST-type transition temperatures in 5 wt% aqueous solution containing inorganic salts of **poly(M-3)** series. In H_2O: a) **poly(M-3)$_{40}$**, b) **poly(M-3)$_{50}$**, c) **poly(M-3)$_{245}$**, and d) **poly(M-3)$_{425}$** and in D_2O: e) **poly(M-3)$_{80}$**. (■) = NaCl, (●) = NaBr, (▲) = Na_2SO_4, and (▼) = $(NH_4)_2SO_4$.

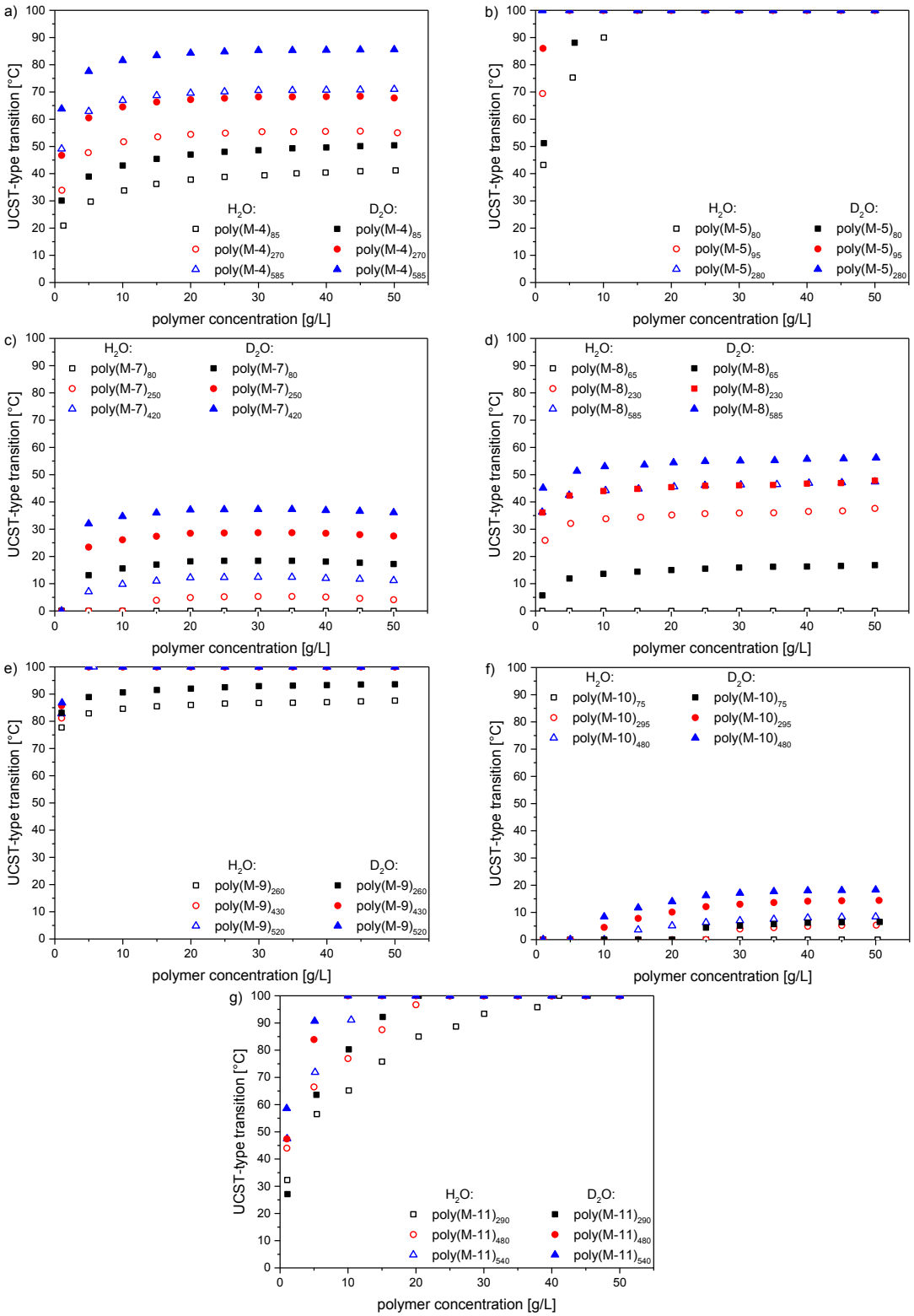

Figure A.52. Concentration dependent evolution of UCST-type transition temperatures in H_2O (open symbols) and D_2O (close symbols) of a) **poly(M-4)**, b) **poly(M-5)**, c) **poly(M-7)**, d) **poly(M-8)**, e) **poly(M-9)**, f) **poly(M-10)**, and g) **poly(M-11)**. The phase transition of **poly(M-6)** in H_2O and in D_2O is below 0 °C.

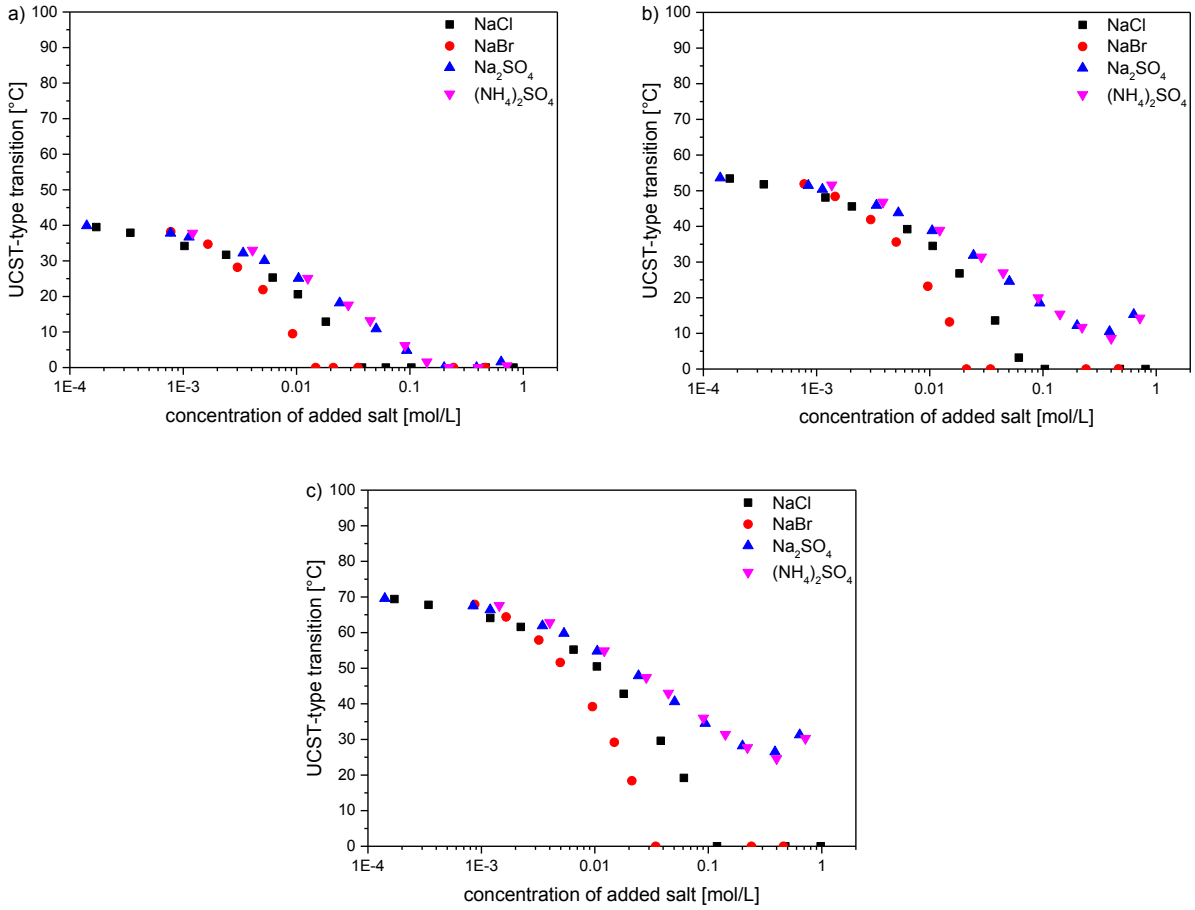

Figure A.53. Evolution of UCST-type transition temperatures in 5 wt% H_2O containing inorganic salts of **poly(M-4)** series. a) P**oly(M-4)$_{85}$**, b) **poly(M-4)$_{270}$**, and c) **poly(M-4)$_{585}$**. (■) = NaCl, (●) = NaBr, (▲) = Na_2SO_4, and (▼) = $(NH_4)_2SO_4$.

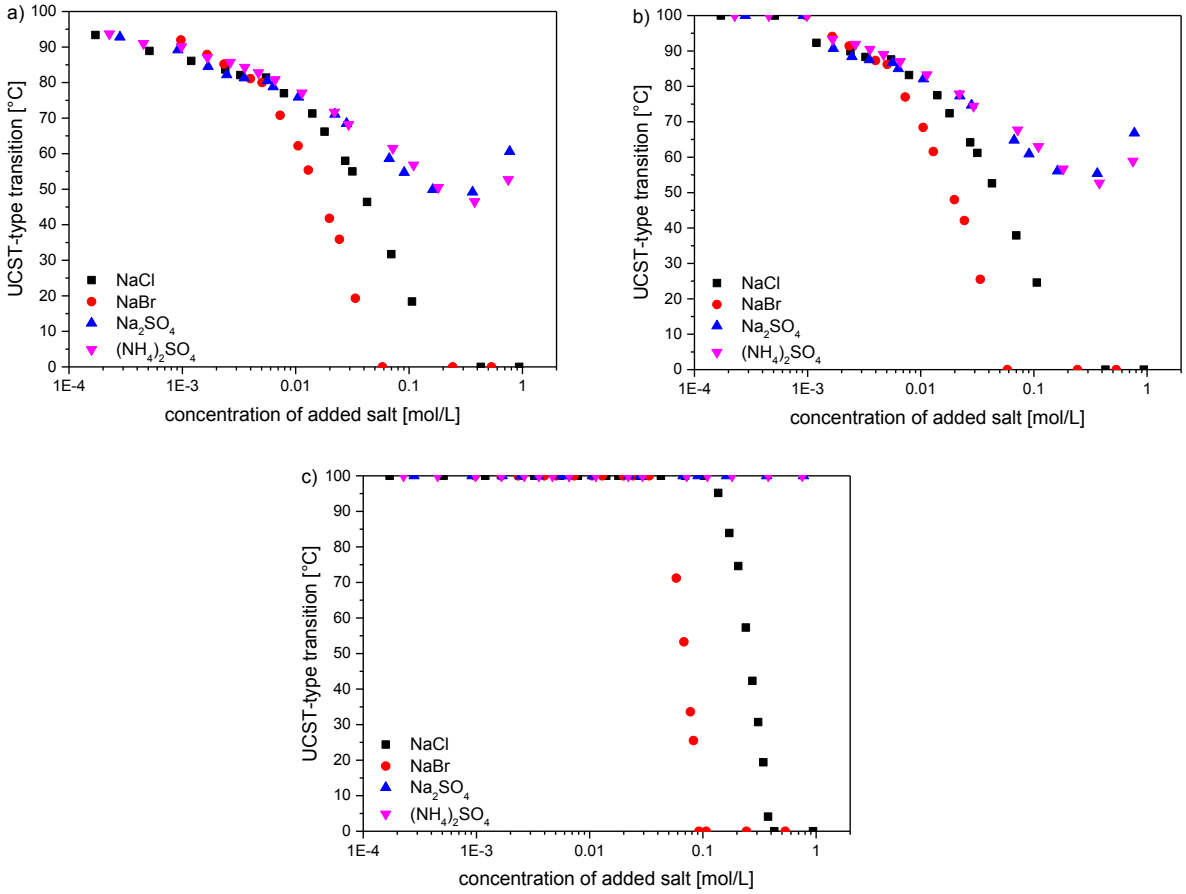

Figure A.54. Evolution of UCST-type transition temperatures in 5 wt% H_2O containing inorganic salts of **poly(M-5)** series. a) **Poly(M-5)$_{80}$**, b) **poly(M-5)$_{95}$**, and c) **poly(M-5)$_{280}$**. (■) = NaCl, (●) = NaBr, (▲) = Na_2SO_4, and (▼) = $(NH_4)_2SO_4$.

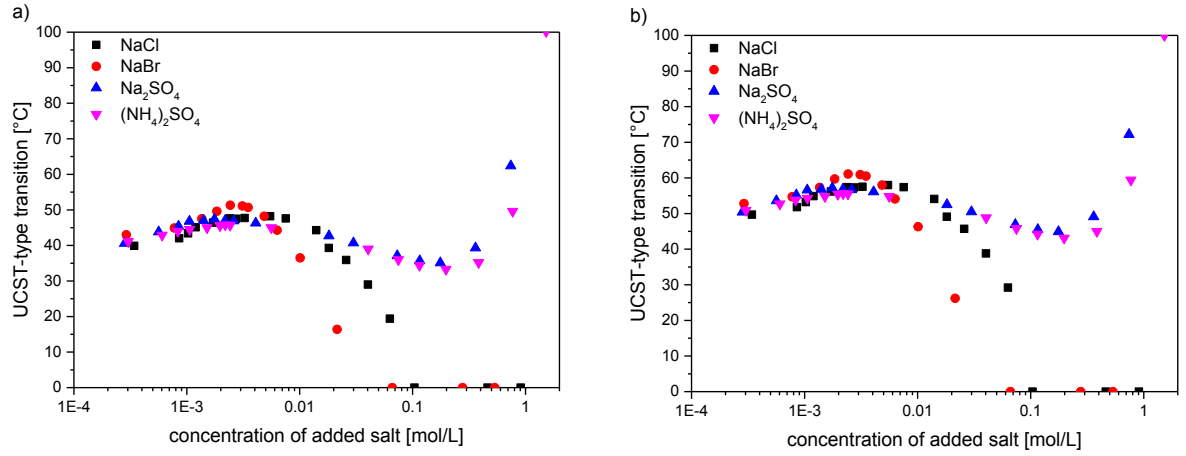

Figure A.55. Evolution of UCST-type transition temperatures in 5 wt% H_2O containing inorganic salts of **poly(M-8)** series. a) **Poly(M-8)$_{230}$**, and b) **poly(M-8)$_{585}$**. (■) = NaCl, (●) = NaBr, (▲) = Na_2SO_4, and (▼) = $(NH_4)_2SO_4$.

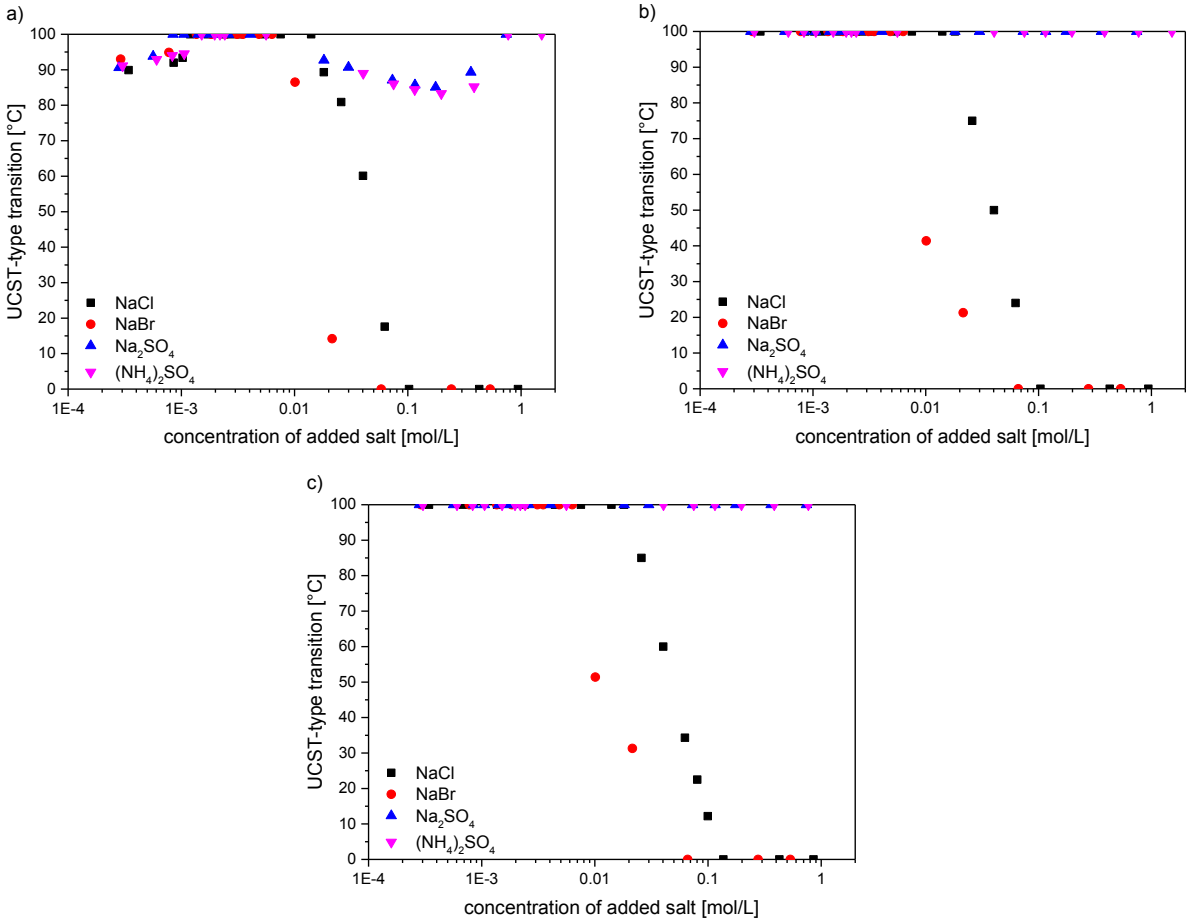

Figure A.56. Evolution of UCST-type transition temperatures in 5 wt% H_2O containing inorganic salts of **poly(M-9)** series. a) P**oly(M-9)$_{260}$**, b) **poly(M-9)$_{430}$**, and c) **poly(M-9)$_{520}$**. (■) = NaCl, (●) = NaBr, (▲) = Na_2SO_4, and (▼) = $(NH_4)_2SO_4$.

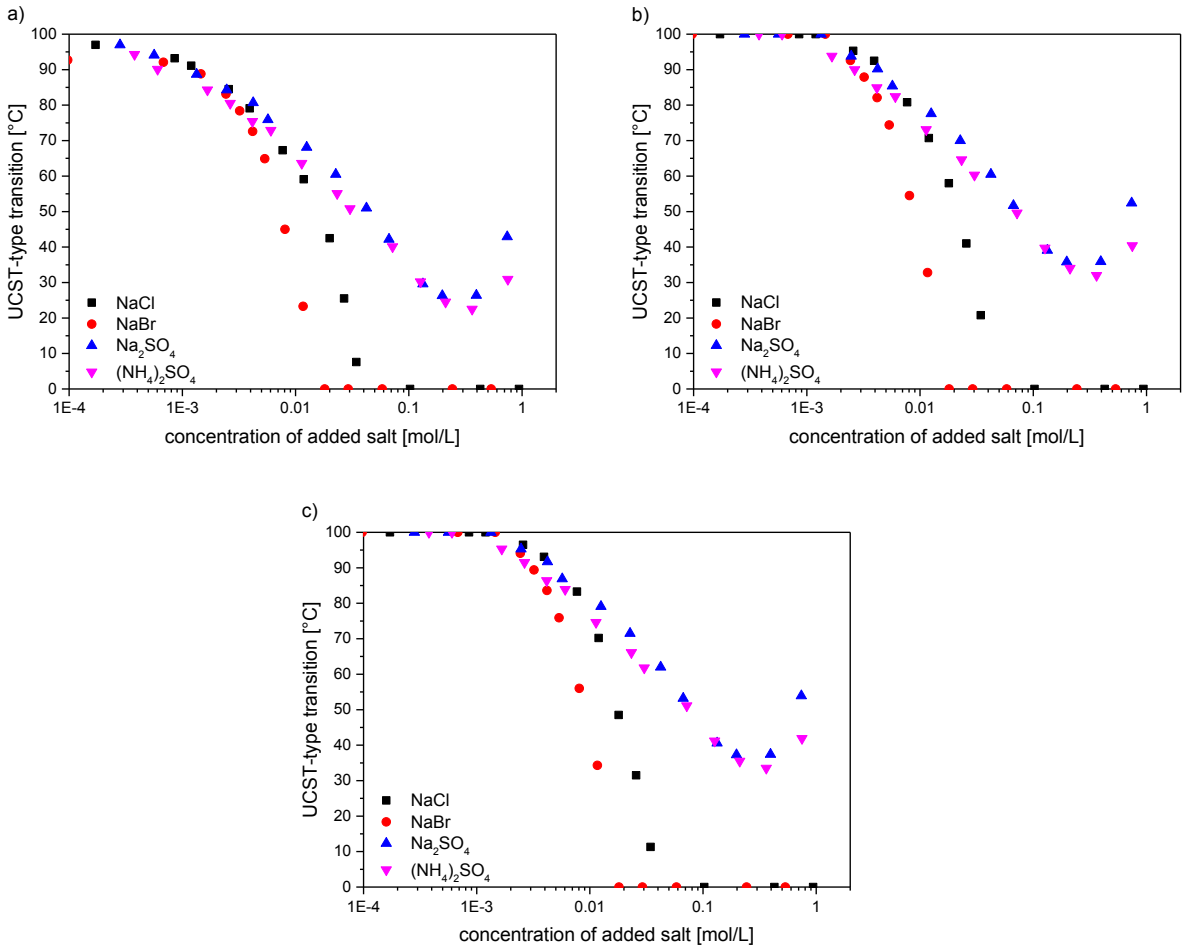

Figure A.57. Evolution of UCST-type transition temperatures in 5 wt% H_2O containing inorganic salts of **poly(M-11)** series. a) P**oly(M-11)$_{290}$**, b) **poly(M-11)$_{480}$**, and c) **poly(M-11)$_{540}$**. (■) = NaCl, (●) = NaBr, (▲) = Na_2SO_4, and (▼) = $(NH_4)_2SO_4$.

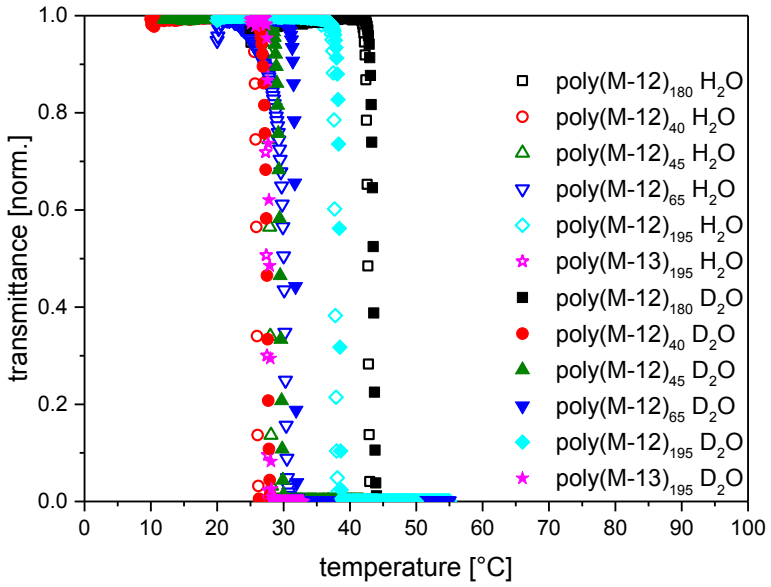

Figure A.58. Temperature dependent turbidity (heating runs) of 5 wt% aqueous solutions of **poly(M-12)** and **poly(M-13)** in H_2O (open symbols) and D_2O (close symbols). a) **CTA-1** was used to synthesize **Poly(M-12)$_{180}$**.

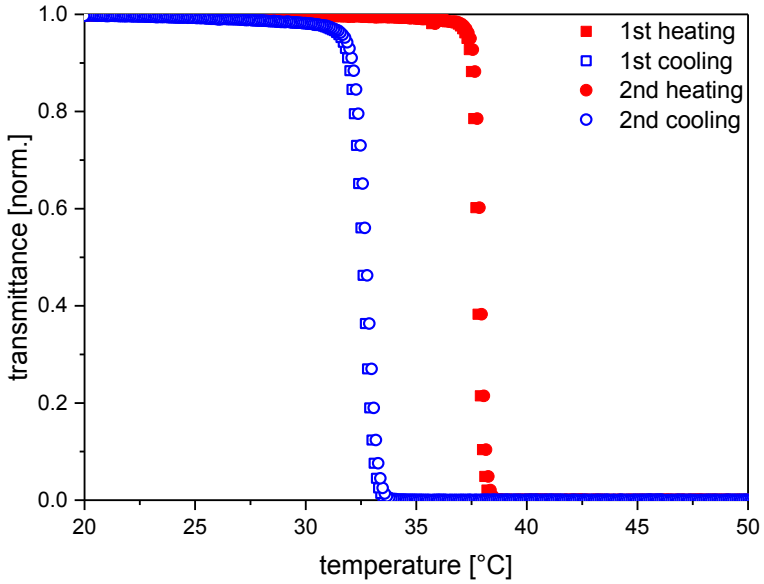

Figure A.59. Reproducible hysteresis of turbidimetry using the example of **poly(M-12)$_{195}$** (5 wt% in H_2O).

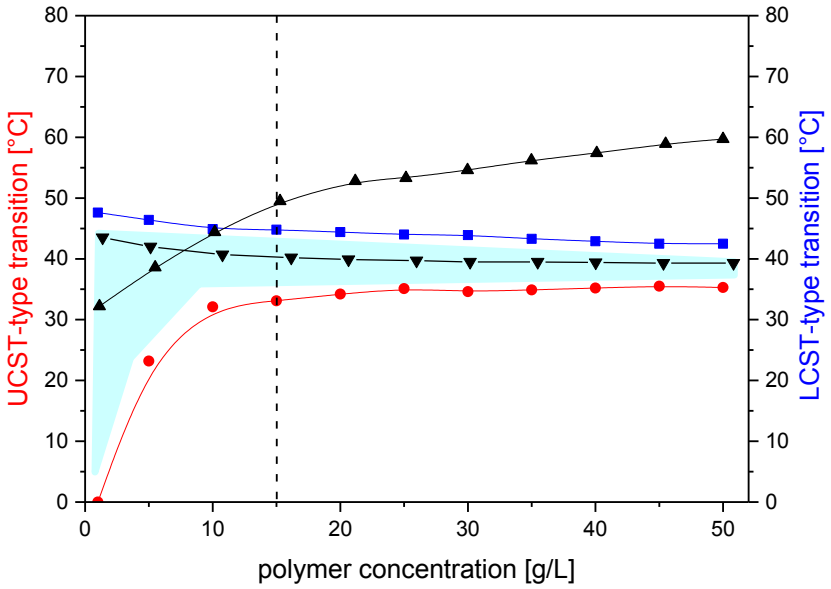

Figure A.60. Turbidity of polymer solutions in H_2O of (–▲–) **poly(M-3)$_{40}$** (cooling runs), (–▼–) **poly(M-12)$_{195}$** (heating run) and (–●– /–■–) **poly(M-3)$_{40}$-*block*-(M-12)$_{190}$** (heating run) at different polymer concentration. Block copolymer is dissolved at intermediate temperatures (cyan).

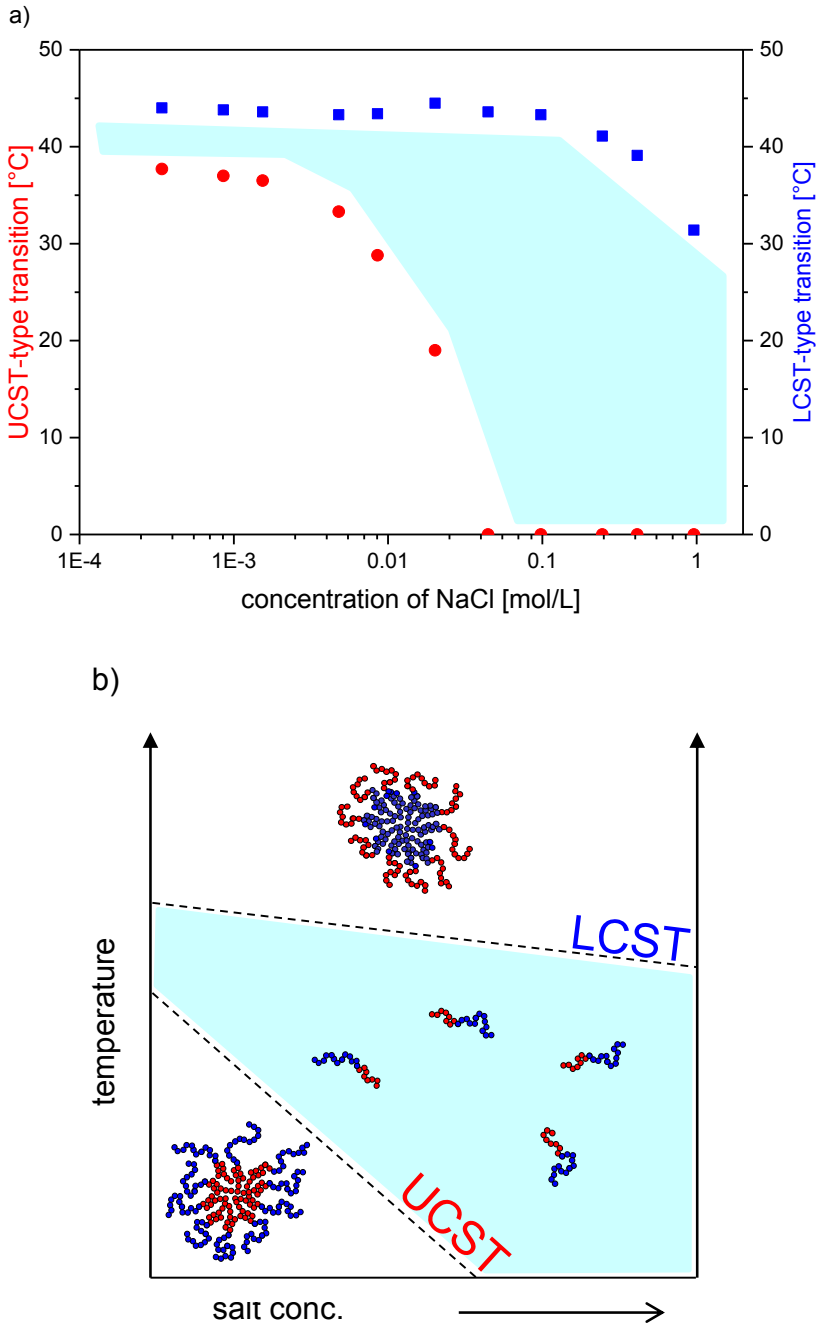

Figure A.61. a) Turbidity of 5 wt% solutions in H_2O of **poly(M-3)$_{50}$-*block*-(M-12)$_{155}$** containing NaCl. b) Schematic illustration of the modulation of thermoresponsive behavior via electrolyte-sensitivity.

Tables

Table A.1. Extinction coefficients ε, maximum absorbance wavelengths λ_{max}, maximum emission wavelengths λ_{PL} of **I-1** in various solvents, and empirical solvent polarity $E_T(30)$ parameter[147]. Excitation and ε at λ_{max3}.

sample	solvent	$\varepsilon_{max,3}$ [10^4 L·mol^{-1}·cm^{-1}]	$\lambda_{max1,2,3}$ [nm]	λ_{PL} [nm]	$E_T(30)$ [kcal·mol^{-1}]
I-1	chloroform	1.11	- , - , 420	505	39.1
I-1	ethanol	0.98	260, - , 418	529	51.9
I-1	trifluoroethanol	1.98	258, 286, 444	542	59.8

Calculations

Calculation of monomer conversion

Monomer conversions were calculated from the comparison of ^{1}H NMR spectra taken at the beginning and at the end of the polymerization. As an example, spectra in D_2O of the RAFT polymerization of **M-10** using **CTA-3** and V-501 in TFE are shown (**Figure A.62**).

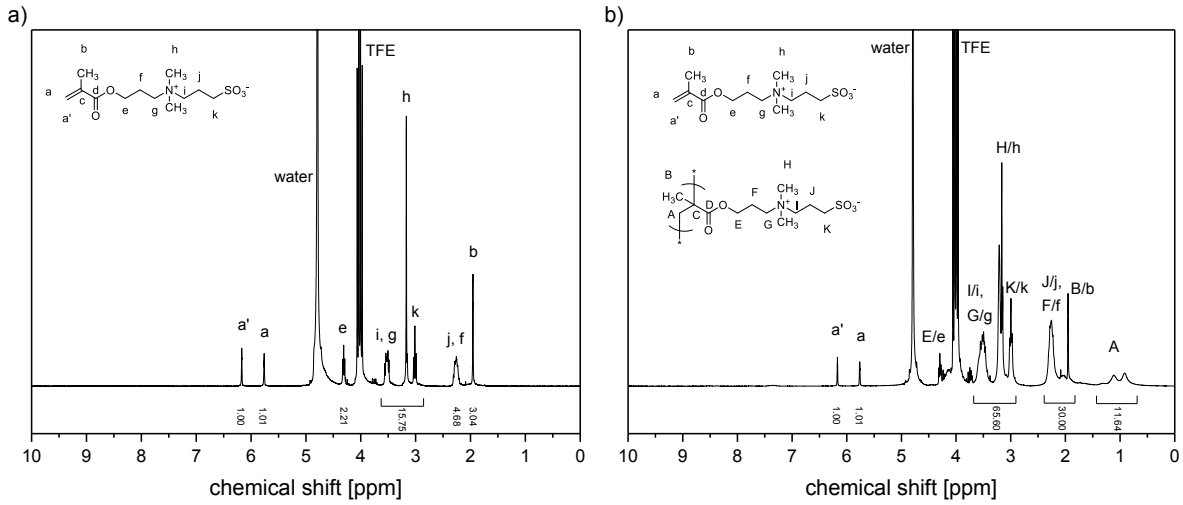

Figure A.62. ^{1}H NMR spectra of a RAFT polymerization of **M-10** in D_2O for calculating monomer conversions. a) Before polymerization, b) crude product after polymerization (2 h, conversion: 0.76). Polymerizations at 75 °C in TFE, using **CTA-3** and V-501. The molar ratio **M-10** : **CTA-3** : V-501 was 100 : 1 : 0.2. The monomer concentration was 30 wt%.

In both spectra, the integral of signal **a** at about 6.2 ppm is set as 1.00 ($N_{H(olefin)}$), as it is due to 1 proton of the methacrylic double bond. In correspondence to the reference value, the integral of the signals **i**, **g**, **h**, and **k** at about 2.8 – 3.6 ppm (**Figure A.62a**) is 15.75 ($N_{H(monomer)}$), which is set as the number as protons for the monomer. Note that the theoretically number of protons for the monomer is expected to be 16.00. However, the discrepancy of 1.5 % between the theoretical and the experimental number of protons is still acceptable for ^{1}H NMR analysis. The integral

of the signals of polymer and monomer **I/i**, **G/g**, **H**,**h**, and **K/k** is 65.60 ($N_{H(polymer+monomer)}$). Then, the conversion of monomer is calculated via **equation A.1**.

$$conversion = 1 - monomer_{unconverted}$$

$$conversion = 1 - \frac{\frac{N_{H(olefin)}}{N_{H(polymer+monomer)}}}{\frac{N_{H(olefin)}}{N_{H(monomer)}}} = 1 - \frac{\frac{1}{65.60}}{\frac{1}{15.75}} = 0.76 \qquad \textbf{(A.1)}$$

List of Figures

LIST OF FIGURES

List of Tables

Bibliography

[1] V. Aseyev, H. Tenhu, F. Winnik. *Adv. Polym. Sci.* **2011**, *242*, 19-50.
[2] I. Dimitrov, B. Trzebicka, A. H. E. Müller, A. Dworak, C. B. Tsvetanov. *Prog. Polym. Sci.* **2007**, *32*, 1275-1343.
[3] J. Madsen, S. P. Armes. *Soft Matter.* **2012**, *8*, 592-605.
[4] S. Sugihara, S. Kanaoka, S. Aoshima. *J. Polym. Sci., Part A: Polym. Chem.* **2004**, *42*, 2601-2611.
[5] D. Xie, X. Ye, Y. Ding, G. Zhang, N. Zhao, K. Wu, Y. Cao, X. X. Zhu. *Macromolecules.* **2009**, *42*, 2715-2720.
[6] J. Weiss, A. Laschewsky. *Langmuir.* **2011**, *27*, 4465-4473.
[7] V. Bütün, N. C. Billingham, S. P. Armes. *J. Am. Chem. Soc.* **1998**, *120*, 11818-11819.
[8] M. Arotçaréna, B. Heise, S. Ishaya, A. Laschewsky. *J. Am. Chem. Soc.* **2002**, *124*, 3787-3793.
[9] V. Bütün, S. Liu, J. V. M. Weaver, X. Bories-Azeau, Y. Cai, S. P. Armes. *React. Funct. Polym.* **2006**, *66*, 157-165.
[10] H. Mori, I. Kato, S. Saito, T. Endo. *Macromolecules.* **2010**, *43*, 1289-1298.
[11] H.-Y. Tian, J.-J. Yan, D. Wang, C. Gu, Y.-Z. You, X.-S. Chen. *Macromol. Rapid Commun.* **2011**, *32*, 660-664.
[12] Y.-J. Shih, Y. Chang, A. Deratani, D. Quemener. *Biomacromolecules.* **2012**, *13*, 2849-2858.
[13] Q. Zhang, J.-D. Hong, R. Hoogenboom. *Polym. Chem.* **2013**, *4*, 4322-4325.
[14] D. Wang, T. Wu, X. Wan, X. Wang, S. Liu. *Langmuir.* **2007**, *23*, 11866.
[15] V. A. Vasantha, S. Jana, S. S.-C. Lee, C.-S. Lim, S. L.-M. Teo, A. Parthiban, J. G. Vancso. *Polym. Chem.* **2015**, *6*, 599-606.
[16] A. Can, Q. Zhang, T. Rudolph, F. H. Schacher, J.-F. Gohy, U. S. Schubert, R. Hoogenboom. *Eur. Polym. J.* **2015**, *69*, 460-471.
[17] Y. Kawauchi, A. Kouka, S. Guragain, B. P. Bastakoti, S.-i. Yusa, K. Nakashima. *Colloids and Surfaces A: Physicochemical and Engineering Aspects.* **2013**, *434*, 56-62.
[18] A. E. Smith, X. Xu, S. E. Kirkland-York, D. A. Savin, C. L. McCormick. *Macromolecules.* **2010**, *43*, 1210-1217.
[19] Z. Ge, Y. Cai, J. Yin, Z. Zhu, J. Rao, S. Liu. *Langmuir.* **2007**, *23*, 1114-1122.
[20] Y. Cai, S. P. Armes. *Macromolecules.* **2005**, *38*, 271-279.

[21] M. d. R. Rodriguez-Hidalgo, C. Soto-Figueroa, L. Vicente. *Soft Matter.* **2013**, *9*, 5762-5770.
[22] X. Cai, L. Zhong, Y. Su, S. Lin, X. He. *Polym. Chem.* **2015**, *6*, 3875-3884.
[23] Y.-H. Tang, Z. Li, X. Li, M. Deng, G. E. Karniadakis. *Macromolecules.* **2016**, *49*, 2895-2903.
[24] J. Seuring, S. Agarwal. *Macromol. Rapid Commun.* **2012**, *33*, 1898-1920.
[25] S. Kudaibergenov, W. Jaeger, A. Laschewsky. *Adv. Polym. Sci.* **2006**, *201*, 157-224.
[26] A. Laschewsky. *Polymers.* **2014**, *6*, 1544-1601.
[27] M. B. Huglin, M. A. Radwan. *Polym. Int.* **1991**, *26*, 97-104.
[28] P. Köberle, A. Laschewsky, T. D. Lomax. *Makromol. Chem., Rapid Commun.* **1991**, *12*, 427-433.
[29] P. Koeberle, A. Laschewsky. *Macromolecules.* **1994**, *27*, 2165-2173.
[30] P. Mary, D. D. Bendejacq, M.-P. Labeau, P. Dupuis. *J. Phys. Chem. B.* **2007**, *111*, 7767-7777.
[31] J. Virtanen, M. Arotçaréna, B. Heise, S. Ishaya, A. Laschewsky, H. Tenhu. *Langmuir.* **2002**, *18*, 5360-5365.
[32] Y.-J. Che, Y. Tan, J. Cao, G.-Y. Xu. *J. Macromol. Sci, Part B.* **2010**, *49*, 695.
[33] E. Wischerhoff, K. Uhlig, A. Lankenau, H. G. Börner, A. Laschewsky, C. Duschl, J.-F. Lutz. *Angew. Chem. Int. Ed.* **2008**, *47*, 5666-5668.
[34] A. M. Breul, M. D. Hager, U. S. Schubert. *Chem. Soc. Rev.* **2013**, *42*, 5366.
[35] G. Huang, H. Li, S.-T. Feng, X. Li, G. Tong, J. Liu, C. Quan, Q. Jiang, C. Zhang, Z. Li. *Macromol. Chem. Phys.* **2015**, *216*, 1014-1023.
[36] V. O. Aseyev, H. Tenhu, F. M. Winnik. *Adv. Polym. Sci.* **2006**, *196*, 1-85.
[37] W. Blokzijl, J. B. F. N. Engberts. *Angew. Chem. Int. Ed. Engl.* **1993**, *32*, 1545-1579.
[38] J. Jiang, X. Tong, D. Morris, Y. Zhao. *Macromolecules.* **2006**, *39*, 4633.
[39] P. Schattling, F. D. Jochum, P. Theato. *Chem. Commun.* **2011**, *47*, 8859.
[40] M. Mertoglu, S. Garnier, A. Laschewsky, K. Skrabania, J. Storsberg. *Polymer.* **2005**, *46*, 7726-7740.
[41] S. Fujishige, K. Kubota, I. Ando. *J. Phys. Chem.* **1989**, *93*, 3311-3313.
[42] S.-i. Yamamoto, J. Pietrasik, K. Matyjaszewski. *Macromolecules.* **2008**, *41*, 7013-7020.
[43] D. Yu, C. Luo, W. Fu, Z. Li. *Polym. Chem.* **2014**, *5*, 4561-4568.
[44] S. Glatzel, A. Laschewsky, J.-F. Lutz. *Macromolecules.* **2011**, *44*, 413-415.
[45] A. Laschewsky, E. D. Rekaï, E. Wischerhoff. *Macromol. Chem. Phys.* **2001**, *202*, 276-286.
[46] Q. Zhang, R. Hoogenboom. *Prog. Polym. Sci.* **2015**, *48*, 122-142.
[47] F. Käfer, F. Liu, U. Stahlschmidt, V. Jérôme, R. Freitag, M. Karg, S. Agarwal. *Langmuir.* **2015**, *31*, 8940-8946.
[48] A. Halperin, M. Kröger, F. M. Winnik. *Angew. Chem. Int. Ed.* **2015**, *54*, 15342-15367.
[49] A. S. Hoffman, P. S. Stayton. *Prog. Polym. Sci.* **2007**, *32*, 922-932.
[50] H. G. Schild. *Prog. Polym. Sci.* **1992**, *17*, 163-249.
[51] G. D. Smith, D. Bedrov. *J. Phys. Chem. B.* **2003**, *107*, 3095-3097.
[52] B. Widom, P. Bhimalapuram, K. Koga. *Phys. Chem. Chem. Phys.* **2003**, *5*, 3085-3093.

[53] G. Némethy, H. A. Scheraga. *J. Chem. Phys.* **1962**, *36*, 3382-3400.
[54] J.-F. Lutz, A. Hoth. *Macromolecules.* **2005**, *39*, 893-896.
[55] J. Adelsberger, A. Meier-Koll, A. Bivigou-Koumba, P. Busch, O. Holderer, T. Hellweg, A. Laschewsky, P. Müller-Buschbaum, C. Papadakis. *Colloid. Polym. Sci.* **2011**, *289*, 711-720.
[56] F. M. Winnik. *Polymer.* **1990**, *31*, 2125-2134.
[57] C. W. Scales, A. J. Convertine, C. L. McCormick. *Biomacromolecules.* **2006**, *7*, 1389-1392.
[58] T. Tang, V. Castelletto, P. Parras, I. W. Hamley, S. M. King, D. Roy, S. Perrier, R. Hoogenboom, U. S. Schubert. *Macromol. Chem. Phys.* **2006**, *207*, 1718-1726.
[59] Y. Zhao, T. Bai, Q. Shao, S. Jiang, A. Q. Shen. *Polym. Chem.* **2015**, *6*, 1066.
[60] D. Zhang, S. H. Lahasky, L. Guo, C.-U. Lee, M. Lavan. *Macromolecules.* **2012**, *45*, 5833-5841.
[61] W. Gao, D. Xu, D. W. Lim, S. L. Craig, A. Chilkoti. *Polym. Chem.* **2011**, *2*, 1561-1566.
[62] J. W. Robinson, C. Secker, S. Weidner, H. Schlaad. *Macromolecules.* **2013**, *46*, 580-587.
[63] N. Zhang, S. Salzinger, B. Rieger. *Macromolecules.* **2012**, *45*, 9751-9758.
[64] A. Miasnikova, A. Laschewsky. *J. Polym. Sci., Part A: Polym. Chem.* **2012**, *50*, 3313-3323.
[65] K. Van Durme, G. Van Assche, B. Van Mele. *Macromolecules.* **2004**, *37*, 9596-9605.
[66] R. Liu, M. Fraylich, B. Saunders. *Colloid. Polym. Sci.* **2009**, *287*, 627-643.
[67] I. L. Valuev, Y. A. Talyzenkov, I. V. Obydennova, L. I. Valuev, N. A. Platé. *Polymer Science Series B. 49*, 148-151.
[68] J. Hashizume, A. Teramoto, H. Fujita. *J. Polym. Sci.: Polym. Phys. Ed.* **1981**, *19*, 1405-1422.
[69] A. Nakajima, F. Hamada, S. Hayashi. *J. Polym. Sci., Part C.* **1996**, *15*, 285.
[70] T. G. Fox. *Polymer.* **1962**, *3*, 111-128.
[71] N. Shimada, S. Kidoaki, A. Maruyama. *RSC Advances.* **2014**, *4*, 52346.
[72] Y.-J. Shih, Y. Chang. *Langmuir.* **2010**, *26*, 17286-17294.
[73] C. Cummings, H. Murata, R. Koepsel, A. J. Russell. *Biomacromolecules.* **2014**, *15*, 763-771.
[74] H. Zhang, X. Tong, Y. Zhao. *Langmuir.* **2014**, *30*, 11433-11441.
[75] B. Yang, C. Wang, Y. Zhang, L. Ye, Y. Qian, Y. Shu, J. Wang, J. Li, F. Yao. *Polym. Chem.* **2015**, *6*, 3431-3442.
[76] G. N. Malcolm, J. S. Rowlinson. *Transactions of the Faraday Society.* **1957**, *53*, 921-931.
[77] S. Saeki, N. Kuwahara, M. Nakata, M. Kaneko. *Polymer.* **1976**, *17*, 685-689.
[78] G. Van Assche, B. Van Mele, T. Li, E. Nies. *Macromolecules.* **2011**, *44*, 993.
[79] R. Longenecker, T. Mu, M. Hanna, N. A. D. Burke, H. D. H. Stöver. *Macromolecules.* **2011**, *44*, 8962-8971.
[80] J. Seuring, F. M. Bayer, K. Huber, S. Agarwal. *Macromolecules.* **2012**, *45*, 374-384.
[81] N. Shimada, H. Ino, K. Maie, M. Nakayama, A. Kano, A. Maruyama. *Biomacromolecules.* **2011**, *12*, 3418-3422.

[82] J. Seuring, S. Agarwal. *Macromolecules.* **2012**, *45*, 3910-3918.
[83] R. Buscall, T. Corner. *Eur. Polym. J.* **1982**, *18*, 967-974.
[84] K. Matyjaszewski, N. V. Tsarevsky. *Nat Chem.* **2009**, *1*, 276-288.
[85] G. Moad, E. Rizzardo, S. H. Thang. *Aust. J. Chem.* **2012**, *65*, 985-1076.
[86] A. B. Lowe, C. L. McCormick. *Chem. Rev.* **2002**, *102*, 4177-4190.
[87] A. Laschewsky. *Curr. Opin. Colloid Interface Sci.* **2012**, *17*, 56-63.
[88] Y. Zhang, P. S. Cremer. *Curr. Opin. Chem. Biol.* **2006**, *10*, 658-663.
[89] P. Lo Nostro, B. W. Ninham. *Chem. Rev.* **2012**, *112*, 2286-2322.
[90] J. C. Galin, *Polyzwitterions (Overview)*, CRC Press: Boca Raton, **1996**; Vol. 9.
[91] R. Ohme, D. Ballschuh, H. Seibt. *Tenside Surf. Det.* **1991**, *28*, 235-240.
[92] N. Tarannum, M. Singh. *Rev. Adv. Sci. Eng.* **2013**, *2*, 90-111.
[93] Y. Zhu, J.-M. Noy, A. B. Lowe, P. J. Roth. *Polym. Chem.* **2015**, *6*, 5705.
[94] V. M. Monroy Soto, J. C. Galin. *Polymer.* **1984**, *25*, 121-128.
[95] P. Köberle, A. Laschewsky, D. van den Boogaard. *Polymer.* **1992**, *33*, 4029.
[96] A. Laschewsky, I. Zerbe. *Polymer.* **1991**, *32*, 2070-2080.
[97] T. A. Wielema, J. B. F. N. Engberts. *Eur. Polym. J.* **1987**, *23*, 947-950.
[98] G. W. Fischer, R. Jentzsch, V. Kasanzewa. *J. Prakt. Chem.* **1975**, *317*, 943.
[99] R. Ohme, D. Ballschuh, H. Seibt. *Tenside Surf. Det.* **1991**, *28*, 180-185.
[100] D. Ballschuh, J. Rusche, K. Geneis, R. Ohme, H. Seibt, K. Schaurich. *Tenside Surf. Det.* **1983**, *20*, 155.
[101] H. Seibt, R. Ohme, D. Ballschuh. *Tenside Surf. Det.* **1991**, *28*, 337-347.
[102] M.-L. Seidenfaden. *Parfüm und Kosm.* **1961**, *42*, 203-206.
[103] W. M. Linfield, P. G. Abend, G. A. Davis. *J. Am. Oil Chem. Soc.* **1963**, *40*, 114-117.
[104] W. M. Linfield. *Tenside Surf. Det.* **1974**, *11*, 260-266.
[105] L. Zastrow. *Mitt.-bl. Chem. Ges.* **1984**, *31*, 32-39.
[106] J. B. Schlenoff. *Langmuir.* **2014**.
[107] B. Mojtaba, K. Maryam, D. U. Larry, In *Proteins at Interfaces III State of the Art*, American Chemical Society: 2012; Vol. 1120, pp 621-643.
[108] T. Moro, Y. Takatori, K. Ishihara, T. Konno, Y. Takigawa, T. Matsushita, U.-i. Chung, K. Nakamura, H. Kawaguchi. *Nat Mater.* **2004**, *3*, 829-836.
[109] P. A. Woodfield, Y. Zhu, Y. Pei, P. J. Roth. *Macromolecules.* **2014**, *47*, 750.
[110] J. Wu, W. Lin, Z. Wang, S. Chen, Y. Chang. *Langmuir.* **2012**, *28*, 7436-7441.
[111] J. Yuan, X. Huang, P. Li, L. Li, J. Shen. *Polym. Chem.* **2013**, *4*, 5074-5085.
[112] J. M. Corpart, F. Candau. *Macromolecules.* **1993**, *26*, 1333-1343.
[113] C. L. McCormick, L. C. Salazar. *Macromolecules.* **1992**, *25*, 1896-1900.
[114] C. L. McCormick, C. B. Johnson. *Macromolecules.* **1988**, *21*, 686-693.
[115] J. C. Salamone, W. Volksen, S. C. Israel, A. P. Olson, D. C. Raia. *Polymer.* **1977**, *18*, 1058-1062.
[116] B. Grassl, J. C. Galin. *Macromolecules.* **1995**, *28*, 7035-7045.
[117] B. Grassl, B. Meurer, M. Scheer, J. C. Galin. *Macromolecules.* **1997**, *30*, 236.
[118] P. Favresse, A. Laschewsky. *Polymer.* **2001**, *42*, 2755-2766.
[119] T. A. Wielema, J. B. F. N. Engberts. *Eur. Polym. J.* **1990**, *26*, 639-642.
[120] Y. Maeda, H. Mochiduki, I. Ikeda. *Macromol. Rapid Commun.* **2004**, *25*, 1330-1334.
[121] V. M. Monroy Soto, J. C. Galin. *Polymer.* **1984**, *25*, 254-262.

[122] J. C. Salamone, W. Volksen, S. C. Israel, D. C. Raia, A. Broggi, T.-D. Hsu. *Polym. Prepr.* **1975**, *16*, 731-736.
[123] K. D. Collins. *Biophys. J.* **1997**, *72*, 65-76.
[124] A. Salis, B. W. Ninham. *Chem. Soc. Rev.* **2014**, *43*, 7358-7377.
[125] W. Kunz. *Curr. Opin. Colloid Interface Sci.* **2010**, *15*, 34-39.
[126] J. C. Salamone, W. Volksen, A. P. Olson, S. C. Israel. *Polymer.* **1978**, *19*, 1157-1162.
[127] W.-F. Lee, C.-C. Tsai. *Polymer.* **1994**, *35*, 2210-2217.
[128] W. A. Braunecker, K. Matyjaszewski. *Prog. Polym. Sci.* **2007**, *32*, 93-146.
[129] S. Grajales, Controlled Radical Polymerization Guide. Sigma-Aldrich: **2012**.
[130] K. Matyjaszewski, J. Xia. *Chem. Rev.* **2001**, *101*, 2921-2990.
[131] J. Qiu, K. Matyjaszewski. *Acta Polym.* **1997**, *48*, 169-180.
[132] H. G. Elias, Makromoleküle Band I: Chemische Strukture und Synthesen, 6. Auflage, Wiley-VCH: Weinheim, **1999**.
[133] J. Chiefari, Y. K. Chong, F. Ercole, J. Krstina, J. Jeffery, T. P. T. Le, R. T. A. Mayadunne, G. F. Meijs, C. L. Moad, G. Moad, E. Rizzardo, S. H. Thang. *Macromolecules.* **1998**, *31*, 5559-5562.
[134] D. G. Hawthorne, G. Moad, E. Rizzardo, S. H. Thang. *Macromolecules.* **1999**, *32*, 5457-5459.
[135] C. Barner-Kowollik, M. Buback, B. Charleux, M. L. Coote, M. Drache, T. Fukuda, A. Goto, B. Klumperman, A. B. Lowe, J. B. McLeary, G. Moad, M. J. Monteiro, R. D. Sanderson, M. P. Tonge, P. Vana. *J. Polym. Sci., Part A: Polym. Chem.* **2006**, *44*, 5809-5831.
[136] M. J. Monteiro, H. de Brouwer. *Macromolecules.* **2001**, *34*, 349-352.
[137] D. J. Keddie, G. Moad, E. Rizzardo, S. H. Thang. *Macromolecules.* **2012**, *45*, 5321-5342.
[138] D. Zehm, L. P. D. Ratcliffe, S. P. Armes. *Macromolecules.* **2012**, *46*, 128.
[139] K. Skrabania, A. Miasnikova, A. M. Bivigou-Koumba, D. Zehm, A. Laschewsky. *Polym. Chem.* **2011**, *2*, 2074-2083.
[140] C. Herfurth, P. Malo de Molina, C. Wieland, S. Rogers, M. Gradzielski, A. Laschewsky. *Polym. Chem.* **2012**, *3*, 1606-1617.
[141] M. Päch, D. Zehm, M. Lange, I. Dambowsky, J. Weiss, A. Laschewsky. *J. Am. Chem. Soc.* **2010**, *132*, 8757-8765.
[142] A. Enzenberg, A. Laschewsky, C. Boeffel, E. Wischerhoff. *Polymers.* **2016**, *8*, 109.
[143] S. Inal, J. D. Kolsch, L. Chiappisi, D. Janietz, M. Gradzielski, A. Laschewsky, D. Neher. *J. Mater. Chem. C.* **2013**, *1*, 6603-6612.
[144] C. Barner-Kowollik, *Handbook of RAFT Polymerization*, Wiley-VCH: **2008**.
[145] M. Semsarilar, V. Ladmiral, A. Blanazs, S. P. Armes. *Langmuir.* **2011**, *28*, 914-922.
[146] W. Zhang, Y. Wang, Y. Xu, X. Qian. *Monatsh. Chem.* **2003**, *134*, 393-402.
[147] C. Reichardt. *Chem. Rev.* **1994**, *94*, 2319-2358.
[148] R. M. Duke, E. B. Veale, F. M. Pfeffer, P. E. Kruger, T. Gunnlaugsson. *Chem. Soc. Rev.* **2010**, *39*, 3936-3953.
[149] Y. Chevalier, Y. Storet, S. Pourchet, P. Le Perchec. *Langmuir.* **1991**, *7*, 848.
[150] A. Laschewsky, R. Touillaux, P. Hendlinger, A. Vierengel. *Polymer.* **1995**, *36*, 3045-3049.

[151] P. Mary, D. D. Bendejacq. *J. Phys. Chem. B.* **2008**, *112*, 2299-2310.
[152] S. A. Beckley, J. O. Schreck. *Polymer Preprints.* **2006**, *47*, 455-456.
[153] S. Hashmi, A. GhavamiNejad, F. O. Obiweluozor, M. Vatankhah-Varnoosfaderani, F. J. Stadler. *Macromolecules.* **2012**, *45*, 9804-9815.
[154] F. O. Obiweluozor, A. GhavamiNejad, S. Hashmi, M. Vatankhah-Varnoosfaderani, F. J. Stadler. *Macromol. Chem. Phys.* **2014**, *215*, 1077.
[155] F. O. Obiweluozor, A. GhavamiNejad, S. Hashmi, M. Vatankhah-Varnoosfaderani, F. J. Stadler. *Macromol. Chem. Phys.* **2014**, *215*, 2125.
[156] M. Semsarilar, E. R. Jones, A. Blanazs, S. P. Armes. *Adv. Mater.* **2012**, *24*, 3378-3382.
[157] J. Qui, B. Charleux, K. Matyjaszewski. *Polimery.* **2001**, *46*, 453-460.
[158] A. B. Lowe, C. L. McCormick. *Prog. Polym. Sci.* **2007**, *32*, 283-351.
[159] D. H. Nguyen. Dissertation, Georg-August-Universität zu Göttingen, Göttingen, **2007**.
[160] S. H. Thang, Y. K. Chong, R. T. A. Mayadunne, G. Moad, E. Rizzardo. *Tetrahedron Lett.* **1999**, *40*, 2435-2438.
[161] J. Fabian, S. Scheithauer, R. Mayer. *Journal für Praktische Chemie.* **1969**, *311*, 45-60.
[162] J. Fabian, H. Viola, R. Mayer. *Tetrahedron.* **1967**, *23*, 4323-4329.
[163] W. Rach, G. Gattow. *Z. Anorg. Allg. Chem.* **1988**, *565*, 47-53.
[164] A. M. Bivigou-Koumba, E. Görnitz, A. Laschewsky, P. Müller-Buschbaum, C. M. Papadakis. *Colloid. Polym. Sci.* **2010**, *288*, 499-517.
[165] Y. Isobe, K. Yamada, T. Nakano, Y. Okamoto. *Macromolecules.* **1999**, *32*, 5979-5981.
[166] Y. Miura, T. Satoh, A. Narumi, O. Nishizawa, Y. Okamoto, T. Kakuchi. *Macromolecules.* **2005**, *38*, 1041-1043.
[167] V. Hildebrand, A. Laschewsky, E. Wischerhoff. *Polym. Chem.* **2016**, *7*, 731.
[168] M. Chen, K. P. Ghiggino, A. W. H. Mau, E. Rizzardo, W. H. F. Sasse, S. H. Thang, G. J. Wilson. *Macromolecules.* **2004**, *37*, 5479-5481.
[169] M. Beija, A. Fedorov, M.-T. Charreyre, J. M. G. Martinho. *J. Phys. Chem. B.* **2010**, *114*, 9977-9986.
[170] H. Mao, C. Li, Y. Zhang, S. Furyk, P. S. Cremer, D. E. Bergbreiter. *Macromolecules.* **2004**, *37*, 1031-1036.
[171] M. J. A. Hore, B. Hammouda, Y. Li, H. Cheng. *Macromolecules.* **2013**, *46*, 7894-7901.
[172] N. Endo, H. Shirota, K. Horie. *Macromol. Rapid Commun.* **2001**, *22*, 593.
[173] L. Hou, P. Wu. *Soft Matter.* **2015**, *11*, 7059-7065.
[174] D. N. Schulz, D. G. Peiffer, P. K. Agarwal, J. Larabee, J. J. Kaladas, L. Soni, B. Handwerker, R. T. Garner. *Polymer.* **1986**, *27*, 1734-1742.
[175] J. Cardoso, R. Manrique, M. Albores-Velasco, A. Huanosta. *J. Polym. Sci., Part B: Polym. Phys.* **1997**, *35*, 479-488.
[176] P. Köberle, A. Laschewsky. *Macromol. Symp.* **1994**, *88*, 165-175.
[177] A. B. Lowe, N. C. Billingham, S. P. Armes. *Macromolecules.* **1999**, *32*, 2141-2148.
[178] H. Willcock, A. Lu, C. F. Hansell, E. Chapman, I. R. Collins, R. K. O'Reilly. *Polym. Chem.* **2014**, *5*, 1023-1030.
[179] Q. Yang, M. Ulbricht. *Chem. Mater.* **2012**, *24*, 2943-2951.

[180] J. M. Rathfon, G. N. Tew. *Polymer.* **2008**, *49*, 1761-1769.
[181] W. Fischer, D. Bellus, A. Adler, E. Francotte, R. Achim. *Chimia.* **1985**, *39*, 19-20.
[182] Autorenkollektiv, *Organikum 21. Auflage*, Wiley-VCH: Weinheim, **2001**.
[183] B. Neises, W. Steglich. *Angew. Chem. Int. Ed. Engl.* **1978**, *17*, 522-524.
[184] H.-l. Zhu, Z.-y. Hu, J.-l. Wang, D.-l. Cao. *J Surfact Deterg.* **2013**, 1-5.
[185] F. Dong, L. Jun, Z. Xin-Li, L. Zu-Liang. *Catal. Lett.* **2007**, *116*, 76-80.
[186] V. Bette, H. Bergmann, J. Petzoldt, F. Höfer *Process for preparing (meth)acrylic esters of N,N-substituted amino alcohols*. Patent. **2012**.
[187] Y. Itoh, K. Ogura, T. Hirota, A. Hachimori, K. Abe. *Acta Polym.* **1997**, *48*, 164-168.